UNIVERSITEIT VAN PRETORIA
UNIVERSITY OF PRETORIA
YUNIBESITHI YA PRETORIA

DETERMINATION OF FACTORS INFLUENCING THE DEGREE OF REDUCTION DISINTEGRATION IN NORTHERN CAPE LUMP ORE AND THE ROLE OF GANGUE MINERALS IN THE PROPAGATION OF CRACKS

WF VAN DER VYVER

Dissertation submitted in partial fulfilment of the requirements of the degree Philosophiae Doctor (Metallurgy) in the Faculty Engineering, Built Environment and Information Technology, University of Pretoria, Pretoria

2008-07-29

DETERMINATION OF FACTORS INFLUENCING THE DEGREE OF REDUCTION DISINTEGRATION IN NORTHERN CAPE LUMP ORE AND THE ROLE OF GANGUE MINERALS IN THE PROPAGATION OF CRACKS

WF VAN DER VYVER

Promotor :	**Prof PC Pistorius**
Department	**Material Science and Metallurgical Engineering**
Degree	**Philosophiae Doctor (Metallurgy)**

SYNOPSIS

The fundamental cause of low temperature breakdown (reduction disintegration) is reduction of hematite to magnetite, resulting in a volume expansion and stress relief through the formation of cracks. Serious reduction disintegration causes poor gas permeability, high flue dust production and scaffolding, poor gas distribution, higher fuel consumption and lower productivity.

Northern Cape iron ore generally performs well when tested for reduction disintegration properties both for blast furnaces and Corex; nevertheless, significant breakdown is experienced when used in the Corex process (at Saldanha Steel).

This study was hence conducted to determine the effects of the following on reduction disintegration:

- different ore types (from Northern Cape)
- initial particle size
- temperature range
- reduction gas composition

Although disintegration is clearly triggered by reduction, no direct correlation could be established between the percentage reduction and the percentage fines generated.

The results indicated that the presence of gangue minerals alone does not cause fractures to form, but does influence the direction and intensity of fractures to some extent. In many cases cracks form randomly, with no specific preference for either gangue minerals or iron oxides. For most of the samples, an incubation period was observed before the first cracks formed. No crack propagation was observed after initial cracking.

This study indicates that the degree of reduction disintegration depends mostly on furnace conditions. Reduction disintegration increased with higher hydrogen percentages (>5%), higher temperatures (in the 500ºC-700ºC range) and longer exposure. Disintegration of the samples decreased at temperatures higher than 750°C.

For particles smaller than 16 mm an inverse relationship was found between the average particle size and the percentage of fines generated, in line with the observation that most of the disintegration is due to spalling from particle edges rather than particles breaking into smaller clumps.

The results indicate that it is important to manage the temperature in the top of the blast furnace and the COREX shaft, and the time spent at temperatures below 750°C, to minimize the amount of fines generated.

TABLE OF CONTENT

LIST OF TABLES

LIST OF FIGURES

1 BACKGROUND

"The value of iron ores and agglomerates is determined by the cost of converting it to a desired product. This includes the coke consumption in the blast furnace, the throughput which can be attained, the proportion of charge which leaves the blast furnace in the form of flue dust and the cost of dephosphorization and desulphurization."[i]

New ironmaking processes have been extensively explored with a view to saving resources and energy, as well as reducing environmental pollution. Since the turn of the previous century, many efforts have been made to find an economical alternative to the well established integrated rout of blast furnace ironmaking followed by the oxygen steelmaking route.

Although various direct reduction processes were developed, there was no alternative method for production of hot metal. In 1970s, however, a process for the production of liquid iron without using coke – or using low-grade coke and coal – was patented. The possibility that a smelting-reduction process could be based on the use of coal alone was first investigated by Korf Stahl in 1977.[ii] This was the origin of the Corex Process.

In the next section, the blast furnace and Corex processes are discussed. The main difference between the Corex and the blast furnace are that the Corex uses coal rather than coke, cold oxygen rather than heated blast air and that the Corex separates the melting and solid-state reduction processes between two different reactors.

1.1 IRONMAKING

1.1.1 BLAST FURNACES

The blast furnace remains an important part of modern iron production. Modern furnaces are highly efficient, including Cowper stoves to pre-heat the blast air and employ recovery systems to extract the heat from the hot gases exiting the furnace. Competition in industry drives higher production rates, and the largest blast furnaces produce around 70,000 tonnes of iron per week (according to benchmarking exercise).

This is a great increase from the typical 18th century furnaces, which averaged about 400 tons per year. Variations of the blast furnace, such as the Swedish electric blast furnace, have been developed in countries which have no native coal resources.

Figure 1 illustrates how the blast furnace is charged with alternate layers of coke and iron bearing minerals. These iron-bearing materials consist of combinations of sinter, pellets and iron ore and the ratio varies from furnace to furnace. Limestone, dolomite, quartz and/or serpentine are also added to the blast furnace to regulate the slag composition and viscosity.

The blast furnace shaft is a countercurrent reactor in which hot gas move upward – heating, reducing and melting the charge that moves downward. Preheated air (>1000°C) is blown in at the tuyère level where the coke in the charge undergoes partial combustion, yielding a reduction gas rich in carbon monoxide. Lower levels of hydrogen are also generated. This highly reducible gas is forced upward through the charge, generating different zones of reduction according to the temperature of the charge and the composition of the gas. **Figure 2** is a schematic diagram of the various reduction zones and the temperature profile of the blast furnace.

At the top is a preheating zone where solids are heated from room temperature to about 950°C. After the free water and water of crystallization are driven off hematite, Fe_2O_3 is indirectly reduced to magnetite, Fe_3O_4. Thermal decomposition of carbonates also takes place in this zone.

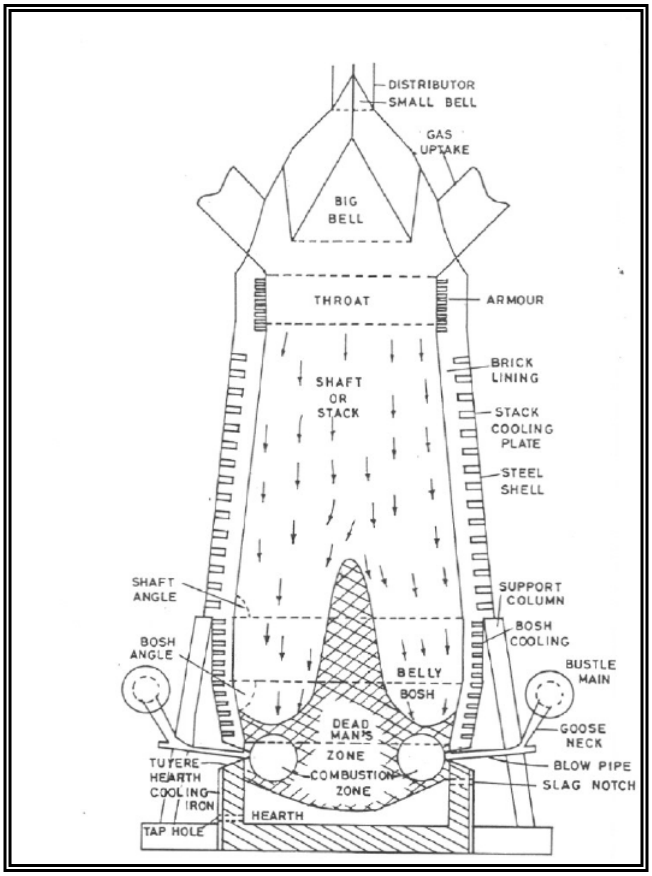

Figure 1: Schematic diagram of the blast furnace.[iii]

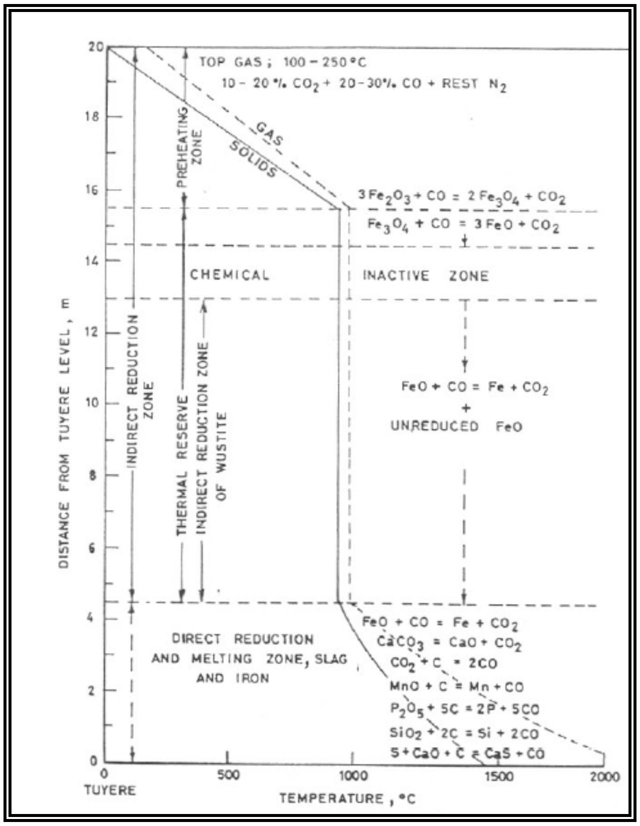

Figure 2: Schematic diagram of the temperature distribution and reduction zones of the blast furnace[iii].

Figure 3: Blast furnace tap hole. (Photo taken at blast furnace at Mittal Vanderbijlpark).

Next is the thermal reserve zone where the temperature remains constant at about 950°C. In this zone the iron bearing charge is indirectly reduced from magnetite, Fe_3O_4, to wustite, FeO. The wustite is to some extent reduced to iron.

Above 1000°C is the direct reduction and melting zone, where the remaining wustite is directly reduced to iron by the carbon in the coke. Thermal decomposition of limestone and dolomite will occur. The reduced iron will melt and slag will form at the surface. Liquid slag is drawn off through the slag notch, while liquid iron is tapped at the tap holes (**Figure 3**).

The mechanical strength of the iron bearing materials is an important factor in the preheating zone where hematite is reduced to magnetite. Reduction of hematite to magnetite involves restructuring of a hexagonal to cubic lattice, which results in some dislocation of the structure.

Shaft permeability and reduction greatly affects the operating parameters and stability of the blast furnace and directly influence the productivity of the blast furnace. Permeability depends on the particle size, distribution of the charge and on the mechanical strength during reduction reaction of both the coke and iron bearing materials. The degree of reduction depends on the reactivity of the coke and on the composition and reducibility of the iron bearing charge.

The stack of material in a shaft furnace is supported largely by the hard and generally resistant lumps of coke and by the gas pressure. If the iron bearing material has a high reduction strength, it is possible to cut down on coke consumption to the quantity actually needed for reduction, while at the same time the movement of material proceeds more smoothly due to a lowering of the gas flow resistance. A further consequence of high iron bearing material strength is that part of the expensive coke charge could be replaced with PCI*, natural gas or oil.

To maximize the throughput of the blast furnace the reduction reaction should proceed as rapidly as possible. The main prerequisites for this are:

1 Uniform permeability of the stock column
  - a Good size grading – eliminating the amount of fines in the charge
  - b Good physical properties which means resistance to mechanical breakdown and abrasion
  - *c Limited low temperature (500°C – 750°C) breakdown also referred to as reduction disintegration*
  - d Softening of charge at high temperatures low down in blast furnace and a short interval between beginning of softening and end of melting

2 Good reducibility

1.1.2 COREX

Figure 4 shows the Corex process developed in Austria. This process is the only new ironmaking process now commercialized, and is in operation with plants having capacities of up to 600,000 ton/year.

---

* PCI – Pulverised-coal injection

The COREX consists of two separate reactors:

- Reduction shaft
- Melter-gasifier

In the reduction shaft a combination of lump ore, pellets, and sinter is pre-reduced to about 90% metallization (sponge iron) by a gas containing CO and H_2 supplied from the melter-gasifier. The sponge iron is delivered hot from the reduction shaft furnace by screw conveyors into the melter-gasifier where melting takes place.

Non-coking coal lump -50mm+6mm in diameter is also fed into the reactor. When the coal comes into contact with the hot gas, the coal is dehydrated and devolatilised and is combusted to form CO and H_2. The gas leaves to furnace at ~1000ºC and is used as the reducing gas in the reduction shaft (following cleaning of the gas in hot dust cyclones). Some unreacted coal forms a char bed at the bottom of the melter-gasifier. The sponge iron descends in the melter-gasifier to melt in the region of the oxygen tuyeres. Hot metal and slag are tapped from the melter-gasifier. The hot metal is similar in composition to blast furnace hot metal.

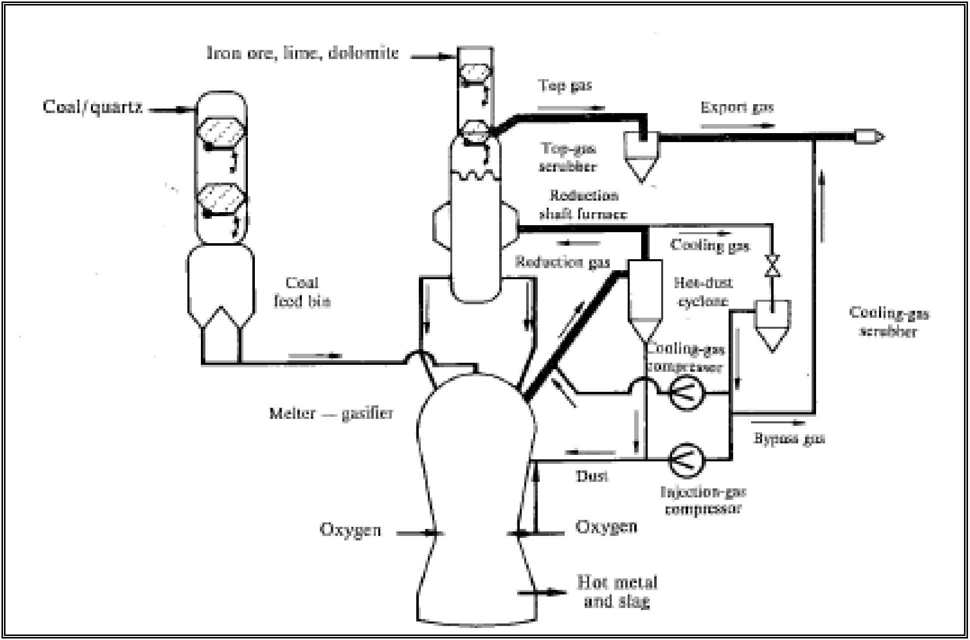

Figure 4: Flowsheet of the COREX process.

1.1.2.1 IRON ORE CHARACTERISTICS FOR THE COREX PLANT

It is generally known that fines – whether present in the feed material or developing during reduction - may have an adverse effect on the gas permeability of the shaft furnace[iv]. However, the rate of reduction decreases with increasing size of the lumps, particularly for lumpy ores. Therefore there are optimum grain sizes for pellet, sinter and lumpy ore, as shown in **Table 1**.

Material	**Grain size (mm)**	
	Tolerable	**Preferred**
Lumpy ore	6 to 30	8 to 20
Pellets	6 to 30	8 to 16
Sinter	6 to 45	10 to 30

Table 1: Optimum grain sizes for lumpy ore, sinter and pellets.[iv]

The following criteria are generally applied in the determination of those properties of the ore that influence its reduction[iv]:

- The size of the lumps and the inherent reducibility of the ores must match if a high degree of metallization is to be realized during the passing of the charge through the shaft of the reduction furnace. "Reducibility" refers to the rate of the gaseous reduction of the ore.
- The tendency to fragmentation of the feed materials should be low; the material should have sufficient strength to withstand rapid heating to the reduction temperature, and should retain their strength throughout the reduction process.
- The tendency of some ores to stick in gas-based direct-reduction plants[iv] is not encountered in the Corex plant because the coal dust serves as lubricant.

1.1.2.2 REDUCIBILITY

During reduction, oxygen is removed from the iron ore by the reduction gas. The kinetics of this process involves various factors:

- Transport of the reduction gas within the pores of the iron ore
- Diffusion of the oxygen in the solid state
- The rate of the reduction reaction

Due to the fact that hematite grains generally possess a certain amount of micro porosity, the reduction of hematite ores normally occurs more rapidly than does the reduction of magnetite[iv]. However the supply of the reduction gas to the reaction zone may be impaired by low porosity.

1.1.2.3 DISINTEGRATION DURING REDUCTION

Disintegration of the feed material during reduction inhibits the gas flow within the burden, influences coal consumption, and affects the quality of the product. Most of the disintegration occurs during the reduction from hematite to magnetite. Given the important effects of disintegration in the furnace, it is important to be able to evaluate the disintegration behavior of the ore: static and dynamic tests are used for this. A short description of the two test methods are given below. A full test procedure is given in **Appendix 2**.

- Reduction disintegration test (static): ISO 4696

  The reduction disintegration test parameters are used to determine the breakdown of material at 500°C. A 500g sample of –12.5+10mm material is heated under inert atmosphere (N_2) to 500°C. When the sample reaches 500°C, the reduction mixture, consisting of 20% CO, 20% CO_2 and 60% N_2 are opened for one hour. The sample is then cooled to room temperature under an inert atmosphere. A drum test and sieve analysis determines the breakdown of the sample.

- Reduction disintegration index (dynamic): ISO 4697

  The test conditions are the same as for the static test except that the rotation of the sample takes place during and not after the test. The rotation takes place at 10rpms. After cooling down the sample, a sieve analysis is performed to determine the breakdown.

In addition to the standard laboratory tests, such as grain size determination, tumble tests and the comprehensive strength evaluations, the Corex Linder test (**Figure 5**) as well as the static Othfresen test (Burghardt) are used in the evaluation of the raw materials for the Corex process. **Figure 6** is a photo of the COREX-Linder test apparatus at Kumba Iron Ore. A short description of the two tests methods are given below. A full description of the test methods are given in **Appendix 2**.

- Burghardt test – Reduction under load): ISO/DOC 3772

  This test is performed to determine the influence of pressure on the sample. A 1 200g sample of –12.5+10mm material is heated under inert atmosphere (N_2) to 1050°C. When the sample reaches 950°C, the reduction mixture, consisting of 40% CO and 60% N_2 are opened. At the same time a pressure of 50kPA are exercised on the sample until 80 per cent of reduction is reached. During the test, the weight loss, pressure drop over the sample as well as the sample height is measured. The sample is then cooled to room temperature under an inert atmosphere. The reduced and compacted sample can be used to determine the *sticking index* of the sample.

- Corex Linder Test

  The test are used to determine the percentage of metallization of the iron bearing material (lumpy ore or pellets) under similar conditions experienced in the COREX shaft. In addition the percentage fine material generated during the dynamic test is measured and recorded. A 500g sample of –12.5+10mm material is heated to 800°C in 30 minutes while the drum is being rotated at 10rpm's. The reduction gas during the heat up phase consist of 30% CO, 50%CO_2 and 20%H_2. When the sample reaches 800°C, the reduction mixture is changed to 70% CO, 5%CO_2 en 25%H_2 and kept at 800°C for 4 hours. After four hours, the sample is cooled to room temperature under an inert atmosphere. Sieve analysis is used to determine the percentage of breakdown while chemical analysis is used to determine the percentage metallization.

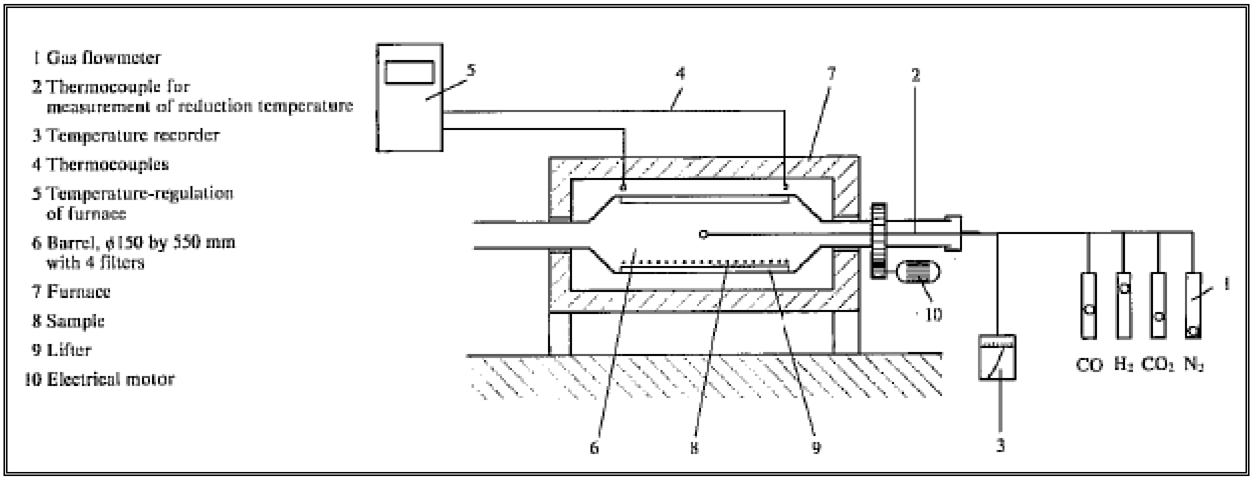

Figure 5: A schematic diagram of the COREX-Linder test apparatus.

Figure 6: Photo of the COREX-Linder test apparatus at Kumba Iron Ore

1.1.3 OTHER

Other new processes for iron making have been attempted in Australia (HIsmelt- and Ausmelt- process), Japan (DIOS process), Russia (Romelt process), and U.S.A. (AISI process), but are still at the pilot plant stage (with the exception of HIsmelt, where a large-scale plant is operated on a test basis). These processes utilize mainly smelting reduction, meaning that the amount of reduction in the molten state is greater than that in the solid state, which is different from that in the BF process. These processes should offer advantages such as: (i) iron ore can be used without agglomeration; (ii) non/weak-coking coals can be used directly without coking; (iii) start up and shut down in operation are much easier than with a BF, and (iv) possible less carbon dioxide is produced. However, many problems have yet to be solved before these processes will become a commercial reality, requiring much research and development.

1.2 IRON ORES

Iron ore naturally occurs as different forms of hematite and magnetite. Due to the relatively slower reduction rate of natural magnetite vs hematite, hematite is the preferred form of iron ore in the blast furnace or Corex. **Figure 7** shows crystals of natural hematite and magnetite[v].

The first step of reduction of hematite ores involves formation of magnetite. Cracking of the ore is often associated with this reduction step. For this reason, data on unit cell volumes of hematite and magnetite are reviewed below.

Hematite has a rhombohedrally centered hexagonal lattice with layers of oxygen ions and layers of iron ion perpendicular to the triad axis.[vii,viii] With 6 formula units (Fe_2O_3) per unit cell, the 18 oxygen ions are arranged in a slightly distorted hexagonal packing while successive cation layers contain equal numbers of iron ions in octahedral coordination. Measurements of the unit cell dimensions of hematite by Taylor[vi] are shown in equations 1-4, relating the unit cell parameters a_0 and c_o (Å) to temperature (°C)

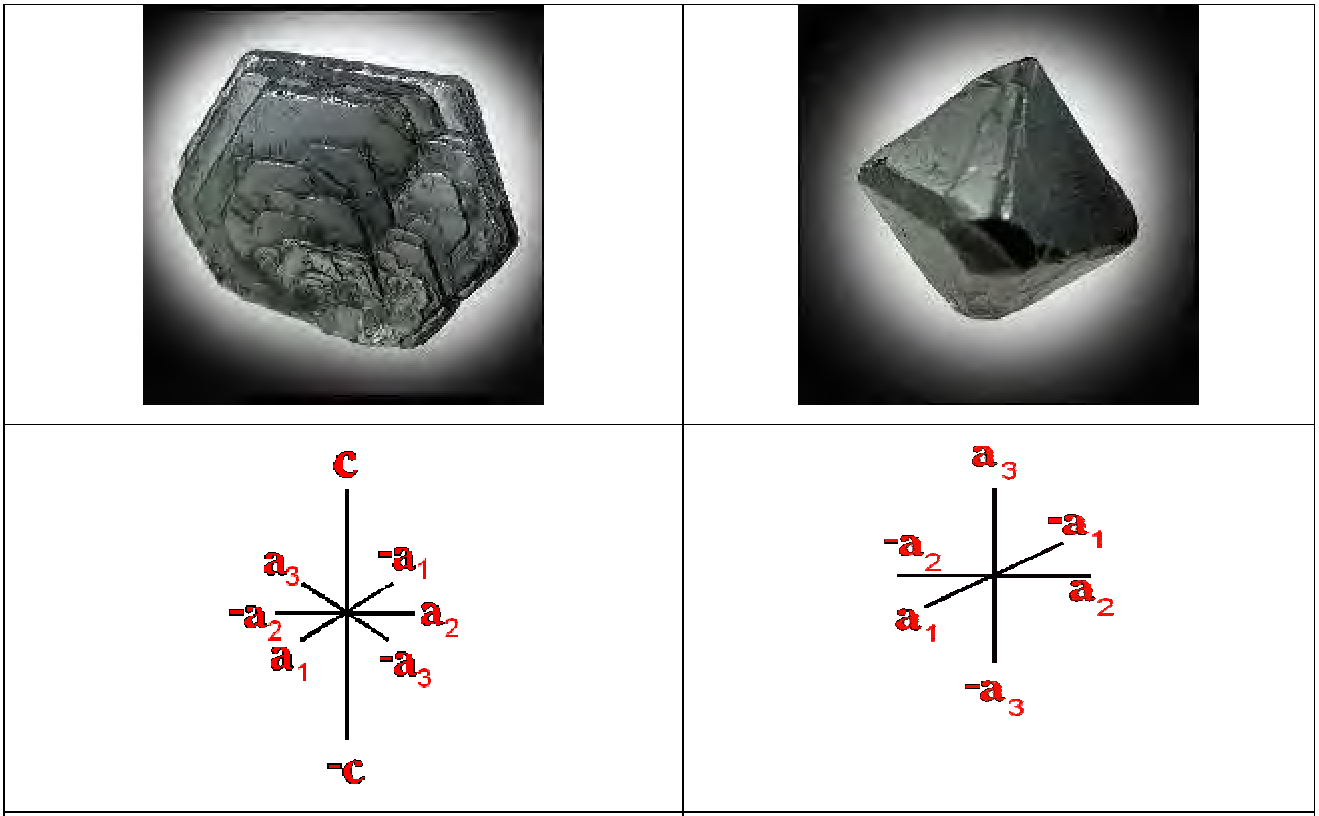

Hematite crystals | **Magnetite crystal**

Figure 7: Crystals of Hematite and Magnetite[v].

For T = 20-650°C

a_0 = 5.0343*(1+7.37E-06*T+9.53E-09*T*T) Å (1)

SE = 0.0008

c_0 = 13.7478*(1+8.48E-06*T+2.80E-09*T*T) Å (2)

SE = 0.0015

For T = 700-1100°C

a_0 = 5.0362*(1+1.32E-05*T) Å (3)

SE = 0.0007

c_0 = 13.7062*(1+1.44E-05*T) Å (4)

SE = 0.0062

Hematite crystals are generally thick to thin tabular {0001}, rarely prismatic [0001] or scalenohedral or rhombohedral {101¯1}, producing pseudo-cubic crystals. It is often found in sub-parallel growths on {0001} or as rosettes but also occurs in micaceous to platy masses (**Figure 7**).

Magnetite has a cubic lattice with an inverse spinel structure. There are 8 formula units (Fe_3O_4) per unit cell and of the 24 iron ions, 8 ferric ions are tetrahedrally coordinated and 8 ferric and 8 ferrous ions are octahedrally coordinated.[vii,viii] Numerous measurements have been made of the unit cell dimension of magnetite. Taylor[ix] has correlated these results and Equations 5 and 6 show the relationships between unit cell dimension a_0 (Å) and temperature T (°C) where SE is the standard error of the correlation.

For T = 19-590°C

a_0 = 8.3965*(1+5.66E-06*T+1.32E-08*T*T) Å (5)

SE = 0.0027

For T = 600-1100°C

a_0 = 8.4452*(1+8.08E-09*T*T) Å (6)

SE = 0.0079

Magnetite crystals are usually octahedral, sometimes dodecahedral, striated on {011} parallel [01¯1]; less frequently with modifying {001} or {hhl}. Cubic occurrences (Balmat, NY) are rare (**Figure 7**). Skeletonized microcrystals are found in igneous rocks. Magnetite varies from massive, granular, coarse to fine.

X-ray studies of the transformation of the spinel (magnetite) to the hexagonal structure (hematite) have shown that the following orientation relationship exists between the two structures (using a three axis system in an orthohexagonal cell for indexing the hematite planes and directions).[x]

$(111)_{mag} \parallel (011)_{hem}$

$[1\bar{1}0]_{mag} \parallel [010]_{hem}$

The habit plane for this transformation is the closed packed plane of α-Fe_2O_3 and Fe_3O_4.

The volume per Fe Atom of magnetite and hematite vs temperature is shown in **Figure 8**.

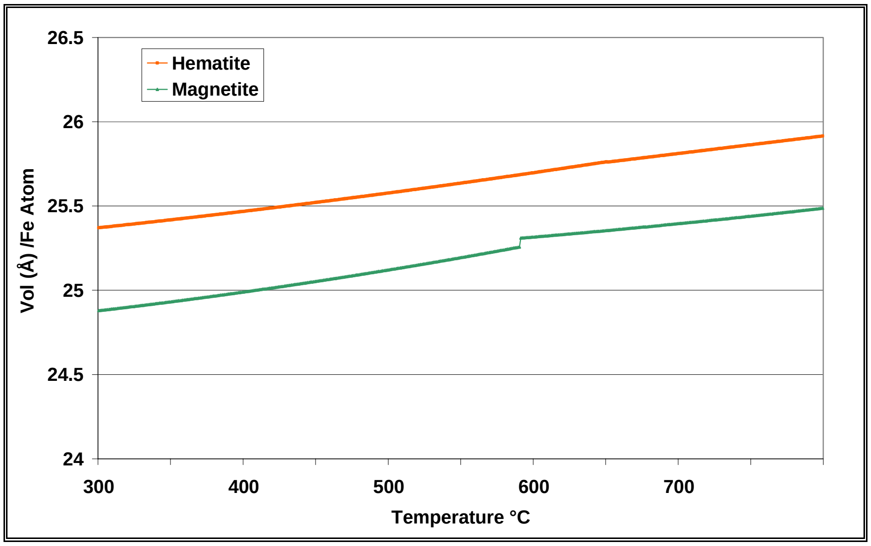

Figure 8: Volume per Fe atom of hematite and magnetite crystals vs temperature.

Between 500°C and 700°C the volume per Fe atom in hematite varies between 25.6$Å^3$ and 25.8$Å^3$ and that of magnetite between 25.1$Å^3$ and 25.4$Å^3$. This indicates a volume decrease from hematite to magnetite of 1.61-1.72% between 550°C and 700°C. (The sharp increase at 600°C in the magnetite curve is due to the change from Equation 5 to Equation 6, - which in practice is not exactly at 600°C. This does however not impact the results of the study and no further attention to detail is given.) In practice however, large apparent volume **increases** (in the order of 25%) are found when hematite is reduced to magnetite. The difference between these two results can be accounted for by the presence of many cracks and pores formed during the reduction process[xi].

1.3 DECREPITATION/DEGRADATION OF IRONBEARING RAW MATERIALS

The fundamental cause of low temperature breakdown (reduction disintegration) is hematite reducing to magnetite, resulting in a volume expansion and the relieving of stress through the formation of cracks, which then become passages for the reducing gases to penetrate easily into the inner regions of ore or sinter particles[i,xii]. Hematite present along the walls of the cracks is then reduced, inducing new stresses and leading to the propagation of the formed crack or the formation of new cracks. Serious low temperature breakdown or reduction disintegration leads to poor permeability for gas, high flue dust production and scaffolding, impedes gas distribution, raises fuel consumption and diminishes production capacity.[i]

It is generally agreed that RDI$_{-3.15mm}$ below 40% is acceptable for blast furnace operation. However practice in China showed that RDI$_{-3.15mm}$ have a notable influence upon the smooth BF operation and stack permeability even if it is less than 20%. It was found that when a sinter RDI$_{3.15mm}$ of 20% was reduced by 5%-10% the coke ratio will decrease 10kg/t and the hot metal production will increase with up to 5%.[xiii]

Although theoretically a contraction is predicted for the stage of reduction from fully hematite to fully dense magnetite, the experimental evidence contradicts this. Instead of a contraction, an expansion has been observed by various authors, and different values of expansion have been reported. It has been estimated that when hematite is reduced to magnetite at temperatures between 525 and 625°C there is a volume increase of around 25%.[xiv] This induces stresses in the materials surrounding the reduced area. Material degradation will not occur if the surrounding areas are able to contain the stresses. Normally, however, the magnitude of the induced stresses is large and cracks are formed to relieve them. The severity of the cracking depends on the degree of reduction and the properties of the surrounding material. The relevant material property appears to be fracture toughness since this parameter is a measure of how easily cracks are propagated through a material[xv].

It is theoretically possible that very tough phases, if present around the reduced areas, could contain the stresses and it is likely that in such circumstances the fracture toughness of these surrounding, non–reducing phases could influence and even prevent degradation.[xv] Loo and Bristow[xv] proposed a mechanism of crack propagation, shown in **Figure 9**. This mechanism models two sinters that are composed of hematite grains in a bonding matrix. The sinters are identical in structure except that the bonding matrix of one sinter has significantly higher fracture toughness values.

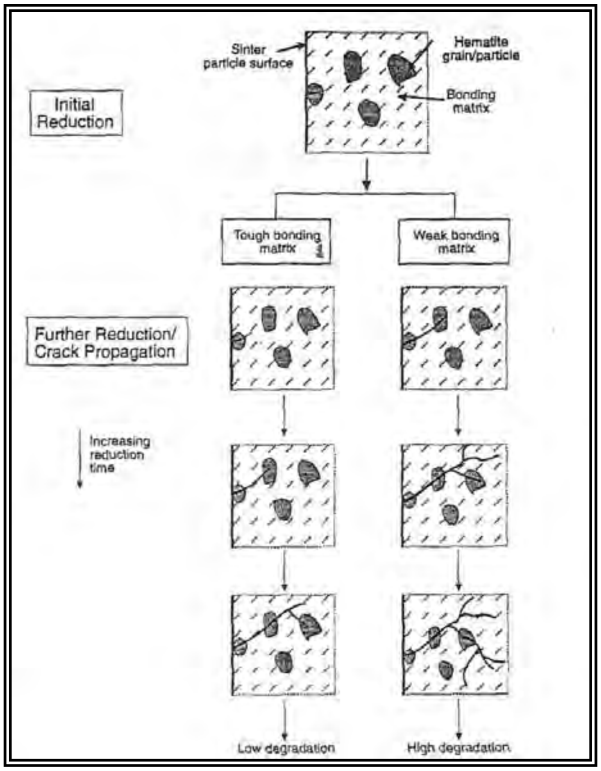

Figure 9: Schematic representation of reduction degradation process in sinter.[xv]

If one applied this model to lump ore, the low temperature reduction degradation properties of lump ore are a function of porosity and the fracture toughness of the material. Experience at the Newcastle Laboratories[xv] has generally shown that highly reducible lump ores have high porosities and higher RDI[†] than dense ores, which is consistent with the proposed mechanism. However studies of a certain dense lump ore with a polycrystalline structure revealed inter-grain cracking and a tendency for the

---

[†] RDI – Reduction Disintegration Index

hematite crystallites to separate during RDI tests. This results in high RDI values even though the ore is very dense, suggesting that cracking behaviors and planes of weakness can also influence degradation. Unfortunately, insufficient information is available on the fracture toughness of lump ores to allow an assessment of the importance of this parameter.[xv]

Figure 11 and Figure 12 is a graphical representation of the necluation and growth of magnetite laths or plates from hematite as proposed by Hayes et al[xvi]. They suggest that when hematite is exposed to the reducing gas, the sample tends to achieve local equilibrium with the gas resulting in an increase in iron/oxygen ratio in the oxide (reaction path a-b **Figure 11**). This leads to unstable α-Fe_20_3 with respect to an intermediate oxide, possibly β-Fe_20_3 which has a defect α-structure. The iron ions in this metastable β-phase are arranged such that the shear transformation by oxygen ions, results in the formation of cubic γ-Fe203 (reaction path c-d, **Figure 11**). The formation of the γ-Fe_20_3 nucleus provides a sink for excess iron ions from the surrounding α-Fe_20_3 and thus a continual increase in iron content of this structure takes place until the stoichiometry of the nucleus approaches equilibrium with the reducing gas i.e. it approaches Fe_30_4 (reaction path d-e, **Figure 11**). The Fe_30_4 lath then moves into the bulk solid as excess iron ions are added through bulk diffusion in α-Fe_2O_3. If the incubation period before the nucleation of y-Fe_20_3 or the metastable oxide has been sufficiently long then the whole of the α-Fe_20_3 should approach equilibrium with the reducing gas and thus after nucleation excess iron ions will be provided to the magnetite phase so that it can continue to grow across the whole thickness of the specimen. If only a short time elapses before nucleation then only the surface layers of α-Fe_20_3 will be supersaturated with iron ions because of the low mobility of iron ions in the bulk phase and the initial growth of the laths will be limited to this surface region. The initial growth of the laths occurs until the iron ion super saturation ahead of the growing magnetite lath tip is eliminated. The removal of oxygen atoms continues at the hematite/gas interface and the excess iron ions are transferred by surface diffusion to the Fe_20_3/Fe_30_4 interface. The growth of the magnetite plates then occurs by the inward migration of iron ions at the Fe_20_3/Fe_3O_4

interface from the gas/oxide interface (**Figure 12**). This latter step obviously becomes slow when the diffusion distances become larger with lath growth.

A study by Husslage et al[xvii] found that the reduction conditions and the reductant couple influence the reduction mechanism and thus the initiation and propagation mechanisms of cracks formed in sinters (**Figure 10**). They indicated that the reductant gases affected the microstructure of the magnetite that formed and thus the dilation behaviour at temperatures below 500°C and below. They indicated that crack initiation in a sinter matrix is dictated by the nature of the dilation in the iron oxide phase during the reduction process, but that the crack propagation was governed by the fracture strength of the magnetite that formed. Both these phenomena combined were proposed to determine the potential for breakdown of sinter during low temperature reduction.

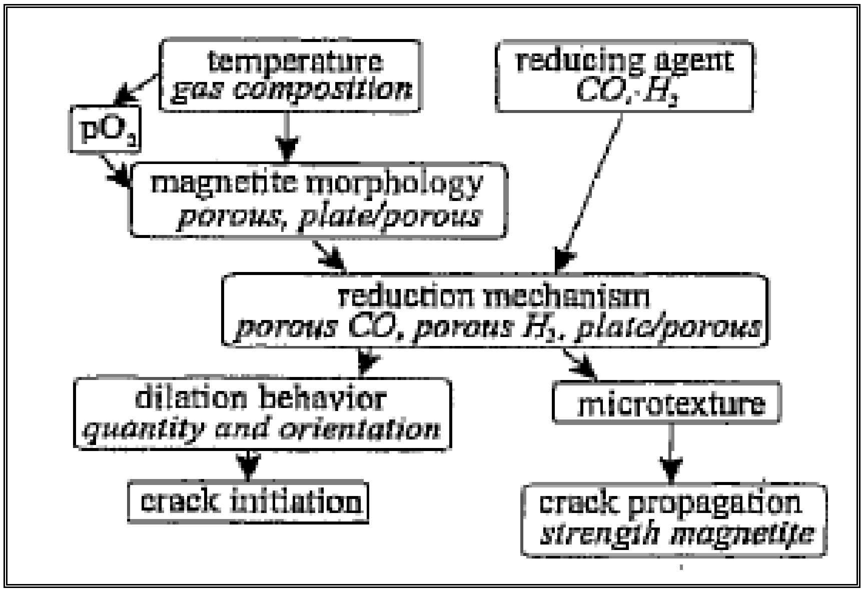

Figure 10: A schematic overview of the relations between the reduction conditions and the initiation and propagation of cracks[xvii].

In studies by Pimanta[xviii], volumetric changes during reduction from hematite to magnetite were determined using dilatometry for pure hematite and solid solutions containing Al_2O_3 and TiO_2, produced synthetically. Results from the dilatrometric studies are shown in Figure 13. The results indicate that pure hematite specimens (Samples 1 and 5) underwent volumetric expansion of ~4%. The presence of Al_2O_3

(Samples 2-4) and TiO_2 (Samples 6-8) in solid solution seemed to result in reduced dilatations.

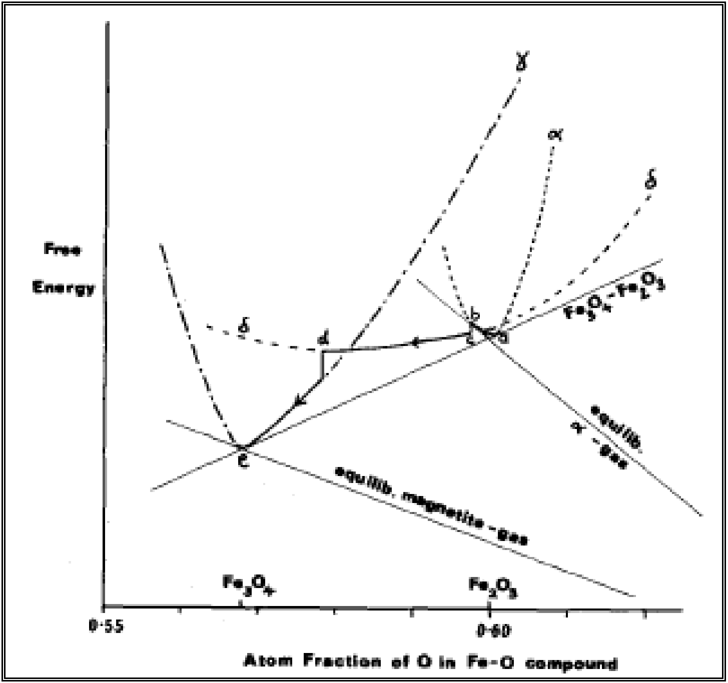

Figure 11: Schematic Free Energy-Composition Diagram for the iron-oxygen system in the Fe_30_4:Fe_20_3 region showing possible reaction paths on reduction of hematite to lath magnetite.[xvi]

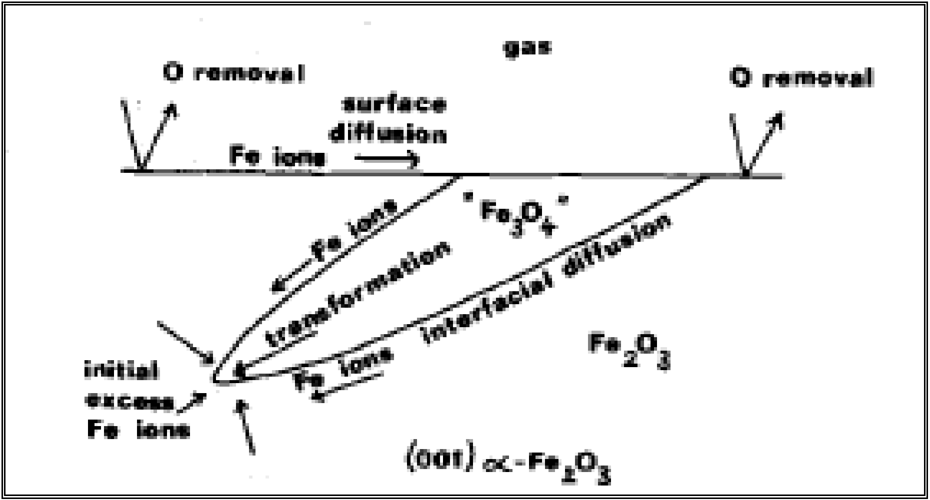

Figure 12: Proposed reactions, mass transport paths and transformations for the formation of lath magnetite on the reduction of hematite.[xvi]

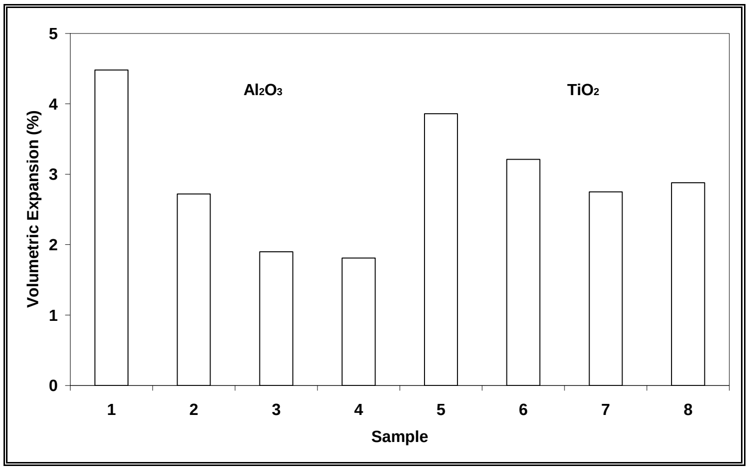

Figure 13: Volumetric changes observed during reduction from hematite to magnetite^{xviii}.

Figure 14 plots the volumetric change as a function of time. It also represents the variation of the extent of reduction with time. It can be seen from the curves that the presence of Al_2O_3 and TiO_2 significantly affected the reduction rate. The presence of TiO_2 influence the rate relatively more than did Al_2O_3.

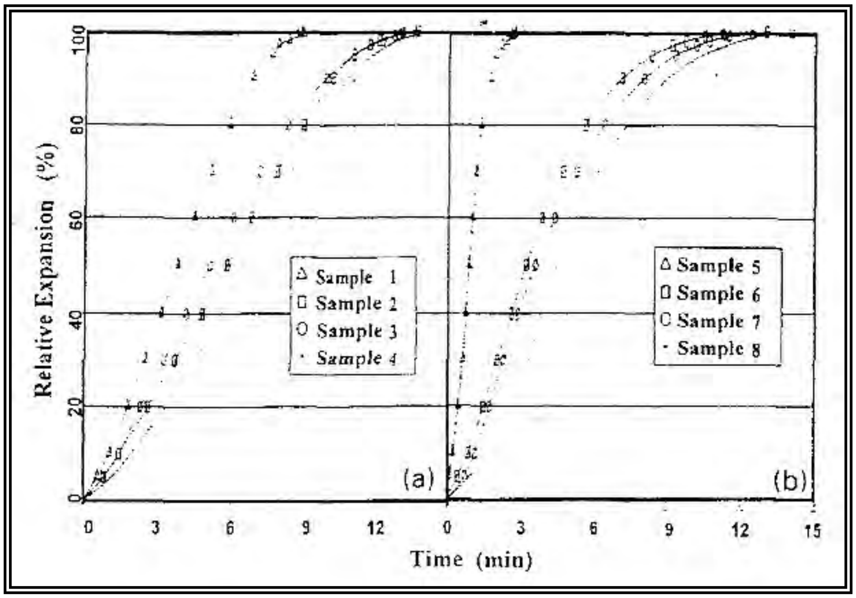

Figure 14: Relative dilatation vs time accompanying reduction of hematite to magnetite^{xviii}.

It has been observed by Hayes et al[xvi] that considerable plastic deformation occurs during the nucleation and growth of lath magnetite from hematite. The lattice strain is such that the plastic deformation provides a self-accelerating transformation front after the initial heterogeneous nucleation of magnetite. The origin of this strain is the mismatch or disregistry δ, of the Fe_2O_3 and Fe_3O_4 lattices and the relative volumes occupied by the parent and product oxides. Defining $\delta = (\delta_{hem} - \delta_{mag})/\delta_{mag}$ where δ is the interplanar spacing it can be shown that δ = 0.153 for the magnetite/hematite interface in $(001)_H$ plane and $<100>_H$ direction. This mismatch is considerable and it is apparent that it can only be accommodated by interracial dislocations, *i.e.* the interface must be semi-coherent.

The other source of strain is the volume of the product phase. If we assume that the above proposed transformation mechanism is correct then the adjustments to the lattice are essentially the arrangement of the oxygen atom packing *i.e.* no long range mass transfer of the oxygen in the lattice occurs, but rather the local addition of iron ions to the magnetite nuclei. The strain is then generated by the difference in volume between hematite and magnetite lattices per mole of oxygen. Assuming the densities of Fe_3O_4 and Fe_2O_3 are 5199 and 5279 kgm^{-3} respectively then the lattice undergoes approximately 10 pct volume expansion/mol oxygen on transformation from hematite to magnetite which accounts for the high dislocation density observed on lath growth.

El-Geassy et al[xix] determined the volume change of iron oxide compacts during reduction with different reducing gases. The relationship of the volume change for the different reducing gases for compacts completely reduced at 973-1373K is shown in **Figure 15**. **Figure 15a** indicates maximum swelling (176%) at 1173K for compacts reduced with CO. This figure also indicates the influence that reduction temperature has on the swelling of the iron oxide compacts. Reduction with H_2, 50% H_2-CO and reformed natural gas (Figure 15b-d) showed similar temperature effects – vastly different from that experienced with CO. El-Geassy concludes that volume change behaviour for compacts reduced with gas mixtures and simulated reformed natural gas depended on both temperature and the relative H_2 content of the reducing gas mixture. An increase in H_2 in the reducing gas the volume change tendency was contractions vs an increase in swelling as the CO content of the gas mixture increased.

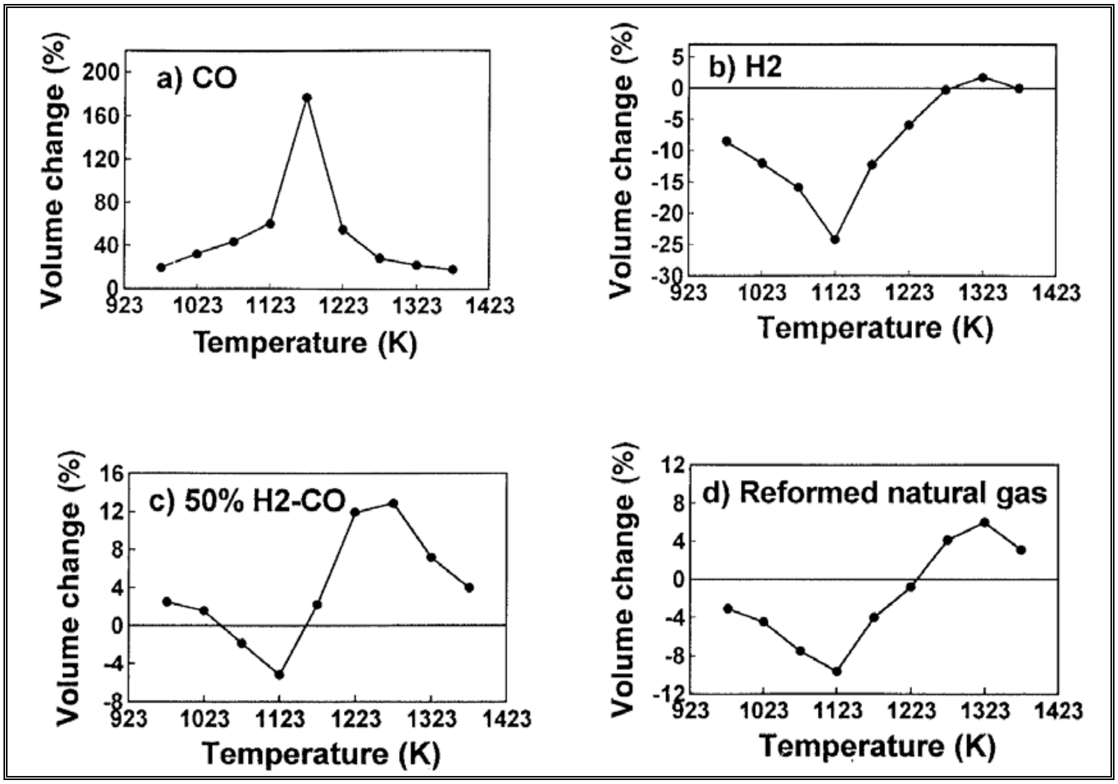

Figure 15: Variation of volume change with temperature for compacts reduced with different gases[xix].

In a study conducted by Loo and Bristow[xii] the results suggest that the microstructure of materials and phase or mineral associations have a very large influence on the exact degradation mechanism. They found that sinters exhibited a degradation mechanism whereby the original pieces degraded into a number of smaller particles, but not many in the –0.5mm size range. On the other hand, pellets degrade by the shedding of outer layers, resulting in a product composed of eroded particles of reduced diameter and –0.5mm material. When lump ores degrade, a larger amount of material in the + 4mm fraction remains in comparison with sinter. There are also particles of very similar size to the original material, suggesting that some particles are very tough and do not degrade at all. The results suggest that volume breakage is an important mechanism causing the formation of fines. Although cracks formed in lump ore would also relieve stress, the crack propagation process appears to be more random than for sinters, where there are clearly paths of least resistance along which the cracks grow.

Another factor to consider when evaluating the reduction disintegration of ores is the heating rate. Loo and Bristow[xv] found that there were large differences in degradation between wall and center profiles, i.e. high and low heating rates for sinter, as was indicated by other studies[xv]. They concluded that the degradation of lump ores was affected more by their inherent properties than by the reducing conditions and temperatures used. The study shows that degradation levels reached a peak at around 650-750ºC indicating negligible degradation beyond these temperatures. However, under some test conditions, degradation did not appear to reach a peak even at 900ºC of the materials studied. Sinter was most susceptible to reduction degradation, and pellets degraded the least. Under certain conditions the degradation of pellets was comparable to that observed for lump ores.

An in-house study by Theron[xx] to investigate the effects of heating rate and gas composition on the degree of breakdown on Sishen STD[‡] indicated that longer heating times (0-900°C in 30min -150min was tested) caused higher degrees of breakdown of the ore (**Figure 16**). It was also found that decreasing the heating time to below 30 minutes also increased the degree of breakdown. This was attributed to thermal spalling. Theron also found that a richer reduction gas has little effect on the degree of breakdown (**Figure 17**).

[‡] Northern Cape STD – The standard commercial mixture of natural hematite from the Northern Cape region

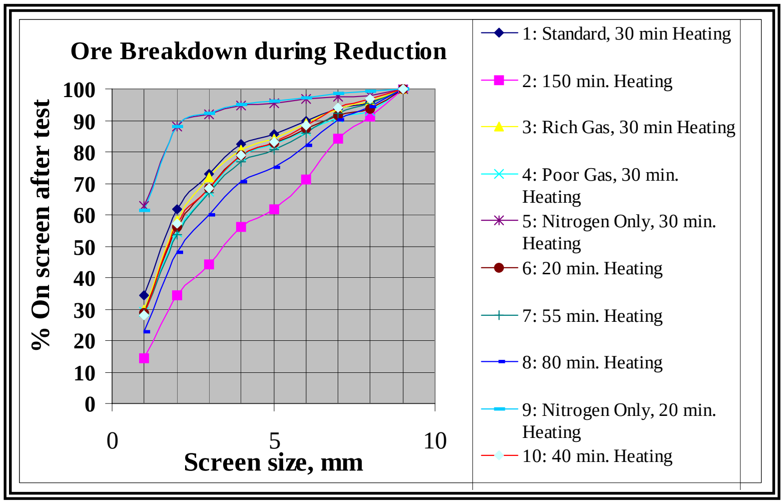

Figure 16: Effect of heating rate on the degree of reduction disintegration[xx].

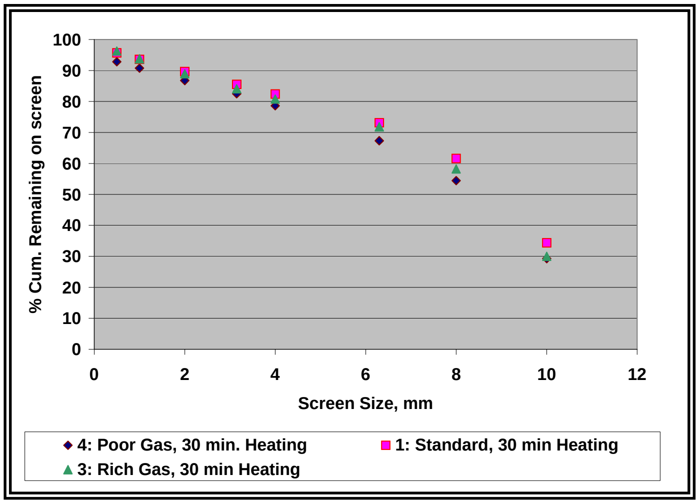

Figure 17: Effect of reducing gas composition on the degree of reduction disintegrationxx. (Poor gas – 45% CO, 33% CO_2, 15% H_2, 7% N_2; Standard gas - 52% CO, 25% CO_2, 17% H_2, 6% N_2; Rich gas - 60% CO, 16% CO_2, 15% H_2, 6% N_2)

Loo and Bristow also indicated that hydrogen has an effect on the reduction disintegration of burden material test and should be included in the RDI testing methods. Their study showed that, unless hydrogen is present, fluxed agglomerates are likely to degrade less than in an actual operating blast furnace. The effect of hydrogen on sinters cannot be predicted at this stage because only certain forms of SFCA[§] are affected. Increasing the level of hydrogen in the furnace, e.g. through increased use of natural gas or pulverized coal would cause increased degradation of sinters. Bapat et al[xxi] found that reduction plays a more important role in the disintegration of the ore pieces than thermal instability (decrepitation as a result of thermal shock). Since decrepitation is measured in terms of the fines (below 5 mm) produced it is likely that when bigger pieces disintegrate the resultant fines are larger in size than 5mm. He further suggests that the introduction of fines (- 10mm) inside the furnace will have a snowballing effect, in that the fines, having a high surface area to mass ratio, will undergo reduction high up in the furnace and, thus, will generate more fines of a smaller size, with a serious implication on the permeability of the furnace.

Figure 18 indicates the volume change of iron oxide compacts at different stages of reduction with different reduction gases as recorded by El-Geassy[xix]. Compacts reduced with CO indicated an increase in the degree of swelling with an increase in the extent of reduction (**Figure 18a**). However, when H2 is introduced into the reduction gas (**Figure 18b-d**), the compacts swelled at the initial stages of reduction but ended up with overall contraction for the completely reduced compacts. El-Geassy found that this agreed with the findings that the swelling of the compacts in the initial stages of reduction is due to the anisotropic transformation of hematite to magnetite while the swelling mechanism in the middle and latter stages of reduction is dependant on the formation of gas bubbles at the iron/wustite interface. Equilibrium bubbles gas pressure for the CO/CO_2 system is much higher than that of the H_2/H_2O system and therefore the disintegration of iron grains and volume expansions are greater when reduced with CO rich mixtures than with H_2 rich mixtures.

[§] SFCA – Silico ferrite containing calcium and alumina

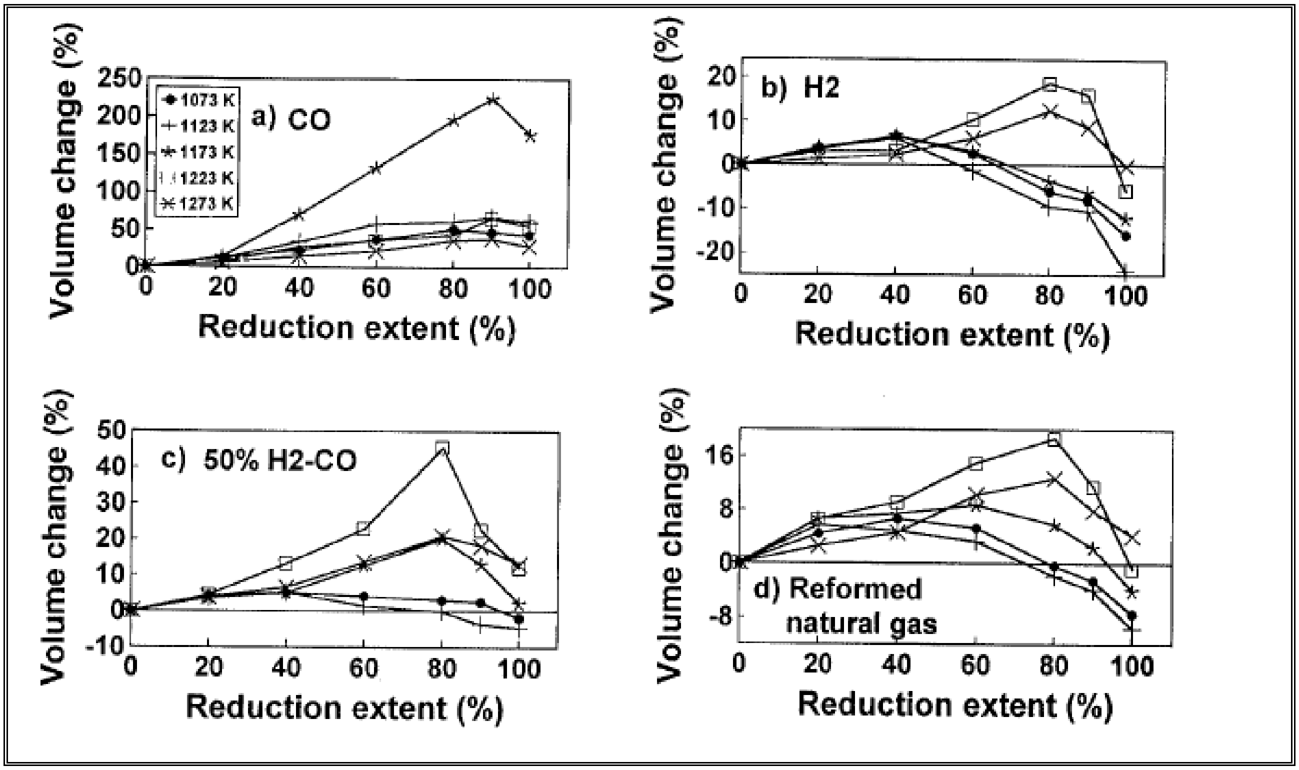

Figure 18: Variation of volume change with reduction extent for compacts reduced with different gases[xix].

Other research conducted by Bapat et al[xxi] on two different ores confirmed that reduction plays a greater role in degradation of iron ores, compared with thermal gradients in the ore body for the three different size ranges tested. He found that decrepitation is more for smaller sizes, progressively coming down for the larger fractions. The decrepitation was the highest at 550°C, compared with that at 700°C and 850°C.

Brill-Edwards et al[xiv] found that the nature of the interface, the apparent volume expansion, the cracking and the porosity induced by reduction are related to the processing temperature. The results confirmed that the hematite/magnetite interface at temperatures between 400°C and 500°C is hemispherical, whereas the interface above 700°C is conical, tapering away from an elliptical base at the grain surface. They indicated a significant volume increase during the reduction of hematite to magnetite. The expansion decreased from 25.6% at 525°C to 16.2% at 825°C (**Figure 19**). In addition to grain boundary failure, which is apparent at all reduction temperatures, they indicated extensive transgranular cracking, predominantly at temperatures below 700°C.

Microscopic examinations indicated that low temperature transgranular cracking results from a different stress system from that causing failure at high temperatures. This change in fracture mode above and below 700°C is attributed to the hematite/magnetite interface morphology. At low temperatures the failure occurs in the magnetite phase at the grain boundaries and along the plane of contact between two magnetite growths within the same hematite grain. The process of reduction is illustrated in **Figure 20**. It is believed that magnetite nucleates simultaneously at many points on the hematite boundary (**Figure 20a**). These nuclei grow radically, ultimately touch each other and isolate regions of unreduced hematite on either side of the contact bridge **(Figure 20b**). As shown in **Figure 20c** cracking between two growths may occur at this stage, when a large area of planar contact exists, but in no instance did it extend into the hematite. When the hematite is eventually surrounded, numerous cracks will have formed, extending radially from the grain surface through the magnetite to the hematite/magnetite interface.

A further structural change accompanying the reduction process is the development of pores, whose size, shape and number are related to the reduction temperature. When reduction is carried out between 400°C and 600°C small spherical and randomly distributed pores are formed, which when the reduction temperature is raised to 700 or 800°C, becomes elongated and exhibit a preferred growth direction.[xiv]

Reduction testwork conducted by Gudenau et al[xxii] conducted on Sishen ore shows the different reduction effects of hydrogen and carbon monoxide in relation to the reduction rate and the mechanisms of crack forming. They found that due to the appearance and expansion of a few large cracks the specimen reduced with CO shows a steady increase in volume (**Figure 21**). The reduction with hydrogen leads to a swelling of up to 15% in the first minutes because of the extensive forming of small cracks (**Figure 22**). Further reduction shows a decrease in volume, due to the fast reduction and the appearance of rather dense and sintered layers of reduction products (**Figure 23**).

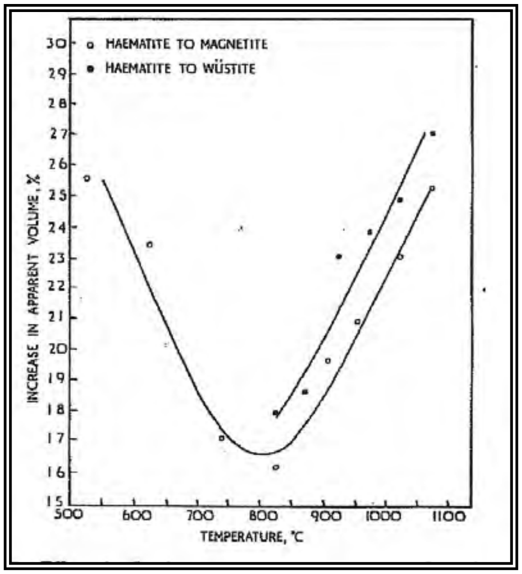

Figure 19: Effect of reduction temperature on apparent volume increase of hematite.[xiv]

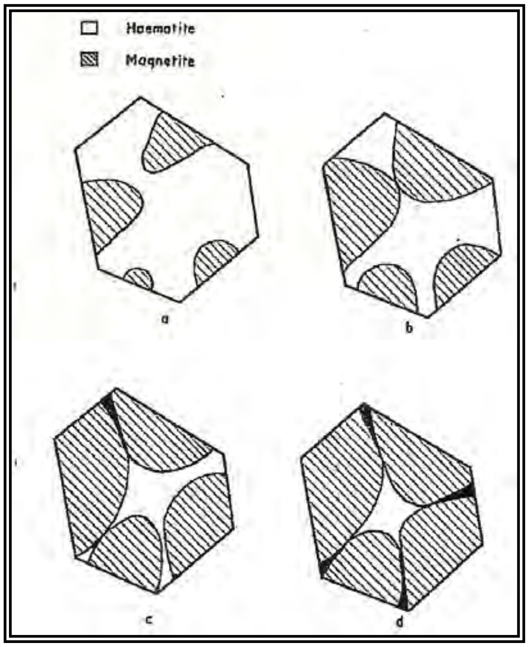

Figure 20: Stages in low temperature reduction of hematite.[xiv]

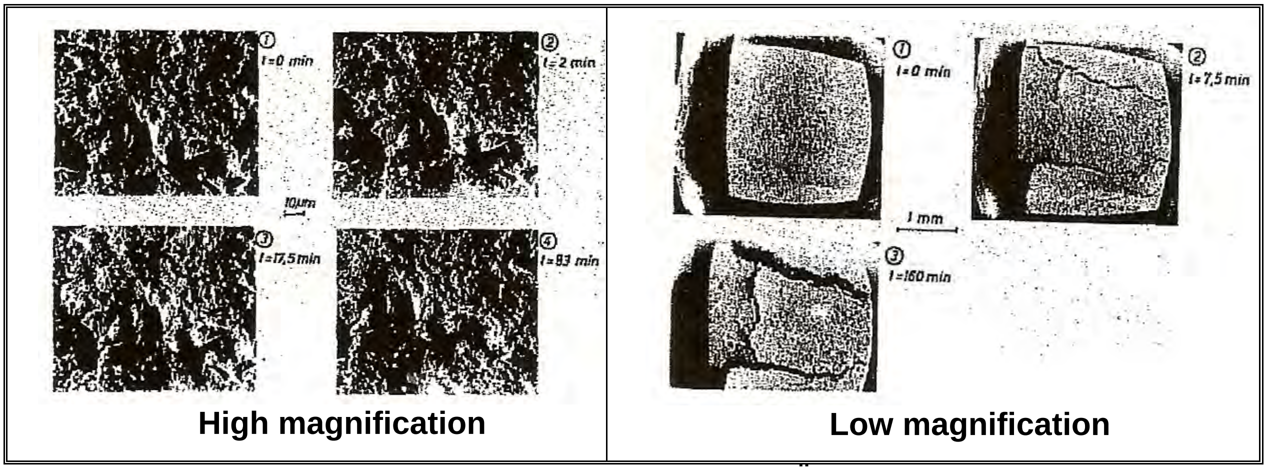

High magnification

Low magnification

Figure 21: Sishen ore, Reduction with CO, T = 850°C[xxii].

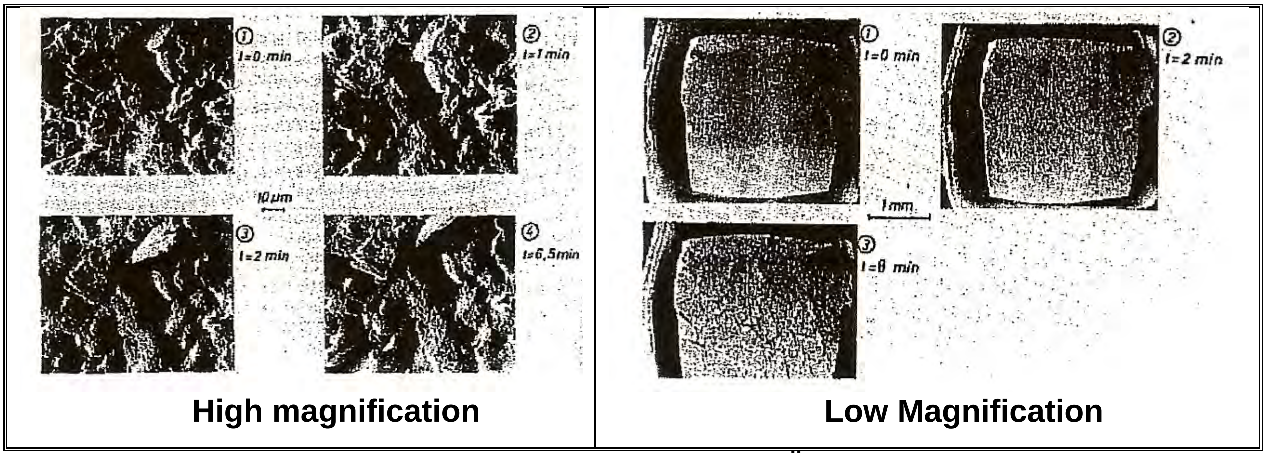

High magnification

Low Magnification

Figure 22: Sishen Ore, Reduction with H_2, T = 850°C[xxii].

They also found that the reduction of the specimen surface with hydrogen was finished after 6.5 minutes, compared to more than an hour with carbon monoxide.

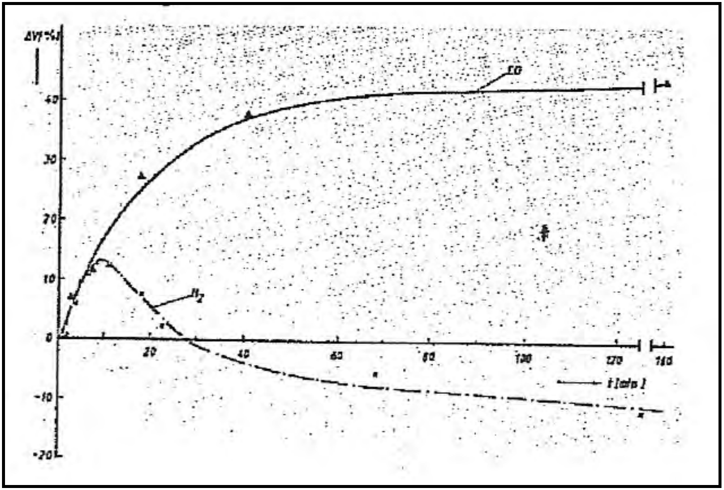

Figure 23: Change in volume of Sishen ore during reduction with CO and H_2[xxii].

Adam et al[xxiii] found that cracking was more prominent at lower temperatures and higher CO_2 percentages in the CO/CO_2 mix (**Figure 24**). A transition region between regions with and without cracking in the (CO/CO_2, T) plane was found. In the "cracking region", the reaction proceeds mainly along the cracks, while in the "topochemical region", the reaction interface moves from the outer surface towards the centre of the particle

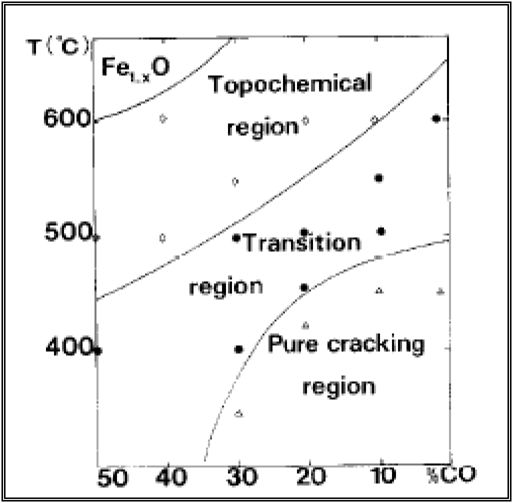

Figure 24: Map of morphological regions given in the (T, CO/CO_2) plane.[xxiii]

When the temperature is raised, an increase in the number of magnetite nuclei is found, giving a more symmetrical stress field. It was also shown by Porter and

Swann[xxiv] that two neighboring nuclei produce antagonistic stresses which tend to cancel each other out. Hence, the temperature should be raised to minimize cracking. Adam et al[xxiii] also argues that more magnetite nuclei are formed with an increase in the reducibility of the gas composition. It was also found that nucleus growth increases with an increase in the CO/CO_2 ratio. But, it was found that the nucleation frequency is roughly proportional to the CO/CO_2 ratio and the growth of nuclei is first order relative to the p_{CO}. Hence a high CO/CO_2, ratio favors nucleation over growth. They therefore conclude that a high CO/CO2 ratio decrease the incidence of cracking.

Adam et al[xxiii] found that although the pre-treatment (annealing) of hematite crystals to eliminate micro-cracks increased the induction period necessary for the cracks to form significantly, no decrease in the amount of cracks that formed were found (**Figure 25**).

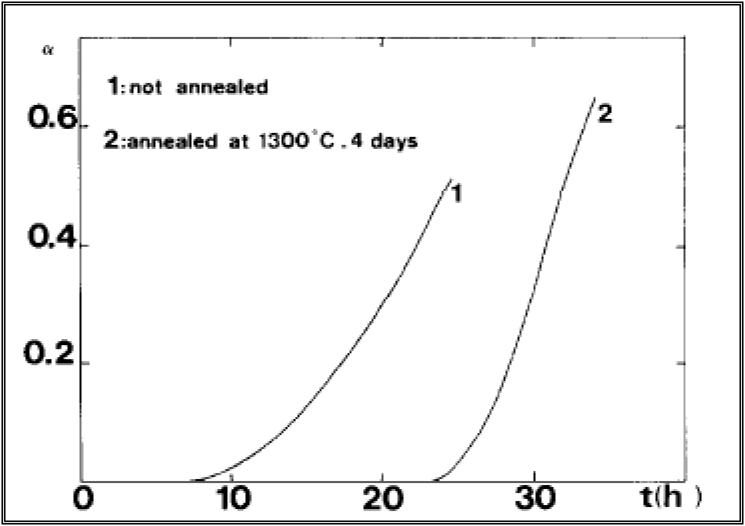

Figure 25: Cracking (α) vs time (h) of samples reduced at 350°C in CO/CO_2 (20/80) gas mixture.[xxiii] (A sample was annealed at 1300° C for 4 days in oxygen to avoid any dissociation).

However, different ore types with similar reduction properties fare differently when it comes to reduction disintegration properties. In a study conducted by Martens et al[xxv] the microstructure of the lump ore is used to predict the reduction disintegration behaviour of lump ore. By using indices like LOI[**], vol. % of water-bearing minerals, porosity, cohesion of crystals, crystal size and orientation and distribution of small pores,

---

[**] LOI = Loss of Ignition

they have constructed an ore structure chart to predict the reduction disintegration behaviour of lump ore. It is important to notice that the presence, structure or compositions of gangue minerals is not considered in their model.

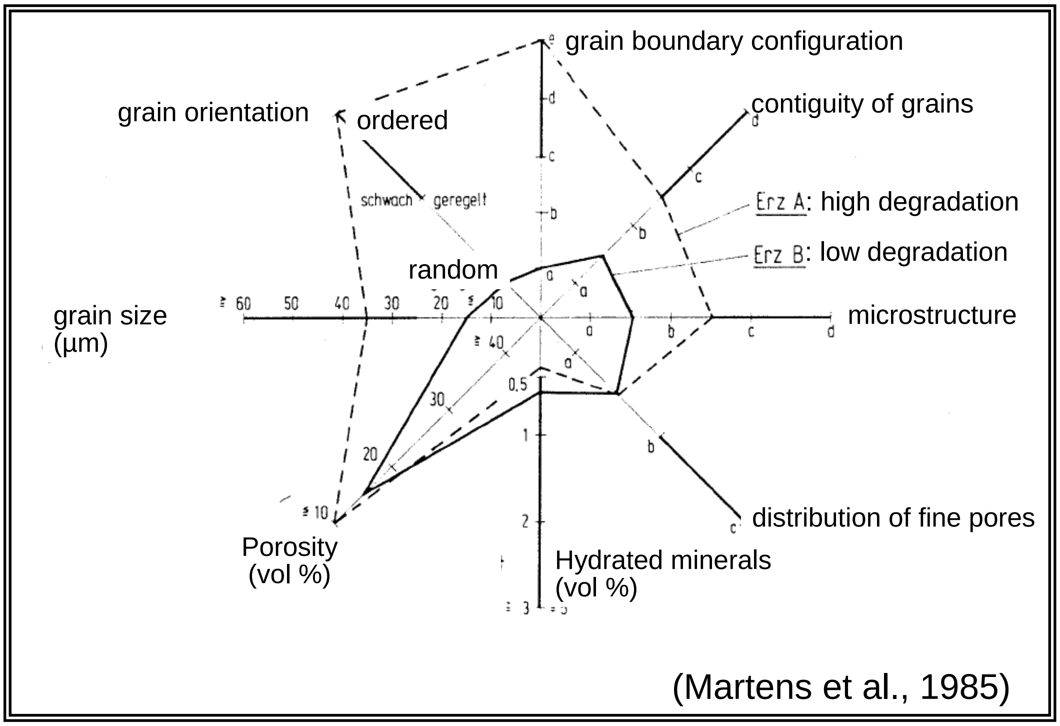

(Martens et al., 1985)

Figure 26: Ore structure chart constructed by Martens et al.[xxv]

1.4 PROBLEM STATEMENT

Northern Cape iron ore generally fares well when tested for reduction disintegration properties. **Table 2** gives a comparison of the reduction disintegration properties of Northern Cape iron ore and Brockman iron ores. **Figure 27** indicates the extent of breakdown of the Northern Cape ore vs that of the Brockman ores. Results of a Corex test as described in section 1.1.2.3 (performed by Kumba Iron Ore) are shown in **Table 3**.

Despite all the indications that Northern Cape iron ore has good low temperature breakdown properties, significant breakdown is experienced when used in the Corex process (at Saldanha Steel). This cause permeability problems in the shaft and an increase in the reductant cost. Previous testwork conducted by Theron[xx] indicated that the retention time in the reduction zone as well as the heating rate plays a role in amount of breakdown experienced.

Table 2: Comparison of reduction disintegration properties of Northern Cape Iron ore and Brockman ores.

Test Method	**% -6.3mm**		
	Northern Cape	**Brockman 1**	**Brockman 2**
RDI Static ISO 4696	**11.4**	**40.0**	**28.3**
RDI Dynamic (Kumba Method)	**8.8**	**59.9**	**44.3**
RDI Static (Kumba Method	**8.3**	**42.5**	**30.2**

Table 3: COREX test results of Northern Cape iron ore.

Size fraction (mm)	**Cumulative mass percentage on sieve**	
	1991	**2007**
+12.5	0	0
+10	45.7	35.1
+6.3	76.1	72.4
+3.15	87.1	84.2
+0.5	97.6	97.1
-05	2.4	2.9

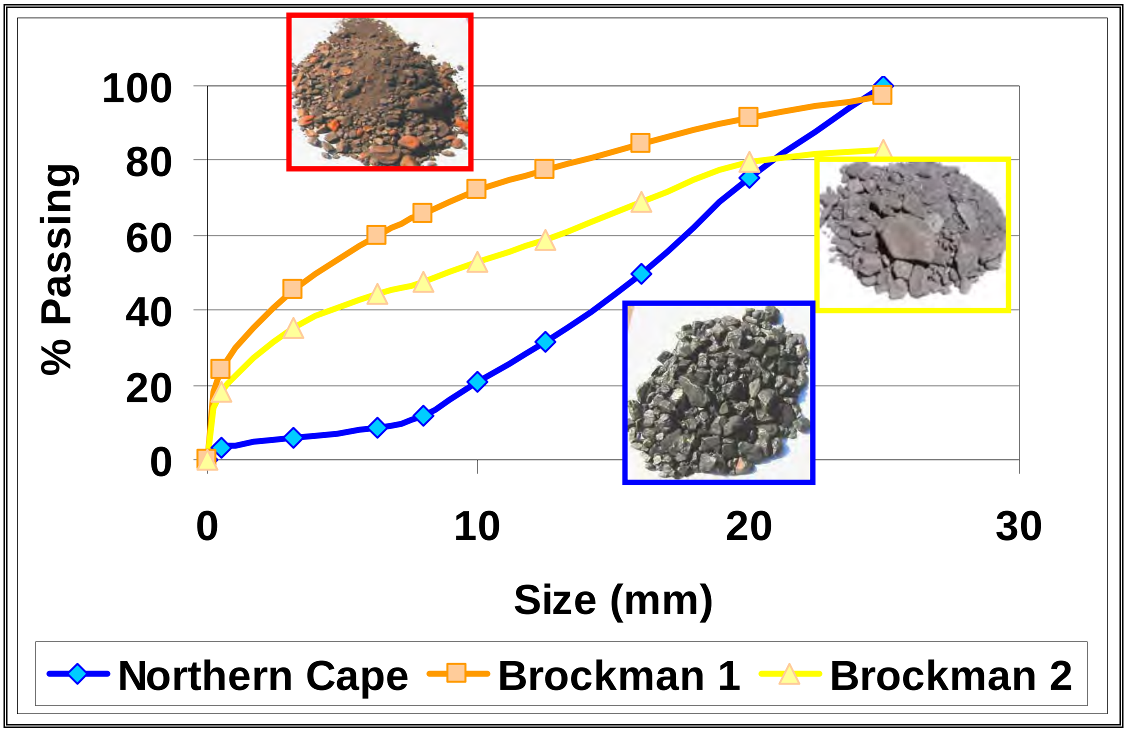

Figure 27: Particle distribution of Northern Cape and Brockman ores after dynamic reduction disintegration tests.

This study was hence conducted to determine the following:

1. Extent of the breakdown for the various Northern Cape iron ore types. The following questions needed to be answered:
    - Does the microstructure play a role during breakdown?
    - What is the effect of impurities or gangue minerals?
    - What is the mechanism for crack generation and propagation?
    - Could the elimination of certain ore types in the mixture reduce the amount of breakdown experienced in the Corex?
2. The effect of particle size on disintegration.
3. The temperature zone where reduction disintegration takes place.
4. The effect of reduction gas on the extent of reduction disintegration.

1.5 MINERALOGICAL EVALUATION

As background to the possible effect of microstructure on the reduction disintegration, the mineralogy of the Northern Cape ore is briefly reviewed below.

Northern Cape iron ore mine is an example of a superior type Banded Iron Formation (BIF), this type is characterized by ,” *banded cherty oolitic iron ores which lack spatial associations with volcanic rocks, are of regional extent and are predominantly of early Proterozoic age.”*

The Northern Cape iron-ore bearing horizon is a conglomerate located at the base of the Northern Cape Formation, Gamagara Subgroup, Olifantshoek Supergroup. This overlies a laminated massive horizon of the Asbestos Hills Subgroup of the Transvaal Supergroup and is overlain by flagstones and shales of the Northern Cape Formation, Olifantshoek Supergroup.

The mineral composition and type were determined for the various samples by Dr Kleyenstüber[xxvi] A short description of the various ore types are given. An alphabetical listing of the minerals mentioned in this report, their ideal chemical formulae and the theoretical iron content of the minerals is given in **Appendix 1**.

In a study by Dr Kleyenstüber, all samples were prepared as polished sections and observed under an optical microscope. The samples were also analyzed by X-Ray Diffraction (XRD) to determine the minerals present and to obtain semi-quantitative information on the sample composition. The samples were also prepared as polished briquettes and studied under the optical microscope

1.5.1 Northern Cape Ore Type 1

Northern Cape Ore type 1 contains both laminated and brecciated ore particles (**Figure 28).** In the brecciated ore particles the fragments show distinct rounding, typical of a fine-grained conglomeritic material. Massive as well as laminated ore fragments make up the composite breccia particles, with large open voids among the ore fragments. In some instances quartz is present as secondary filler mineral in the open voids. The ore fragments range in size from 1 to 10mm.

The matrix of all the ore particles is characterized by a relatively large amount of acicular specular hematite that range in size from 250µm down to 35µm. Granular specular hematite grains are also present. These commonly have an irregular shape and are 35 to 50µm in size. With the large amount of acicular hematite present the ore particles show a relatively large open pore texture. Pore up to 100µm in diameter are present. In many instances these pores have been filled by secondary quartz.

Laminations in the ore particles are due to alternating hematite and quartz lamellae. The quartz does not form continuous lamellae, but tends to show higher concentration levels in some of the pores thereby accentuating the laminations. Furthermore, laminations are shown by a variation in hematite lamellae with more and less open pores, as well as alternating granular and acicular hematite lamellae. The latter exhibit a more open porosity.

Quartz is the only gangue mineral identified in this ore sample.

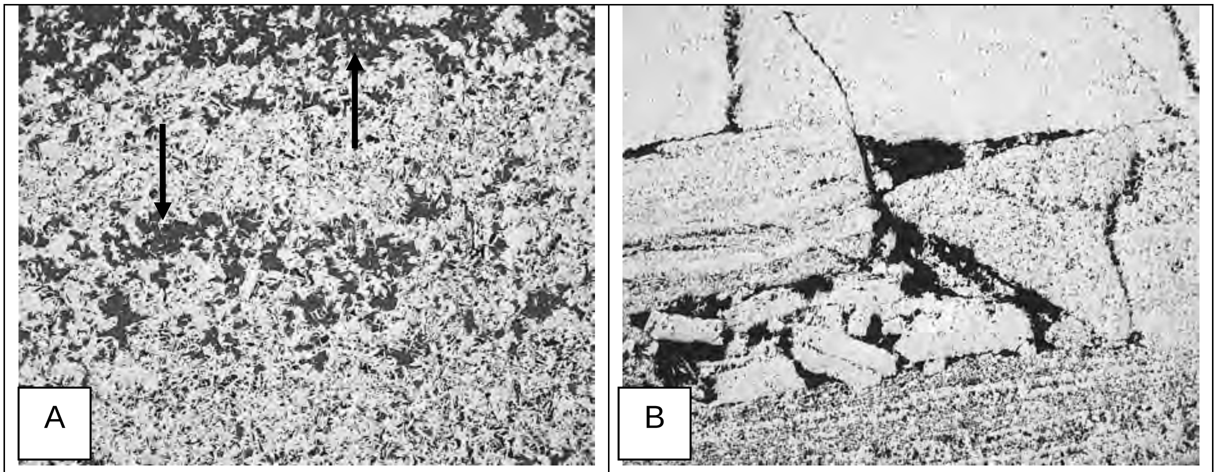

Figure 28: Photomicrographs of the textures observed in Northern Cape Ore type 1. Magnification 30x

A = Indistinct layering due to quartz distribution (arrows) in ore particle.

B = Massive ore particle showing brecciation of hematite layer, which creates open porosity (black) in particle.

1.5.2 Northern Cape Ore Type 2

Three distinct ore types were observed in samples from Northern Cape Ore type 2, namely brecciated ore, laminated ore and massive ore. The “massive ore” does show lamination on a microscopic scale. The “laminated ore” comprises dense, finely crystalline hematite microlaminae alternating with coarser, specularitic mesolaminae. The latter are thicker than 300µm.

Typically clastic-textured (brecciated) ore exhibits dull reddish, porous, earthy laminations, comprising specularitic and earthy hematite. Laminations are wavy and distorted, consistent with soft sediment deformation. The lamellae vary in thickness between 100 and >300µm. The same textures are observable macroscopically.

Throughout Northern Cape South Mine, clastic textured ore is intensely brecciated. Ore fragments are commonly cemented by lenticular specularite lathes, silica, phosphates and alumino-silicates. The ore is also relatively porous. The association of contaminants within brecciated matrix and fracture fillings suggests that with crushing and abrasion they should be liberated, since ore fragments are likely to fracture preferentially along these planes and zones of weakness. Clay minerals are relatively common in the matrix. In places, quartz and possibly some phosphates were also observed in the breccia matrix. There appears to be a spatial association between phosphate and alumino-silicate (kaolinite) occurrence in the hematite matrix. This suggests these contaminants were introduced in the same secondary fluid event associated with a specific deformational episode.

Some residual primary quartz (chert) microlaminae may be intercalated within hematite laminae.

The hematite grains in the ore comprise acicular, granular and earthy hematite. The acicular hematite commonly lines open voids in the ore matrix.

1.5.3 Northern Cape Ore Type 3

Iron ore from this locality exhibits laminated, “clastic-textured” and brecciated subordinate ore types. Typically, the laminated ore type comprises dense, finely crystalline granular specular hematite alternating with coarse, porous, recrystallised, acicular specular hematite. Cavities within these coarse laminae are locally filled with silica and possibly phosphates (although no phosphates could be conclusively identified).

1.5.4 Northern Cape Ore Type 4

Brecciated, laminated and massive ore particles are encountered in this ore (**Figure 29**). All of these particles are characterized by a high concentration of acicular specular hematite. Some of the ore particles contain a Northern Cape proportion of quartz in association with the open textured acicular hematite matrix.

The massive ore particles consist of both granular and acicular hematite grains and some of the particles exhibit open pore structures up to 300µm in diameter that are partially filled with slender hematite needles.

Laminated ore particles typically exhibit their laminations by alternating granular and acicular hematite lamellae, variations in open porosity as well as higher concentration levels of quartz in the open pores of the hematite matrix.

- Brecciated ore particles consist of fragments made up of an acicular hematite matrix, cemented together by acicular hematite.
- Some of the ore particles also contain small areas of earthy hematite intergrown with specular hematite.

The individual hematite grains range in size from 35 to 50µm, although longer hematite needles are present in the open pores of the massive ore particle.

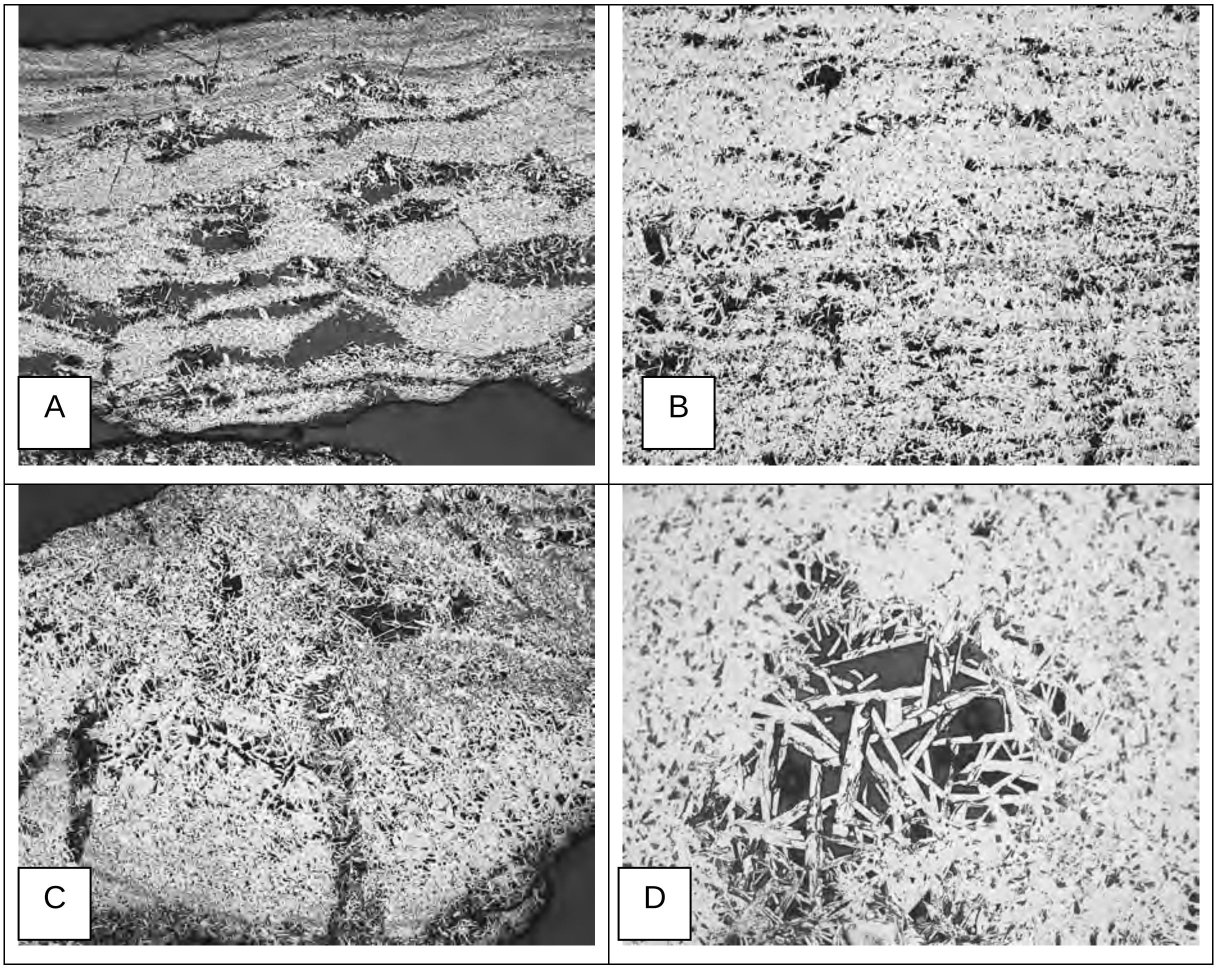

Figure 29: Photomicrographs of ore textures observed in ore sample Northern Cape Ore type 4

A = Layered ore particle with irregular quartz distribution (black) and numerous acicular hematite grains in the quartz matrix. Magnification 30x.

B = Laminated ore particle due to alternating granular and acicular hematite grains, as well as open porosity (black). Magnification 30x.

C = Brecciated ore particle consisting of acicular hematite surrounded by an acicular hematite matrix. Magnification 30x.

D = Patches of very long acicular hematite in matrix of massive acicular hematite ore particle. Magnification 125x.

1.5.5 Northern Cape Ore Type 5

These samples of conglomeratic ore typically comprise angular to subangular ore fragments consisting of specular hematite set in an aluminous matrix. The matrix consists of extremely finely crystalline alumino-silicate groundmass containing euhedral phosphates with lesser quartz and specular hematite. In some instances the matrix phosphates may occur in a cryptocrystalline form, such that they are almost indistinguishable from the enclosing alumino-silicate groundmass.

1.5.6 Northern Cape Ore Type 6

This Northern Cape ore type consist of distinct massive specularitic hematite particles, earthy hematite particles and particles exhibiting an alternating layering of earthy and specular hematite layers.

These thin laminations range in thickness from 50 up to 300µm. Lamination is accentuate in the ore particles by more than one feature. Alternating granular and acicular specular hematite layers, where the acicular layering shows distinct open porosity where the individual needles terminate against each other. In some particles the layering consists of hematite lamellae alternating with gangue minerals such as quartz and kaolinite. Finally the layering can be due to alternating earthy and specular hematite lamellae. The earthy hematite matrix can contain finely dispersed specular hematite needles that are <5µm thick and only 30µm long.

Brecciation was observed in some ore particles, where massive specular hematite particles earthy hematite particles make up the matrix of the composite particle.

Figure 30 gives examples of the textures observed in this ore type.

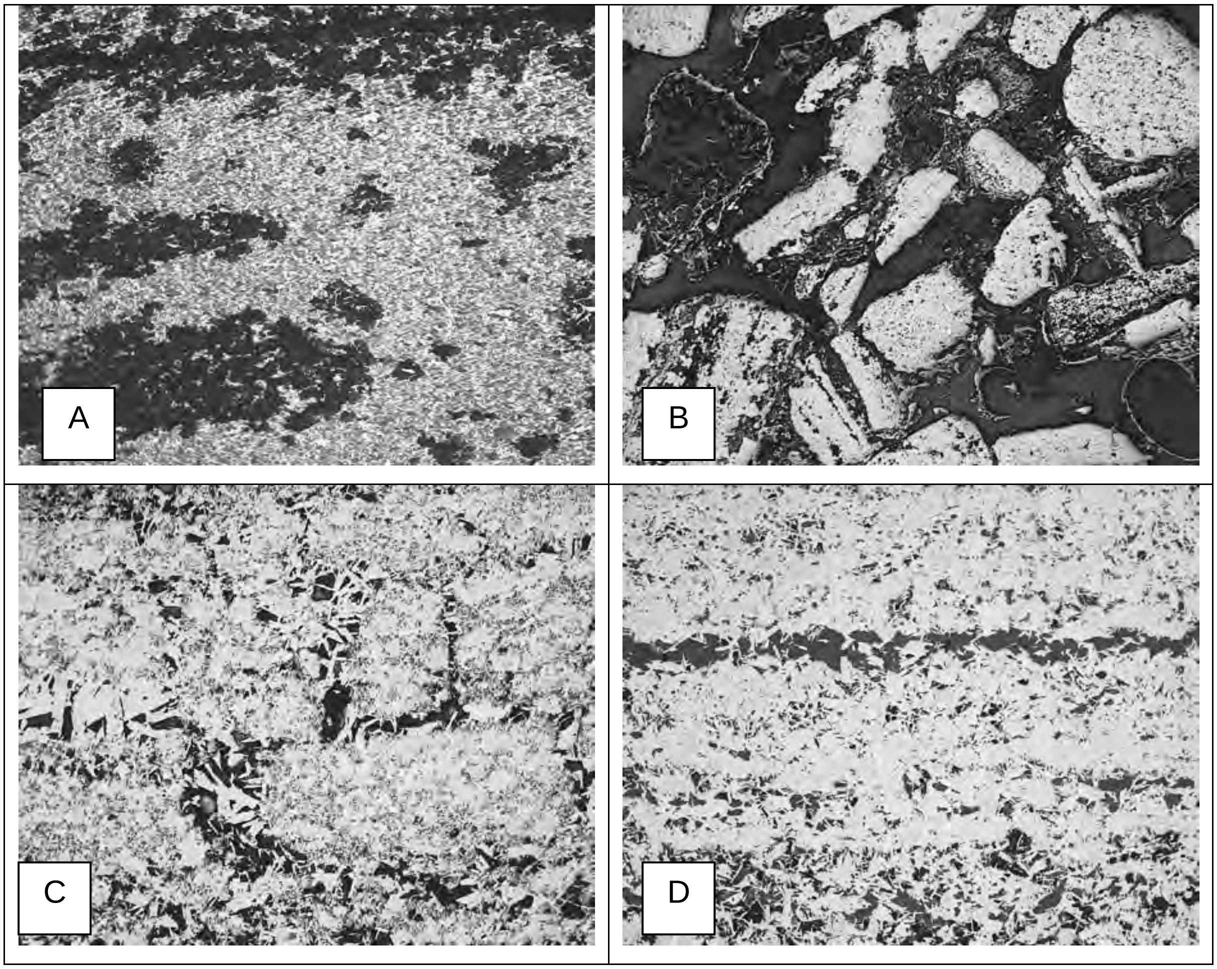

Figure 30: Photomicrographs showing the different textures in Northern Cape ore type 6

A = Earthy hematite ore particle (dark areas) partially altered to specular hematite (white area). Magnification 63x.

B = Brecciated and rounded fragments of specular hematite (white) and quartz (black) in a ore type 6 matrix. Magnification 30x.

C = Massive ore particle comprising both granular and acicular specular hematite, with the acicular grains contributing to the open pores (black). Magnification 63x.

D = Quartz inclusions (black) in ore particle, both as individual patches and as thin lamellae. Magnification 63x.

1.5.7 Northern Cape Ore Type 7

This banded ironstone ore exhibits a varied texture (**Figure 31**). Some of the ore particles consist of massive hematite containing only acicular specular hematite grains and open porosity where the individual needles terminate in the hematite matrix. Some of the open pores can be up to 200µm in diameter and are distinctly lined by acicular specularite that has grown into the void from the hematite matrix. Some of the needles attain a length of 200µm. These open voids are reminiscent of leaching textures, where the quartz has been removed.

Other ore particles show a distinct brecciation between denser and less dense hematite particles forming composites.

Then there are the typical banded ironstone ore particles with an intricate intergrow, on a microscopic scale, between specular hematite and quartz. Some of the particles contain very little quartz, whereas others up to 50% of the total ore matrix. Some of these quartz patches can reach a diameter of 400µm but most of them are seldom larger than 100µm. Very rarely do these ore particles show the alternating layering of quartz and hematite typical of banded ironstone ores.

Generally the specular hematite grains are 50µm in diameter. Quartz is the only gangue mineral observed under the optical microscope (**Figure 31d**).

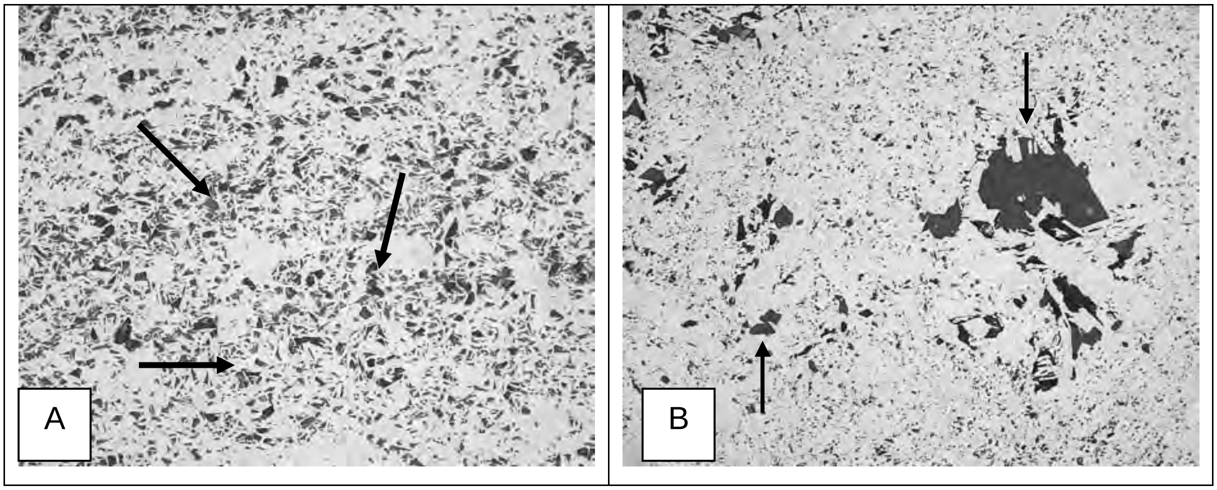

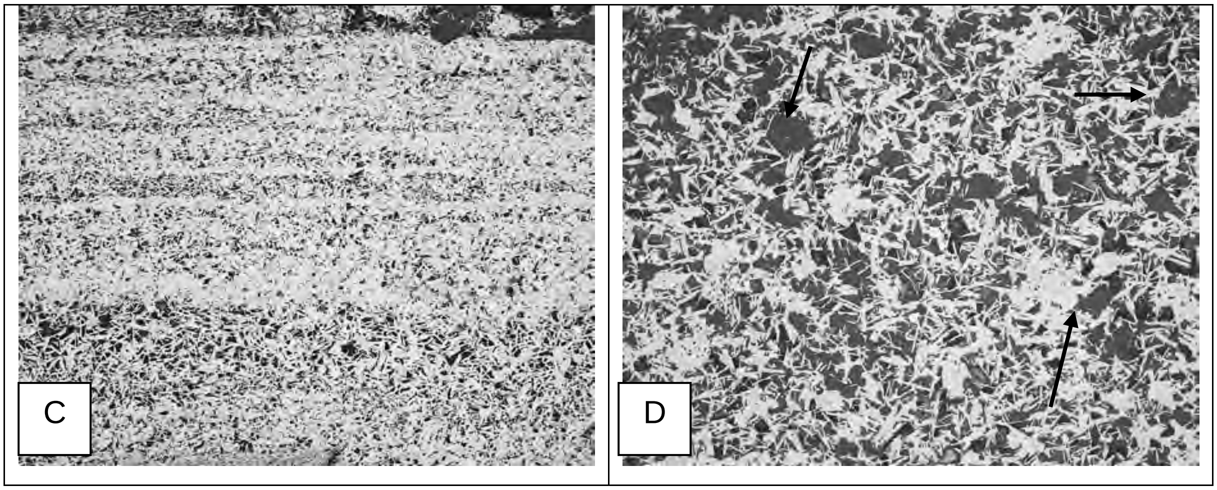

Figure 31: Photomicrographs showing the various textures encountered in Northern Cape Ore type 7.

A = Massive hematite particle comprising both acicular and granular specular hematite, with the acicular hematite contributing to the open porosity of the particle, while quartz (arrows) fills some of the pores. Magnification 125x.

B = Irregular secondary quartz distribution (arrows) in massive hematite particle. Magnification 63x.

C = Lamination in ore particle due to alternating lamellae of granular and acicular hematite. Porosity (black areas) created by acicular hematite. Magnification 30x.

D = Quartz distribution (arrows) in an ore particle comprising only acicular specular hematite. Magnification 125x.

1.5.8 Scanning Electron Microscopy (SEM) Analysis

Gangue minerals identified by SEM for selected ores are given in **Table 4**. These minerals are usually present below the detection limit of the X-ray diffraction analysis and are commonly found as minute inclusions within the hematite matrix, filling voids or occupying thin fracture fillings.

These minerals are present in trace amounts only, mostly intergrown with the hematite matrix filling fractures or pores.

Table 4: Minerals identified by means of SEM analysis in the various ore types

NORTHERN CAPE ORE TYPE 2	NORTHERN CAPE ORE TYPE 3	NORTHERN CAPE ORE TYPE 5
Quartz	Quartz	Quartz
Phosphate (apatite)	Phosphates	Apatite
Kaolinite	Kaolinite	Kaolinite

2 TESTWORK

Reduction disintegrations test were conducted on a samples of Northern Cape STD, as well as several ore types from the Northern Cape deposit.

The chemical analysis of the samples before and after testing was used to determine the degree of reduction obtained during testing. The chemical analysis of the samples before testing is given in **Table 5**.

Table 5: Chemical analysis of samples before testing.

	Northern Cape STD[††]	Northern Cape OT[‡‡] 1	Northern Cape OT 2	Northern Cape OT 3	Northern Cape OT 4	Northern Cape OT 5	Northern Cape OT 6	Northern Cape OT 7
Fe (tot)	65.2	67.6	67.7	65.8	66.9	66.5	64.9	65.6
Fe2O3	92.3	96.3	96.7	93.9	95.1	94.3	92.1	93.6
FeO	0.76	0.23	0.11	0.16	0.47	0.68	0.55	0.12
Fe°	0.05	0.02	0.02	0.04	0.06	0.06	0.06	0.07
CaO	0.055	0.250	0.036	0.094	0.167	0.028	0.077	0.200
MgO	0.018	0.060	0.022	0.025	0.017	0.016	0.025	0.070
SiO2	4.06	1.73	1.96	3.92	1.60	2.86	3.51	3.66
Al2O3	1.20	0.65	0.31	0.85	1.33	1.01	2.22	1.26
K2O	0.149	0.050	0.027	0.161	0.173	0.018	0.162	0.033
Na2O	0.011	0.010	0.019	0.020	0.020	0.010	0.008	0.010
TiO2	0.062	-	0.021	0.073	0.049	0.054	0.105	0.044
MnO	0.016	0.030	0.007	0.050	0.013	0.011	0.014	0.016
P	0.048	0.037	0.036	0.028	0.068	0.040	0.044	0.035
S	0.006	0.015	0.033	0.006	0.007	0.008	0.009	0.015
C	0.035	0.023	0.022	0.028	0.036	0.042	0.046	0.038

[††] Northern Cape STD – the standard commercial mixture of natural hematite from the northern Cape region

[‡‡] OT - Ore Type

All the ore types have a good grade above 63% Fe. Of the various Northern Cape ore types OT 6 contains the lowest iron values at 64.9%. From **Table 5** it can also be seen that this ore has the highest Al_2O_3 content at 2.2%, followed by Northern Cape OT 4

The highest phosphorus is associated with the Northern Cape OT 4 lump ore at 0.068%, followed by the Northern Cape Lump STD ore, while Northern Cape OT 5 contains a maximum of 0.045% P.

Regarding K_2O levels in the lumpy ore the Northern Cape OT 6 contains the highest amounts at 0.162%, followed by the Northern Cape Lump STD ore.

2.1 REDUCTION DISINTEGRATION

To examine possible micro-structural effects, Northern Cape STD (mixed ore) and seven individual ore types from Northern Cape were tested to determine the relative reduction disintegration properties. Tests were also conducted to determine the effect of time, temperature, gas composition and size fractions on the reduction disintegration properties of the various samples.

Different standards are available to measure the low temperature reduction disintegration of ore, sinter and pellets. The method described in ISO 4696 (**Appendix 2**) was used as a basis for the test[xxvii]. During the standard test a 500g sample of –12.5+10mm material is heated under inert atmosphere (N_2) to 500°C. When the sample reaches 500°C the sample is reduced for one hour with a reducing mixture, consisting of 20% CO, 20% CO_2 and 60% N_2. The sample is then cooled down to room temperature under an inert atmosphere. A drum test and sieve analysis determines the breakdown of the sample. Results of the standard RDI test (ISO 4696) are given in **Table 6**. Because degree of reduction, gas composition and temperature were identified as factors which can influence reduction disintegration, this work included changes to the test method to determine the effect of time, temperature, size fraction and gas composition on the reduction disintegration of the various ores and ore types. The different tests are listed in

Table 7. Tests were completed in duplicate and the standard deviation was within the guidelines of the ISO standard. Similar tests on the Northern Cape samples were also conducted by SGA and the standard deviation between the two laboratories were also within the guidelines.

The furnace temperature, heating cycle and gas mixture were computer controlled to ensure repeatability of the tests. The gas flow was controlled with mass flow meters and spot checks were executed on a regular basis by means of a mass spectrometer. The temperatures were controlled within ±10°C of the desired temperature. The tests were conducted in duplicate according to the specifications in ISO 4696 and the average of the test results is reported.

Table 6: RDI results of samples according to ISO 4696

Sample	**ISO 4696**		
	RDI$_{+6.3mm}$	**RDI$_{+3.15mm}$**	**RDI$_{-0.5mm}$**
Northern Cape STD	90.86	94.10	1.93
NORTHERN CAPE OT 1	90.00	93.90	2.10
Northern Cape OT 2	76.90	84.96	6.15
Northern Cape OT 3	87.20	93.40	1.70
Northern Cape OT 4	98.92	99.34	0.30
Northern Cape OT 5	89.92	93.96	1.77
Northern Cape OT 6	79.57	87.35	3.59
Northern Cape OT 7	90.80	95.10	1.80

Table 7: List of different tests performed.

Test nr	Ore Type	Size fraction	Changes made to ISO 4696
1	Northern Cape STD	-25+20mm	Size Fraction
2	Northern Cape STD	-20+16mm	Size Fraction
3	Northern Cape STD	-16+12.5mm	Size Fraction
4	Northern Cape STD	-12.5+10mm	No Change
5	Northern Cape STD	-10+8mm	Size Fraction
6	Northern Cape OT 1	-12.5+10mm	No Change
7	Northern Cape OT 2	-12.5+10mm	No Change
8	Northern Cape OT 3	-12.5+10mm	No Change
9	Northern Cape OT 4	-12.5+10mm	No Change
10	Northern Cape OT 5	-12.5+10mm	No Change
11	Northern Cape OT 6	-12.5+10mm	No Change
12	Northern Cape OT 7	-12.5+10mm	No Change
13	Northern Cape STD	-25+20mm	Size Fraction, Increase time 90 min
14	Northern Cape STD	-20+16mm	Size Fraction, Increase time 90 min
15	Northern Cape STD	-16+12.5mm	Size Fraction, Increase time 90 min
16	Northern Cape STD	-12.5+10mm	Increase time 90 min
17	Northern Cape STD	-10+8mm	Size Fraction, Increase time 90 min
18	Northern Cape STD	-25+20mm	Size Fraction, Increase time 120 min
19	Northern Cape STD	-20+16mm	Size Fraction, Increase time 120 min
20	Northern Cape STD	-16+12.5mm	Size Fraction, Increase time 120 min
21	Northern Cape STD	-12.5+10mm	Increase time 120 min
22	Northern Cape STD	-10+8mm	Size Fraction, Increase time 120 min
23	Northern Cape STD	-12.5+10mm	Increase Temp 550°C
24	Northern Cape STD	-12.5+10mm	Increase Temp 600°C
25	Northern Cape STD	-12.5+10mm	Increase Temp 650°C
26	Northern Cape STD	-12.5+10mm	Increase Temp 700°C
27	Northern Cape STD	-12.5+10mm	Enrich gas composition 5% H_2
28	Northern Cape STD	-12.5+10mm	Enrich gas composition 10% H_2
29	Northern Cape STD	-12.5+10mm	Increase Temp 600°C, Increase time 90 min
30	Northern Cape STD	-12.5+10mm	Increase Temp 600°C, Increase time 120 min
31	Northern Cape STD	-12.5+10mm	Increase Temp 700°C, Increase time 90 min
32	Northern Cape STD	-12.5+10mm	Increase Temp 700°C, Increase time 120 min
33	Northern Cape STD	-12.5+10mm	Increase Temp 750°C, 60 min
34	Northern Cape STD	-12.5+10mm	Increase Temp 800°C, 60 min

2.2 EVALUATION OF CRACK OCCURANCE AND PROPAGATION

Samples of the different size fractions generated during the reduction disintegration tests were analyzed using a scanning electron microscope (SEM). The aim of this part of the study was to determine whether the cracks are significantly associated with specific phases, i.e. to determine whether the cracks follow ore particles, and whether they occur in the hematite matrix or the gangue portion of the ore.

Five different ore types were examined, namely:

- Northern Cape STD -10+8mm (Test 5)
- Northern Cape OT 2 (Test 7)
- Northern Cape OT 4 (Test 9)
- Northern Cape OT 5 (Test 10)
- Northern Cape OT 6 (Test 11)

2.2.1 Analysis Method

A point counting method was used to evaluate the images from the SEM analysis and only images of the same magnification (X120) were considered for analyses. A representative pool image was used for the counts.

A grid was used for the fracture distribution determination. The number of cracks that fell on the intersection was counted: it was recorded whether the crack occurred in the iron ore matrix or in gangue minerals. The same grid was used to record the percentage of gangue minerals vs hematite in the samples. The methodology is illustrated in **Figure 32**. **Table 8** is a summary of the results as presented in **Figure 32**. It should be noted that this is merely a demonstration and does not apply to any of the data discussed.

Table 8: Illustrative data using Figure 32 to illustrate the methodology used to evaluate the occurrences of cracks using SEM analysis.

	Cracks assoc. with Ore	Cracks assoc. with gangue	Gangue	Hematite
Count	1	3	16	55
Percentage	25	75	22.5	77.5

SEM analysis was carried out on all the size fractions produced during the reduction disintegration tests.

2.3 HIGH TEMPERATURE MICROSCOPE REDUCTION TESTS

High temperature microscopy was performed during reduction, to follow crack formation and crack propagation. **Figure 33** is a graphical representation of the high temperature microscope at Wollongong University, which is the instrument that was used. The sample is heated with the halogen lamp (1kW). The lamp is air cooled, with the furnace housing water-cooled. The samples were prepared to fit in a 10mm outer diameter (alumina) 8mm inner and 3mm high alumina crucible. The samples were polished to get an even surface to simplify the use of the microscope. A Lasertec microscope (Model 1LM21) was used, while the video signal was captured using a Snazzi AVIO capturecard.

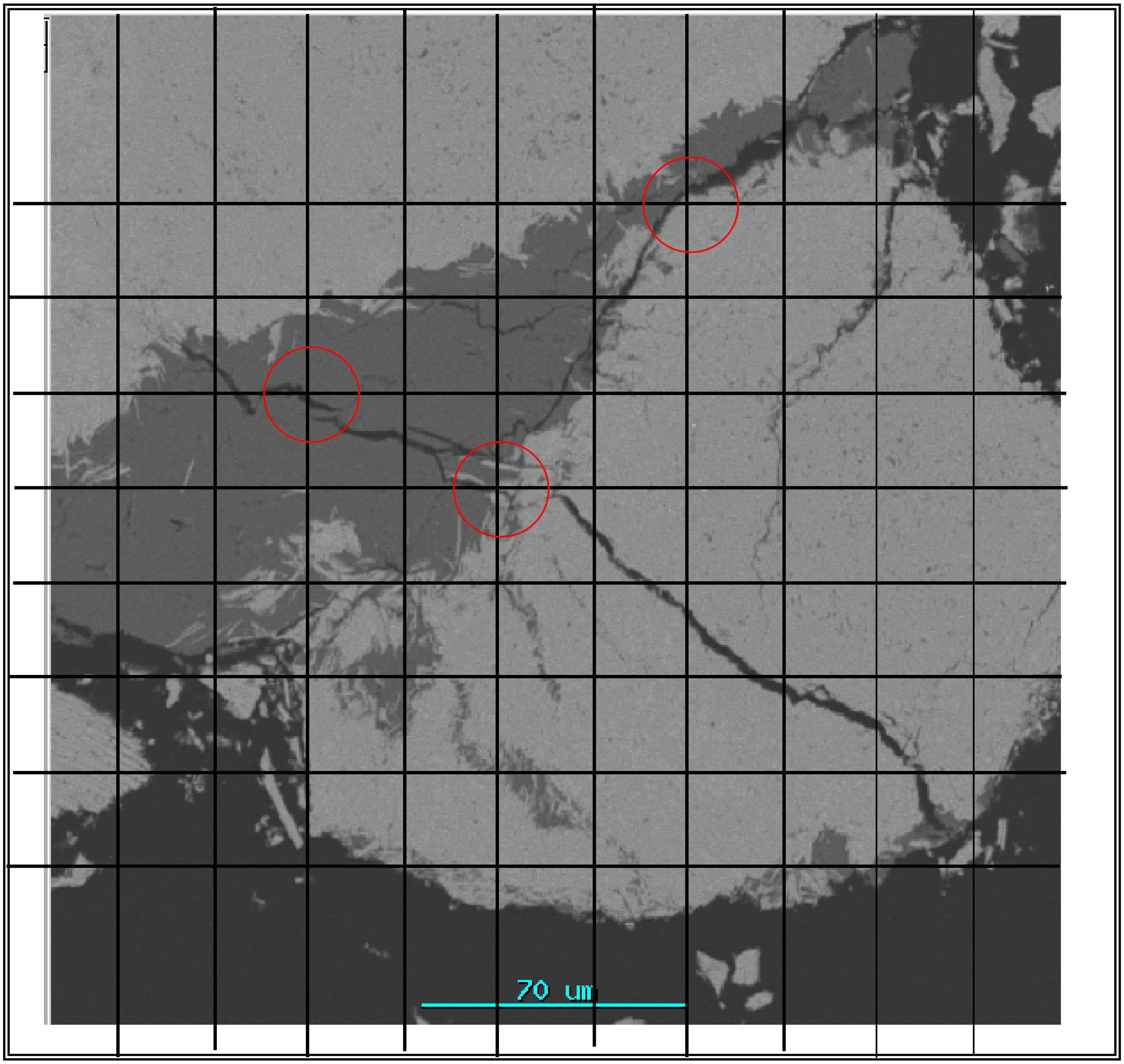

Figure 32: Illustration of methodology used to evaluate the occurrences of cracks using SEM images.

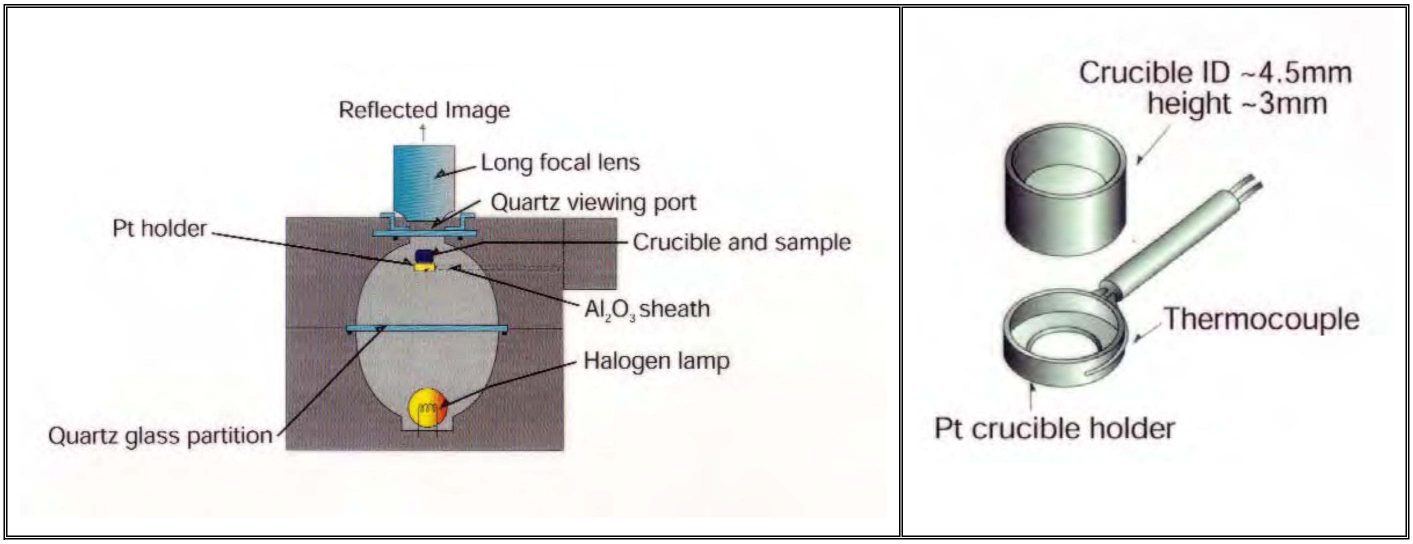

Figure 33: Graphical representation of high temperature microscope.

Table 9 lists the original sample labels as well as the reduction atmosphere under which the samples were heated. The test procedure of ISO 4696 was used as basis for the test procedure. During heating and cooling, BOC UHP (ultra high purity) Ar was passed through a Vici He purifier (used for all noble gasses) and used as inert atmosphere. A pre-mix gas from Air Liquide (20% CO, 20% CO_2 and 60% N_2) was used as a reduction gas for the CO runs. BOS Argoplas 5 (5% H_2 in Ar) was used for the hydrogen runs. A flow rate of approximately 2l/min was used.

Due to non-uniform heating of the sample (under inert conditions), the heating rate was decreased so that the samples were heated from 0-500ºC in one hour. **Figure 34** is an illustration of the test conditions used in the high temperature microscope. During the tests, a video recording was made of the entire test. Emphasis was placed on crack formation and propagation. A magnification of 10 times (objective) was used.

After the reduction test, the samples were mounted in epoxy resin, polished and coated with gold in a sputter coater. They were observed in a JOEL 5800 scanning electron microscope at the Department of Microscopy and Micro-Analysis at the University of Pretoria.

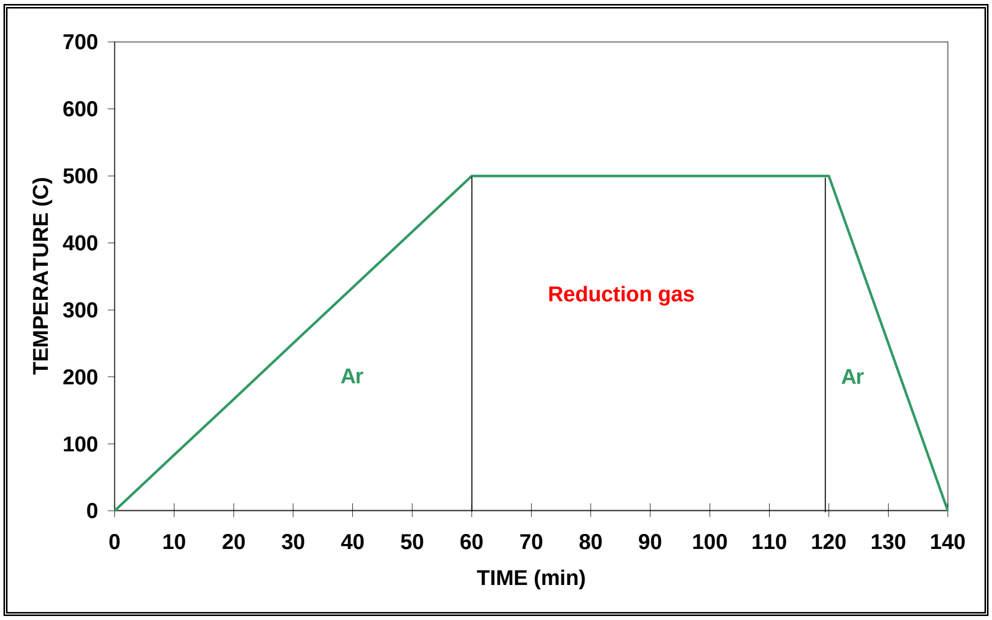

Figure 34: Illustration of test conditions used in the high temperature microscope.

Table 9: List and test conditions of samples reduced under the high temperature microscope.

Sample No.	Sample Name	Date	Reduction gas composition (%) Remaining = Ar	Time (min) and reduction temp (ºC)
1	Northern Cape OT 5	13/06/06	20 CO, 20 CO_2	60; 500
2	Northern Cape OT 2	14/06/06	20 CO, 20 CO_2	60; 500
3	Northern Cape OT 4	09/06/06	20 CO, 20 CO_2	60; 500
6	Northern Cape OT 2	13/06/06	20 CO, 20 CO_2	60; 500
8	Northern Cape STD	09/06/06	20 CO, 20 CO_2	60; 500
10	Northern Cape OT 4	09/06/06	20 CO, 20 CO_2	60; 500
12	Northern Cape OT 2	14/06/06	20 CO, 20 CO_2	60; 500
13	Northern Cape STD	12/06/06	20 CO, 20 CO_2	60; 500
14	Northern Cape OT 6	13/06/06	20 CO, 20 CO_2	60; 500
15	Northern Cape OT 6	14/06/06	20 CO, 20 CO_2	60; 500
16	Northern Cape STD	12/06/06	20 CO, 20 CO_2	60; 500
17	Northern Cape OT 4	12/06/06	20 CO, 20 CO_2	60; 500
18	Northern Cape STD	27/02/07	5 H_2	120; 500
19	Northern Cape STD	1/3/2003	5 H_2	180; 500
20	Northern Cape STD	7/3/2007	5 H_2	180; 500
21	Northern Cape STD	9/3/2003	20 CO, 20 CO_2	90; 700

3 RESULTS

3.1 REDUCTION DISINTEGRATION

The results of the sieve analysis and the degree of reduction after the various reduction disintegration tests are given in **Table 10**. All the results were within the prescribed repeatability procedure given in the ISO standard (ISO 4696) where the difference of the two duplicate tests should be less than 0.5. The forms of iron used to calculate the percentage reduction is given in **Table 11** for the different ore types. The variance of the chemical analysis was stated 0.12 for Fe(tot) (wet chemical) and 0.28 for FeO (ICP). It should be noted that the Fe_2O_3 value is a calculated value. **Table 12** shows the XRD-analysis for the different ore types. These results indicate that the FeO measured during the wet chemical analysis is in the form of magnetite and no wüstite was formed during reduction. More comprehensive tables are given in **Appendix 3.**

Figure 35 indicates the effect of burden size on the degree of reduction disintegration on Northern Cape STD. From the graphs it is clear that the degree of reduction disintegration is very similar despite differences in the burden size. It is only for the burden size -10+8mm that a significant increase in the percentage fine material is noted. This is mainly due to the fact that the burden material size fraction is merely +8mm, hence only a small degree of size degradation is required to produce a significant amount of -8mm material.

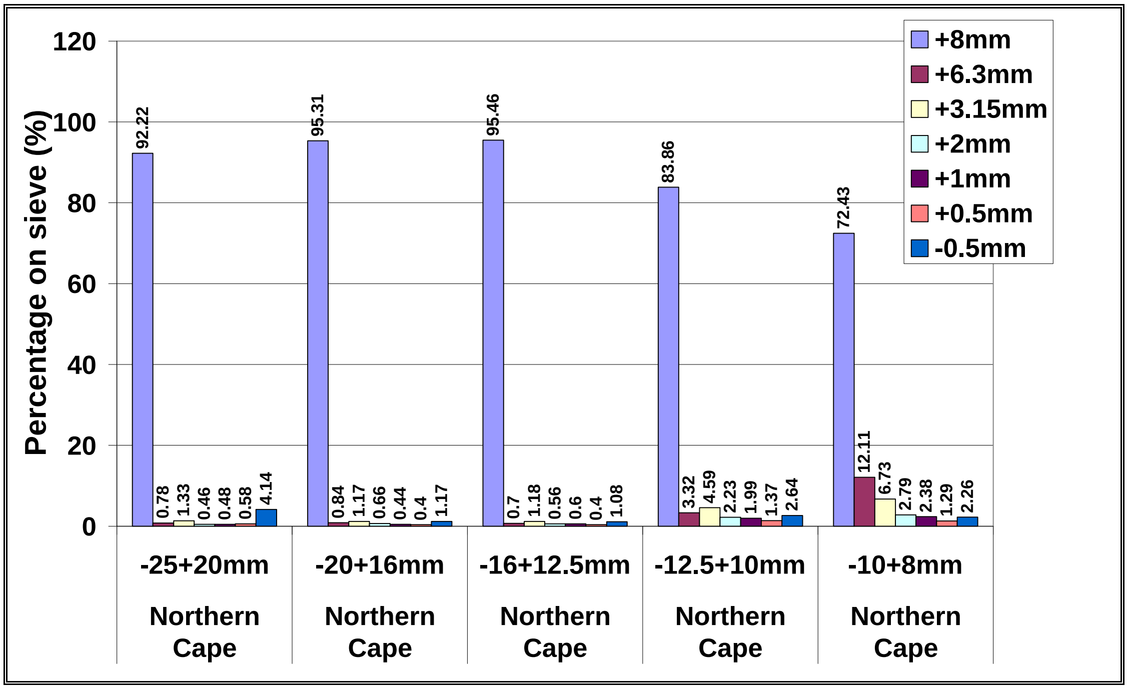

Figure 35: Effect of burden size on the degree of reduction disintegration on Northern Cape STD.

Table 10: Results of sieve analysis and fractional reduction after reduction disintegration testing

Test no.	Ore Type	Size fraction (Original)	Size fraction after RDI		% Reduction		
			+6.3mm	-6.3mm	+6.3mm	-6.3mm	Total
1	Northern Cape STD	-25+20mm	93.00	6.99	1.29	1.78	1.36
2	Northern Cape STD	-20+16mm	96.15	3.84	0.78	0.00	0.75
3	Northern Cape STD	-16+12.5mm	96.16	3.82	1.09	0.00	1.05
4	Northern Cape STD	-12.5+10mm	90.86	9.14	1.73	5.49	2.07
5	Northern Cape STD	-10+8mm	84.54	15.45	2.78	4.13	2.99
6	Northern Cape OT 1	-12.5+10mm	90.00	10.10	0.42	4.43	0.83
7	Northern Cape OT 2	-12.5+10mm	76.90	23.10	0.94	4.11	1.67
8	Northern Cape OT 3	-12.5+10mm	87.20	12.80	1.43	4.40	1.81
9	Northern Cape OT 4	-12.5+10mm	98.92	1.08	0.03	12.76	0.17
10	Northern Cape OT 5	-12.5+10mm	89.92	10.09	2.37	6.06	2.74
11	Northern Cape OT 6	-12.5+10mm	79.57	20.43	3.44	4.31	3.62

Test no.	Ore Type	Size fraction (Original)	Size fraction after RDI		% Reduction		
			+6.3mm	-6.3mm	+6.3mm	-6.3mm	Total
12	Northern Cape OT 7	-12.5+10mm	90.80	9.20	5.06	7.05	5.25
13	Northern Cape STD	-25+20mm	98.59	1.40	0.00	0.00	0.00
14	Northern Cape STD	-20+16mm	90.25	9.74	0.32	5.54	0.82
15	Northern Cape STD	-16+12.5mm	86.61	13.38	0.00	0.00	0.00
16	Northern Cape STD	-12.5+10mm	83.61	16.39	2.27	5.75	2.84
17	Northern Cape STD	-10+8mm	78.29	21.71	2.42	4.60	2.90
18	Northern Cape STD	-25+20mm	94.21	5.78	0.00	0.00	0.00
19	Northern Cape STD	-20+16mm	87.24	12.76	0.00	0.00	0.00
20	Northern Cape STD	-16+12.5mm	77.46	22.54	3.26	5.69	3.81
21	Northern Cape STD	-12.5+10mm	82.60	17.40	0.78	6.17	1.72
22	Northern Cape STD	-10+8mm	71.88	28.12	2.79	4.78	3.35
23	Northern Cape STD	-12.5+10mm	86.70	13.30	3.05	5.80	3.42
24	Northern Cape STD	-12.5+10mm	87.10	12.90	0.82	6.88	1.60
25	Northern Cape STD	-12.5+10mm	87.80	12.20	1.63	7.68	2.37
26	Northern Cape STD	-12.5+10mm	87.30	12.70	4.60	9.78	5.26
27	Northern Cape STD	-12.5+10mm	91.00	9.00	3.41	6.16	3.66
28	Northern Cape STD	-12.5+10mm	87.10	12.90	7.42	6.50	7.30
29	Northern Cape STD	-12.5+10mm	86.45	13.55	2.12	8.36	2.96
30	Northern Cape STD	-12.5+10mm	76.30	23.70	5.12	6.27	5.39
31	Northern Cape STD	-12.5+10mm	88.40	11.60	6.25	10.72	6.77
32	Northern Cape STD	-12.5+10mm	80.80	19.20	4.25	11.65	5.67
33	Northern Cape STD	-12.5+10mm	92.00	8.00	3.19	15.07	4.14
34	Northern Cape STD	-12.5+10mm	94.70	5.30	4.63	15.09	5.19

Table 11: Chemical analysis of the different size fractions after reduction disintegration tests for the different ore types.

Sample Name/ Test no.	Ref No.	Size Fraction	Fe_{total}	Fe^o	FeO	Fe_2O_3
Northern Cape STD/Test no 4	RMT 2540	+8mm	66.65	0.07	5.40	89.20
	RMT 2541	+6.3mm	68.08	0.18	9.21	86.86
	RMT 2542	+3.15mm	68.96	0.04	14.17	82.80
	RMT 2543	+1mm	70.01	3.46	23.55	68.98
	RMT 2544	-0.5mm	68.62	Insufficient Sample		98.13
Northern Cape OT 1/ Test no 6	RMT 2545	+10mm	68.29	0.14	3.17	93.93
	RMT 2546	+8mm	68.29	0.13	4.74	92.20
	RMT 2547	+6.3mm	70.16	0.20	8.83	90.22

	RMT 2548	+3.15mm	69.81	0.07	14.95	83.10
	RMT 2549	+2mm	70.85	0.55	22.74	75.24
	RMT 2550	+1mm	70.98	0.21	25.29	73.08
	RMT 2551	+0.5mm	70.38	Insufficient Sample		100.64
	RMT 2552	-0.5mm	68.99	0.24	24.49	71.08
Northern Cape OT 2/ Test no 7	RMT 2553	+10mm	68.85	0.12	6.28	91.30
	RMT 2554	+8mm	69.24	0.13	7.24	90.78
	RMT 2555	+6.3mm	68.65	0.09	9.70	87.25
	RMT 2556	+3.15mm	70.42	0.18	12.25	86.82
	RMT 2557	+2mm	70.22	0.16	18.46	79.66
	RMT 2558	+1mm	70.88	0.03	24.87	73.66
	RMT 2559	+0.5mm	70.41	0.53	24.22	73.00
	RMT 2560	-0.5mm	69.39	0.09	25.75	70.47
Northern Cape OT 3/ Test no 8	RMT 2561	+10mm	65.93	0.03	3.48	90.37
	RMT 2562	+8mm	67.91	0.18	4.39	91.97
	RMT 2563	+6.3mm	65.05	0.05	4.07	88.42
	RMT 2564	+3.15mm	66.51	0.08	9.19	84.78
	RMT 2565	+2mm	68.19	0.34	16.93	78.20
	RMT 2566	+1mm	68.36	0.20	21.47	73.59
	RMT 2567	+0.5mm	67.82	0.11	22.40	71.92
	RMT 2568	-0.5mm	65.02	0.46	21.64	68.26
Northern Cape OT 4/ Test no 9	RMT 2569	+10mm	67.16	0.20	1.80	93.75
	RMT 2570	+8mm	65.75	0.17	1.93	91.63
Northern Cape OT 5/ Test no 10	RMT 2571	+10mm	66.74	0.13	4.61	90.13
	RMT 2572	+8mm	67.39	0.18	5.88	89.57
	RMT 2573	+6.3mm	68.28	0.12	10.10	86.24
	RMT 2574	+3.15mm	68.24	0.04	12.31	83.84
	RMT 2575	+2mm	67.88	0.41	17.51	77.01
	RMT 2576	+1mm	67.85	Insufficient Sample		97.03
	RMT 2577	+0.5mm	68.54	0.08	21.76	73.70
	RMT 2578	-0.5mm	66.20	0.13	22.59	69.36
Northern Cape OT 6/ Test no 11	RMT 2611	+10mm	64.81	0.10	3.81	88.30
	RMT 2612	+8mm	66.26	0.15	5.49	88.43
	RMT 2613	+6.3mm	68.67	0.22	8.21	88.75
	RMT 2614	+3.15mm	68.20	0.13	12.36	83.60
	RMT 2615	+2mm	68.40	Insufficient Sample		97.81
	RMT 2616	+1mm	69.61	0.04	23.15	73.74
	RMT 2617	+0.5mm	68.42	Insufficient Sample		97.84
	RMT 2618	-0.5mm	66.36	0.19	23.04	69.00
Northern Cape OT 7/ Test no 12	RMT 3197	+10mm	65.00	0.01	5.11	87.20
	RMT 3198	+8mm	65.90	0.01	6.00	87.60
	RMT 3199	+6.3mm	64.00	0.07	7.21	83.40
	RMT 3200	+3.15mm	66.80	0.03	10.10	84.20
	RMT 3201	+2mm	66.30	0.03	15.70	77.30
	RMT 3202	+1mm	67.40	0.19	20.80	73.00
	RMT 3203	+0.5mm	67.60	0.20	25.00	68.60
	RMT 3204	-0.5mm	65.80	0.19	23.90	67.20

Table 12: XRD analysis of the different size fractions after reduction disintegration tests for the different ore types.

Sample Name/ Test no.	Ref No.	Size Fraction	% Hematite	% Magnetite	% Quartz	% Calcite	% Clay
Northern Cape STD/Test no 4	RMT 2540	+8mm	78.6	13.5	7.9	-	-
	RMT 2541	+6.3mm	72.7	24.9	2.4	-	-
	RMT 2542	+3.15mm	60	35	5	-	-
	RMT 2543	+1mm	18.5	73.3	8.2	-	-
	RMT 2544	-0.5mm	14.6	68.4	16.9	-	-
Northern Cape OT 1/ Test no 6	RMT 2545	+10mm	82.7	11.4	3.2	-	2.8
	RMT 2546	+8mm	85.3	10.3	4.5	-	-
	RMT 2547	+6.3mm	75	22.4	2.5	-	-
	RMT 2548	+3.15mm	61.2	36.5	2.3	-	-
	RMT 2549	+2mm	30.6	66	3.4	-	-
	RMT 2550	+1mm	17.4	79.8	2.8	-	-
	RMT 2551	+0.5mm	10.6	83.8	5.5	-	-
	RMT 2552	-0.5mm	7.7	81.3	11	-	-
Northern Cape OT 2/ Test no 7	RMT 2553	+10mm	84.4	12.4	3.2	-	-
	RMT 2554	+8mm	81.6	15.5	2.9	-	-
	RMT 2555	+6.3mm	76.3	19.9	3.8	-	-
	RMT 2556	+3.15mm	75.8	22.7	1.4	-	-
	RMT 2557	+2mm	44.6	50.9	4.5	-	-
	RMT 2558	+1mm	23.3	72.8	3.9	-	-
	RMT 2559	+0.5mm	12.5	82	5.4	-	-
	RMT 2560	-0.5mm	9.4	82.2	8.4	-	-
Northern Cape OT 3/ Test no 8	RMT 2561	+10mm	83.3	8.8	8	-	-
	RMT 2562	+8mm	85.3	9.4	5.4	-	-
	RMT 2563	+6.3mm	82.3	6.4	11.3	-	-
	RMT 2564	+3.15mm	67.3	20.4	12.3	-	-
	RMT 2565	+2mm	53.8	37.4	8.9	-	-
	RMT 2566	+1mm	27.9	58.7	13.4	-	-
	RMT 2567	+0.5mm	16.9	67.3	15.8	-	-
	RMT 2568	-0.5mm	12.8	64.7	22.5	-	-
Northern Cape OT 4/ Test no 9	RMT 2569	+10mm	95.6	3.1	1.2	-	-
	RMT 2570	+8mm	94.4	0	3	-	2.6
Northern Cape OT 5/ Test no 10	RMT 2571	+10mm	83.5	10.3	6.2	-	-
	RMT 2572	+8mm	82	13.4	4.6	-	-
	RMT 2573	+6.3mm	78.7	19.3	2.1	-	-
	RMT 2574	+3.15mm	72.1	23.5	4.4	-	-
	RMT 2575	+2mm	53.4	38.7	7.7	-	-
	RMT 2576	+1mm	18.2	73.1	8.7	-	-
	RMT 2577	+0.5mm	36.4	57.2	6.4	-	-
	RMT 2578	-0.5mm	11	78.6	10.4	-	-
Northern Cape OT 6/ Test no 11	RMT 2611	+10mm	86.9	6.6	2.1	-	4.5
	RMT 2612	+8mm	87	10	3	-	-
	RMT 2613	+6.3mm	83.3	13.7	3	-	-
	RMT 2614	+3.15mm	67.9	24.6	4.5	-	3
	RMT 2615	+2mm	47	48.7	4.3	-	-
	RMT 2616	+1mm	22.8	73.8	3.4	-	-
	RMT 2617	+0.5mm	13.6	79.2	7.2	-	-
	RMT 2618	-0.5mm	7.1	80.5	8.2	-	4.1

Figure 36 indicates the effect of ore composition and microstructure on the degree of reduction disintegration. The results indicate that Northern Cape OT 4 is very stable with 98 percent of the material greater than 8mm. This correlates with the low degree of reduction that was recorded for this ore type. In contrast, Northern Cape OT 7, that performed second best with regards to the degree of reduction disintegration, recorded the highest average degree of reduction of 5.2%. On the other hand for Northern Cape OT 2 and Northern Cape OT 6 only 70-75 percent of the material is greater than 8mm. Although the general thinking is that the disintegration is mainly due to the reduction process, the average degree of reduction for Northern Cape OT 2 is 1.7 percent while that of Northern Cape OT 6 is 3.8 percent (**Figure 37**).

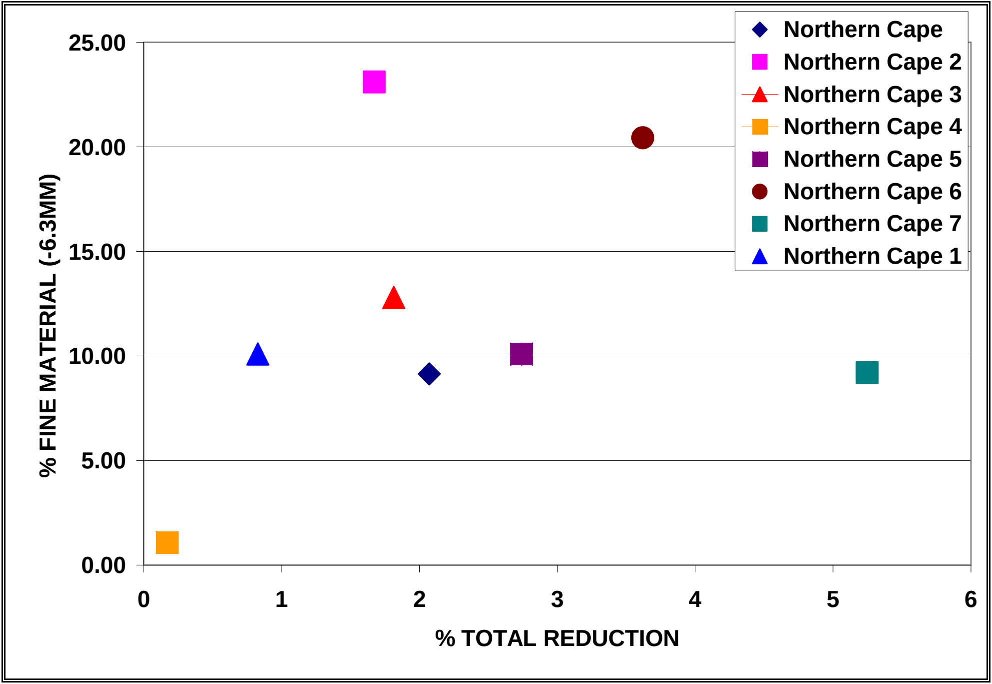

Figure 37 These results suggest that the degree of breakdown depends both on the reduction process as well as the microstructure of the ore.

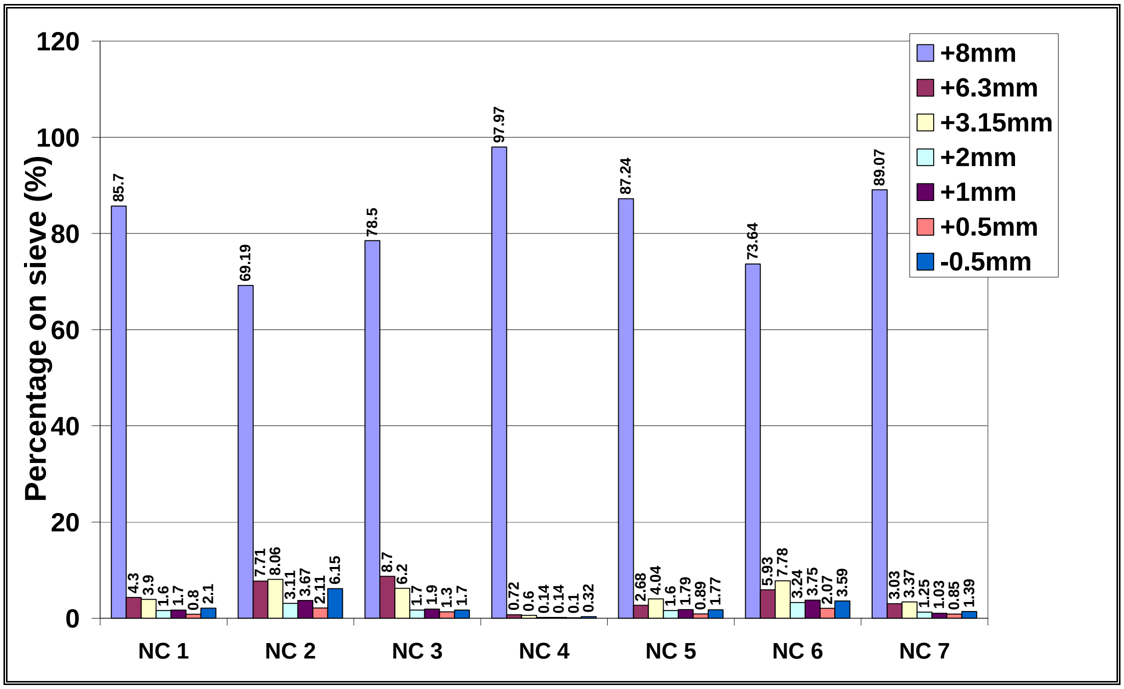

Figure 36: Degree of reduction disintegration for the different Northern Cape Ore types.

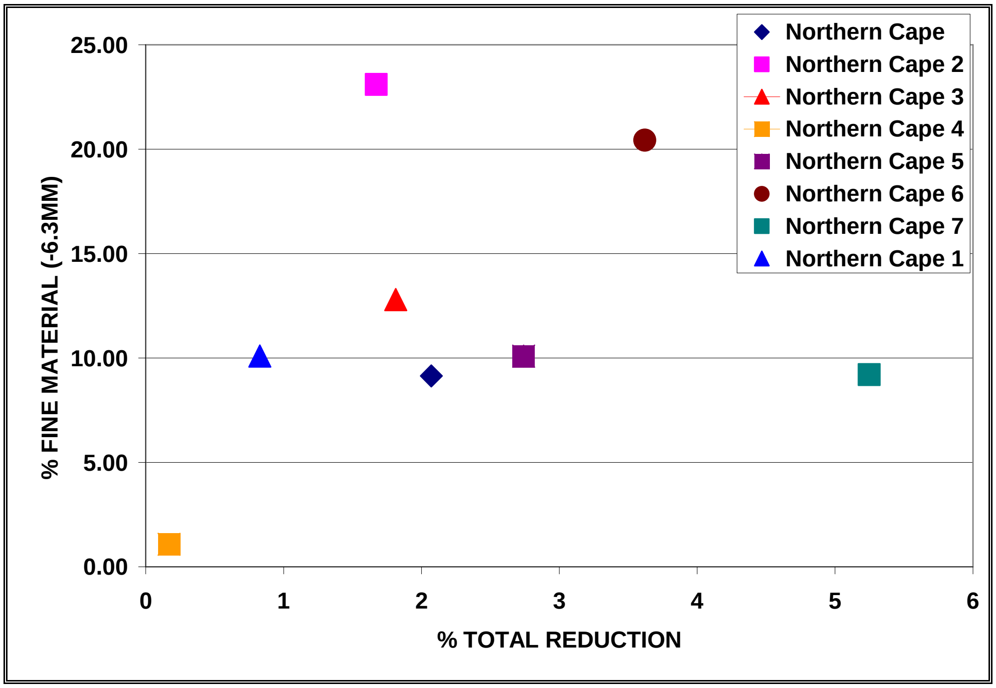

Figure 37: Percentage reduction after reduction disintegration tests for Northern Cape STD and the various ore types plotted against the % fine material (-6.3mm) generated during the test.

The effect of H_2 on the degree of reduction and the percentage fine material generated is indicated in **Figure 38**. In the first test where 5% H_2 is added to the reduction mix, the percentage reduction nearly doubled, without increasing the % fines generated. Doubling the amount of H_2 in the reduction mixture again doubles the percentage reduction, but the percentage fines generated only increases with about 40%.

Figure 39 is a graphical representation of the effect of reduction time on reduction disintegration for samples of different sizes tested for Northern Cape STD. For the -25+20mm burden, an increase in reduction time apparently leads to a decrease in the degree of reduction disintegration (this effect is likely to be reflect test-to-test variation rather than any fundamental effect). The -20+16mm burden material indicated a slight increase in the percentage +16mm, but there is also an increase in the percentage finer material that forms with an increase in time from 60 minute to 90 minutes. Increasing the reduction time further to 120 minutes leads to a general increase in the degree of reduction disintegration.

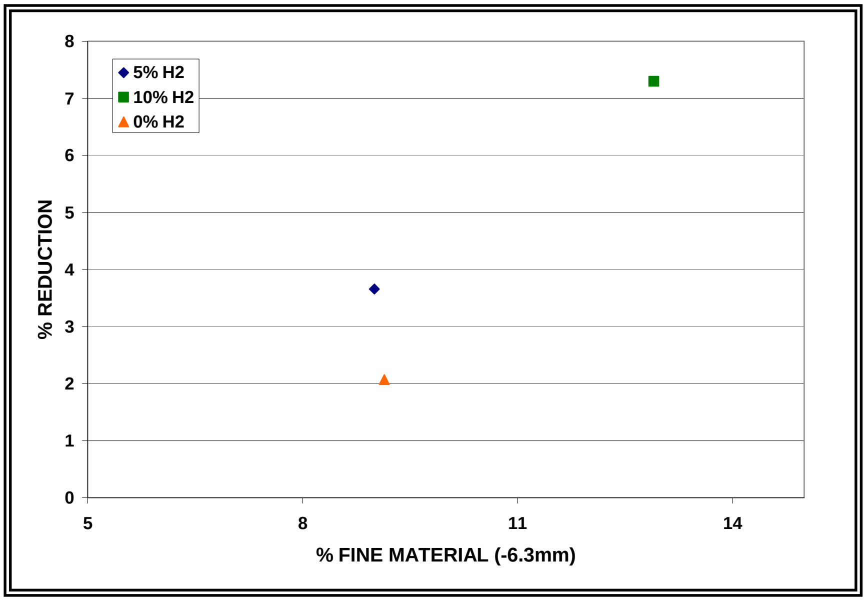

Figure 38: Effect of gas composition on the degree of reduction and the percentage fine material generated.

For the -16+12.5mm, -12.5+10mm and -10+8mm starting materials, a general trend was noted of an increase in the degree of reduction disintegration with an increase in reduction time. To determine whether the same tendency is valid at higher temperatures, tests were also conducted at 600°C and 700°C with the -12.5+10mm burden. The results of these tests are indicated in **Figure 40**. This graph confirms that an increase in reduction time leads to a general increase in the degree of reduction disintegration, independent of the reduction temperature.

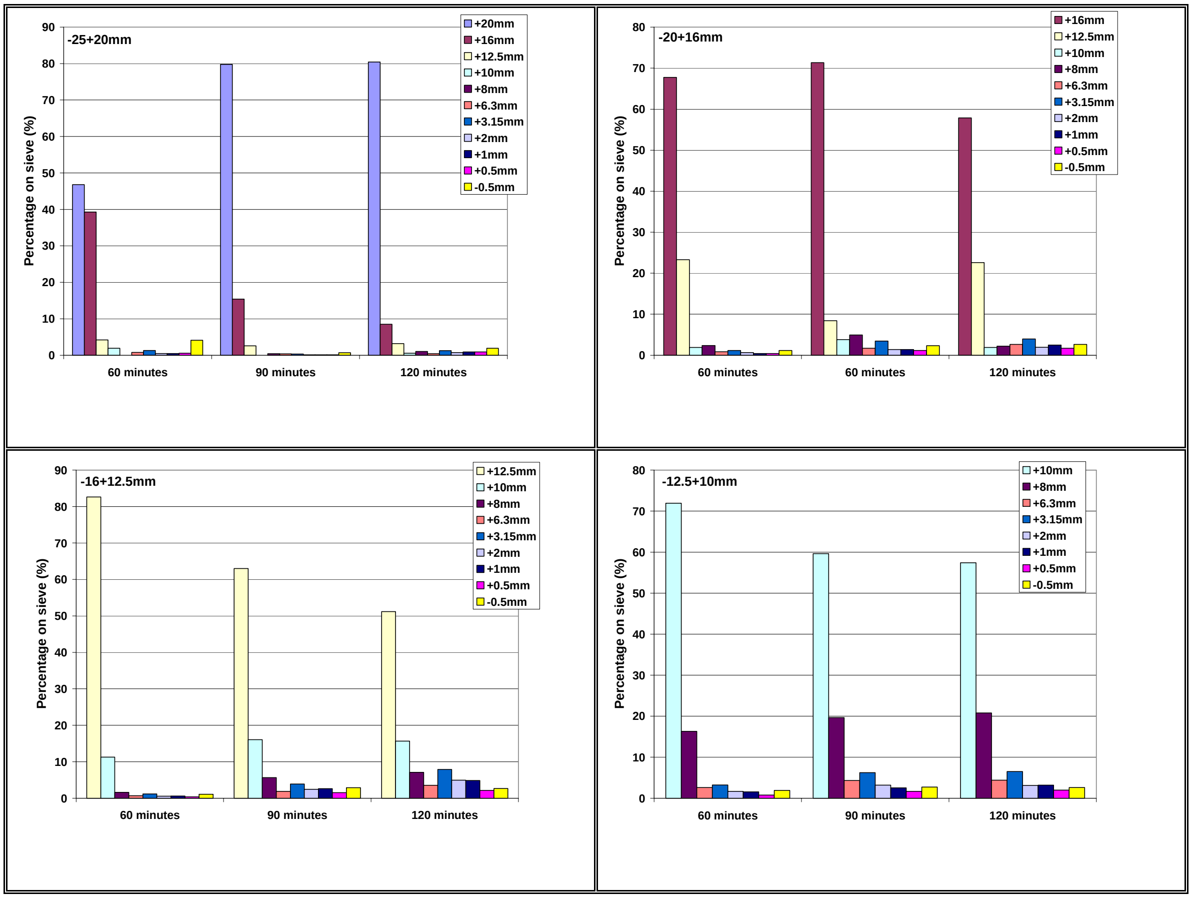

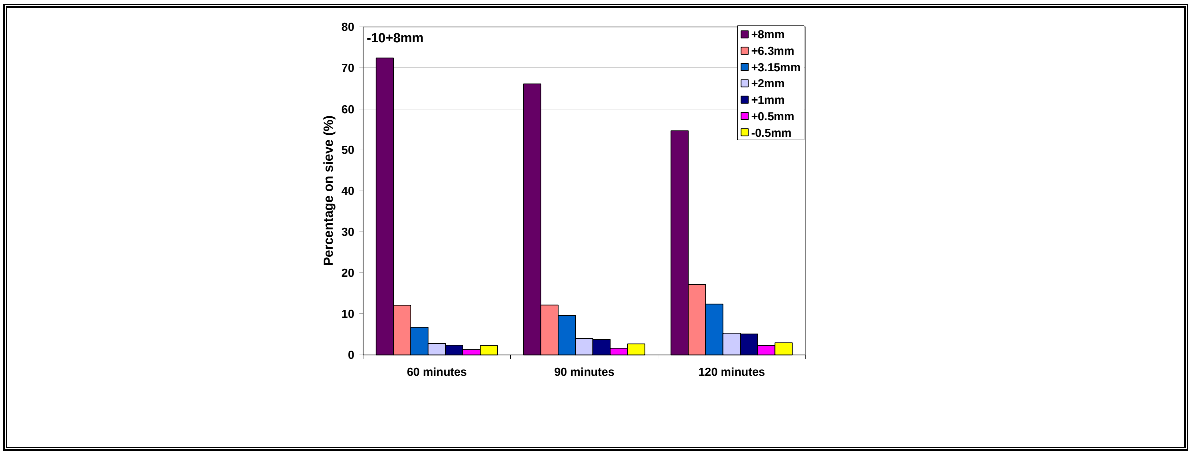

Figure 39: Effect of reduction time on the degree of reduction disintegration for samples of different sizes of Northern Cape STD.

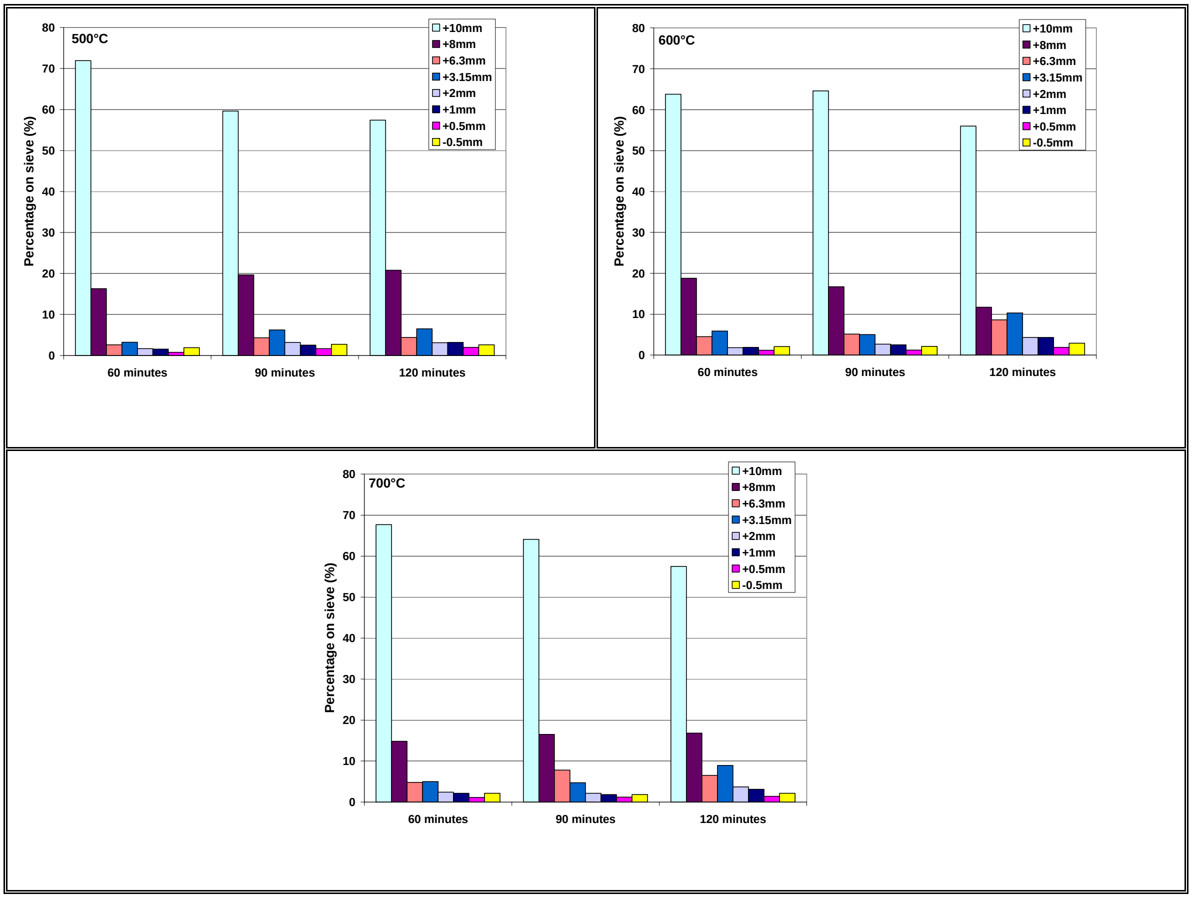

Figure 40: Effect of temperature on reduction disintegration for -12.5+10mm burdens after 60, 90 and 120 minutes of Northern Cape STD.

Figure 41 indicates the effect of reduction time and temperature on the percentage fines generated. This graph shows a general upward trend in the percentage fine generated for increasing temperatures and increasing reduction times.

Figure 42 indicates the effect of reduction temperature on the degree of reduction disintegration on a -12.5+10mm fraction burden for Northern Cape STD. The figure confirms that between 500°C and 700°C similar degrees of reduction disintegration is noted, but with a decline in the degree of reduction disintegration above 700°C. **Figure 43** represents the same results as percentage fines generated compared to reduction temperature. From the figure it is clear that at temperature between 550°C and 700°C the percentage fines generated increase by 50 percent and more compared to temperatures of 500°C, 750°C and 800°C.

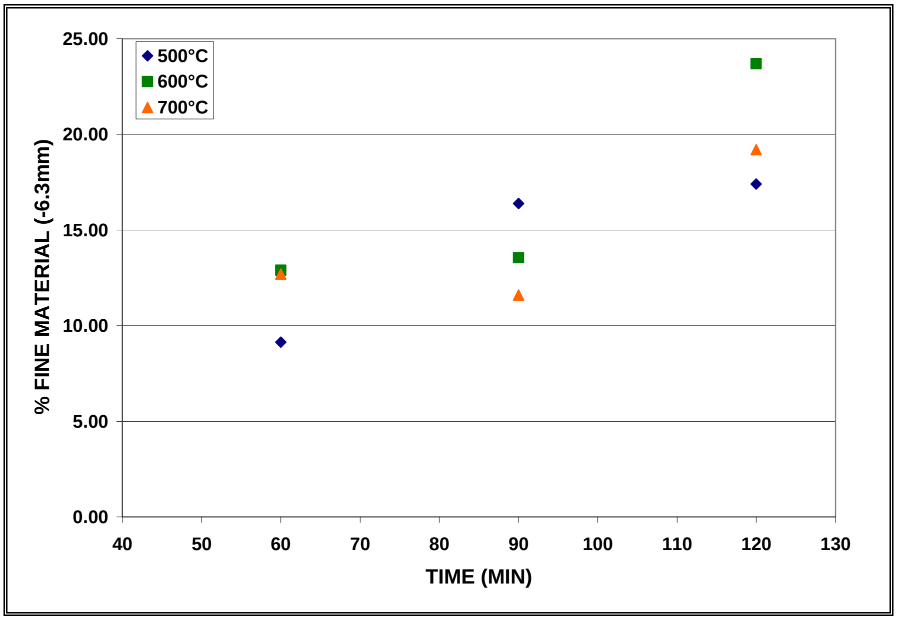

Figure 41: Effect of time and temperature on the reduction disintegration of Northern Cape STD

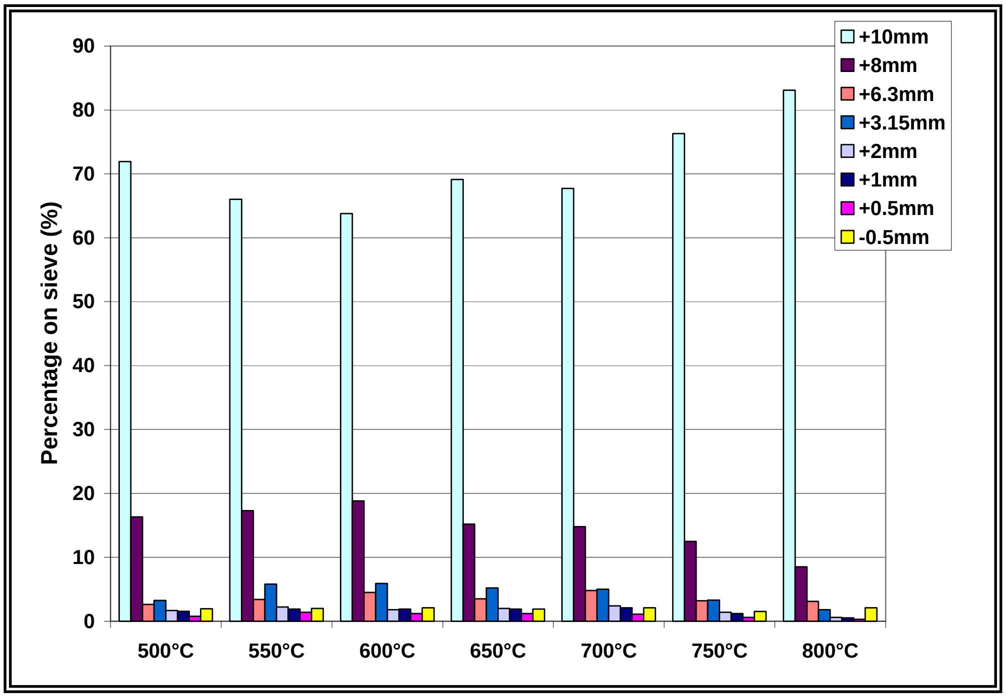

Figure 42: Effect of temperature on the reduction disintegration of Northern Cape STD. The burden was -12.5+10mm and the reduction time 60 minutes.

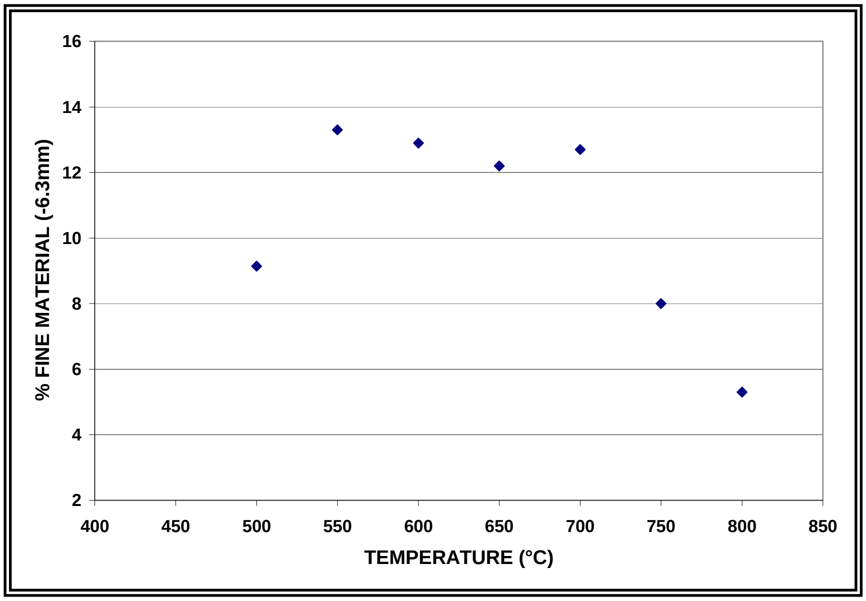

Figure 43: Effect of Temperature on the reduction disintegration of Northern Cape STD

3.2 EVALUATION OF CRACK FORMATION AND PROPAGATION

As shown by the results presented in the previous section, Northern Cape OT 4 has the lowest low temperature breakdown, while Northern Cape OT 2 gave the most low temperature breakdown. **Figure 44** - **Figure 59** are SEM images of the typical occurrences of cracks for the different size fractions after reduction disintegration for these two ore types. All of these images were obtained using back-scattered electron imaging. The brightest regions are iron oxide, the black regions mounting resin or pores and the grey regions gangue.

The results regarding crack association with gangue are given in **Table 13 – Table 17** for the individual samples with graphical representation of the results in **Figure 60 - Figure 64.**

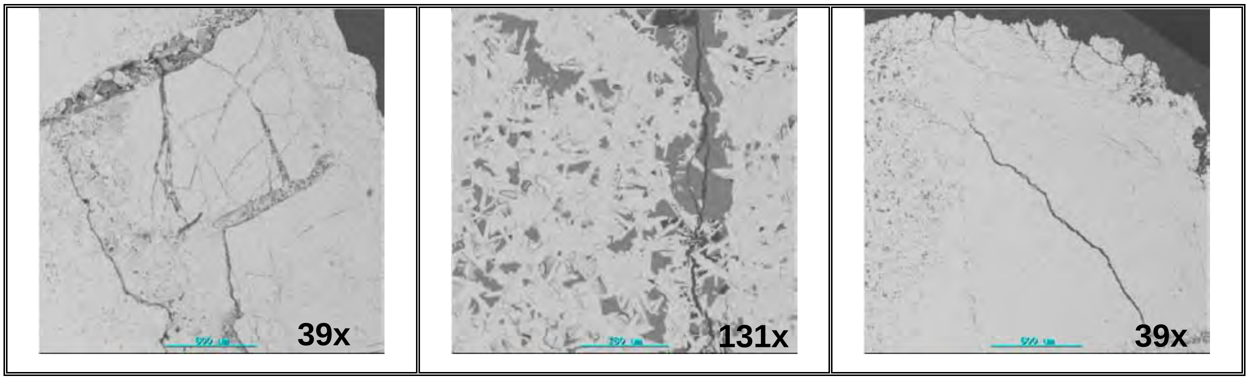

Figure 44: SEM images of the -12+10mm fraction after reduction disintegration test for Northern Cape OT 2.

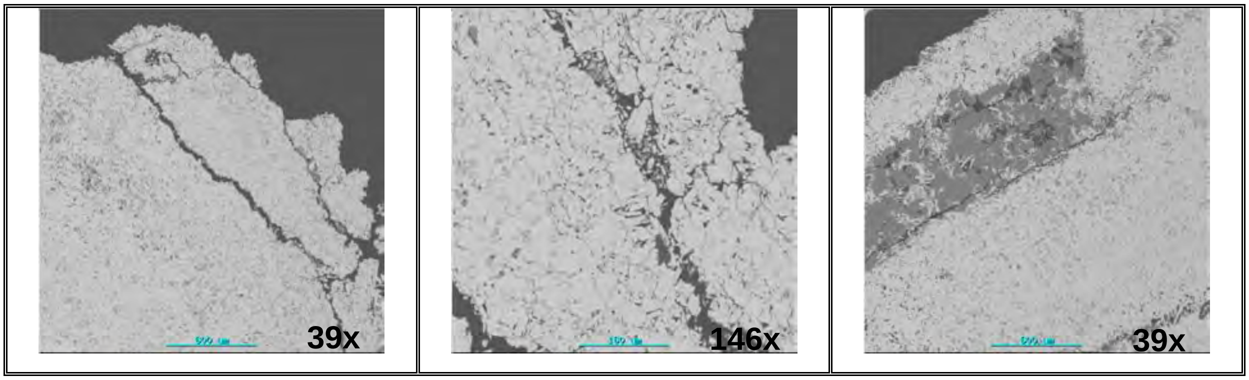

Figure 45: SEM images of the -10+8mm fraction after reduction disintegration test for Northern Cape OT 2.

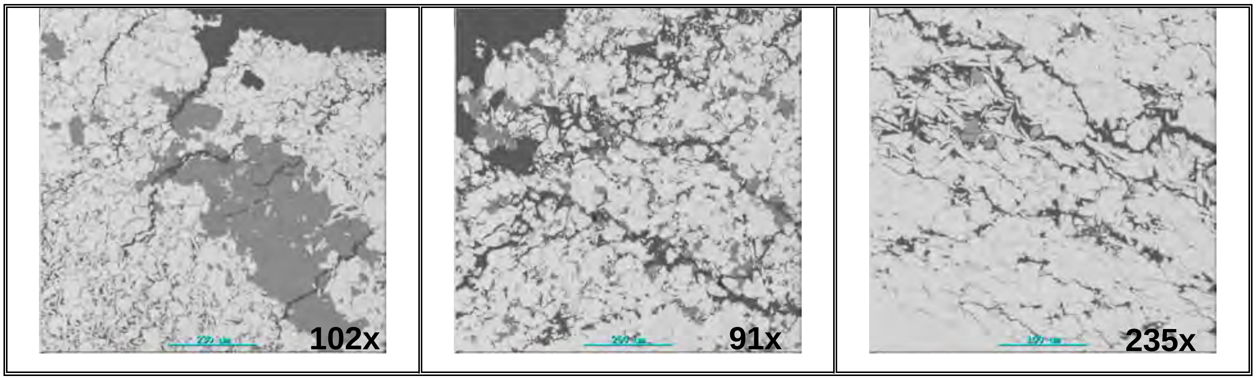

Figure 46: SEM images of the -8+6.3mm fraction after reduction disintegration test for Northern Cape OT 2.

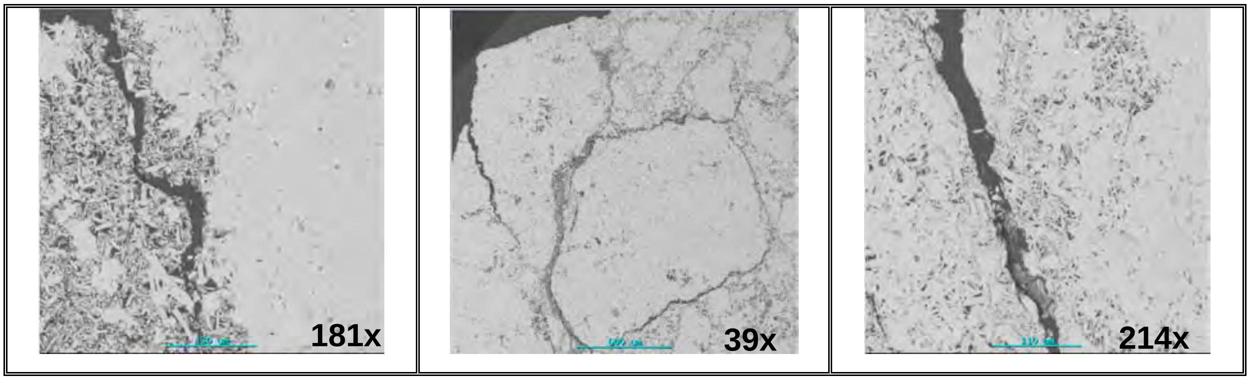

Figure 47: SEM images of the -6.3+3.15mm fraction after reduction disintegration test for Northern Cape OT 2.

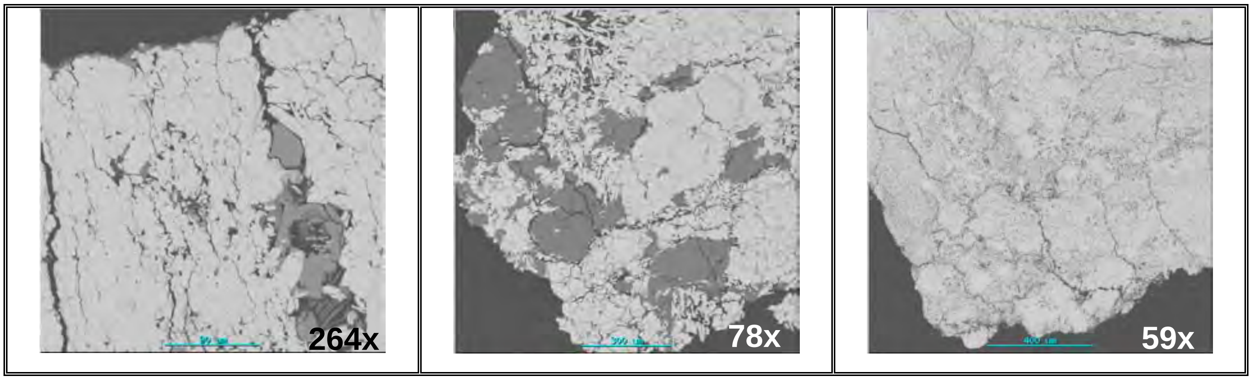

Figure 48: SEM images of the -3.15+2mm fraction after reduction disintegration test for Northern Cape OT 2.

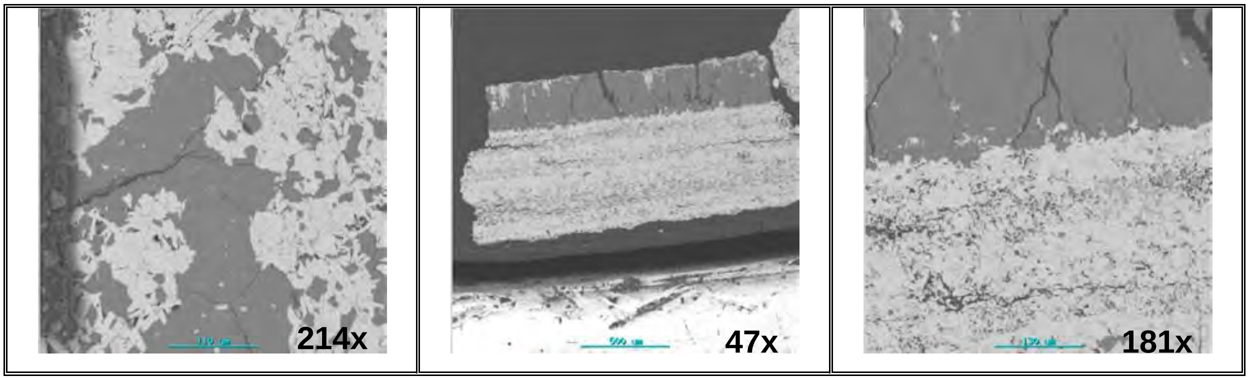

Figure 49: SEM images of the -2+1mm fraction after reduction disintegration test for Northern Cape OT 2.

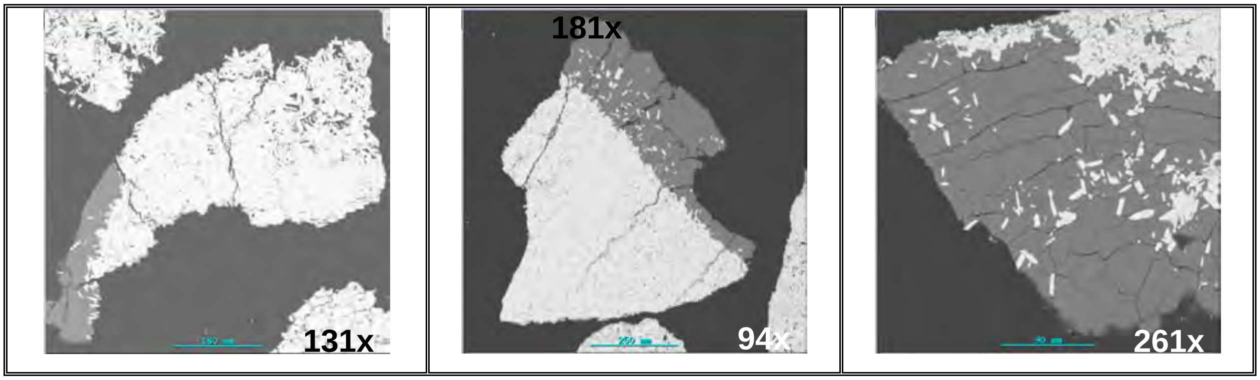

Figure 50: SEM images of the -1+0.5mm fraction after reduction disintegration test for Northern Cape OT 2.

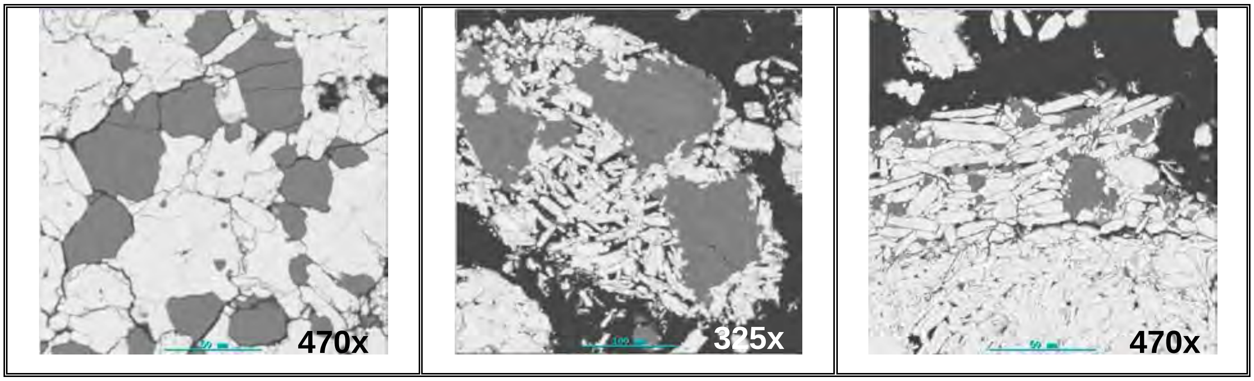

Figure 51: SEM images of the -0.5mm fraction after reduction disintegration test for Northern Cape OT 2.

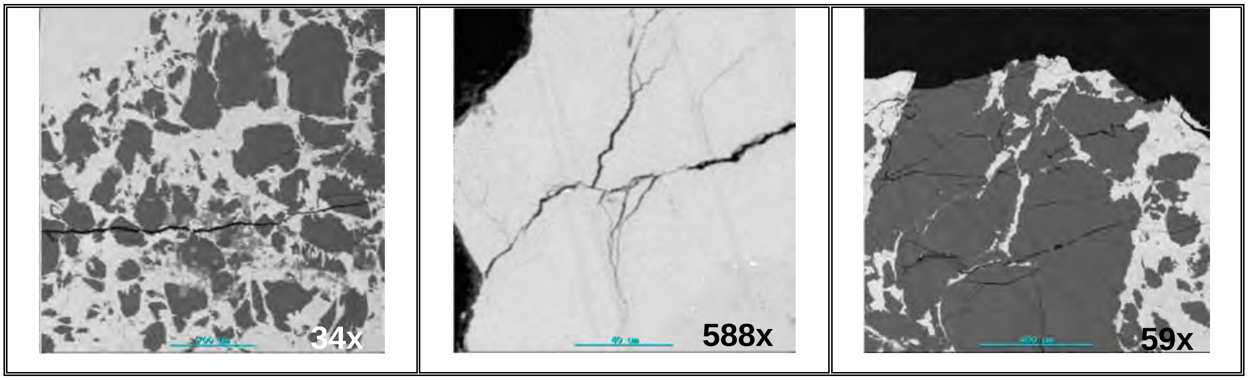

Figure 52: SEM images of the -12+10mm fraction after reduction disintegration test for Northern Cape OT 4.

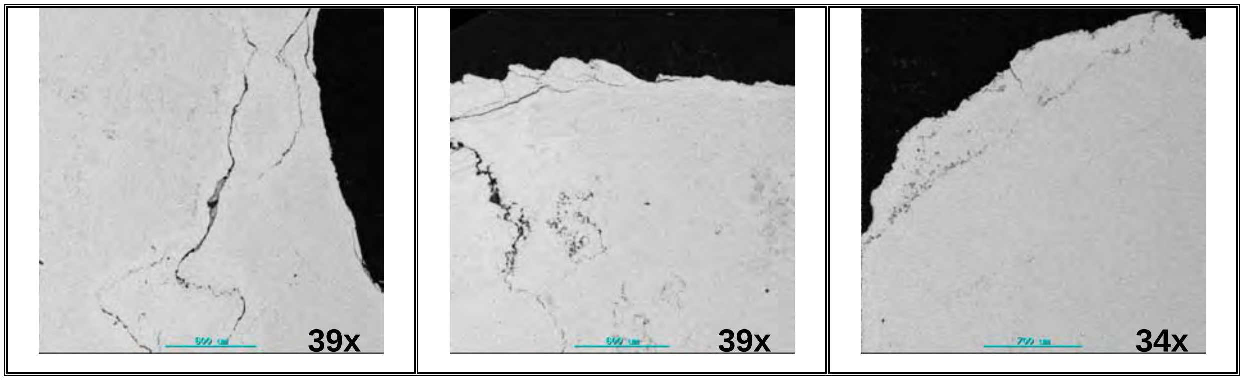

Figure 53: SEM images of the -10+8mm fraction after reduction disintegration test for Northern Cape OT 4.

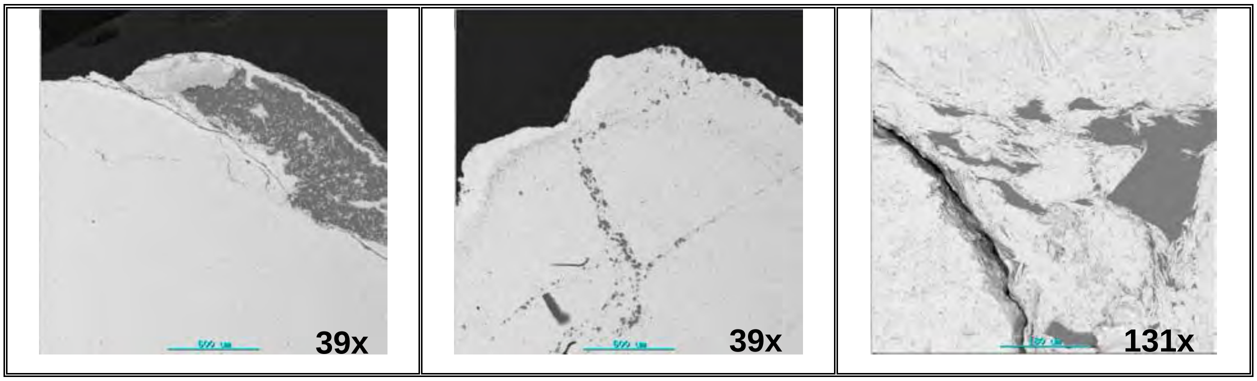

Figure 54: SEM images of the -8+6.3mm fraction after reduction disintegration test for Northern Cape OT 4.

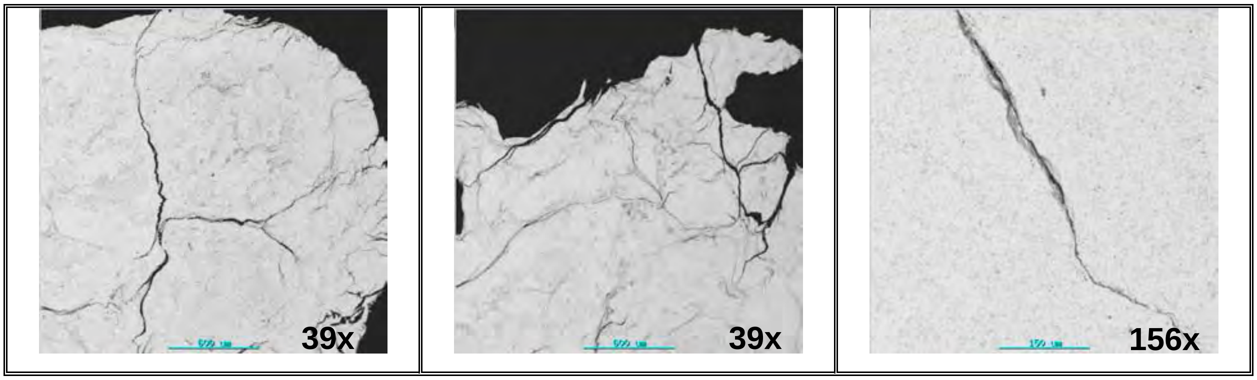

Figure 55: SEM images of the -6.3+3.15mm fraction after reduction disintegration test for Northern Cape OT 4.

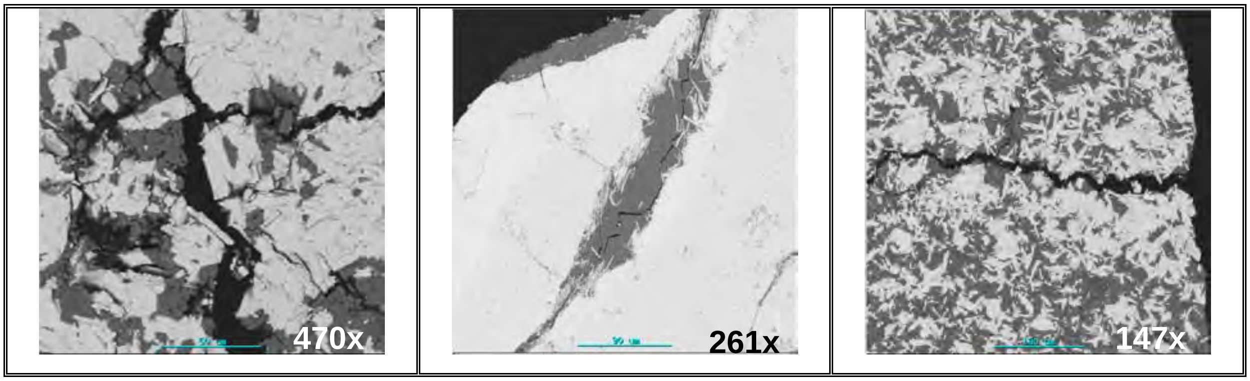

Figure 56: SEM images of the -3.15+2mm fraction after reduction disintegration test for Northern Cape OT 4.

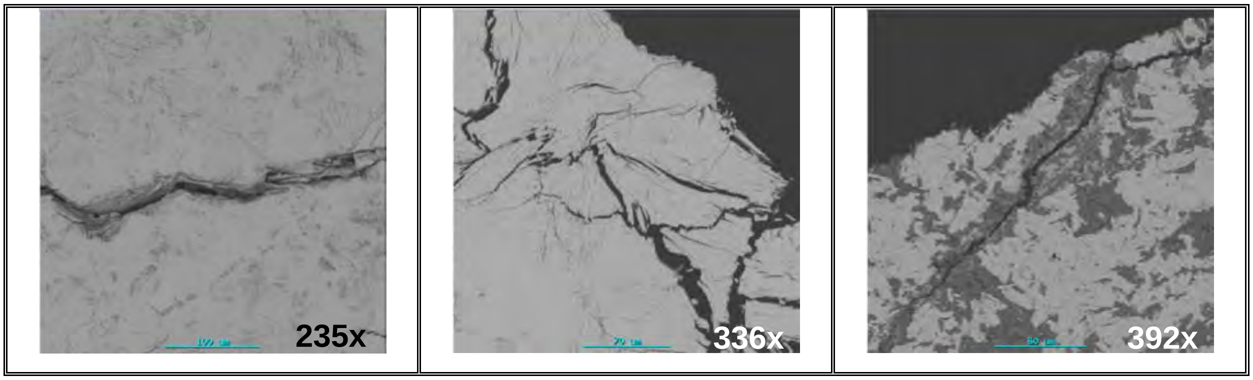

Figure 57: SEM images of the -2+1mm fraction after reduction disintegration test for Northern Cape OT 4.

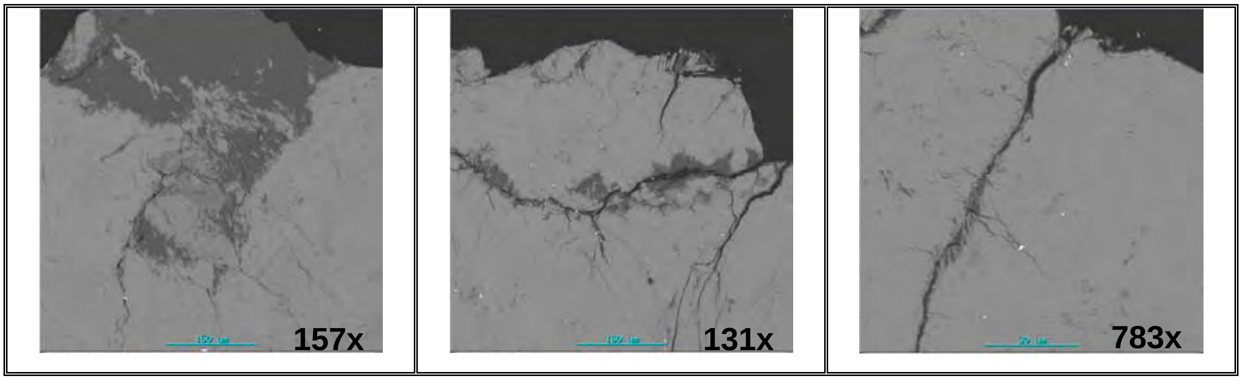

Figure 58: SEM images of the -1+0.5mm fraction after reduction disintegration test for Northern Cape OT 4.

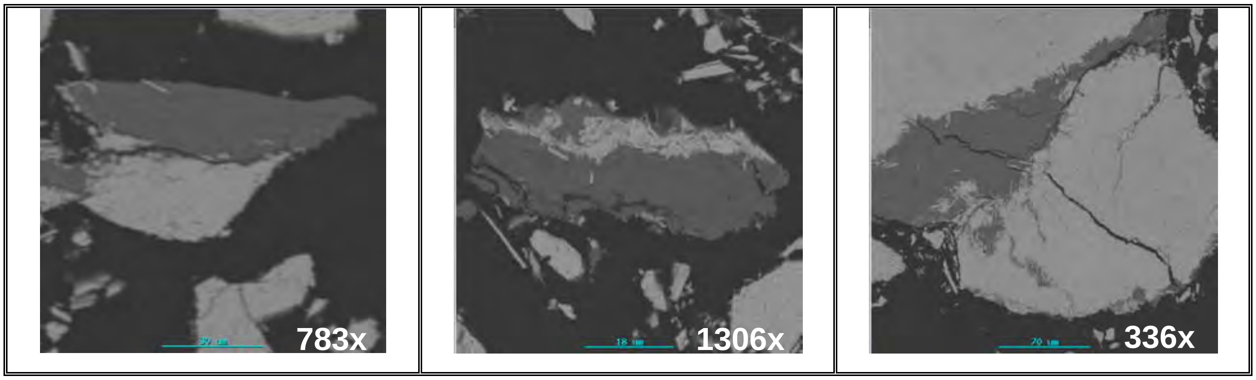

Figure 59: SEM images of the -0.5mm fraction after reduction disintegration test for Northern Cape OT 4.

Table 13: Crack association in the different size fractions of Northern Cape STD (-10+8mm) as determined from SEM images.

Size Fraction,mm	Image Ref No.	% Cracks assoc. with iron oxide	%Cracks assoc. with gangue	% v/v Gangue	% v/v iron oxide
-6.3 + 3.15	B	100	0	4	96
-6.3 + 3.15	C	82	18	23	87
-10 + 8	P	15	85	34	66
-10 + 8	Q	90	10	42	58

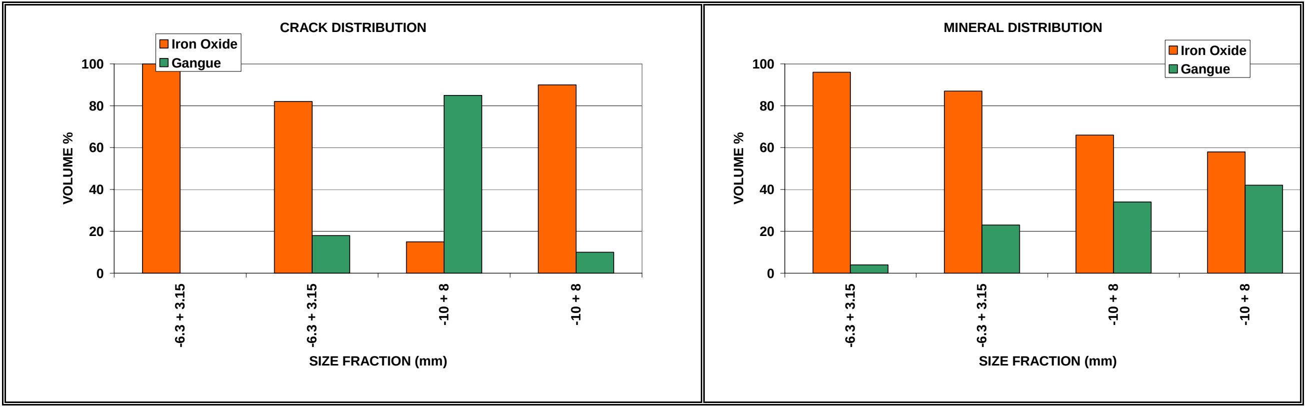

Figure 60: Graphical representation of crack association in the different size fractions of Northern Cape STD (-10+8mm).

Table 14: Crack association in the different size fractions of Northern Cape OT 2 as determined from SEM images.

Size Fraction,mm	Image Ref No.	% Cracks assoc. with iron oxide	%Cracks assoc. with gangue	% v/v Gangue	% v/v iron oxide
-0.5	1.1.1_1	69	31	20	80
-0.5	2.1.1_1	76	24	14	86
-0.5	3.1.1_1	71	29	15	85
-0.5	5.1.1_1	82	18	11	89
-0.5	9.1.1_1	59	41	25	75
-1 + 0.5	1.1.1_2	98	2	6	94
-1 + 0.5	5.1.1_1	100	0	0	100
-1 + 0.5	7.1.1_1	85	15	7	93
-1 + 0.5	9.1.1_1	100	0	5	95
-2 + 1	5.1.1_1	100	0	2	98
-3.5 + 2	2.1.1_1	72	28	22	78
-6.3 + 3.15	1.1.1_1	100	0	0	100
-6.3 + 3.15	3.1.1_1	87	13	30	70
-10+ 8	1.1.1_1	100	0	0	100
-10+ 8	2.1.1_1	83	17	20	80
-12 + 10	1.1.1_1	89	11	17	83
-12 + 10	1.5.1_1	87	13	9	91
-12 + 10	3.3.1_1	91	9	11	89

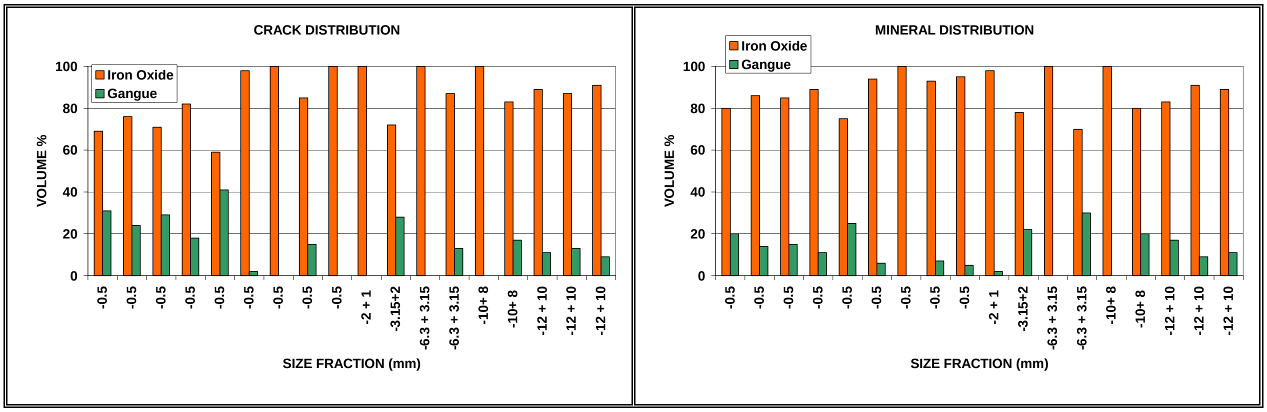

Figure 61: Graphical representation of crack association in the different size fractions of Northern Cape OT 2.

Table 15: Crack association in the different size fractions of Northern Cape OT 4 as determined from SEM images.

Size Fraction,mm	Image Ref No.	% Cracks assoc. with iron oxide	%Cracks assoc. with gangue	% v/v Gangue	% v/v iron oxide
-12.5 + 10	2.10.1_1	20	80	27	73
-12.5 + 10	2.2.1_1	65	35	53	47
-2+1	1.1.1_1	100	0	0	100
-2+1	6.1.1_1	74	26	35	65
-6.3+3.15	3.1.1_1	100	0	7	93

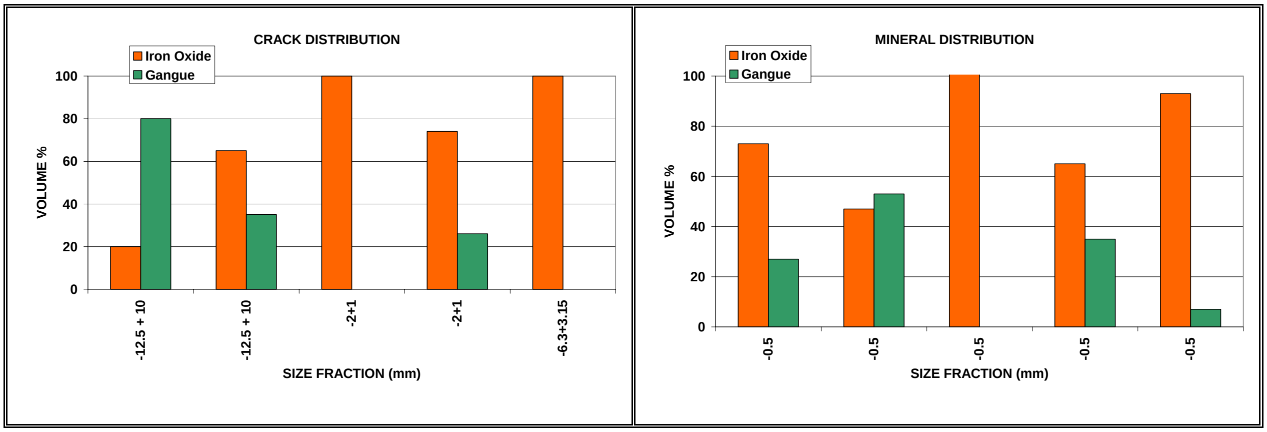

Figure 62: Graphical representation of the crack association in the different size fractions of Northern Cape OT 4.

Table 16: Crack association in the different size fractions of Northern Cape OT 5 as determined from SEM images.

Size Fraction,mm	Image Ref No.	% Cracks assoc. with iron oxide	%Cracks assoc. with gangue	% v/v Gangue	% v/v iron oxide
-0.5	1.1.1_1	97	3	8	92
-1 + 0.5	5.1.1_1	87	13	17	83
-1 + 0.5	8.1.1_1	72	28	35	75
-2+1	10.1.1_1	29	71	80	20
-2+ 1	12.1.1_1	86	14	10	90
-3.15 + 2	1.1.1_1	83	17	25	75
-3.15+ 2	5.2.2_1	61	39	28	72
-10+8	1.5. 1_1	68	32	35	75
-12+10	2.1.1_1	77	23	18	82

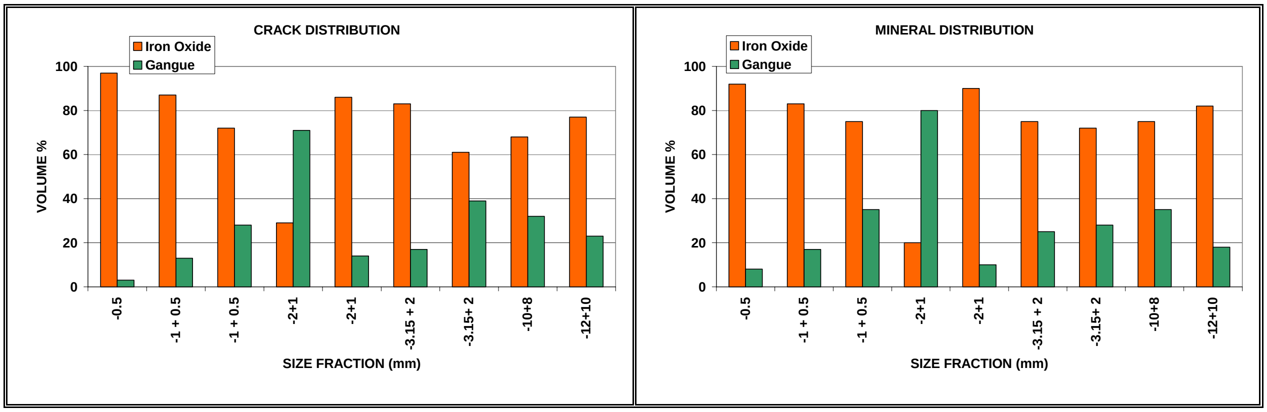

Figure 63: Graphical representation of the crack association in the different size fractions of Northern Cape OT 5.

Table 17: Results of the crack association in the different size fractions of Northern Cape OT 6 as determined from SEM images.

Size Fraction,mm	Image No.	% Cracks assoc. with iron oxide	%Cracks assoc. with gangue	% v/v Gangue	% v/v iron oxide
-0.5	4.1.1_1	84	16	30	70
-1 + 0.5	4.1.1_1	89	11	22	78
-2 +1	6.1.1_1	85	15	29	71
-3.5+ 2	10.1.1_1	73	27	38	62
-6.3+ 3.15	1.2.1_1	71	29	25	75
-8+ 6.3	1.2.1_1	75	25	27	73
-10+ 8	3.3.2_1	100	0	6	94

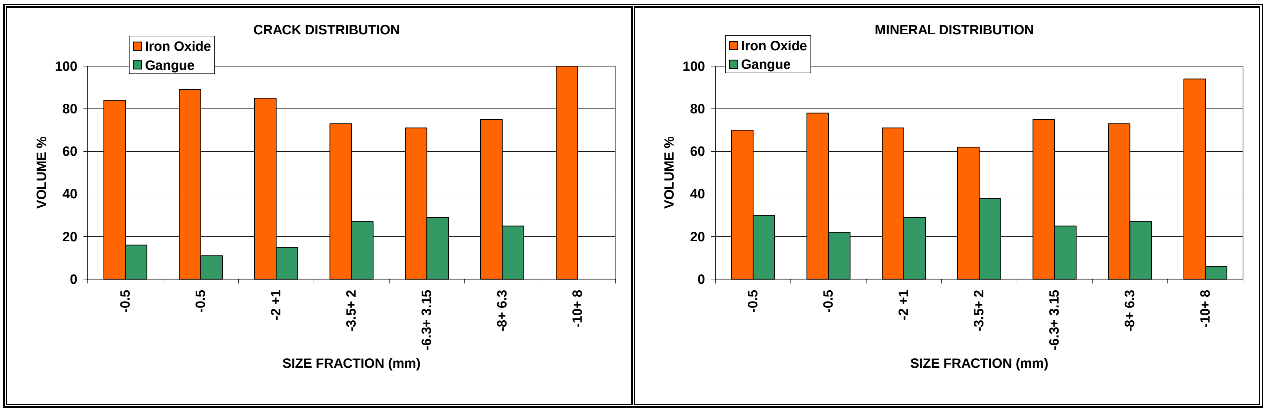

Figure 64: Graphical representation of the crack association in the different size fractions of Northern Cape OT 6.

3.3 HIGH TEMPERATURE MICROSCOPE REDUCTION TESTS

During the high temperature test a video recording was made for the duration of the test. This was evaluated afterwards for crack generation and propagation. During three of the tests the first crack was generated during the warming up cycle. The rest of the tests indicated that the first crack only appears 12-30 minutes after the reduction gas has been introduced. Only one sample (sample 1) demonstrated catastrophic cracking[§§]

[§§] Catastrophic Cracking – Sample forms huge cracks and physically breaks into two ore more portions

(**Figure 65**) during the test. Most of the samples cracked only once. Volume expansion was noticed in the form of cracks widening after the initial cracking took place.

Propagation of a crack was only observed in one sample (Sample 16). To confirm these initial results, the test was repeated under an inert atmosphere. No cracking was observed. The reduction time was also increased to see whether new cracking (due to increased reduction at the crack face) would commence after a while. However, the same tendency as in the original tests was observed. The influence of reduction gas and temperature on the crack formation and propagation was also tested by using H_2 as the reduction gas (Test 18-20) and increasing the temperature to 700ºC (Test 21). The data captured on video was evaluated and the cracks were defined as “large” cracks (Cracks that would lead to failure during tumbling), “internal” cracks (thin/hairline cracks that would not lead to failure) and “border” cracks (cracks on the edges of sample that would cause fine particles to spall of the edges of the sample). A summary of the results of the high temperature microscope test is given in **Table 18**. **Figure 65**-**Figure 85** is optical microscope photos of the cracks observed during the tests. **Table 19** is a summary of the SEM analysis of the samples after reduction in the high temperature microscope.

Table 18: Summary of the cracks observed during and after reduction tests in high temperature microscope.

Sample No.	Sample Name	Time before 1st crack	No. of large cracks	No. of cracks growing from large cracks	Internal cracks	Border cracks
1	Northern Cape OT 5	17	3	5	6	5
2	Northern Cape OT 2	0	2	3	2	2
3	Northern Cape OT 4	15	0	0	1	3
6	Northern Cape OT 2	0	4	3	2	5
8	Northern Cape STD	26	0	0	3	2
10	Northern Cape OT 4	0	2	0	2	3
12	Northern Cape OT 2	1	1	0	1	1
13	Northern Cape	21	1	0	0	4

	STD					
14	Northern Cape OT 5	16	1	3	1	2
15	Northern Cape OT 5	12	1	2	3	6
16	Northern Cape STD	18	3	5	8	5
17	Northern Cape OT 4	12	2	0	2	3
18	Northern Cape STD	30	3	4	3	5
19	Northern Cape STD	-	0	0	0	0
20	Northern Cape STD	30	3	0	4	2
21	Northern Cape STD	34	0	0	0	2

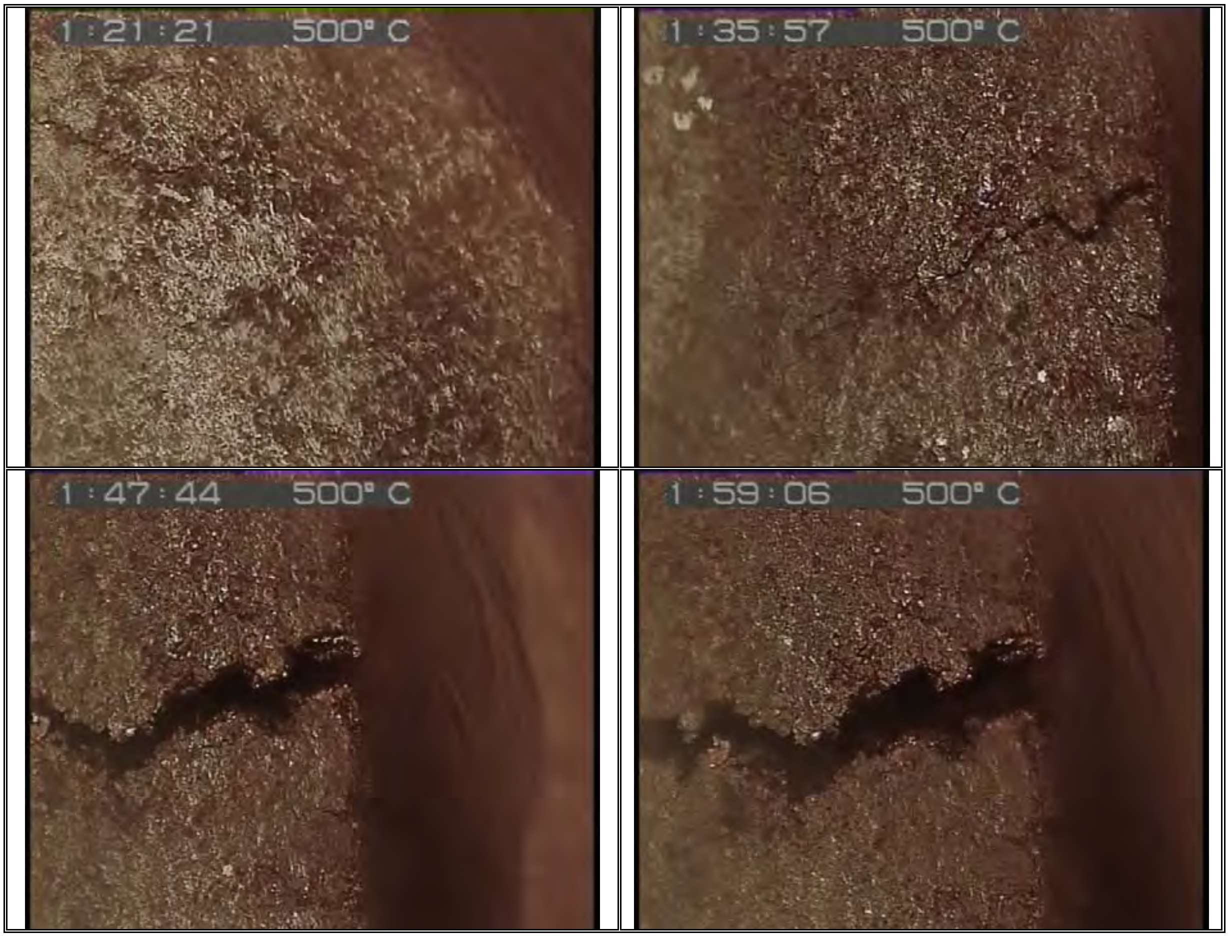

Figure 65: Optical microscope image during the high temperature microscope reduction test of Sample 1

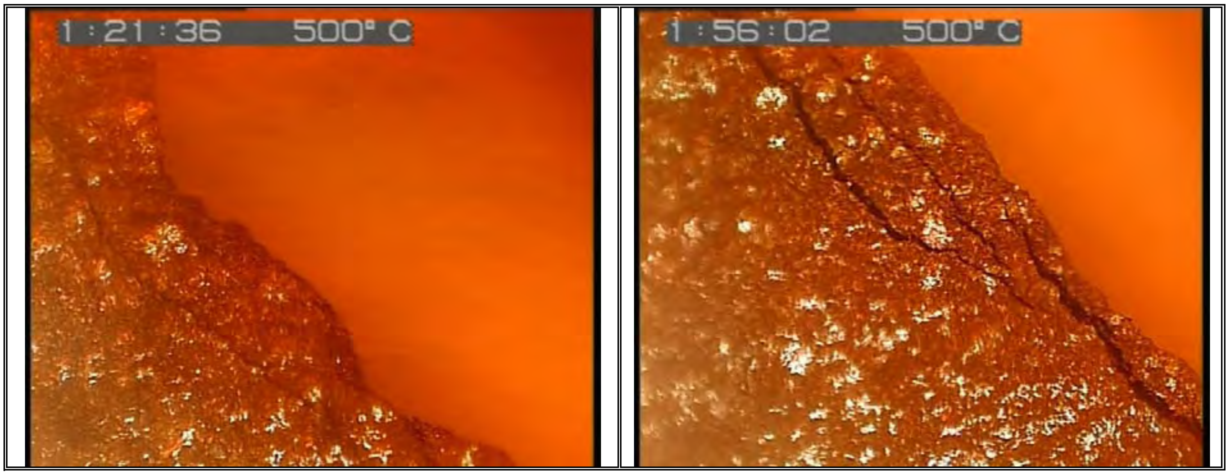

Figure 66: Optical microscope image during the high temperature microscope reduction test of Sample 13.

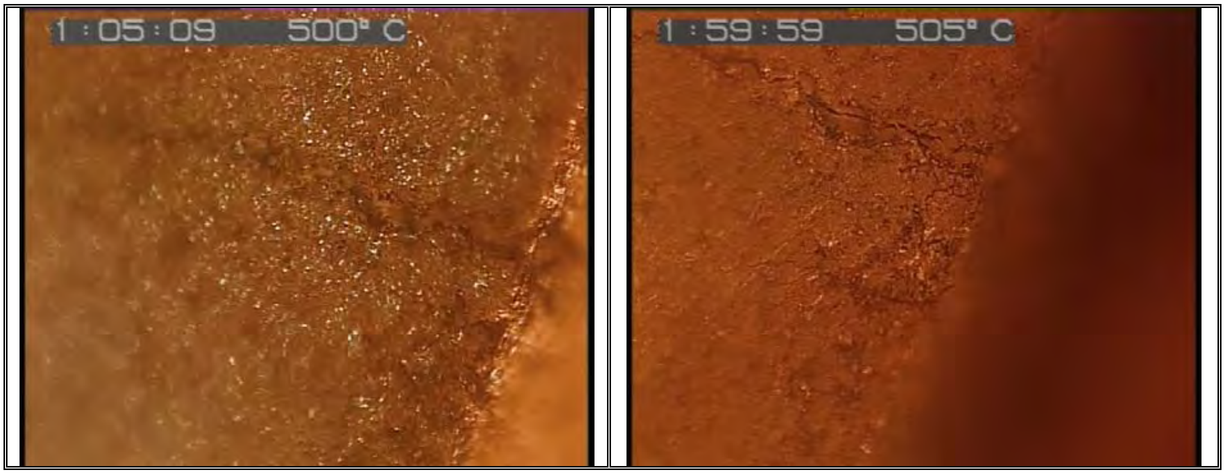

Figure 67: Optical microscope image during the high temperature microscope reduction test of Sample 14.

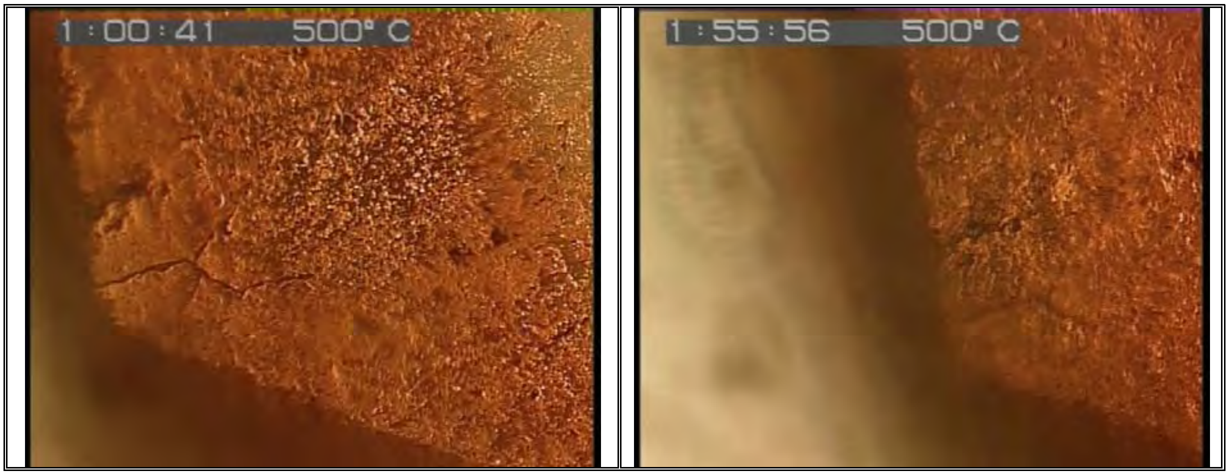

Figure 68: Optical microscope image during the high temperature microscope reduction test of Sample 15.

Figure 69: Optical microscope image during the high temperature microscope reduction test of Sample 16.

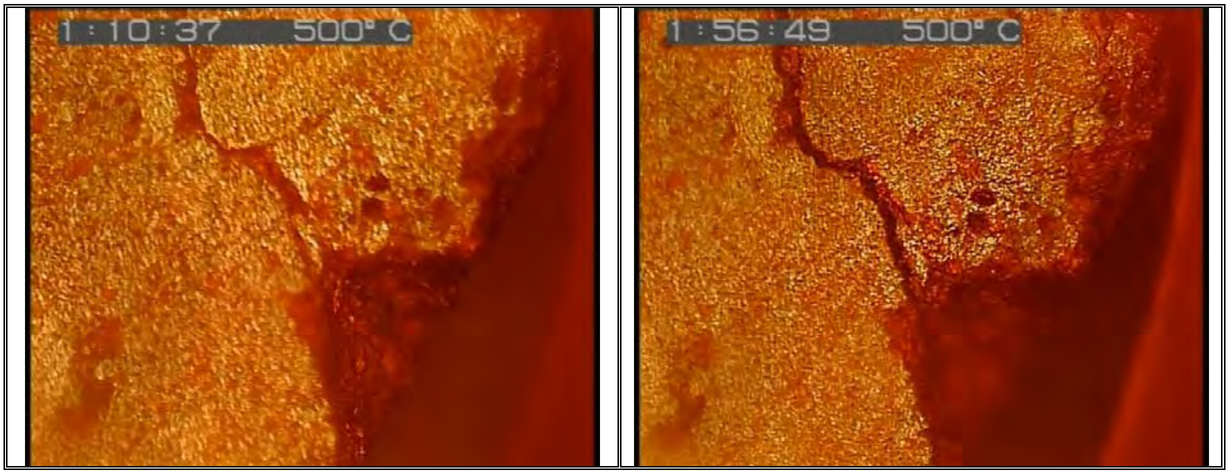

Figure 70: Optical microscope image during the high temperature microscope reduction test of Sample 16.

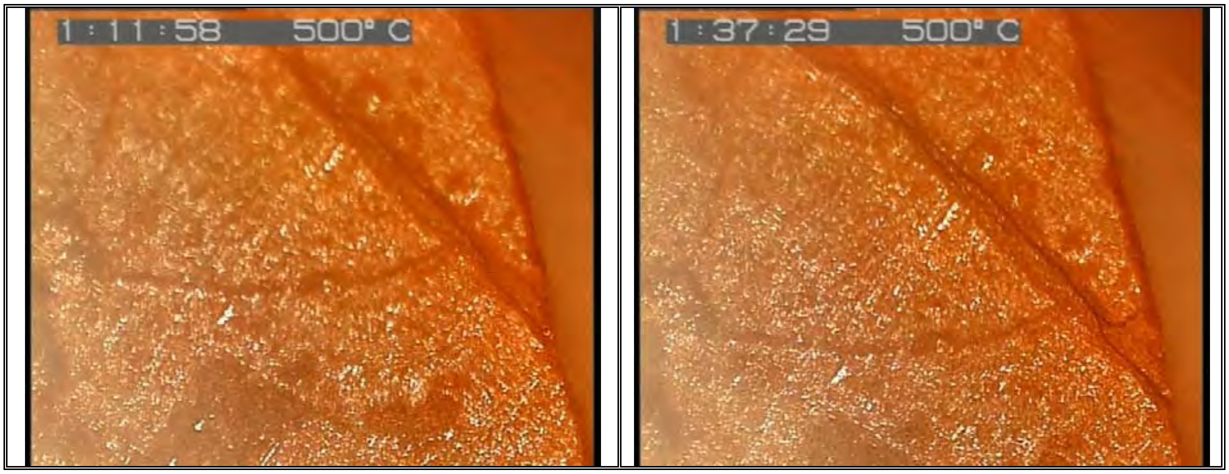

Figure 71: Optical microscope image during the high temperature microscope reduction test of Sample 17.

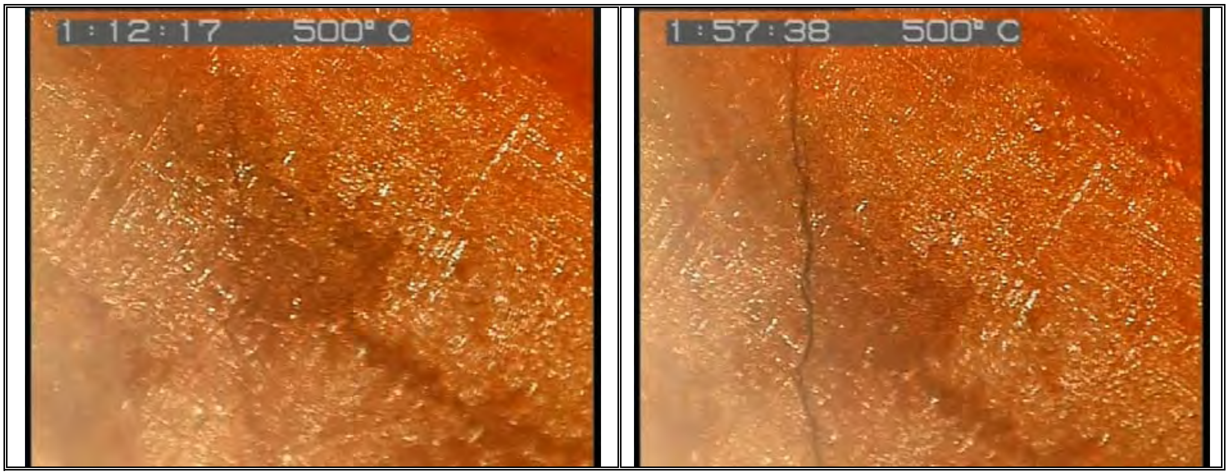

Figure 72: Optical microscope image during the high temperature microscope reduction test of Sample 17.

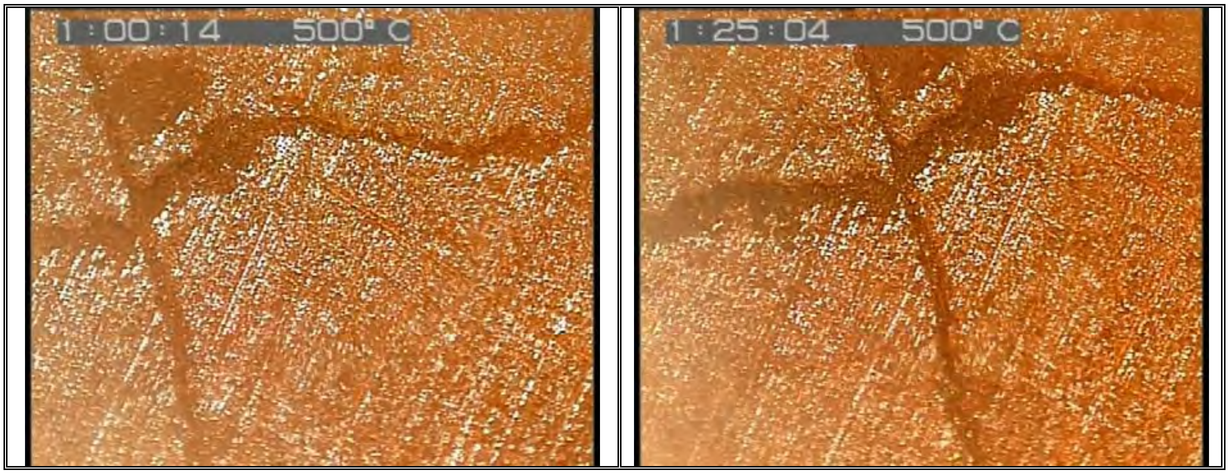

Figure 73: Optical microscope image during the high temperature microscope reduction test of Sample 17.

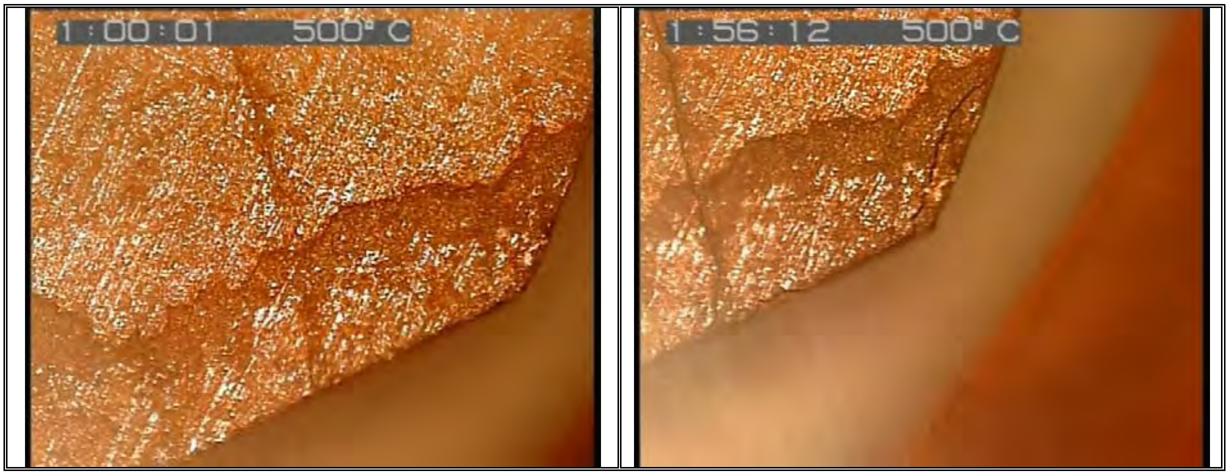

Figure 74: Optical microscope image during the high temperature microscope reduction test of Sample 17.

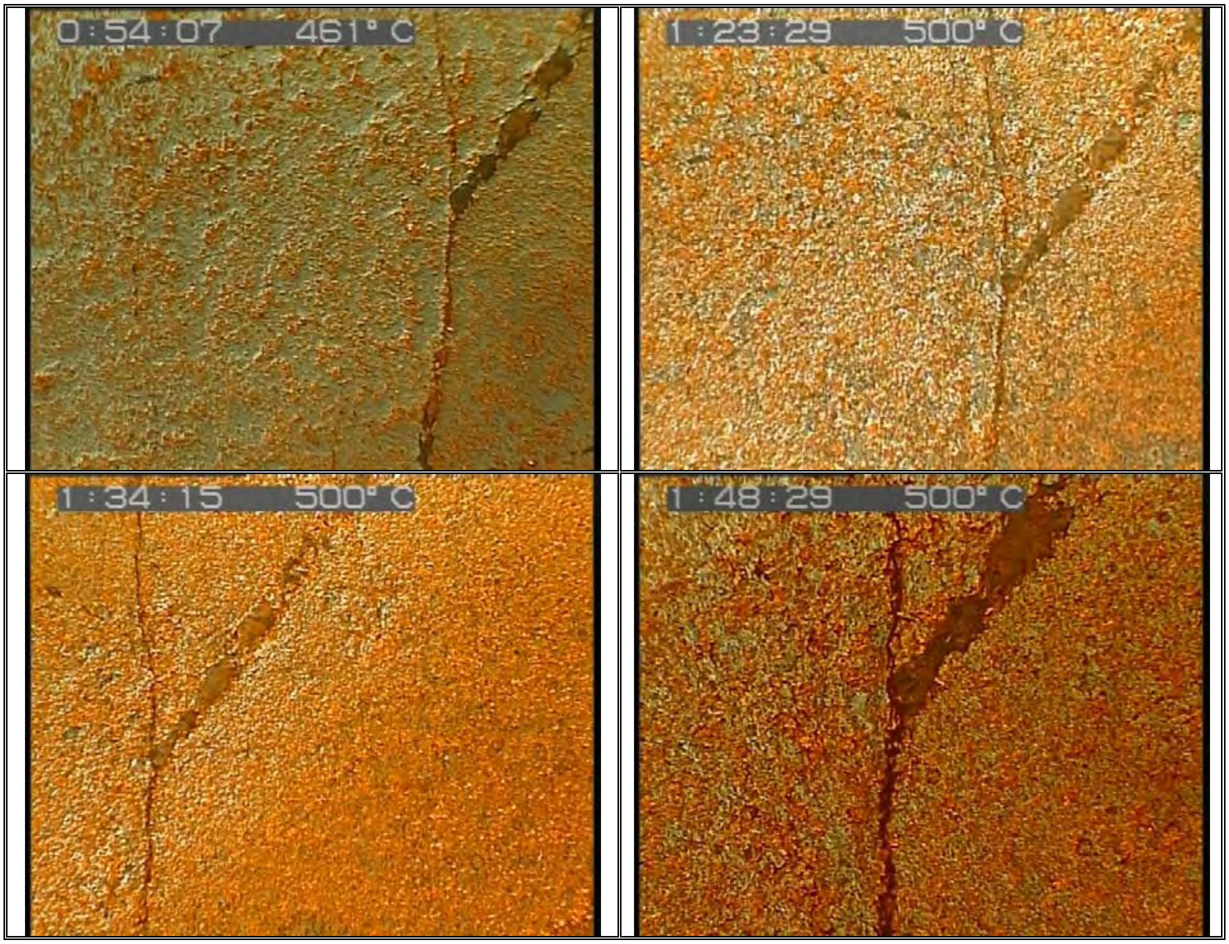

Figure 75: Optical microscope image during the high temperature microscope reduction test of Sample 18.

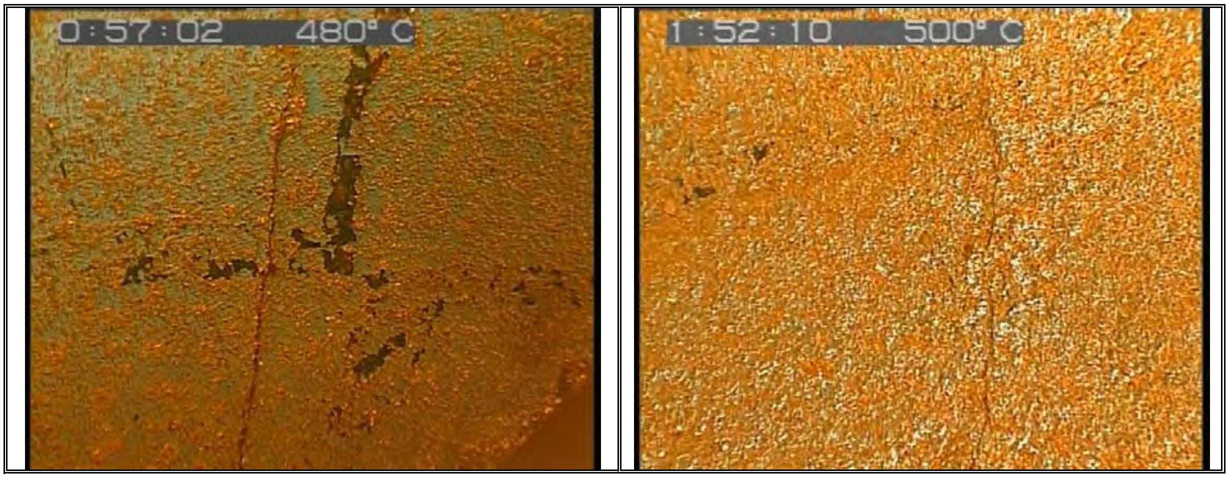

Figure 76: Optical microscope image during the high temperature microscope reduction test of Sample 18.

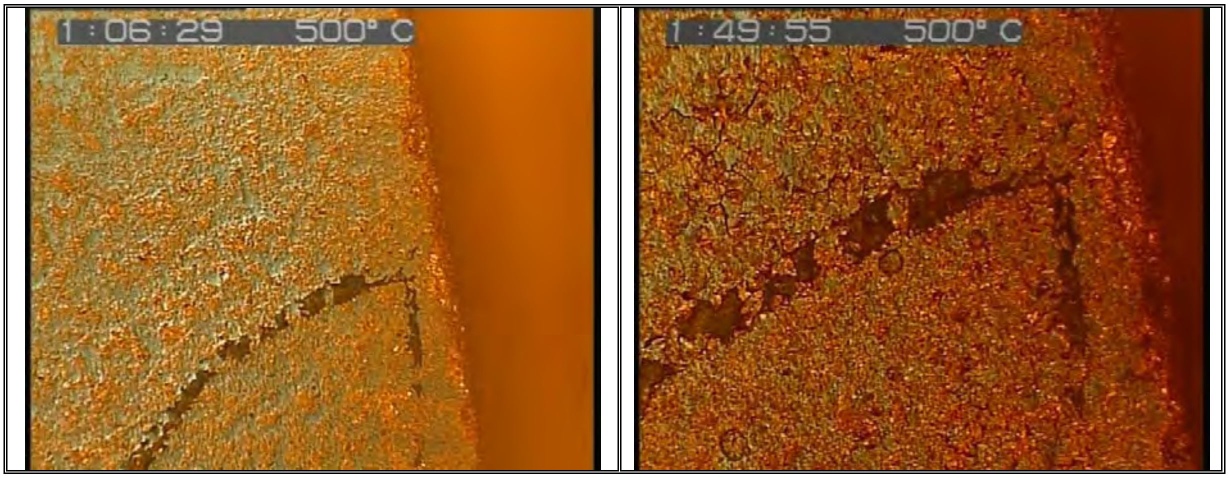

Figure 77: Optical microscope image during the high temperature microscope reduction test of Sample 18.

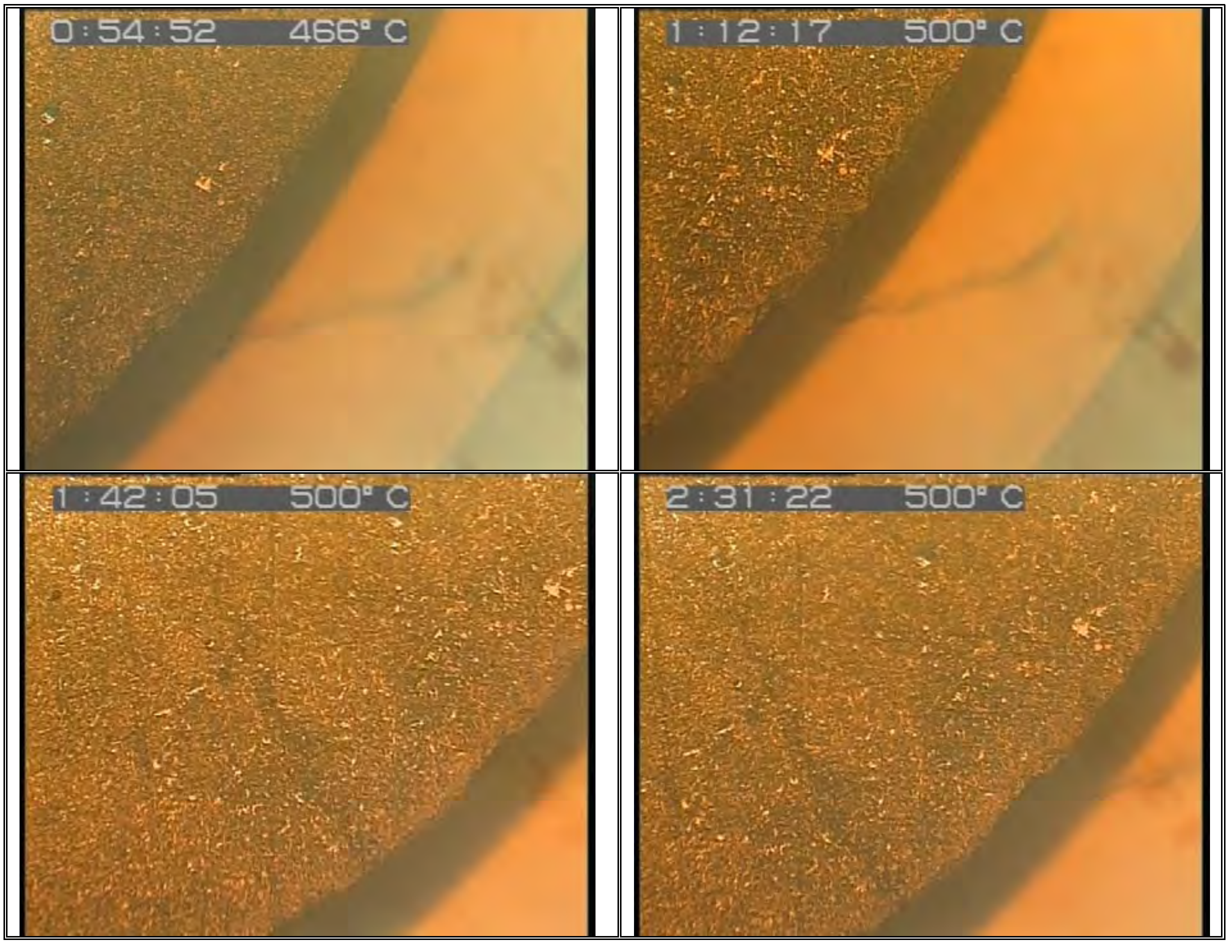

Figure 78: Optical microscope image during the high temperature microscope reduction test of Sample 19.

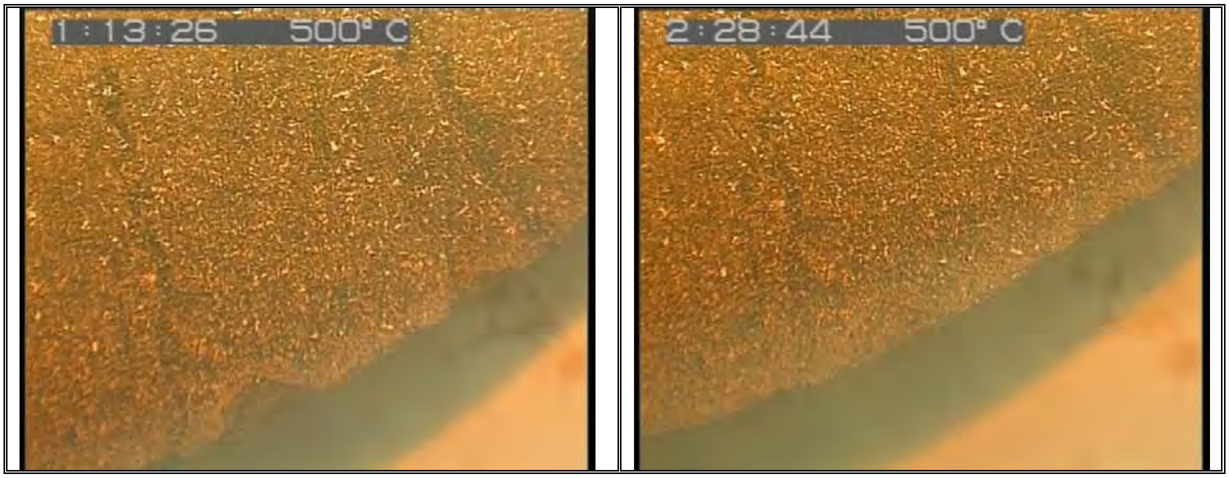

Figure 79: Optical microscope image during the high temperature microscope reduction test of Sample 19.

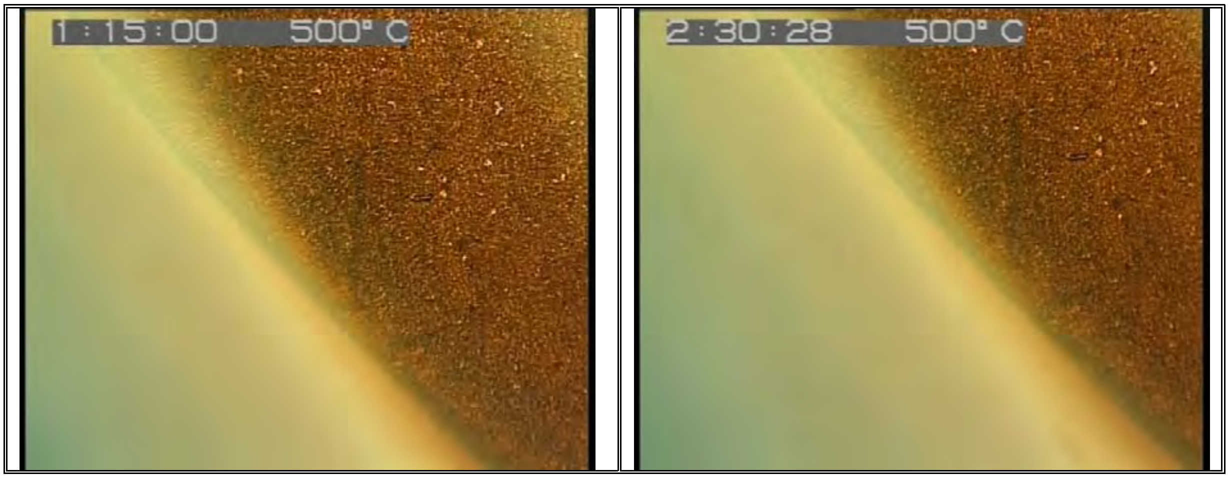

Figure 80: Optical microscope image during the high temperature microscope reduction test of Sample 19.

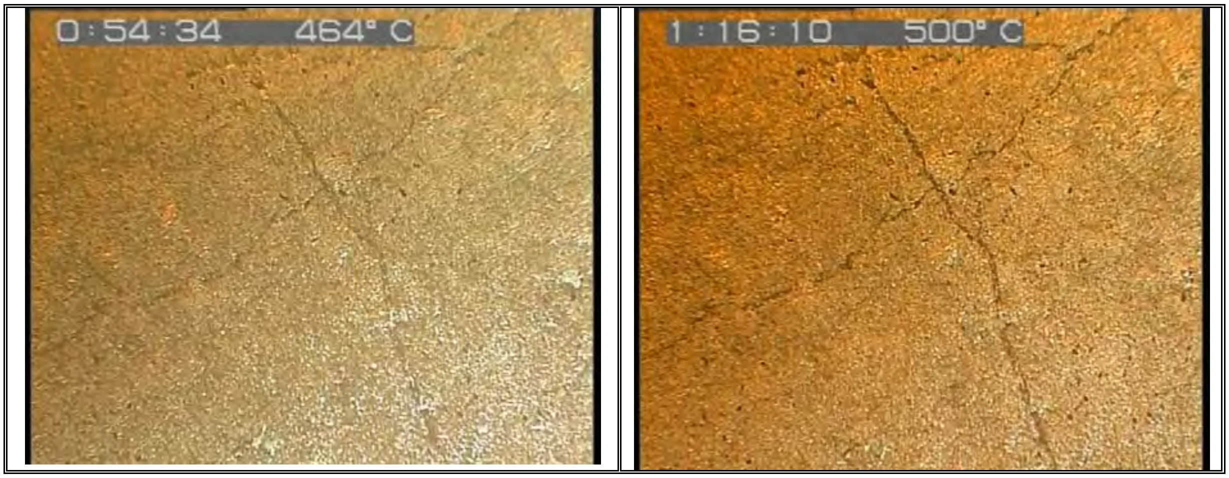

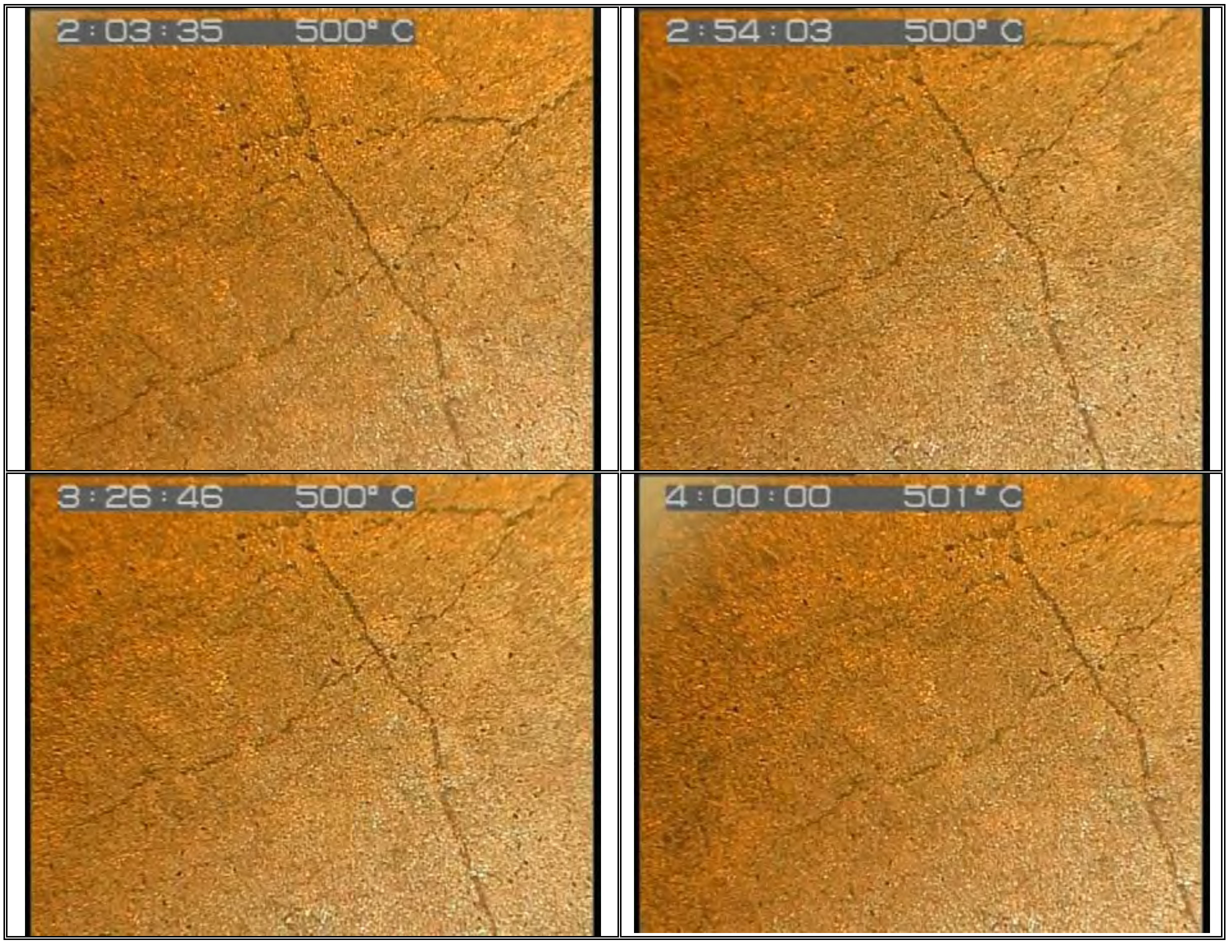

Figure 81: Optical microscope image during the high temperature microscope reduction test of Sample 20.

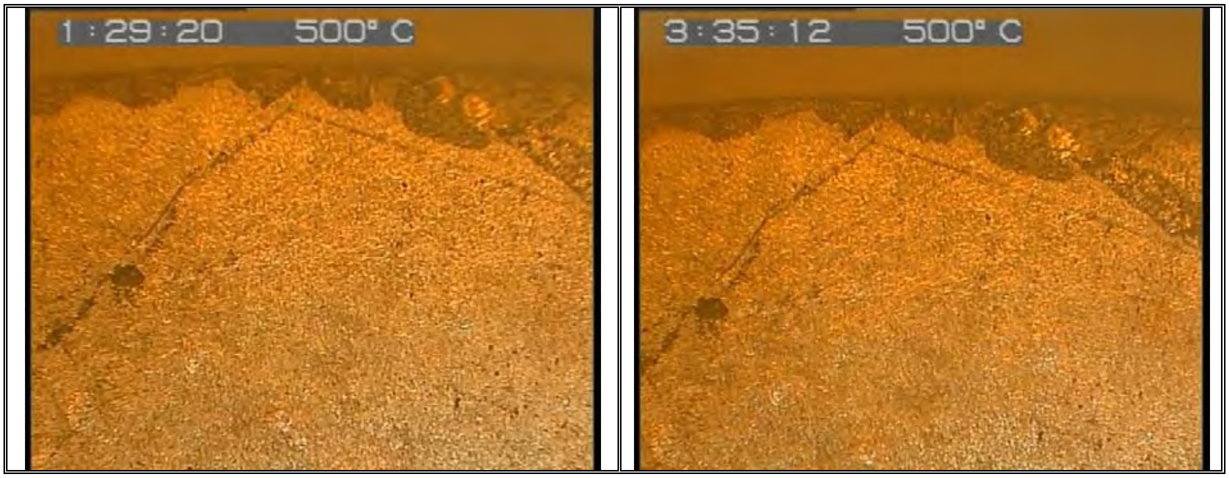

Figure 82: Optical microscope image during the high temperature microscope reduction test of Sample 20.

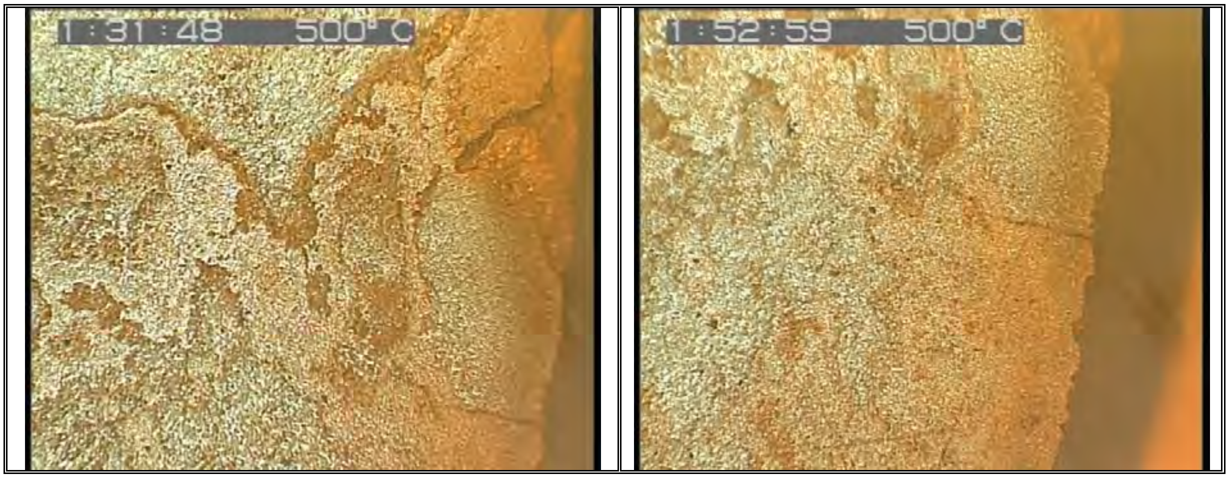

Figure 83: Optical microscope image during the high temperature microscope reduction test of Sample 20.

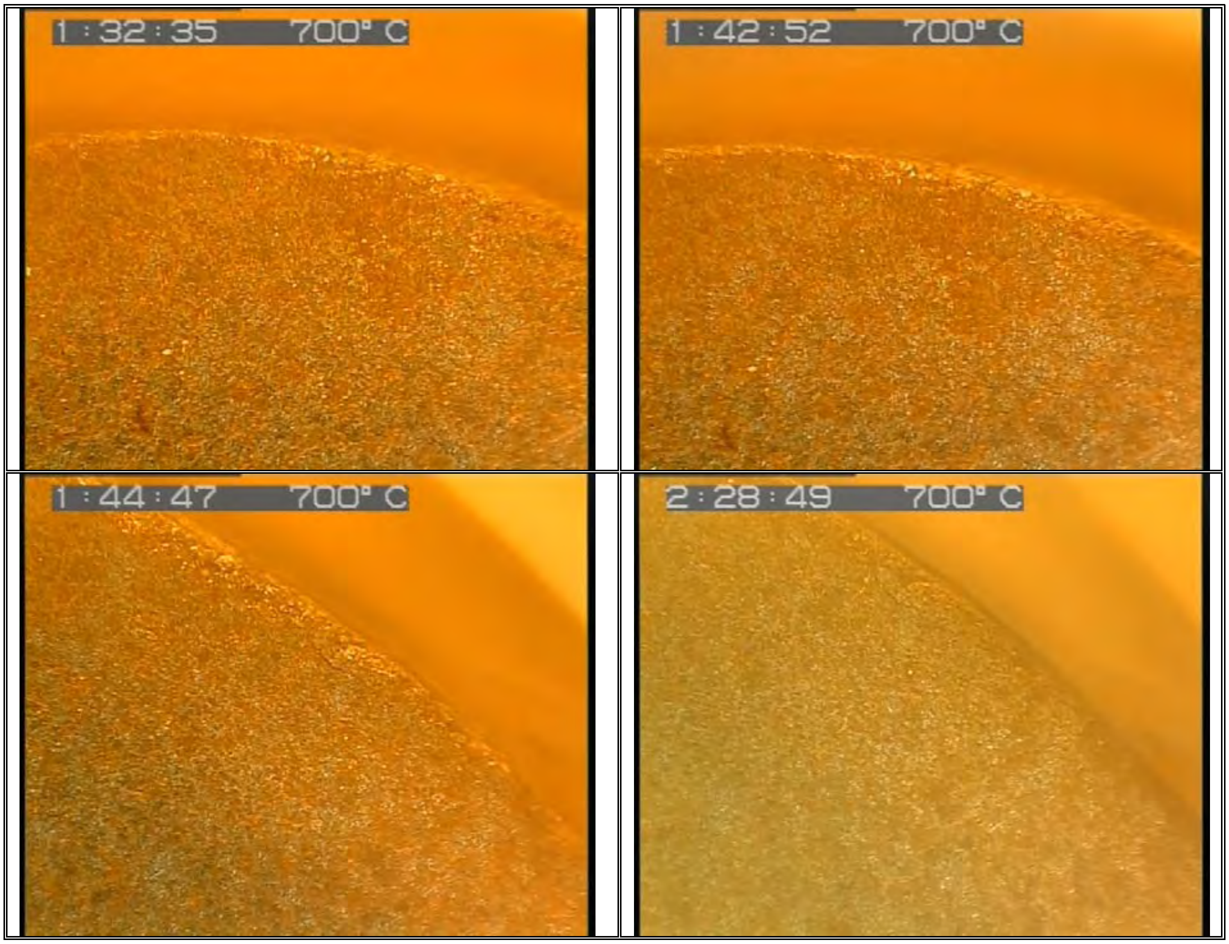

Figure 84: Optical microscope image during the high temperature microscope reduction test of Sample 21.

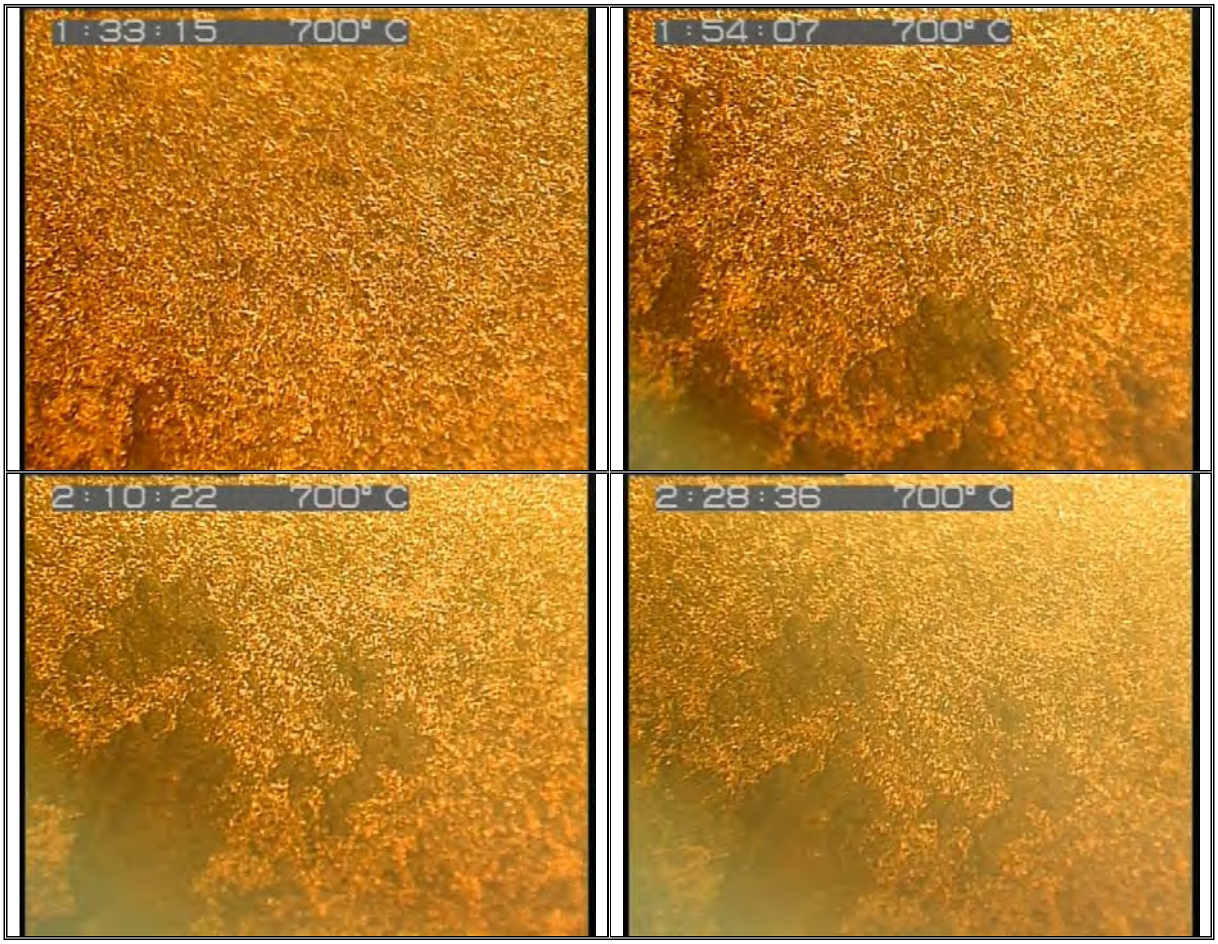

Figure 85: Optical microscope image during the high temperature microscope reduction test of Sample 21.

Table 19: Summary of SEM-analysis of iron ore samples after reduction under high temperature microscope.

Sample No.	Sample Name	Group	Gangue	Porosity	Fracture type
1	Northern Cape OT 5	Poly-mineralic samples	Apatite/Quartz	Low	Extensive, throughout the sample
2	Northern Cape OT 2	Porous	-	Variable	Regular network[***]
3	Northern Cape OT 4	Mono-mineralic hematite samples	-	Low	Perpendicular to edge
6	Northern Cape OT 2	Other	Quartz	Low	Parallel to foliation
8	Northern Cape STD	Mono-mineralic hematite samples	-	Low	Perpendicular to edge
10	Northern Cape OT 4	Poly-mineralic samples	Quartz/Muscovite	Low	Parallel to edge
12	Northern Cape	Mono-mineralic	-	Low	Parallel/Perpenducular

[***] Regular network - network of fractures that occur at right angles to each other.

	OT 2	hematite samples			to edge
13	Northern Cape STD	Mono-mineralic hematite samples	-	Low	Parallel/Perpenducular to edge
14	Northern Cape OT 5	Poly-mineralic samples	Apatite/Quartz	Low	Parallel/Regular network to edge
15	Northern Cape OT 5	Poly-mineralic samples	Al-Silicates	Low	None
16	Northern Cape STD	Porous	-	Low	Associated with Specularite
17	Northern Cape OT 4	Mono-mineralic hematite samples	-	Low	Parallel to edge
18	Northern Cape STD	Poly-mineralic samples	Apatite/Quartz	Medium, small pores	Perpendicular/Parallel
19	Northern Cape STD	Poly-mineralic samples	Muscovite/Apatite	Low	Parallel
20	Northern Cape STD	Mono-mineralic hematite samples	Muscovite	Low	Perpendicular
21	Northern Cape STD	Mono-mineralic hematite samples	Muscovite	Small pores and large infill pores	Perpendicular/Parallel

3.4 SEM ANALYSIS

When observing samples under the SEM that have undergone deformation, with the aim of understanding the mechanisms of deformation and metamorphism, one must be mindful of the fact that the sample is only being observed in two dimensions whilst deformation has taken place in three dimensions.

In this study we only observe brittle deformation mechanisms in samples comprising predominantly of hematite with minor amounts of gangue minerals. This indicate that although the samples were between 500°C and 700°C, the stresses induced due to the reduction process taking place led to brittle cracks and that no shearing took place. **Appendix 1** list the minerals identified in this study. In this study, most samples consist predominantly of hematite and the small amount of gangue minerals present is unlikely to have an influence on the overall stress supporting network.

Each sample is discussed and described individually (**Appendix 4**). The samples were classified into four distinct groups according to the predominant feature observed in the sample. Samples were allocated into the following groups:

1. Mono-mineralic hematite samples	(Samples 3, 8, 12, 13, 17, 20, 21)
2. Poly-mineralic samples	(Samples 1, 10, 14, 15 18, 19)
3. Porous samples	(Samples 2 and 16)
4. Other	(Sample 6)

3.4.1 GROUP 1: MONO-MINERALIC HEMATITE SAMPLES

These samples consist primarily of hematite and they have very similar physical and micro-fracture characteristics. The samples have low porosity with very little or no gangue minerals present.

In these samples fractures occurs mainly perpendicular to the sample edges – the first place in which reduction occurs. The fractures only penetrate as far as the sample has been reduced. When internal fractures do occur, they are present in a network of fractures that occur at right angles to each other – commonly known as a regularly spaced framework.

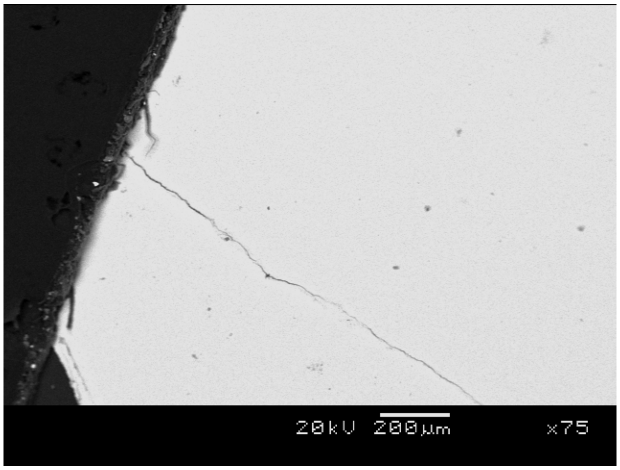

Figure 86: Electron backscatter image of sample 3 showing the homogeneity of the sample. The sample is essentially mono-mineralic and comprises almost exclusively of hematite. Small radial fractures occur at the edge of the sample, where it has been reduced.

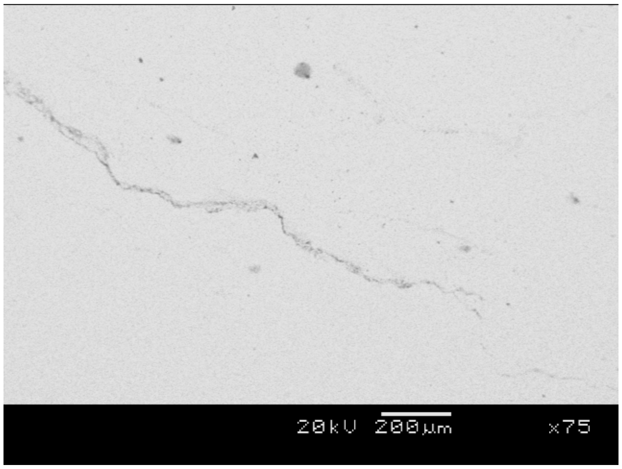

Figure 87: Electron backscatter image of sample 3 showing a rare internal fracture. This fracture is not associated with gangue minerals, porosity or reduction.

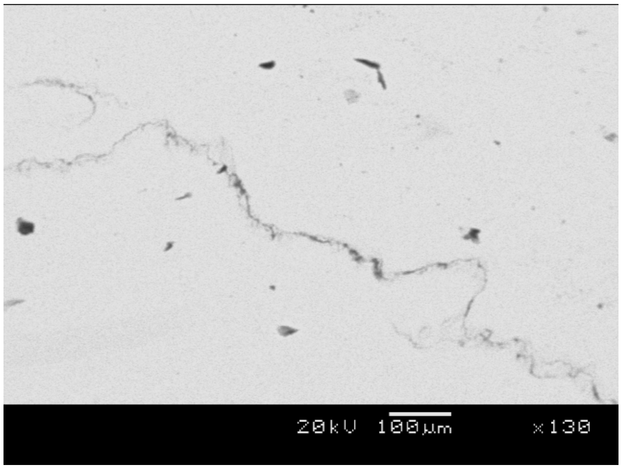

Figure 88: Electron backscatter image of sample 3 showing a pre-existing fracture filled with muscovite.

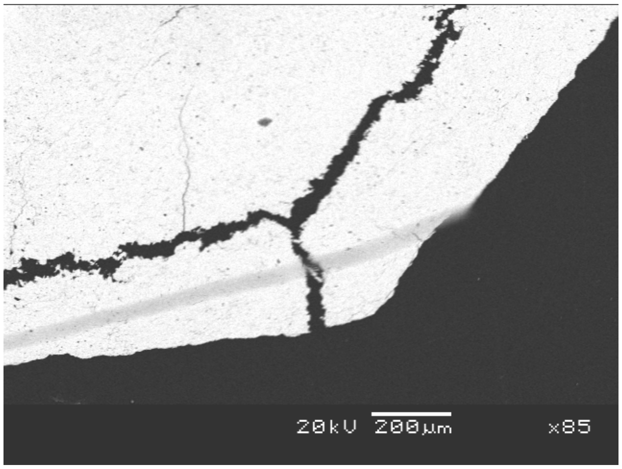

Figure 89: Electron backscatter image of sample 12 showing large fractures perpendicular and parallel to the edge of the sample. Smaller fractures occur perpendicular to the edge of the sample.

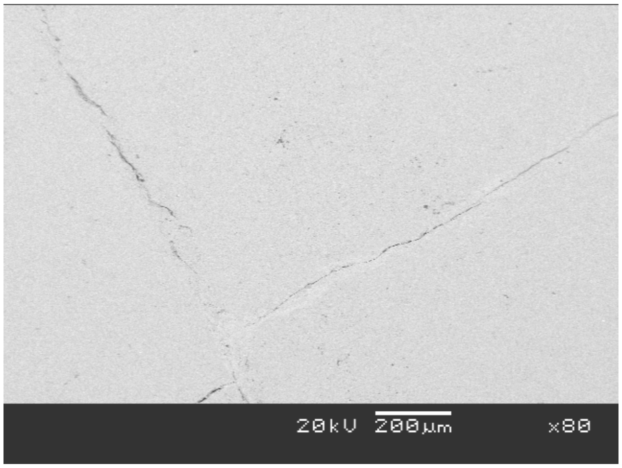

Figure 90: Electron backscatter image of sample 17 showing regularly spaced fracture/joint set in the sample.

3.4.2 GROUP 2: POLY-MINERALIC SAMPLES

This group of samples have a significant proportion of gangue minerals. The results from the various samples in this group indicates that the presence of gangue minerals alone do not cause fractures to form. However, the gangue minerals do influence the direction and intensity of fractures and gangue minerals. Especially quartz, that is much harder than hematite tend to fracture more easily than hematite.

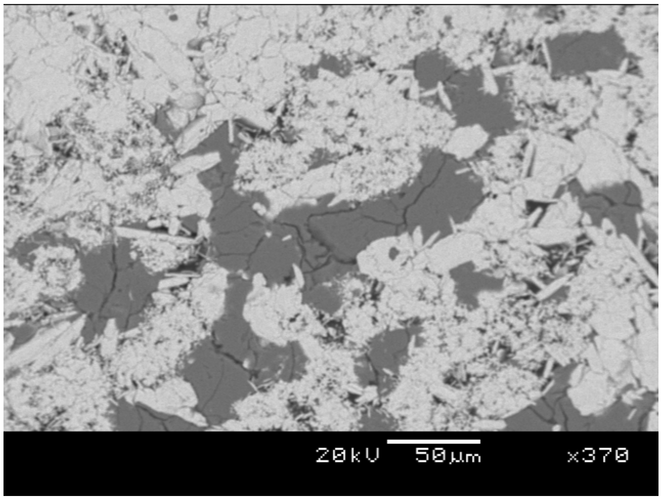

Figure 91: Electron backscatter image of sample 1 showing fractures originating and terminating within quartz (grey) without extending into the surrounding hematite.

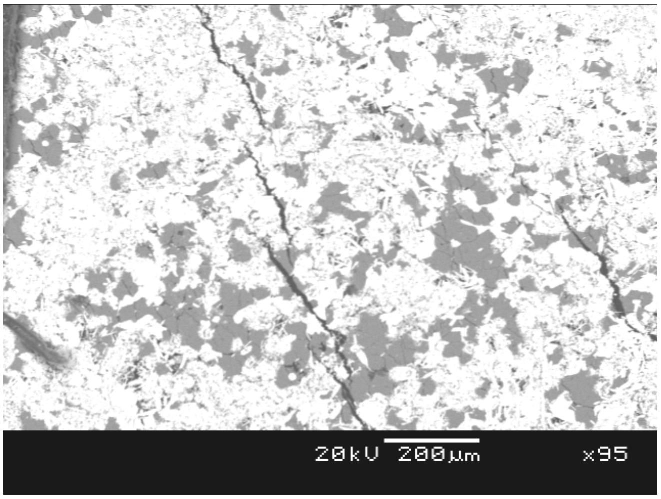

Figure 92: Electron backscatter image of sample 1 showing large fractures that do not appear to be influenced by the sample mineralogy. The fractures propagate through both gangue and ore minerals.

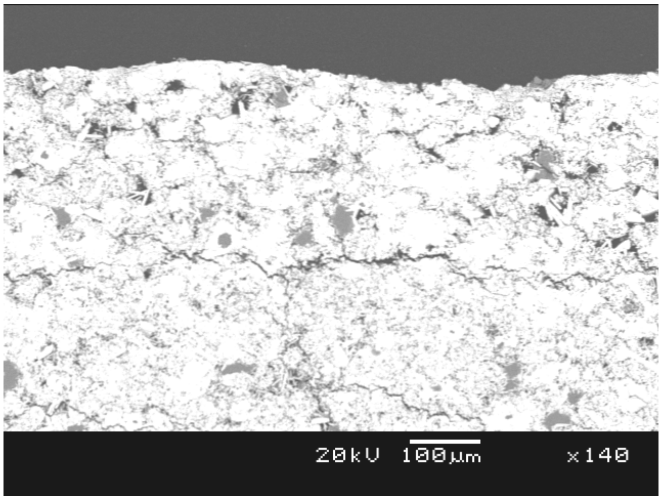

Figure 93: Electron backscatter image of sample 1 showing regularly spaced fractures at the edge of the sample, related to the volume change during the reduction of hematite to magnetite.

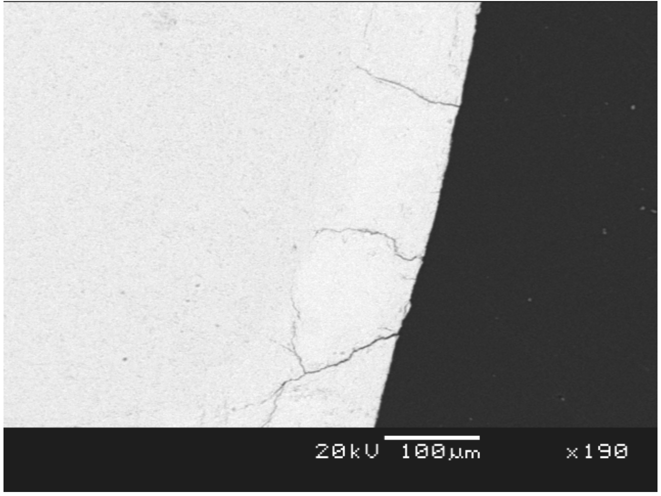

Figure 94: Electron backscatter image of sample 10 showing the development of fractures along the edge of the samples, where it has been reduced. The stippled line indicates where the sample has been reduced.

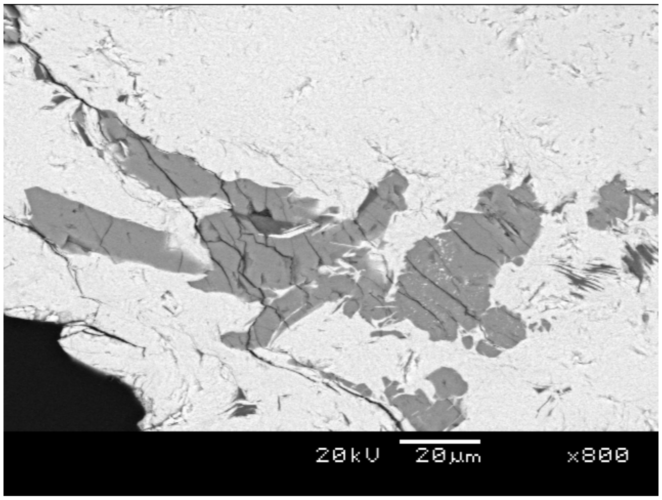

Figure 95: Electron backscatter image of sample 10 showing the development of fractures in quartz. The secondary fractures do not extend into the surrounding hematite.

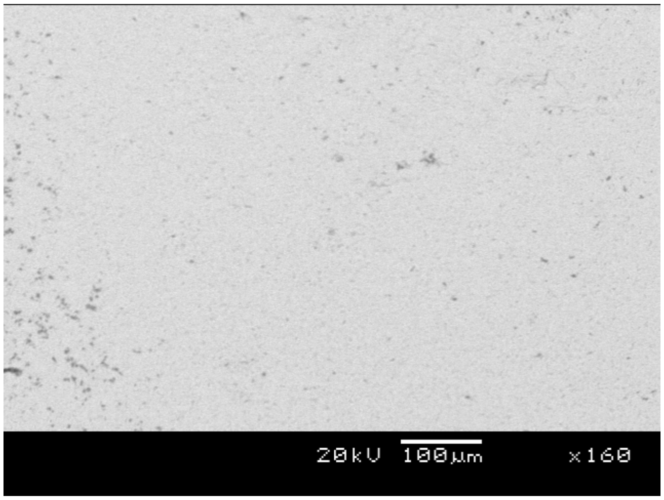

Figure 96: Electron backscatter image of sample 10 showing an area within the sample where no reduction or fracturing has occurred.

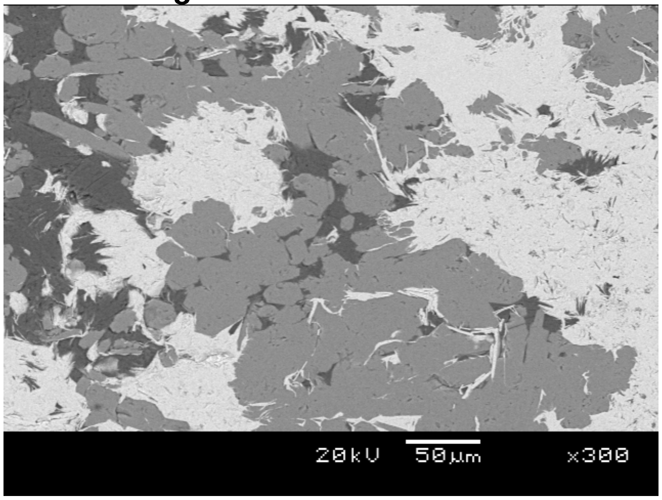

Figure 97: Electron backscatter image of sample 10 showing intergrown hematite and gangue. The presence of gangue phases does not necessarily lead to fracture formation.

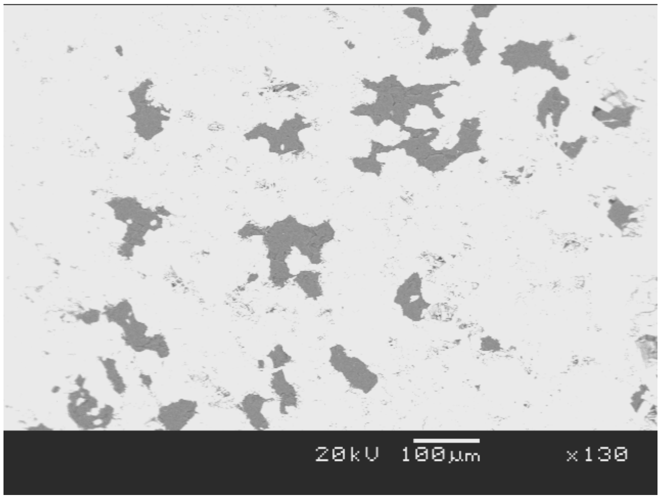

Figure 98: Electron backscatter image of sample 14 showing intergrown hematite and quartz in the center of the sample. There are o fractures observed here as no reduction has been able to occur with the low sample porosity.

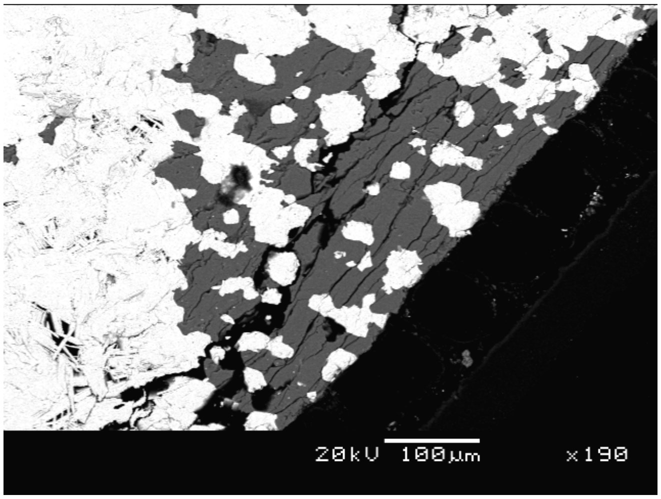

Figure 99: Electron backscatter image of sample 14 showing fractures developed at the edge of the sample where reduction has occurred. Notice how the gangue allows for more extensive development of the fracture network that does not extend into the surrounding hematite.

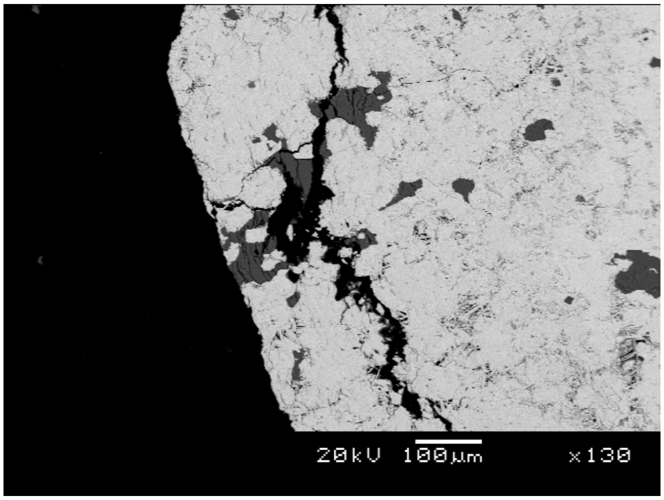

Figure 100: Electron backscatter image of sample 14 showing fractures developed along the edge of the sample where it has been reduced. Where a fracture intersects gangue minerals the gangue appears to facilitate the development of fractures.

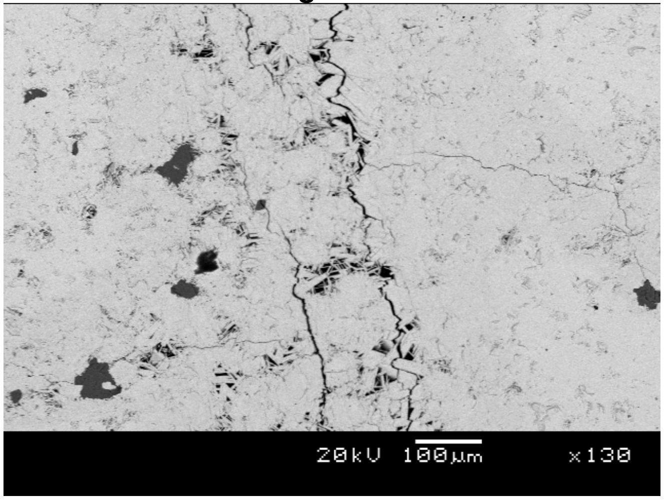

Figure 101: Electron backscatter image of sample 14 showing fractures developed within the sample. The fractures appear to join open pores where reduction has occurred.

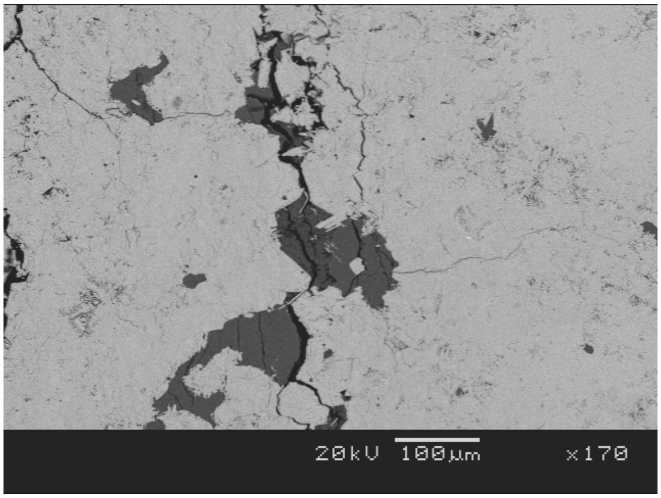

Figure 102: Electron backscatter image of sample 14 showing fractures developed within the sample. Where a fracture intersects gangue minerals the gangue appears to facilitate the development of fractures that do not extend into the surrounding hematite.

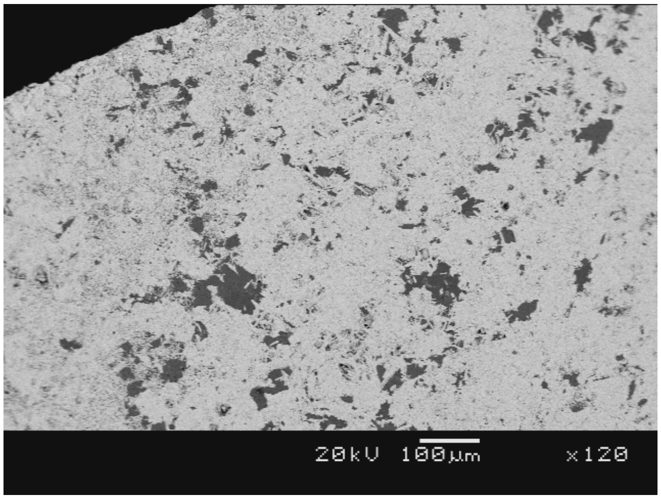

Figure 103: Electron backscatter image of sample 15 showing intergrown hematite and gangue with very low porosity and no visible fractures, even at the edge of the sample where fractures are unusually prolific.

3.4.3 GROUP 3: POROUS SAMPLES

Only two porous samples were identified in the study. Sample 2 consists of bands of acicular hematite with very high porosity whilst sample 16 has a homogenous high-porosity texture throughout the sample. Neither sample exhibits extensive fracturing. One could argue that the numerous open voids present in the samples could possibly accommodate for the volume change that takes place during reduction and thus less fracturing is observed in these samples.

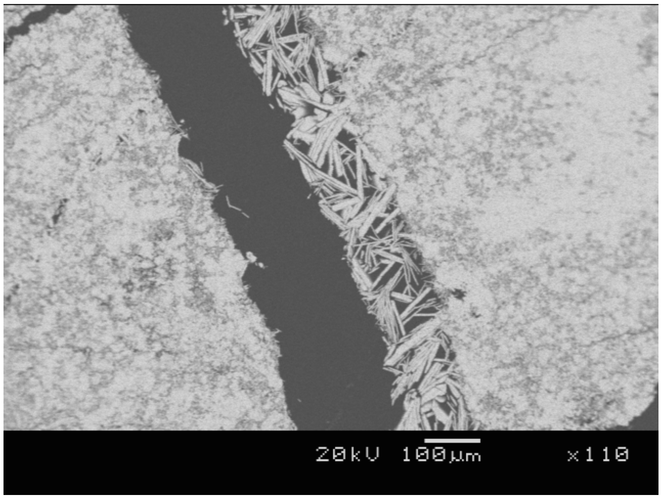

Figure 104: Electron backscatter image of sample 2 showing a very large fracture that has occurred at a boundary between granular hematite (left) and porous specularite (acicular hematite).

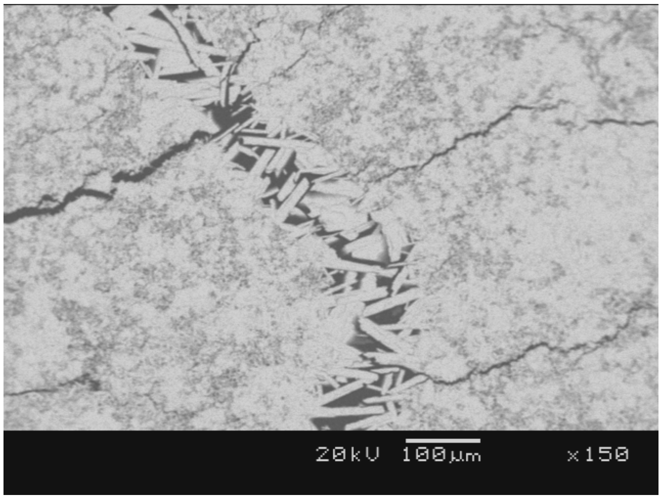

Figure 105: Electron backscatter image of sample 2 showing large fractures originating/terminating in areas of low porosity.

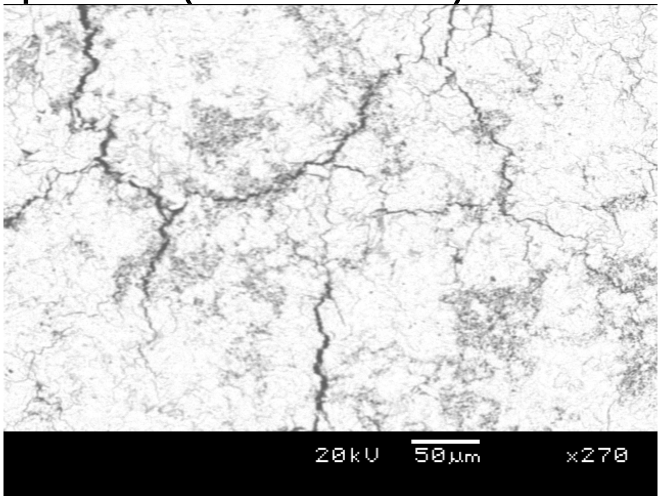

Figure 106: Electron backscatter image of sample 2 showing a network or regularly spaced and oriented fractures formed in an area of dense homogenous ore.

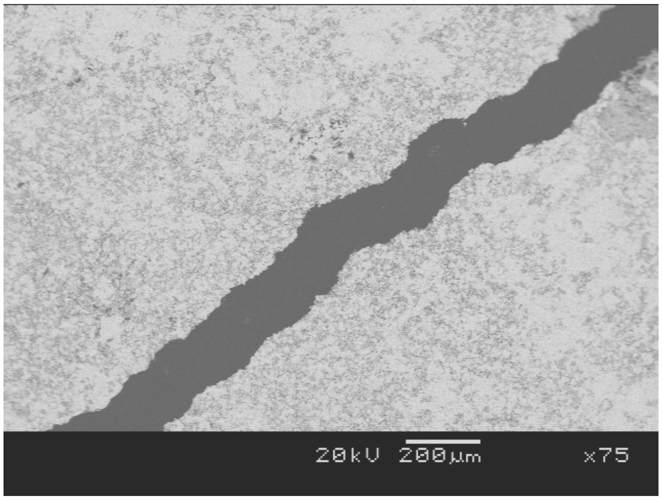

Figure 107: Electron backscatter image of sample 2 showing a large fracture through low porosity granular hematite. The fracture occurs without a large network of feeder fractures or ancillary fractures.

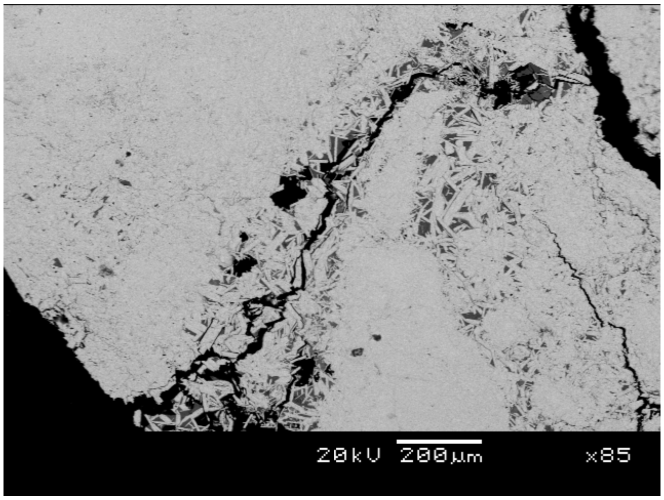

Figure 108: Electron backscatter image of sample 16 showing a large fracture associated with acicular hematite.

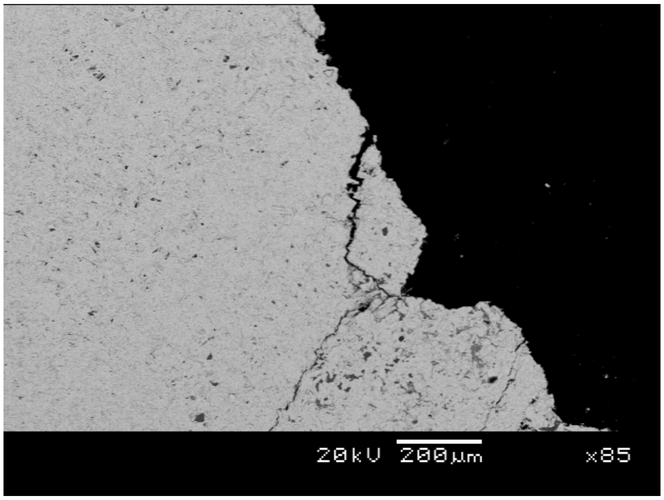

Figure 109: Electron backscatter image of sample 16 showing a small fracture at the edge of the sample associated with reduction of hematite.

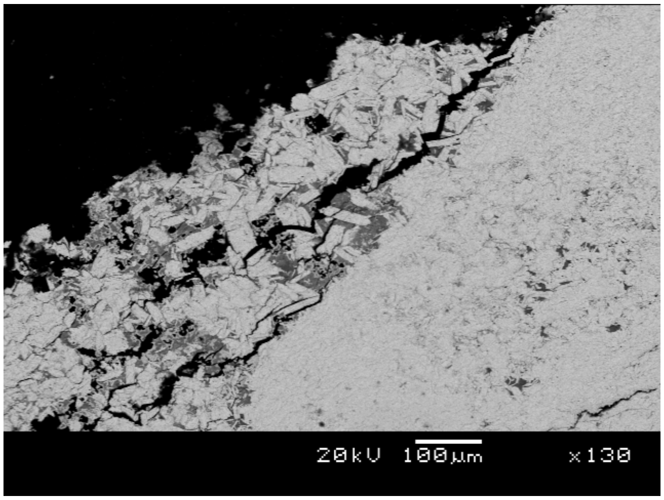

Figure 110: Electron backscatter image of sample 16 showing fractures at the edge of the sample where reduction has taken place. The influence of acicular hematite and gangue minerals is uncertain.

3.4.4 GROUP 4: OTHER

Only in one sample, Sample 6, could the fracture patterns not be linked to any compositional or textural features in the sample. Fractures were orientated parallel to the foliation fabric or in a regularly spaced network of fractures that occurred at right angles to each other.

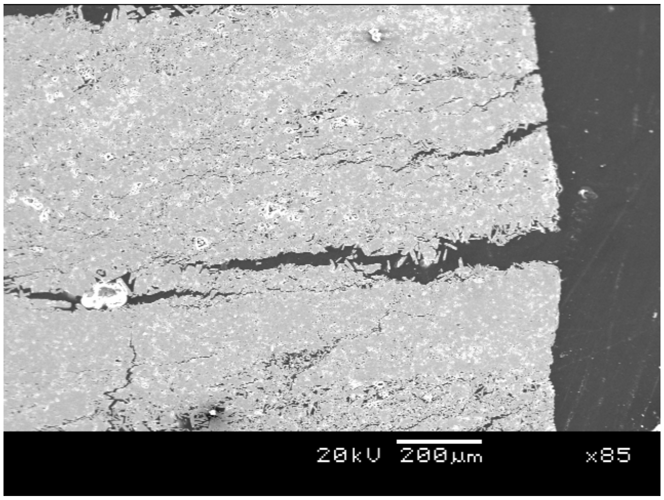

Figure 111: Electron backscatter image of sample 6 showing fractures oriented parallel to the foliation fabric.

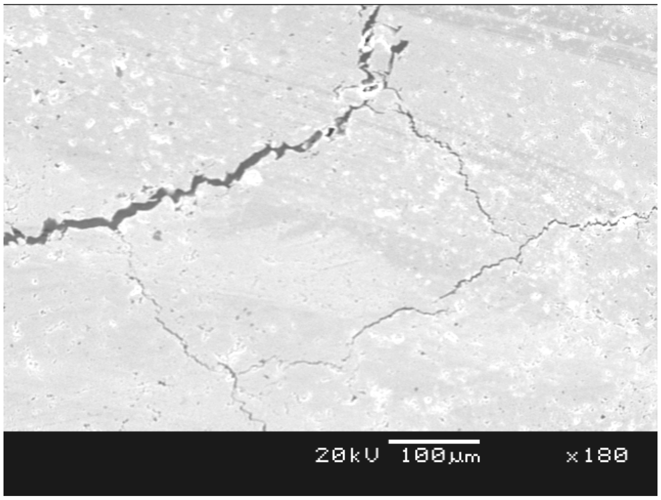

Figure 112: Electron backscatter image of sample 6 showing a regularly spaced network of fractures that occur at right angles to each other. There are no compositional or textural features to influence the fracture orientation.

4 DISCUSSION

The standard reduction disintegration test results indicates that at least 80 percent of the Northern Cape lump ore remains larger than 8mm and that it should not present any problems in a shaft furnace. It must be recognized that the conditions in the standard test represents only a small fraction of the conditions in the complete shaft furnace operation. This study has indicated that burden size, gas composition, reduction temperature reduction time and microstructure do have an effect on the performance of Northern Cape ore in a shaft furnace and will be discussed in detail.

4.1 EFFECT OF BURDEN SIZE

The percentage unchanged material (material remaining in the same size before and after the reduction disintegration test) increased from 47 percent (-25+20mm) to 72 percent (-10+8mm) with a decrease in burden particle size. However, the standard reduction disintegration test results indicated that, irrespective of the burden size, at least 80 percent of the Northern Cape lump ore remains bigger than 8mm and should not present any problems in a shaft furnace. These findings correlates with those of Loo and Bristow[xii] that also found particles of very similar size to the original material, suggesting that some particles are very tough and do not degrade at all. They found that, although cracks formed in lump ores, the crack propagation process appears to be more random than for sinters, where there are clearly paths of least resistance for the cracks to run.

4.2 EFFECT OF GAS COMPOSITION

The results obtained with the H_2 in the reduction gas also indicate that factors other than percentage reduction influence the degree of reduction disintegration. As Loo and Bristow indicated, H_2 has an effect on the percentage reduction. This study however indicates that lower percentages (less that 5 percent) of H_2 do not have an effect on the degree of reduction disintegration (**Figure 113**). With 10 percent H_2 however the degree of reduction doubled while the percentage fine material increased only from 9 to 13 percent. This compares well with the findings of El-Geassy[xix] (**Figure 18**) that indicated that when H2 is introduced into the reduction gas the compacts swelled at the initial stages of reduction but ended up with overall contraction for the completely reduced compacts.

Contrary to the testwork conducted by Gudenau et al[xxii] no difference was observed in the appearances of the cracks when hydrogen was used as reduction gas compared to carbon monoxide. This might be because of the high temperature (850°C) considered by Gudenau et al.

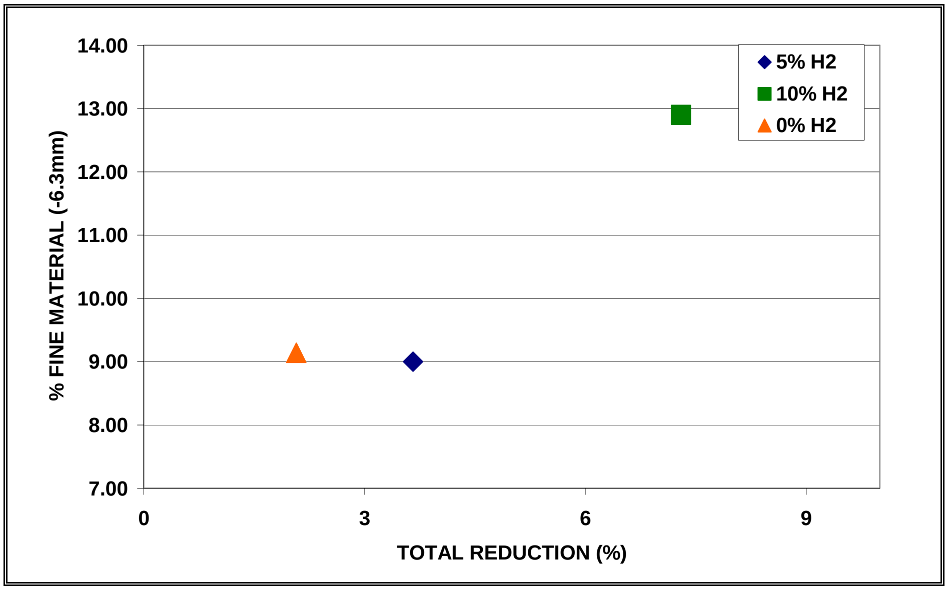

Figure 113: Effect of gas composition on the percentage fine material (-6.3mm) vs the total percentage reduction.

4.3 EFFECT OF REDUCTION TEMPERATURE AND REDUCTION TIME

Figure 114 indicate that reduction disintegration is most severe between 550°C and 750°C for Northern Cape STD. At temperatures above 800°C, more than 80 percent of the particles remain the same size. Similar results were obtained in test 21 of the high temperature microscope, where little cracking was observed at 700°C. This correlates with the work done by Husslage et al[xvii] that indicated that this behaviour could be related to a change in the morphology and the fracture toughness of the magnetite at higher temperatures. Increasing the reduction times, **Figure 41** showed a general upward trend in the percentage of fines generated with an increase in the reduction time. Although there is a decline in the fines generated at higher temperatures, **Figure 114** indicates a general increase in the percentage reduction with an increase in the reduction temperature. **Figure 115** indicates that at 600ºC an increase in the reduction time leads to an increase in the percentage reduction. At 500ºC and 700ºC, the effect is clear.

The results indicate that it is important to manage the temperature in the blast furnace and the COREX shaft as well as the time spent at temperature to minimize the amount of fines generated.

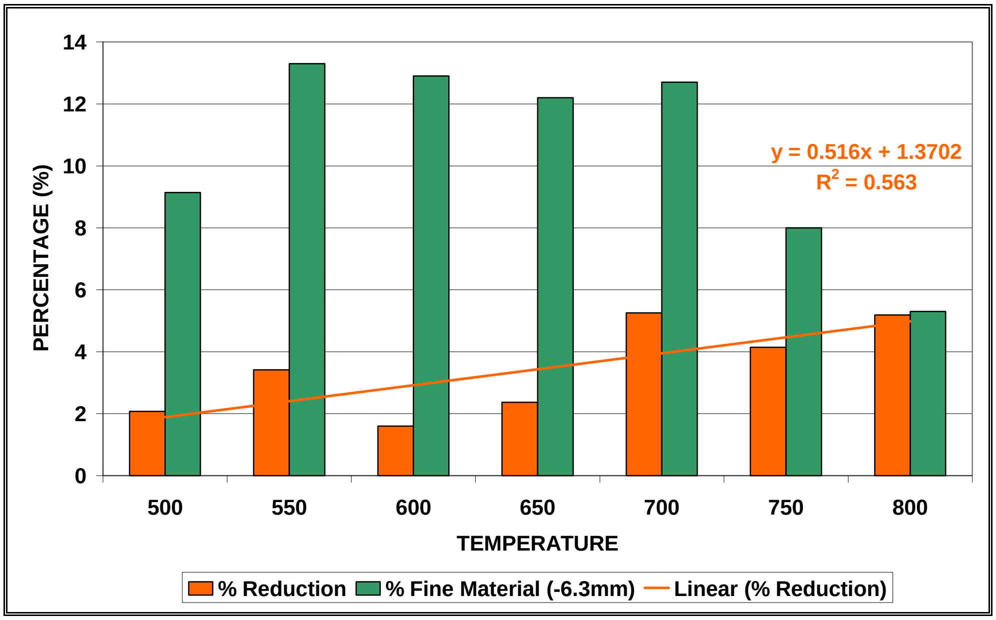

Figure 114: Effect of temperature on the magnitude of breakdown and reduction during reduction disintegration tests.

4.4 EFFECT OF REDUCTION

The degree of reduction was determined for the coarse (+6.3mm) and fine (-6.3mm) fractions, as present after reduction. **Figure 116** is a plot of the coarse and fine fractions vs the fractional reduction of the specific fractions for all the samples tested, that is for a range of temperatures, gas compositions, feed sizes and times. The fines are significantly more highly reduced than the coarse material, as expected from the effect of surface area on reduction rate. What is notable is that there is no strong correlation between the amount of material remaining in the +6.3 mm fraction, and the percentage reduction of this coarse fraction. This lack of a relationship, between disintegration and the degree of reduction of the remaining coarse material, is in contrast with the observation that the degree of fines formation increases with the percentage reduction *of the whole sample*.

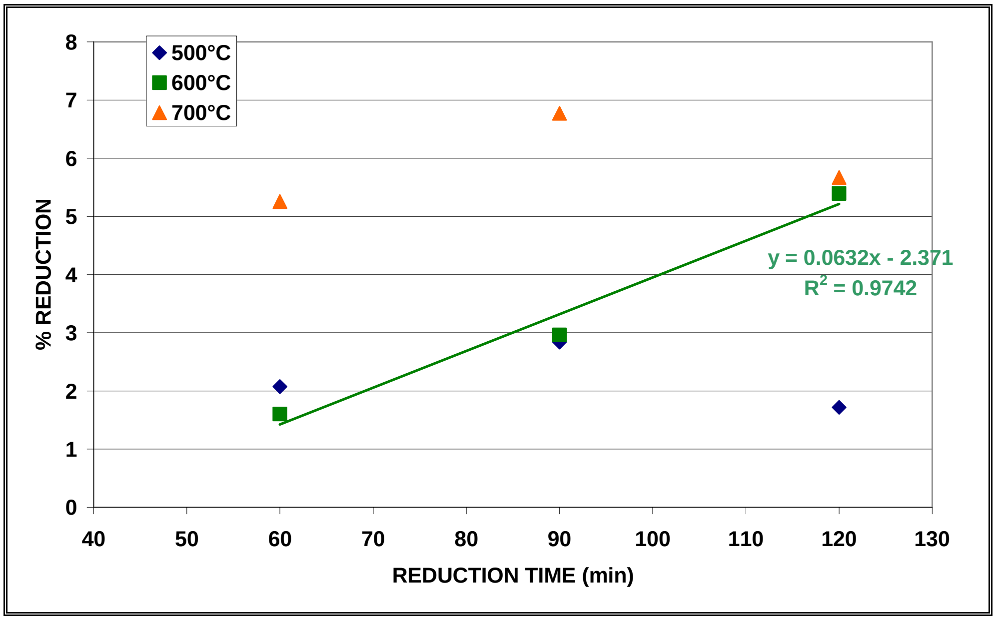

Figure 115: Effect of temperature and reduction time on the total percentage reduction vs the reduction time.

Figure 116 suggests that the observed relationships between the *overall* degree of reduction and fines formation may simply be an artifact: the mechanistic relationship may be that material which form more fines are more highly reduced simply because the fines once formed, have higher reduction rates. In this view, fines formation would be the cause and the degree of reduction would be the effect. The results obtained in the present study did not allow this possibility to be tested further, but it would be an interesting topic for further study.

Although the general thinking is that the disintegration is mainly due to the reduction process, no direct correlation could thus be established between the percentage reduction and the percentage fines generated. Clearly other factors in addition to the reduction process influence the degree of reduction disintegration. That is, the differences in disintegration behaviour of different ore types are not just caused by differences in reduction rate.

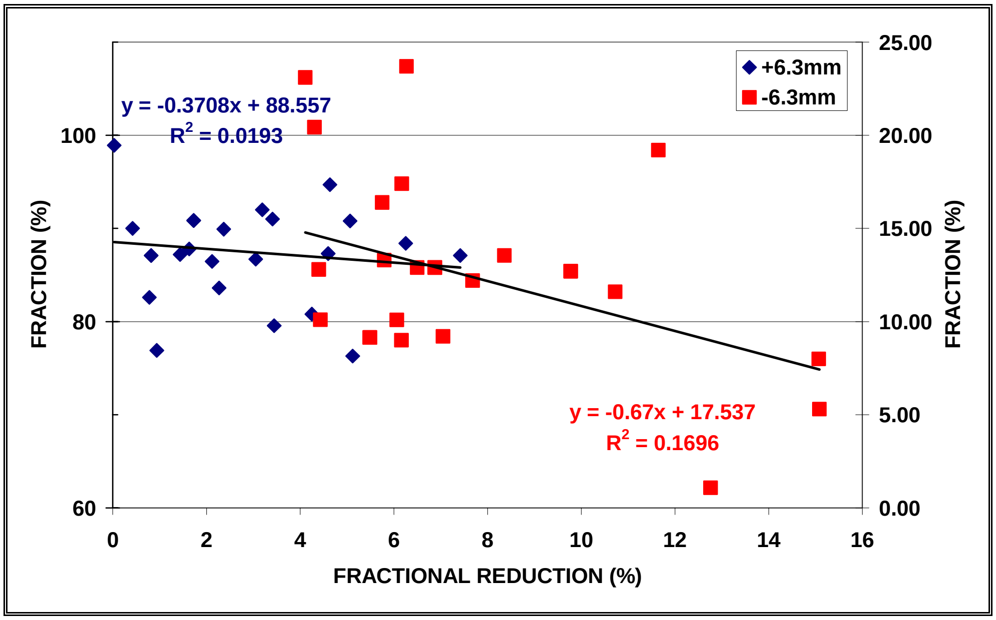

Figure 116: Fractional reduction of the +6.3mm and -6.3mm fractions for all the samples.

4.5 ORE COMPOSITION AND MICROSTRUCTURE

The results indicate that ore composition and microstructure have a definite effect on the degree of reduction disintegration. The fraction of material remaining in the +8mm size range after reduction varied between 70% and 98% for the different ore types (**Figure 117**). **Figure 118** and **Figure 119** however indicate that there is no correlation between the chemical analysis (gangue content) and the percentage fines generated. This conclusion is supported by **Figure 120** which plots the fraction of cracks which are associated with gangue minerals vs the percentage gangue minerals in the samples. Points plotted above the black line would indicate a preference of cracks forming in gangue minerals, while points plotted below the black line would indicate a preference to cracks forming in the iron oxide matrix. From **Figure 120** it is clear that the cracks formed randomly with no preference to gangue minerals or iron oxide. This is in line with the ore structure chart developed by Marten et al[xxv] that indicated that although various micro-structural features impacts in the reduction disintegration of lump ores, gangue minerals is not considered to be an important one.

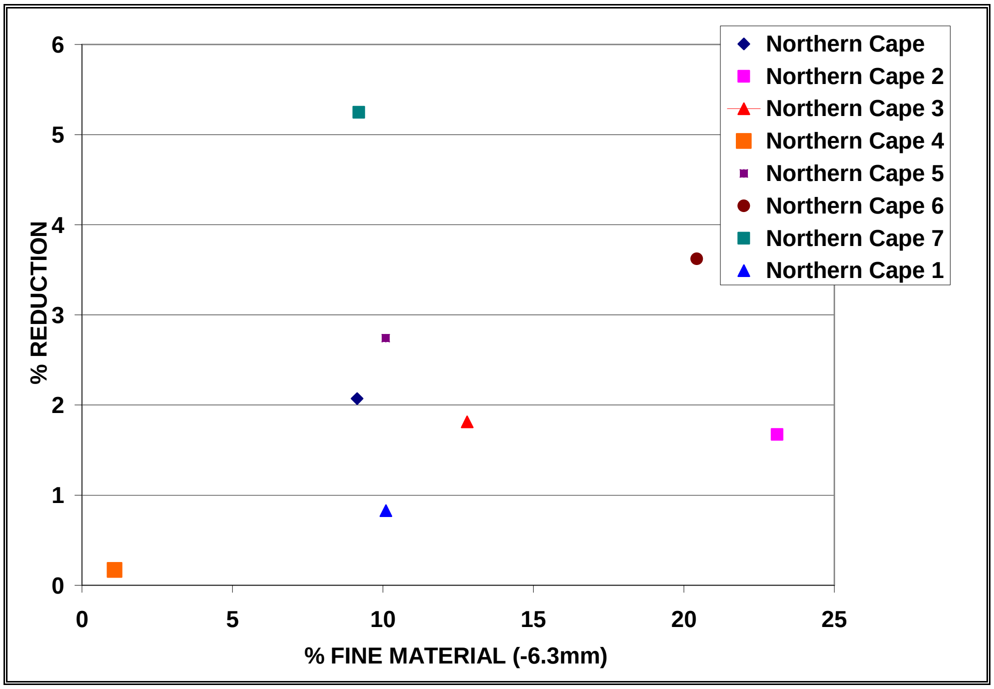

Figure 117: % Fine material (-6.3mm) vs % reduction for the different ore types.

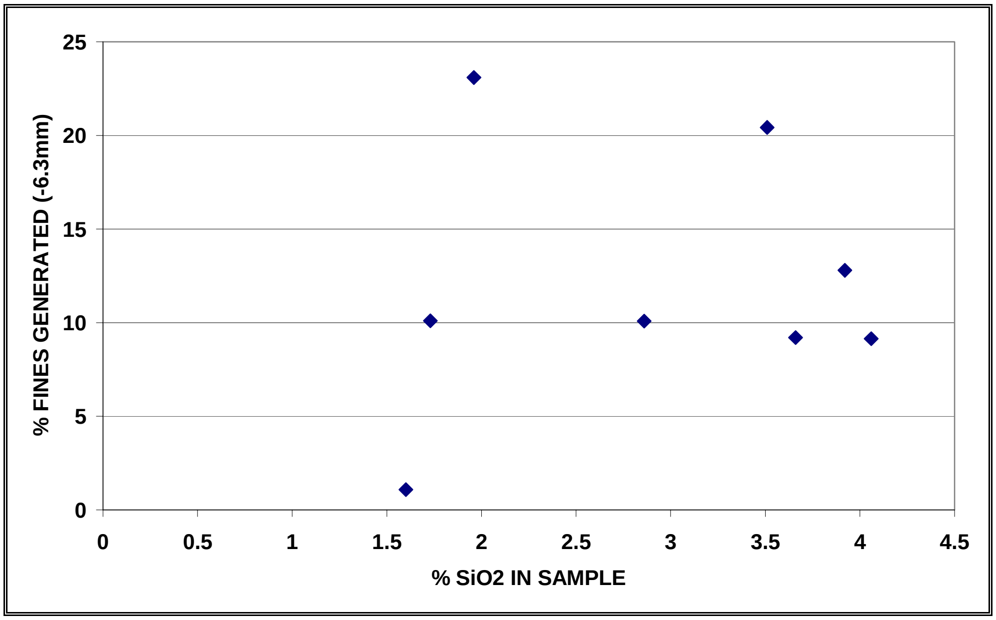

Figure 118: % Fine material (-6.3mm) vs % SiO_2 in samples for the different ore types.

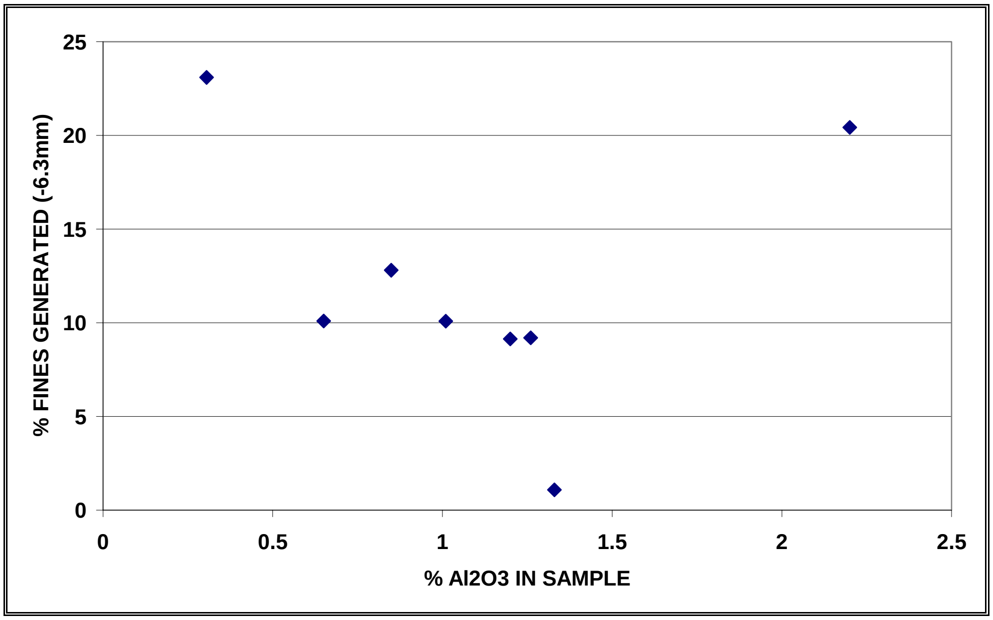

Figure 119: % Fine material (-6.3mm) vs % Al_2O_3 in samples for the different ore types.

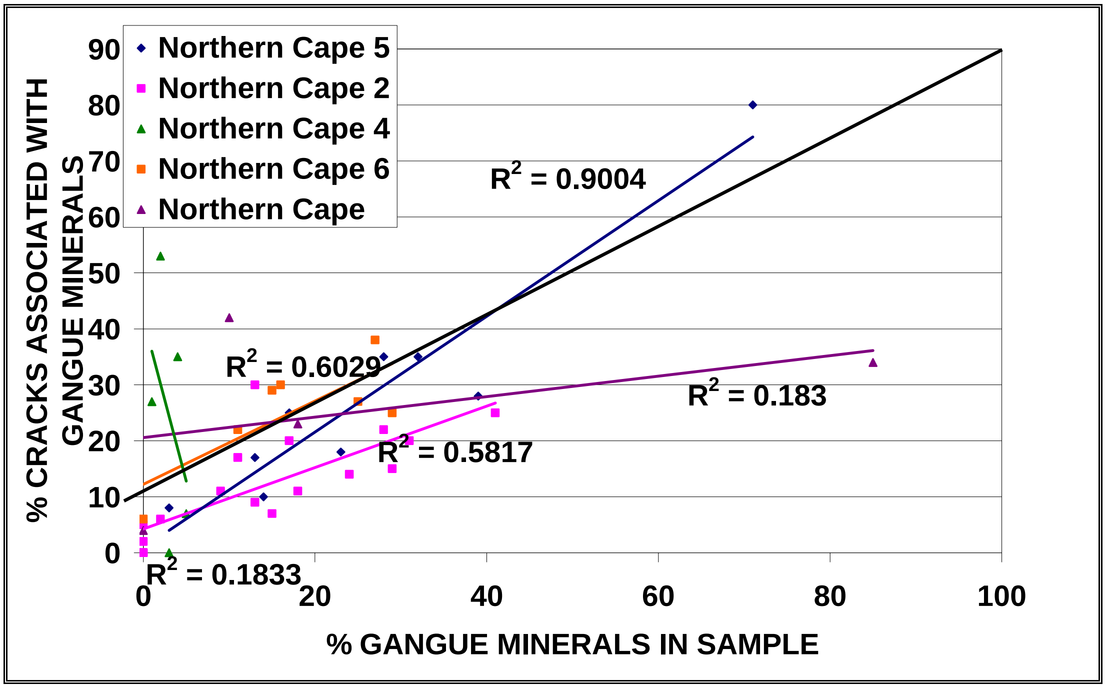

Figure 120: Percentage cracks associated with gangue minerals vs the percentage gangue minerals in the sample.

From the SEM investigation the appearance of cracks was classified in four distinct groups:

- Radial fractures occurring on the edges of particles penetrating the sample to the depth of reduction. These fractures appear to be directly related to the volume change during reduction.

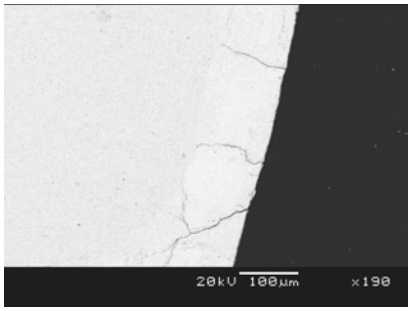

- Internal fractures that occur regularly spaced at right angles to one another – forming a matrix of internal cracks.

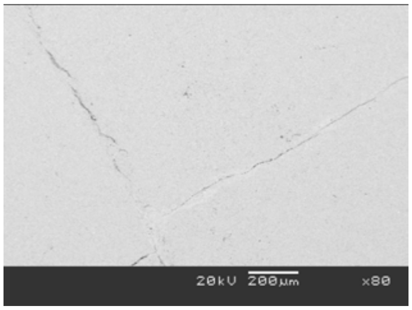

- Fractures that occurred perpendicular to the edge of the sample, where the sample has been reduced.

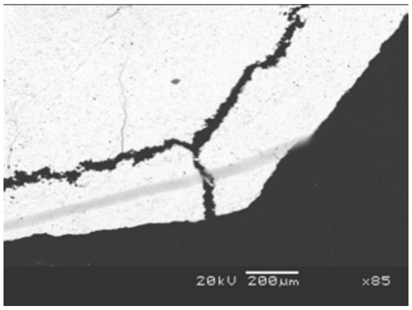

- Fractures associated with gangue minerals or internal structures (internal foliation, open pores or acicular hematite)

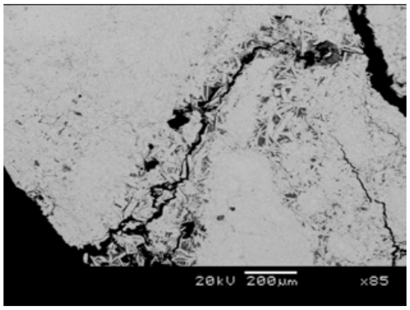

Features such as internal foliation fabric and/or bedding planes have a significant influence on the orientation of fractures as the foliation/bedding plane is the primary plane of weakness in the sample. However, cracks occurred randomly in samples where internal foliation fabric was present. Cracks that occurred perpendicular to internal foliation fabric was also observed (**Figure 121**). The results indicated that the presence of gangue minerals alone do not cause fractures to form. However, the gangue minerals do influence the direction and intensity of fractures. It was observed that the presence of gangue minerals only appears to have an impact on the fracture path up until a certain size of fracture is reached. Thereafter with large fractures, the fracture propagates irrespective of the presence or absence of gangue minerals. However, the presence of gangue minerals does not imply crack formation, as was shown previously.

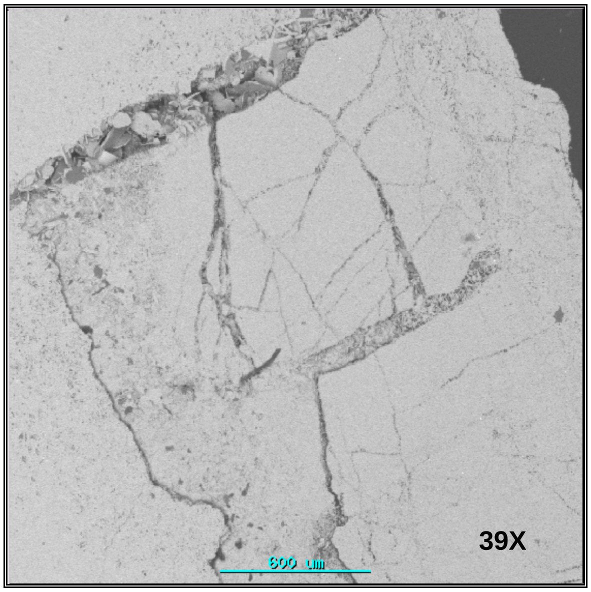

Figure 121: SEM images of the -12+10mm fraction after reduction disintegration test for Northern Cape OT 2

Hardness tests of the different minerals present in the ores would have been valuable to understand this phenomenon better. Although it was never observed (during the SEM analysis or the high temperature microscope work) that the formation of a crack was influenced due to a new mineral coming in the path of the crack as was observed by Loo and Bristow[XV], fractures often dilate as they pass through gangue minerals and a secondary network of smaller fractures is often developed, especially in quartz (**Figure 122**). No occurrences were observed where secondary fractures extended into the surrounding hematite. It appears as though the more brittle gangue mineral would absorb the stresses by breaking up extensively – as indicated in **Figure 122**, and thus “stop” the crack of propagating. This however also occurred without the presence of a large crack as indicated by **Figure 123**, and not at all as indicated by **Figure 124**.

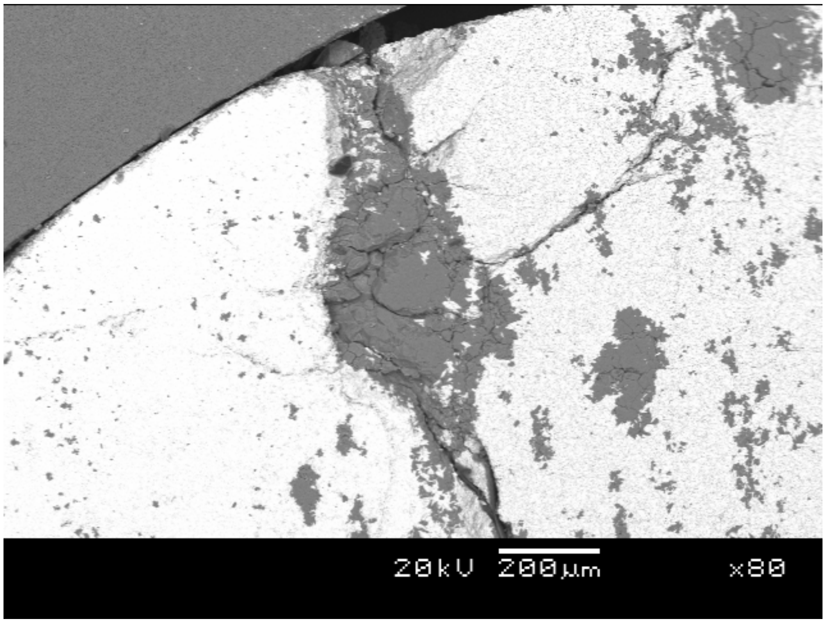

Figure 122: Fracture forming secondary cracks in quartz.

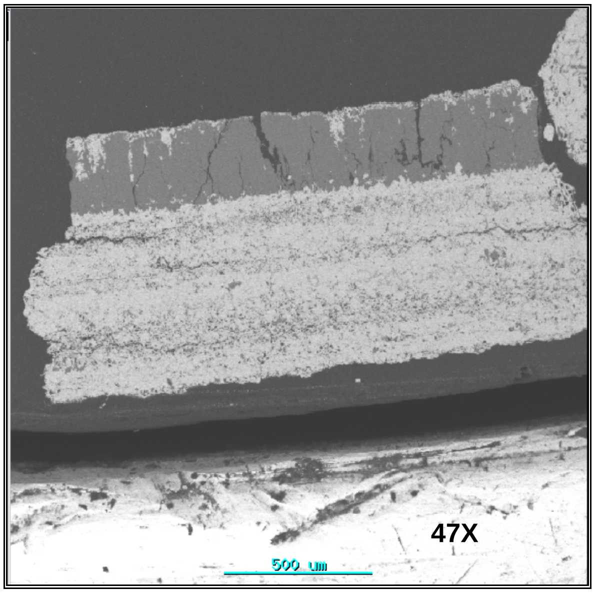

Figure 123: SEM images of the -2+1mm fraction after reduction disintegration test for Northern Cape OT 2

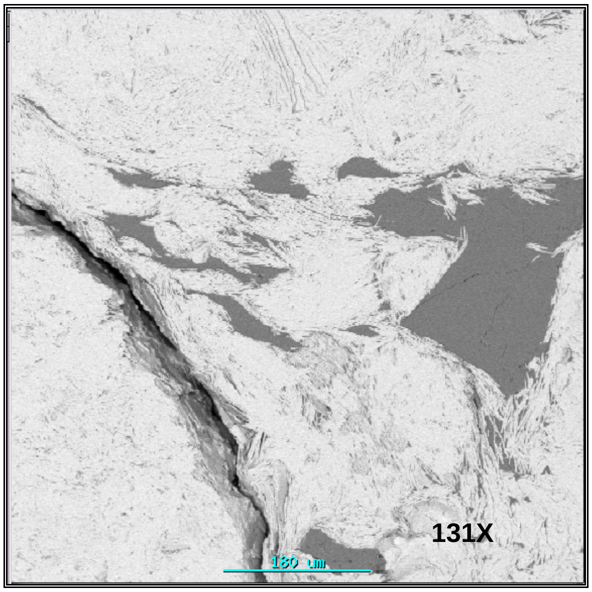

Figure 124: SEM images of the -8+6.3mm fraction after reduction disintegration test for Northern Cape OT 4

Porous samples appear to be less fractured as the open pores impede fracture formation as the pores is able to accommodate the strain of the volume increase during reduction.

Where there are no compositional or textural features in a sample that can have an influence on fracture propagation then fractures will form at regular intervals with similar orientations, often at right angles to one another.

Table 18 which gave a summary of the high temperature microscope work indicated that most of the cracks occurred as smaller internal cracks (that does not lead to breakdown) or border cracks (which relates to small particles breaking off the edges) rather than large cracks that would split the sample. This conclusion is supported by **Figure 125** which plots the percentage fines generated during reduction disintegration vs the inverted average particle size. There is a strong relation between the original particle size and the fraction of fines formed during reduction disintegration for particles smaller than 16mm which confirms that fines are created by spalling from the outside surface. It however appears that the largest particles deviate from proportionality.

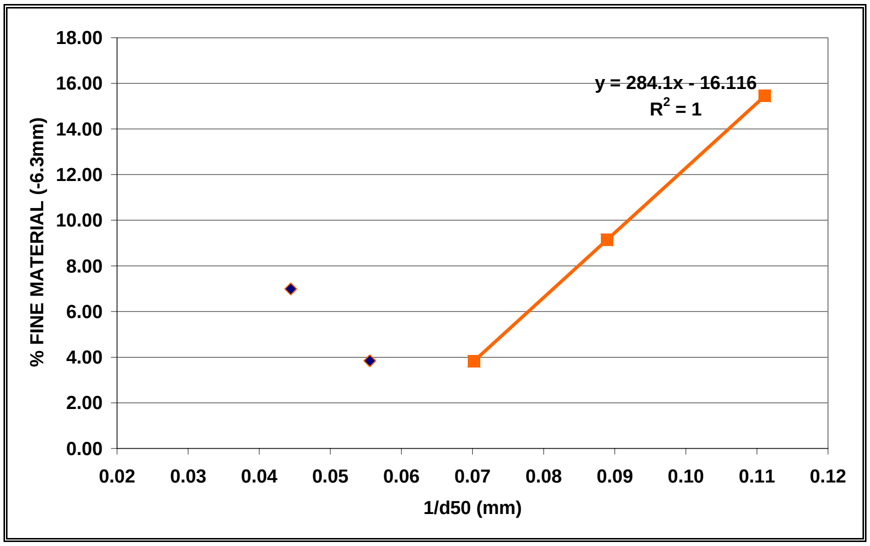

Figure 125: Effect of burden size on the percentage fine material generated during reduction disintegration tests.

This is also confirmed by the size distribution of the ore after reduction disintegration as illustrated in **Figure 126.** The graph indicates that for larger particles (-25+20mm) less than 50 percent of the particles are unchanged, while 70-80 percent of the particles is unchanged when smaller particles are tested.

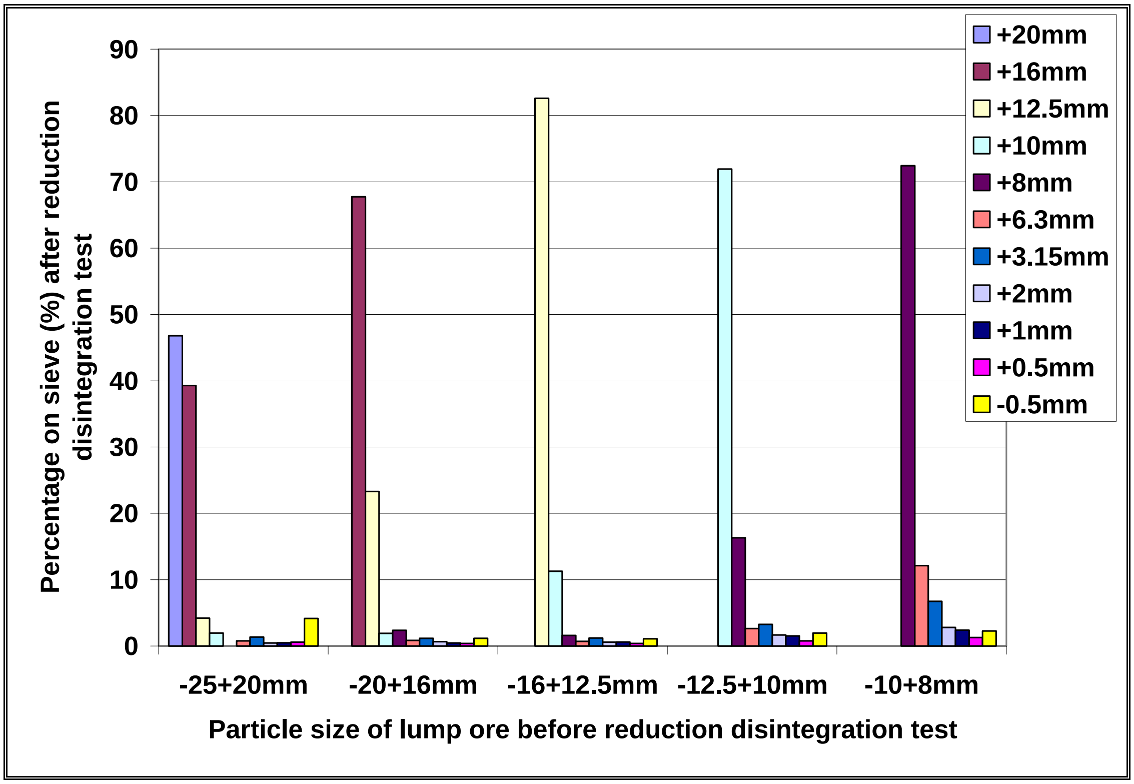

Figure 126: Size distribution of Northern Cape STD ore after reduction disintegration test for different ore sizes as raw material.

This study has indicated that at although Northern Cape lump ore consist of various ore types with varying microstructures, the degree of reduction disintegration depends mostly on the furnace conditions. Indeed, this study has shown that reduction disintegration increases with higher percentages of H_2 and longer periods in the 500ºC-750ºC temperature zone. An inverted relationship between the average particle size and the percentage of fines generated was established for particles smaller than 16mm which confirms that most of the disintegration is due to spalling from the edges rather than particles breaking into smaller clumps. Although the general thinking is that the disintegration is mainly due to the reduction process, no direct correlation could however be established between the percentage reduction and the percentage fines generated. It was also indicated that the presence of gangue minerals alone do not cause fractures to form. However, the presence of gangue minerals does influence the direction and intensity of fractures.

The high temperature microscope testwork revealed that for most of the samples, an incubation period was observed before the first cracks were formed. No crack propagation was observed after the initial cracking of the sample – even in tests extended to more than three hours.

The results indicate that it is important to manage the temperature in the top of the blast furnace and the COREX shaft as well as the time spent at temperatures below 750°C to minimize the amount of fines generated.

5 RECOGNITIONS

Arno Kleyenstüber
Kobus Vreugdenburg
Mandlakazi Mashao
Kobus Theron
Leonie Reyneke
L.N. Shago
Gerhard van Niekerk
Stephan Mokwana
Stewart Brand
Danie Krige
Lourina de Beer
Kumba Iron Ore

6 REFERENCES

1. Von Bogdandy, L.; Engell, H.J.; 1971; The Reduction of Iron Ores; *SPRINGER-VERLAG*; Berlin

2. Keplinger, W., Maschlanka, W., Wallner, F.; 1990; The Corex Process – Development And Further Plans; *COREX SYMPOSIUM, SAIMM* SP4; pp 5-20.

3. Biswas, A.K.; Principles Of Blast Furnace Ironmaking; *COOTHA PUBLISHING HOUSE*, Australia; pp 1-13.

4. Hauk, R.; 1990; Raw Materials For The Corex Process; COREX SYMPOSIUM, SAIMM SP4; pp 21-34

5. http://www.mindat.org/min-1856.html; Oktober 2007

6. Taylor,D.; 1984; Thermal Expansion Data: III Sesquioxides, M_2O_3, With The Corundum And The A-, B- and C-M2O_3 Structures; *BRIT CERAM SOC;* J and Trans; Vol. 83; p92

7. Megaw, H.D.; 1973; Crystal Structures: A Working Approach; *SAUNDERS;* Philadelphia

8. Deer, W.A., Howie, R.A., Zussman, J.; 1971; In Introduction To The Rock-Forming Minerals; *LONGMAN*, London

9. Taylor,D.; 1985; Thermal Expansion Data VI: Complex Oxides, AB_2O_4, The Spinels; *BRIT CERAM SOC;* J and Trans; Vol 84; p121

10 Bernal, J.D., Dasgapta, D.R., Mackay, A.L.; 1957; Nature; Vol. 180; pp645-647.

11. Roller, P.W.; 1986; Letter to the editor: The Theoretical Volume Decrease On Reduction Of Hematite To Magnetite; ISIJ; pp834-835

12. Loo, C.E., Bristow, N.J.;1998; Properties Of Iron Bearing Materials Under Simulated Blast Furnace Indirect Reduction Conditions Part 2 Reduction Degradation, RDI; *IRONMAKING AND STEELMAKING;* Vol. 25; No. 4; pp287-295

13. Yang, J., Cheng, G.; 1998; A Process For Minimizing Reduction Degradation Of Iron Ore Agglomerates Has Been Put In Practice; *ICSTI/IRONMAKING CONFERENCE PROCEEDINGS*; p1687

14 Brill-Edwards, H., Daniell, B.L., Samuel, R.L.; 1965; Structural Changes Accompanying The Reduction Of Polycrystalline Hematite; *J ISI*; pp361-368.

15. Loo, C.E.; Bristow, N.J.; 1994; Mechanism Of Low Temperature Reduction Degradation Of Iron Ore Sinters; *TRANS. INSTN MIN. METALL*. (sect C: Mineral Process. Extr Metall.); p103

16. Hayes, P.C., Grieveson, P.; 1981; Microstructural Changes On The Reduction Of Hematite To Magnetite; *METALLURGICAL TRANSACTIONS B*; American Society for Metals and The Metallurgical Society of AIME; Vol. 12B; pp579-587

17. Husslage, W.M., Bakker, T., Kock, M.E.m Heerema, R.H.; 1999; Influence Of Reduction Conditions On The Expansion And Microstexture Of Sintered Hematite Compacts During The Transition To Magnetite; *MINERALS AND METALLURGICAL PROCESSING;* Vol. 16; No. 3; pp23-33

18 Pimenta, H.P.; 2002; Influence Of Al_2O_3 And TiO_2 On The Reduction Degradation Behaviour Of Sinter And Hematite At Low Temperatures; *IRONMAKING AND STEELMAKING*; Vol 29; No 3; pp175-179

19 El-Geassy, A.A., Nasr, M.I., Hessien, M.M.; 1996; Effect Of Reducing Gas On The Volume Change During Reduction Of Iron Oxide Compacts; *ISIJ INTERNATIONAL;* Vol 36; No. 6; pp640-649

20. Theron, J.A.; 2002; Effect Of The Heating Rate And Other Parameters On Breakdown Of Iron Ore In The Saldanha Steel Corex Shaft – A Laboratory Scale Study

21. Bapat, S.P., Chakravarty, A.K., Mitra, A.N., Mukherjee, T.;1977; Assessment Of The Low-Temperature Breakdown And Swelling Characteristics Of Noamundi Ore, Joda Ore And Sinter; *TISCO*

22. Gudenau, H.W., Burchard, W.G., Rupp, H.; 1979; Direct Observation Of Reduction And Disintegration Processes In The Scanning Electron Microscope, *IRONMAKING PROCEEDINGS;* Vol 38; pp230-234

23. Adam, F., Dupre, B., and Gleitzer, C.; 1988; Cracking Of Hematite Crystals During Low Temperature Reduction Into Magnetite; *REACTIVITY OF SOLIDS;* Vol. 5; pp101-114

24. Porter, J, Swann, P; 1977; High-Voltage Microscopy Of Reduction Of Hematite To Magnetite; *IRONMAKING AND STEELMAKING*; p300.

25. Martens, R., Rausch, H., Serbent, H., Westenberger, H.; 1985; Investigation Of The Interrelation Of Microstructure And Disintegration Behaviour Of Hematite Lump Ores In The Reduction Process; *STEEL RESEARCH 56*, No.3; pp147-152

26. Vreugdenburg, J.C., Van der Vyver, W.F., Kleyenstuber, A.; 2004; Iron Ore Characterization; Kumba Research and Development

27. ISO 4696

APPENDIX 1

ALPHABETICAL LISTING OF THE MINERALS MENTIONED IN THIS REPORT, THEIR IDEAL CHEMICAL FORMULAE AND THE THEORETICAL IRON CONTENT OF THE MINERALS AND DEFINITIONS

Alphabetical listing of the minerals mentioned in this report, their ideal chemical formulae and the theoretical iron content of the minerals and definitions

Mineral	**Ideal chemical formula**	**Theoretical iron content in mass %**
Anatase	TiO_2	
Ankerite	$Ca(Fe,Mg,Mn)(CO_3)_2$	16.24
Apatite	$Ca_5(PO_4)_3(OH)$	
Barite	$BaSO_4$	
Calcite	$CaCO_3$	
Celestite	$SrSO_4$	
Diaspore	$AlO(OH)$	
Dolomite	$CaMg(CO_3)_2$	
Goethite	α-FeOOH	62.85
Greenalite	$(Fe^{2+},Fe^{3+})_{2-3}Si_2O_5(OH)_4$	44.14
Hematite	Fe_2O_3	69.94
Illite	$(K,H_3O)(Al,Mg,Fe)_2(Si,Al)_4O_{10}[(OH)_2,H_2O]$	
Jacobsite	$MnFe_2O_4$	48.43
Kaolinite	$Al_2Si_2O_5(OH)_4$	
Lithiophorite	$(Al,Li)MnO_2(OH)_2$	
Magnetite	Fe_3O_4	72.36
Muscovite	$KAl_3Si_3O_{10}(OH)_2$	
Pyrophyllite	$Al_2Si_4O_{10}(OH)_2$	
Quartz	SiO_2	
Rhodochrosite	$MnCO_3$	
Rutile	TiO_2	
Siderite	$FeCO_3$	48.20
Stilpnomelane	$K(Fe^{2+},Mg,Fe^{3+})_8(Si,Al)_{12}(O,OH)_{27}$	30.40

Specularite	A platy, metallic variety of hematite
Acicular	Slender and pointed, needle-like
Brecciated	A textural term used to describe a rock comprised of angular clasts.
Relict	Term used to describe a mineral that is a remnant or fragment that remains from what was more widely distributed
Earthy	The non-metallic mineral lustre of porous mineral aggregates such as clays.
Microlaminae	Rock layers less than 1cm thick are referred to as laminae, microlaminae are less than 3mm in thickness
Texture	The general character of a rock, shown by its component particles

	in terms of grain size and shape, degree of crystallinity and arrangement.
Mesolaminae	Layers less than 1cm thick are referred to as laminae, mesolaminae are thicker than 3mm but less than 1cm.

APPENDIX 2

TEST METHODS

DRAFT INTERNATIONAL STANDARD ISO/DIS 4696-1

ISO/TC **102**/SC **3** Secretariat: **ABNT**

Voting begins on:
2005-04-11

Voting terminates on:
2005-09-12

INTERNATIONAL ORGANIZATION FOR STANDARDIZATION • МЕЖДУНАРОДНАЯ ОРГАНИЗАЦИЯ ПО СТАНДАРТИЗАЦИИ • ORGANISATION INTERNATIONALE DE NORMALISATION

Iron ores for blast furnace feedstocks — Determination of low-temperature reduction-disintegration indices by static method —

Part 1:
Reduction with CO, CO_2, H_2 and N_2

Minerais de fer pour l'alimentation des hauts-fourneaux — Détermination des indices de désagrégation par réduction à basse température par méthode statique —

Partie 1: Réduction avec CO, CO_2, H_2 et N_2

[Revision of first edition (ISO 4696-1:1996)]

ICS 73.060.10

In accordance with the provisions of Council Resolution 15/1993 this document is circulated in the English language only.

Conformément aux dispositions de la Résolution du Conseil 15/1993, ce document est distribué en version anglaise seulement.

To expedite distribution, this document is circulated as received from the committee secretariat. ISO Central Secretariat work of editing and text composition will be undertaken at publication stage.

Pour accélérer la distribution, le présent document est distribué tel qu'il est parvenu du secrétariat du comité. Le travail de rédaction et de composition de texte sera effectué au Secrétariat central de l'ISO au stade de publication.

PDF disclaimer

This PDF file may contain embedded typefaces. In accordance with Adobe's licensing policy, this file may be printed or viewed but shall not be edited unless the typefaces which are embedded are licensed to and installed on the computer performing the editing. In downloading this file, parties accept therein the responsibility of not infringing Adobe's licensing policy. The ISO Central Secretariat accepts no liability in this area.

Adobe is a trademark of Adobe Systems Incorporated.

Details of the software products used to create this PDF file can be found in the General Info relative to the file; the PDF-creation parameters were optimized for printing. Every care has been taken to ensure that the file is suitable for use by ISO member bodies. In the unlikely event that a problem relating to it is found, please inform the Central Secretariat at the address given below.

Copyright notice

This ISO document is a Draft International Standard and is copyright-protected by ISO. Except as permitted under the applicable laws of the user's country, neither this ISO draft nor any extract from it may be reproduced, stored in a retrieval system or transmitted in any form or by any means, electronic, photocopying, recording or otherwise, without prior written permission being secured.

Requests for permission to reproduce should be addressed to either ISO at the address below or ISO's member body in the country of the requester.

ISO copyright office
Case postale 56 • CH-1211 Geneva 20
Tel. + 41 22 749 01 11
Fax + 41 22 749 09 47
E-mail copyright@iso.org
Web www.iso.org

Reproduction may be subject to royalty payments or a licensing agreement.

Violators may be prosecuted.

UNIVERSITEIT VAN PRETORIA
UNIVERSITY OF PRETORIA
YUNIBESITHI YA PRETORIA

Contents

Page

Foreword

ISO (the International Organization for Standardization) is a worldwide federation of national standards bodies (ISO member bodies). The work of preparing International Standards is normally carried out through ISO technical committees. Each member body interested in a subject for which a technical committee has been established has the right to be represented on that committee. International organizations, governmental and non-governmental, in liaison with ISO, also take part in the work. ISO collaborates closely with the International Electrotechnical Commission (IEC) on all matters of electrotechnical standardization.

International Standards are drafted in accordance with the rules given in the ISO/IEC Directives, Part 2.

The main task of technical committees is to prepare International Standards. Draft International Standards adopted by the technical committees are circulated to the member bodies for voting. Publication as an International Standard requires approval by at least 75 % of the member bodies casting a vote.

Attention is drawn to the possibility that some of the elements of this document may be the subject of patent rights. ISO shall not be held responsible for identifying any or all such patent rights.

ISO 4696-1 was prepared by Technical Committee ISO/TC 102, *Iron Ore and Direct Reduced Iron*, Subcommittee SC 3, *Physical Testing*.

This second edition cancels and replaces the first edition (ISO 4696-1:1996),which has been revised to homogenise with other physical test standards.

ISO 4696 consists of the following parts, under the general title *Iron ores for blast furnace feedstocks — Determination of low-temperature reduction-disintegration indices (RDI) by static method*:

— *Part 1: Reduction with CO, CO_2, H_2 and N_2*

— *Part 2: Reduction with CO and N_2*

Introduction

This is one of a number of physical test methods that have been developed to measure various physical parameters and to evaluate the behaviour of iron ores including reducibility, disintegration, crushing strength, apparent density, etc. This method was developed to provide a uniform procedure, validated by collaborative testing, to facilitate comparisons of tests made in different laboratories.

Results of this test should be considered in conjunction with other tests used to evaluate the quality of iron ores as feedstocks for blast furnace and direct reduction processes.

This International Standard may be used to provide test results as part of a production quality control system, as a basis of a contract, or as part of a research project.

Iron ores for blast furnace feedstocks — Determination of low-temperature reduction-disintegration indices by static method — Part 1: Reduction with CO, CO_2, H_2 and N_2

CAUTION This standard may involve hazardous materials, operations and equipment. This standard does not purport to address all of the safety issues associated with its use. It is the responsibility of the user of this International Standard to establish appropriate safety and health practices and determine the applicability of regulatory limitations prior to its use.

1 Scope

Part 1 of this International Standard specifies a method to provide a relative measure for evaluating the degree of size degradation of iron ores when reduced under conditions resembling those prevailing in the low-temperature reduction zone of a blast furnace.

This International Standard is applicable to lump ores, sinters and hot bonded pellets.

2 Normative references

The following referenced documents are indispensable for the application of this International Standard. For dated references, only the edition cited applies. For undated references, the latest edition of the referenced document (including any amendments) applies.

ISO 3082:2000[1)], *Iron ores — Sampling and sample preparation procedures.*

ISO 3310-1:2000, *Test sieves — Technical requirements and testing – Part 1: Test sieves of metal wire cloth.*

ISO 3310-2:1999, *Test sieves — Technical requirements and testing – Part 2: Test sieves of perforated metal plate.*

ISO 4701:1999, *Iron ores - Determination of size distribution by sieving.*

ISO 11323:2002, *Iron ore and direct reduced iron — Vocabulary.*

3 Definitions

For the purpose of this International Standard the definitions given in ISO 11323 apply.

4 Principle

The test portion is isothermally reduced in a fixed bed, at 500 °C, using a reducing gas consisting of CO, CO_2, H_2 and N_2, for 60 min. The reduced test portion is tumbled in a specific tumble drum for 300 revolutions and then sieved with sieves having square openings of 6,3 mm, 3,15 mm and 500 µm. Three reduction-

---

[1)] Under revision to incorporate ISO 10836 – *Iron ores – Method for sampling and sample preparation for physical testing.*

disintegration indices (*RDI*) are calculated as the mass percentage of material greater than 6,30 mm, less than 3,15 mm and less than 500 µm.

5 Sampling, sample preparation and preparation of test portions

5.1 Sampling and sample preparation

Sampling of a lot and preparation of a test sample shall be in accordance with ISO 3082.

The size range for pellets, sinters and lump ores shall be - 12,5 mm + 10,0 mm.

A test sample of at least 2 kg, on dry basis, of the sized material shall be obtained.

Oven-dry the test sample to constant mass at 105 °C ± 5 °C and cool it to room temperature before preparation of the test portions.

NOTE Constant mass is achieved when the difference in mass between two subsequent measurements becomes less than 0,05% of the initial mass of the test sample.

5.2 Preparation of test portions

Collect each test portion by taking ore particles at random.

At least 4 test portions, each of approximately 500 g (± the mass of 1 particle) shall be prepared from the test sample.

Weigh the test portions to the nearest 0,1 g and register the mass of each test portion on its recipient label.

6 Apparatus

6.1 General

Test apparatus shall comprise

a) ordinary laboratory equipment, such as oven, hand tools, time control device and safety equipment;

b) a reduction tube assembly;

c) a furnace;

d) a system to supply the gases and regulate the flow rates;

e) a tumble drum;

f) test sieves;

g) a weighing device.

Figure 1 shows an example of the test apparatus.

6.2 Reduction tube, made of non-scaling, heat-resistant metal to withstand temperatures higher than 600 °C and resistant to deformation. The internal diameter shall be 75 mm ± 1 mm. A removable perforated plate made of non-scaling, heat-resistant metal to withstand temperatures higher than 600 °C shall be mounted in the reduction tube to support the test portion and to ensure uniform gas flow through it. The perforated plate shall be 4 mm thick, with a diameter 1 mm less than the tube internal diameter. The holes in the plate shall be 2 mm to 3 mm in diameter and shall be separated from each other by 4 mm to 5 mm.

Figure 2 shows an example of reduction tube.

6.3 Furnace, having a heating capacity and temperature control able to maintain the entire test portion as well as gas entering the bed at 500 °C ± 5 °C.

6.4 Porcelain balls, having a size range between 10,0 mm and 12,5 mm and enough amount to form a double-layer bed on the perforated plate.

6.5 Gas supply system, capable of supplying the gases and regulating gas flow rates.

6.6 Tumble drum, made of steel, at least 5 mm thick, having an internal diameter of 130 mm and an inside length of 200 mm. Two equally spaced steel lifters 200 mm long, 20 mm high and 2 mm thick shall be mounted longitudinally inside the drum. These may be mounted on a frame that can be inserted inside the vessel from one end. One end of the drum shall be closed and the other open. A close-fitting lid shall be held in place on the opening to ensure a dust-tight seal. The drum shall be replaced in any case when the thickness of the plate is reduced to 3 mm in any area, and the lifters when their height is reduced to less than 18 mm.

Figure 3 shows an example of tumble drum.

6.7 Rotation equipment, capable to ensure that the drum attains full speed in one revolution, rotates at a constant speed of 30 rpm ± 1 rpm and stops within one revolution. The equipment shall be fitted with a revolution counter and with an automatic device for stopping the drum after a predetermined number of revolutions.

6.8 Test sieves, conforming to ISO 3310-1 or ISO 3310-2 and having square apertures of the following nominal sizes: 6,30 mm; 3,15 mm and 500 µm.

6.9 Weighing device, capable of weighing the test sample and test portions to an accuracy of 0,1 g.

7 Test conditions

7.1 General

Volumes and flow rates of gases are as measured at a reference temperature of 0°C and at a reference atmospheric pressure of 101,325 kPa (1,01325 bar).

7.2 Reducing gas

7.2.1 Composition

The reducing gas shall consist of:

CO	20,0 % (V/V) ± 0,5 % (V/V)
CO_2	20,0 % (V/V) ± 0,5 % (V/V)
H_2	2,0 % (V/V) ± 0,5 % (V/V)
N_2	58,0 % (V/V) ± 0,5 % (V/V)

7.2.2 Purity

Impurities in the reducing gas shall not exceed:

O_2	0,1 % (V/V)

H_2O 0,2 % (V/V)

7.2.3 Flow rate

The flow rate of the reducing gas, during the entire reducing period, shall be maintained at 20 L/min ± 1 L/min.

7.3 Heating and cooling gas

Nitrogen (N_2) shall be used as the heating and cooling gas. Impurities shall not exceed 0,1% (V/V).

The flow rate of N_2 shall be maintained at 5 L/min until the test portion reaches 500 °C and at 20 L/min during temperature equilibration period. During cooling it shall be maintained at 5 L/min.

7.4 Temperature of the test portion

The temperature of the entire test portion shall be maintained at 500 °C ± 10 °C during the entire reducing period and, as such, the reducing gas shall be preheated before entering the test portion.

8 Procedure

8.1 Number of determinations for the test

Carry out the test as many times as required by Annex A.

8.2 Reduction

Place a double-layer bed of porcelain balls (6.4) in the reduction tube (6.2) on the perforated plate.

Take at random one of the test portions prepared in Clause 5.2. Place it in the reduction tube (6.2) and level its surface.

Close the top of the reduction tube. Connect the thermocouple, ensuring that its tip is in the centre of the test portion.

Insert the reduction tube into the furnace (6.3).

Connect the gas supply system (6.5).

Pass a flow of N_2 through the test portion at a rate of 5 L/min and commence heating. When the temperature of the test portion approaches 500^{o}C increase the flow rate to 20 L/min. Continue heating while maintaining the flow of N_2 until the test portion reaches 500 °C ± 5 °C. Allow a period of 15 min for temperature equilibration at 500 °C.

DANGER Carbon monoxide and the reducing gas, which contains carbon monoxide, are toxic and therefore hazardous. Testing shall be carried out in a well ventilated area or under a hood. Precautions should be taken for the safety of the operator, in accordance with the safety codes of each country.

Introduce the reducing gas at a flow rate of 20 L/min ± 1 L/min to replace the N_2. After 60 min of reduction turn off the power. Replace the reducing gas with N_2 at a flow rate of 5 L/min and cool the test portion to a temperature below 100 °C.

8.3 Tumbling

Remove the test portion carefully from the reduction tube. Determine its mass (m_0) and place it in the tumble drum (6.6). Fasten the lid tightly and rotate the drum for a total of 300 revolutions at a rate of 30 rpm ± 1 rpm.

8.4 Sieving

Remove all material from the drum, determine and record the mass and hand sieve with care on 6,30 mm, 3,15 mm and 500 µm sieves, in accordance with ISO 4701. Determine and record the mass of each fraction retained on the 6,30 mm (m_1), 3,15 mm (m_2) and 500 µm (m_3) sieve. Material lost during tumbling and sieving shall be considered to be part of the - 500 µm fraction.

9 Expression of results

9.1 Calculation of the reduction-disintegration indices ($RDI\text{-}1_{+6,3}$, $RDI\text{-}1_{-3,15}$, $RDI\text{-}1_{-0,5}$)

The reduction-disintegration indices, $RDI\text{-}1_{+6,3}$, $RDI\text{-}1_{-3,15}$, $RDI\text{-}1_{-0,5}$, expressed as percentages by mass, are calculated from the following equations:

$$RDI-1_{+6,3} = \frac{m_1}{m_0} \times 100$$

$$RDI-1_{-3,15} = \frac{m_0 - (m_1 + m_2)}{m_0} \times 100$$

$$RDI-1_{-0,5} = \frac{m_0 - (m_1 + m_2 + m_3)}{m_0} \times 100$$

where

m_0 is the mass, in grams, of the test portion after reduction and before tumbling;

m_1 is the mass, in grams, of the fraction retained on the 6,30 mm sieve;

m_2 is the mass, in grams, of the fraction retained on the 3,15 mm sieve;

m_3 is the mass, in grams, of the fraction retained on the 500 µm sieve.

Record each result to one decimal place.

9.2 Repeatability and acceptance of test results

Follow Annex A, for each of the *RDI-1* indices, by using the repeatability value given in Table 1. Results shall be reported to one decimal place.

Table 1 — Repeatability (*r*)

Mean value of *RDI-1* **%**	***r*** **(%, absolute)**
0	0
5	1,0
10	2,0
15	3,0
20	4,0
25	4,0
50	4,0
75	4,0
80	4,0
85	3,0
90	2,0
95	1,0
100	0

10 Test Report

The test report shall include the following information:

a) reference to this part of ISO 4696, i.e. ISO 4696-1;

b) all details necessary for the identification of the sample;

c) the name and address of the test laboratory;

d) the date of the test;

e) the date of the test report;

f) the signature of the person responsible for the test;

g) details of any operation and any test conditions not specified in this part of ISO 4696 or regarded as optional, as well as any incident which may have had an influence on the results;

h) the reduction-disintegration indices, $RDI\text{-}1_{+6,3}$, $RDI\text{-}1_{-3,15}$, $RDI\text{-}1_{-0,5}$;

i) the sieving conditions, e.g. the method of sieving and the sieving time;

j) the total mass of the material inserted into the tumble drum and taken from the tumble drum;

k) the types of sieves used.

11 Verification

Regular checking of apparatus is essential to assure test result reliability. The frequency of checking is a matter for each laboratory to determine.

The conditions of the following items shall be checked:

- sieves
- weighing device
- reduction tube
- temperature control and measurement devices
- gas flow meters
- purity of gases
- time control device
- tumble drum
- drum rotation equipment

It is recommended that internal reference material be prepared and used periodically to check test repeatability.

Appropriate records of verification activities shall be maintained.

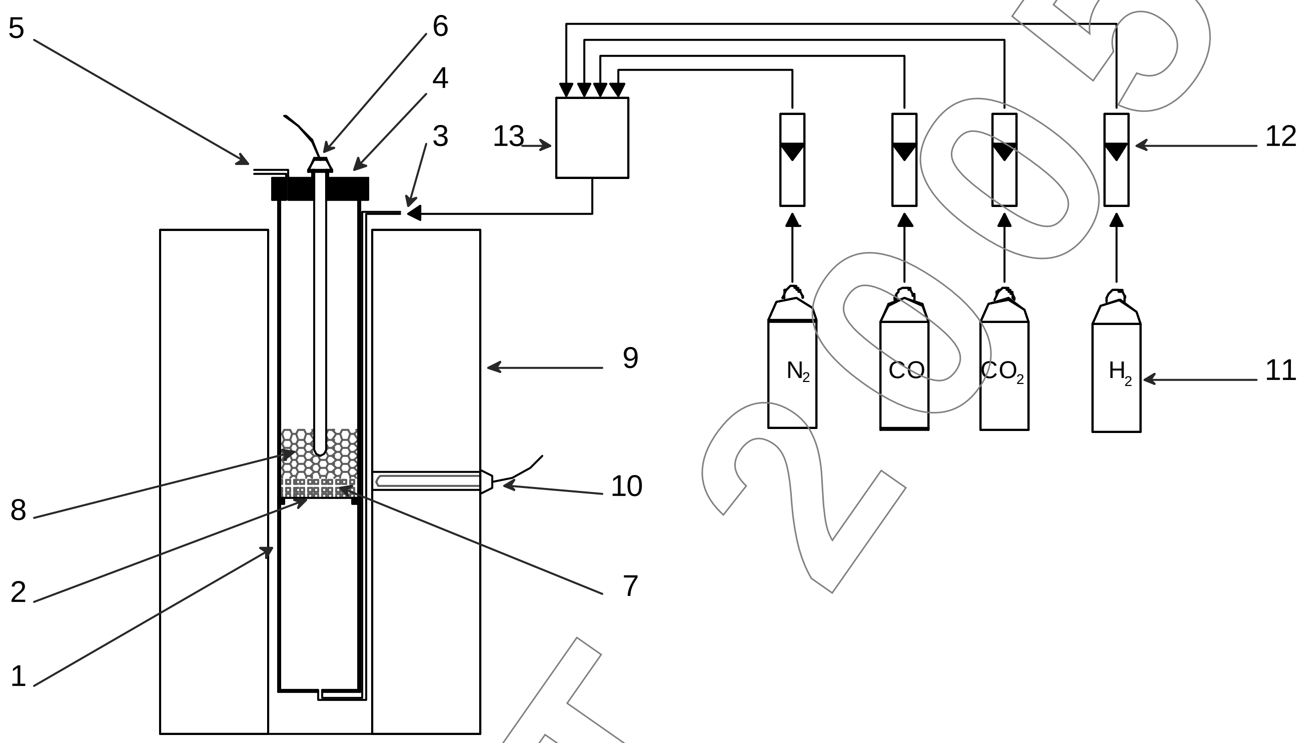

Key:

Reduction tube

1 Reduction tube wall
2 Perforated plate
3 Gas inlet
4 Lid
5 Gas outlet
6 Thermocouple for measuring the reduction temperature
7 Porcelain ball layer
8 Test portion

Furnace

9 Electrically heated furnace
10 Thermocouple for temperature regulation of furnace

Gas supply system

11 Gas cylinders
12 Gas flowmeters
13 Mixing vessel

Figure 1 - Example of test apparatus (schematic diagram)

Dimensions in millimetres

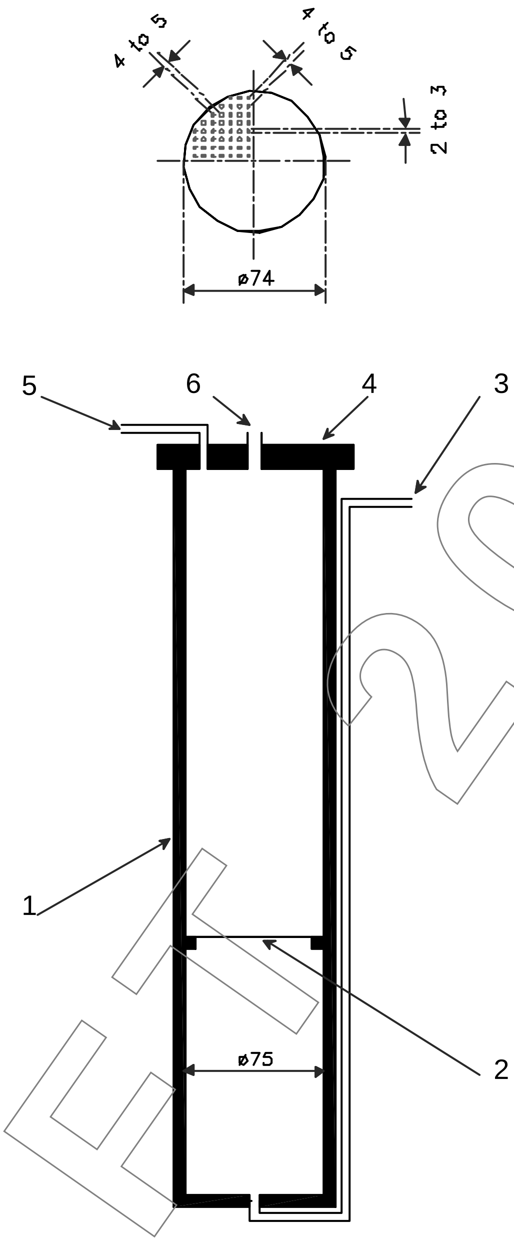

Key:

1 Reduction tube wall
2 Perforated plate
3 Opening for gas inlet
4 Lid
5 Opening for gas outlet
6 Opening for thermocouple insertion

NOTE Dimensions not specified in the apparatus Clause are shown for information only.

Figure 2 - Example of reduction tube (schematic diagram)

Dimensions in millimetres

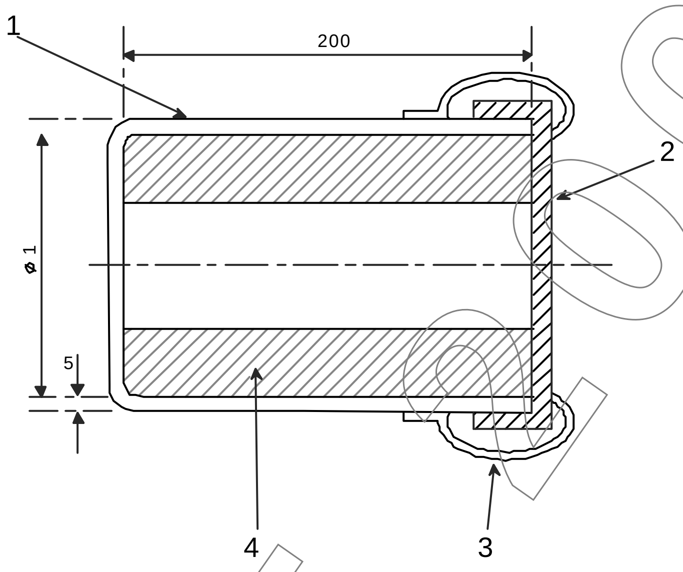

Key:

1	Vessel
2	Lid
3	Clamps
4	Frame with lifters

Lifters: 20 mm wide by 2 mm thick
Material: plain carbon steel

Figure 3 - Example of RDI tumble drum (schematic diagram)

Annex A
(normative)
Flowsheet of the procedure for the acceptance of test results

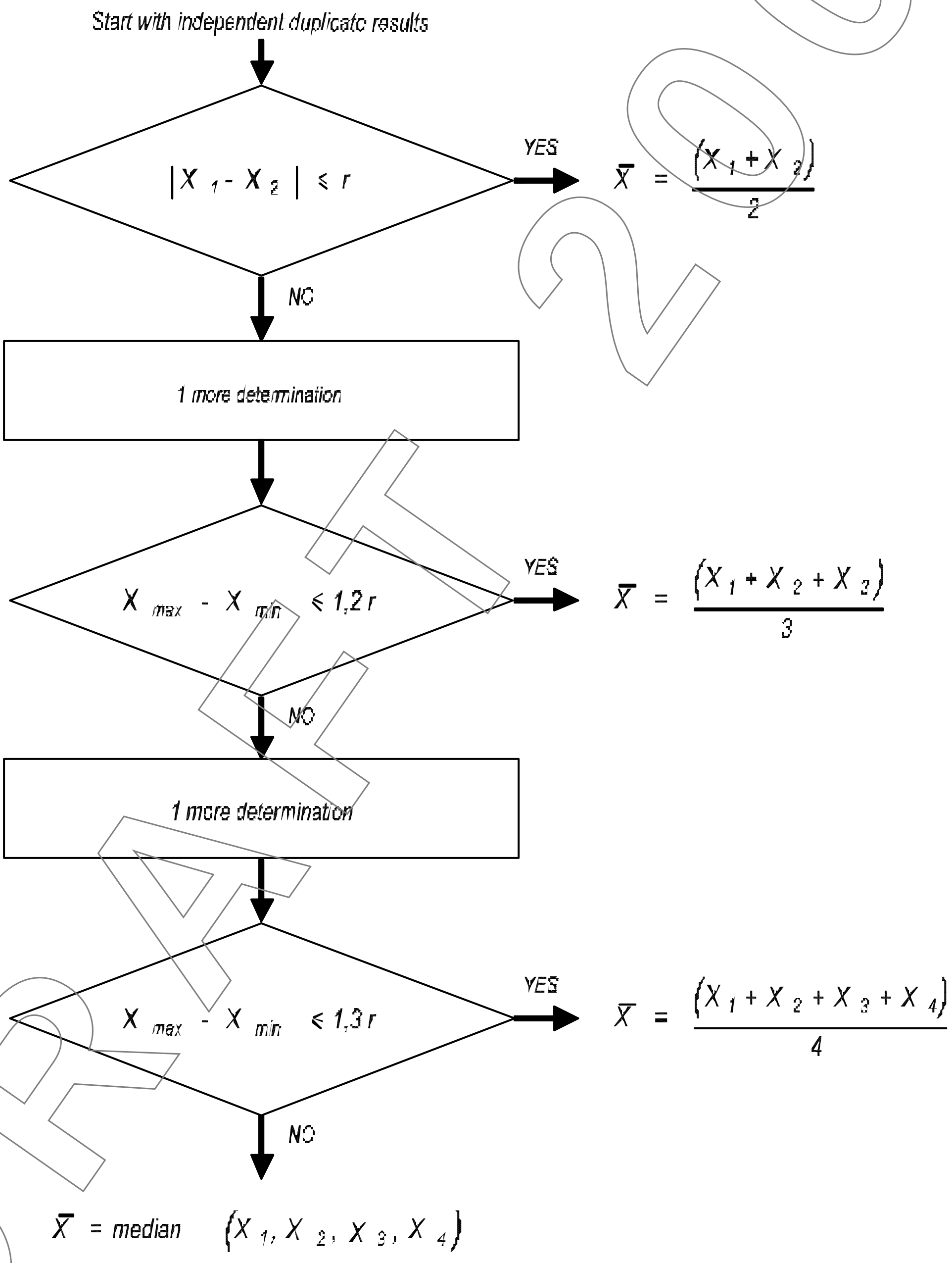

r: see Table 1

APPENDIX 3

TEST RESULTS

Test no.	Ore Type	Size fraction	Changes made to ISO 4696	Sieve analysis after testing (%)										
				+20mm	+16mm	+12.5mm	+10mm	+8mm	+6.3mm	+3.15mm	+2mm	+1mm	+0.5mm	-0.5mm
1	Northern Cape STD	-25+20mm	Size Fraction	46.8	39.28	4.19	1.95	0	0.78	1.33	0.46	0.48	0.58	4.14
2	Northern Cape STD	-20+16mm	Size Fraction		67.74	23.29	1.91	2.37	0.84	1.17	0.66	0.44	0.4	1.17
3	Northern Cape STD	-16+12.5mm	Size Fraction			82.6	11.28	1.58	0.7	1.18	0.56	0.6	0.4	1.08
4	Northern Cape STD	-12.5+10mm	Normal				71.92	16.32	2.62	3.24	1.67	1.53	0.77	1.93
5	Northern Cape STD	-10+8mm	Size Fraction					72.43	12.11	6.73	2.79	2.38	1.29	2.26
6	NORTHERN CAPE OT 1	-12.5+10mm	Normal				64.3	21.4	4.3	3.9	1.6	1.7	0.8	2.1
7	NORTHERN CAPE OT 2	-12.5+10mm	Normal				40.57	28.62	7.71	8.06	3.11	3.67	2.11	6.15
8	NORTHERN CAPE OT 3	-12.5+10mm	Normal				52.1	26.4	8.7	6.2	1.7	1.9	1.3	1.7
9	NORTHERN CAPE OT 4	-12.5+10mm	Normal				81	17.12	0.8	0.42	0.08	0.14	0.14	0.3
10	NORTHERN CAPE OT 5	-12.5+10mm	Normal				58.83	28.41	2.68	4.04	1.6	1.79	0.89	1.77
11	NORTHERN CAPE OT 6	-12.5+10mm	Normal				59.04	14.6	5.93	7.78	3.24	3.75	2.07	3.59
12	NORTHERN CAPE OT 7	-12.5+10mm	Normal				71.3	15.9	3.6	4.3	1.1	1	1	1.8
13	Northern Cape STD	-25+20mm	90 minutes	79.77	15.41	2.57	0	0.44	0.4	0.34	0.1	0.12	0.14	0.7
14	Northern Cape STD	-20+16mm	90 minutes		71.33	8.41	3.81	4.97	1.73	3.45	1.4	1.4	1.16	2.33
15	Northern Cape STD	-16+12.5mm	90 minutes			62.99	16.05	5.68	1.89	3.89	2.42	2.64	1.55	2.88
16	Northern Cape STD	-12.5+10mm	90 minutes				59.64	19.66	4.31	6.24	3.2	2.54	1.67	2.74
17	Northern	-10+8mm	90 minutes					66.12	12.17	9.63	4.01	3.77	1.62	2.68

	Cape STD													
18	Northern Cape STD	-25+20mm	120 minutes	80.46	8.5	3.21	0.54	1.06	0.44	1.27	0.76	0.88	0.92	1.95
19	Northern Cape STD	-20+16mm	120 minutes		57.86	22.6	1.91	2.21	2.66	3.96	1.95	2.5	1.71	2.64
20	Northern Cape STD	-16+12.5mm	120 minutes			51.17	15.66	7.09	3.54	7.87	4.97	4.85	2.17	2.68
21	Northern Cape STD	-12.5+10mm	120 minutes				57.4	20.8	4.4	6.5	3.1	3.2	2	2.6
22	Northern Cape STD	-10+8mm	120 minutes					54.68	17.2	12.41	5.31	5.09	2.34	2.97
23	Northern Cape STD	-12.5+10mm	550°C				66	17.3	3.4	5.8	2.2	1.9	1.4	2
24	Northern Cape STD	-12.5+10mm	600°C				63.8	18.8	4.5	5.9	1.8	1.9	1.2	2.1
25	Northern Cape STD	-12.5+10mm	650°C				69.1	15.2	3.5	5.2	2	1.9	1.2	1.9
26	Northern Cape STD	-12.5+10mm	700°C				67.7	14.8	4.8	5	2.4	2.1	1.1	2.1
27	Northern Cape STD	-12.5+10mm	5% H2				71.4	17.3	2.3	3.2	0.9	1.5	0.9	2.5
28	Northern Cape STD	-12.5+10mm	10% H2				66.2	17	3.9	5.1	2.3	2	1.5	2
29	Northern Cape STD	-12.5+10mm	600°C 90 min				64.6	16.72	5.13	5.03	2.66	2.51	1.22	2.13
30	Northern Cape STD	-12.5+10mm	600°C 120 min				56	11.7	8.6	10.3	4.3	4.3	1.9	2.9
31	Northern Cape STD	-12.5+10mm	700°C 90 min				64.1	16.5	7.8	4.7	2.1	1.8	1.2	1.8
32	Northern Cape STD	-12.5+10mm	700°C 120 min				57.5	16.8	6.5	8.9	3.7	3.1	1.4	2.1
33	Northern Cape STD	-12.5+10mm	750°C 60 min				76.3	12.5	3.2	3.3	1.4	1.2	0.6	1.5
34	Northern Cape STD	-12.5+10mm	800°C 60 min				83.1	8.5	3.1	1.8	0.6	0.5	0.3	2.1

APPENDIX 4

MINERALOGY REPORT

KUMBA RESOURCES

RAW MATERIALS TECHNOLOGY

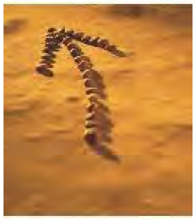

Mineralogical Investigation into the Micro-fracturing of Iron Ore at High Temperature

Prepared for

WF van der Vyver

By

Stewart Brand

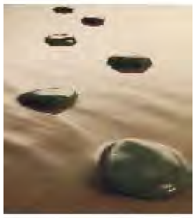

October 2006

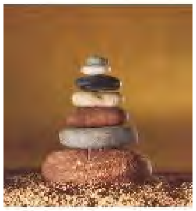

WINNING THROUGH INNOVATION

UNIVERSITEIT VAN PRETORIA
UNIVERSITY OF PRETORIA
YUNIBESITHI YA PRETORIA

Executive Summary

Seventeen different iron ore samples that had been heated to high temperatures, under varying atmospheric conditions, were observed under the Scanning Electron Microscope (SEM). The samples were studied in order to determine the degree of fracturing within the samples and the influence of mineralogy on the propagation, distribution and intensity of micro-fractures. Fracture formation and propagations depends on a variety of inter-related factors including:

1) The presence or absence of gangue phases

The presence of gangue phases appears to enhance fracture formation. Fractures that formed in samples that contain little or no gangue had an evenly spaced regular framework of fractures. Gangue minerals appear to influence the distribution of fractures. Fractures appear to form more prolifically in gangue minerals such as muscovite, the fractures often do not penetrate the surrounding hematite and are terminated at the grain boundary between the hematite and gangue minerals.

Therefore, although gangue minerals may not cause fractures to form, they do allow for fractures to mature more quickly. Furthermore, where gangue minerals occur, fractures deviate towards the gangue. In places where fractures occur and no gangue minerals are present, the fractures tend to form a regular framework.

2) Type of Gangue Mineral

The type of gangue mineral does not appear to be an important factor in the formation or propagation of fractures. Most of the gangue mineral observed in this study have similar densities and all the gangue minerals are significantly less competent than hematite. Quartz appears to fracture slightly more than P bearing minerals as there does not appear to be a network of secondary fractures developed in apatite when it is intersected by a fracture, as is the case when a fracture intersects quartz. The secondary fracture network does not extend into the surrounding hematite and therefore does not play a significant role in the overall fracture development within the sample.

3) Degree of Reduction

The degree of reduction appears to be the primary influence on fracture formation in all the samples observed. The more reduced a sample is, the more fractures there are. In most samples, fracture networks have developed only in areas where the hematite has been reduced and usually do not extend into areas where the ore has not been reduced.

4) Sample Porosity

Extensive sample porosity can reduce the amount of fractures caused by reduction within a sample. The open pores allow for the volume increase without fracturing. Where fracturing does occur it usually originates and terminates at open pores. In samples that have extremely low porosity fractures are also rare as the sample can only be reduced around the edges.

For the maximum amount of fracturing to occur within a sample, the sample must be porous enough to allow for reduction of the sample, whilst not having enough open pores to allow for the volume increase to be accommodated by the pores.

5) Internal structure

Where a preferred orientation or foliation fabric occurs the internal structure of the samples has an influence on fracture propagation as fractures tend to exploit the planes of weakness within the sample.

Table of Contents

1. INTRODUCTION

1.1 AIM

The aim of the investigation is to describe the influence of mineralogy on the micro-structural behavior of iron ore samples heated under various atmospheric conditions with the aim of determining the effects, if any, of mineralogy on the propagation, distribution and intensity of micro-fractures in iron ore samples undergoing reduction at high temperatures (500 ºC - 700 ºC).

1.2 ORIGIN OF SAMPLES

The samples were received as small discs 8mm in diameter and 2m thick. The discs had been heated under reducing conditions in a high temperature microscope.

Table 1 lists the original sample labels as well as the environmental conditions under which the samples were heated.

Table 1: Sample List

	Sample	Temp (ºC)	Time (min)	Atmosphere
1	Ore Type 5 B	500	60	CO/CO_2
2	Ore Type 3 B	500	60	CO/CO_2
3	Ore Type 4 A	500	60	CO/CO_2
4	Northern Cape Std	500	60	CO/CO_2
5	Northern Cape Std B	700	30	CO/CO_2
6	Northern Cape Ore Type 2 C	500	60	CO/CO_2
7	Northern Cape Ore Type 5	500	30	

8	Northern Cape Std C	500	60	CO/CO_2
9	Northern Cape Std Test1	700	30	
10	Ore Type 4 D2	500	60	CO/CO_2
11	Ore Type 4 B	700	30	CO/CO_2
12	Ore Type 3 D	500	60	CO/CO_2
13	Northern Cape Std Test	500	60	CO/CO_2
14	Ore Type 5	500	60	CO/CO_2
15	Ore Type 5 C	500	60	CO/CO_2
16	Northern Cape Std A	500	60	CO/CO_2
17	Ore Type 4 C	500	60	CO/CO_2

METHODOLOGY

Samples were mounted in epoxy resin, polished and coated with gold in a sputter coater. They were observed in a JOEL 5800 scanning electron microscope at the Department of Microscopy and Micro-Analysis at the University of Pretoria,

2. DISCUSSION: MICRO-TECTONICS

Rheology is the study of the quantitative response of rocks to stress. Rocks under stress can deform either by brittle or ductile mechanisms. Brittle behavior takes place at lower temperatures and shallower depths in the Earth's crust than ductile behavior. The deformation of rocks is achieved by a large number of processes on the scale of individual grains.

Mineralogy has been recognized as an influencing factor on the deformation mechanisms of rocks under stress. *Passchier, C.W. and Trouw, R.A.J.* ascribe the deformation mechanisms in rocks to be dependant on their, "mineralogy, composition of inter-granular fluid, grain size, porosity and permeability, temperature, pressure, differential stress and externally imposed strain rate."

In this study we only observe brittle deformation mechanisms in mono-mineralic, bi-mineralic and poly-mineralic samples comprising predominantly of hematite with minor amounts of gangue minerals. **Table 2** lists the minerals identified in this study. The behavior of poly-mineralic samples under stress is complex and one has to take into consideration the concept of a, "stress-supporting network." If "hard" (e.g. hematite) and "soft" (e.g. muscovite) minerals occur together in the same sample the strength of the sample does not increase linearly in relation to the amount of "hard" mineral present. In this study, most samples comprise predominantly of hematite and the small amount of gangue minerals present is unlikely to have an influence on the overall stress supporting network.

When observing samples under the SEM that have undergone deformation, with the aim of understanding the mechanisms of deformation and metamorphism, one must be mindful of the fact that the sample is only being observed in 2 dimensions whilst deformation has taken place in 3 dimensions.

In iron ore samples, the primary mechanism for the formation of fractures under reducing conditions in hematite samples is due to the volume increase as hematite is reduced to a porous form of magnetite.

Table 2: List of Minerals

MINERAL	IDEAL FORMULA
Apatite	Ca5(PO4)3(OH,F,Cl)
Hematite	Fe_2O_3
Magnetite	Fe_3O_4
Muscovite	$KAl_2(Si_3Al)O_{10}(OH,F)_2$
Quartz	SiO_2

3. RESULTS

Each sample is discussed and described individually, however the samples are also grouped according to the predominant feature observed in the sample. Samples were allocated into the following groups:

1. Mono-mineralic hematite samples	(Samples 3, 4, 8, 11, 12, 13 and 17)
2. Poly-mineralic samples	(Samples 1, 5, 7, 10, 14 and 15)
3. Porous samples	(Samples 2, 9 and 16)
4. Other	(Sample 6)

Table 4. Summary of results

	SAMPLE	HEMATITE	GANGUE	GROUP	POROSITY	FRACTURE TYPE
1	Ore Type 5 B	Granular/ Specularite	Apatite/ Quartz	2	Low	Extensive, throughout the sample
2	Ore Type 3 B	Granular/ Specularite	None	3	Variable	Regular network
3	Ore Type 4 A	Granular	None	1	Low	Perpendicular to edge
4	Northern Cape Std	Granular	None	1	Medium	Parallel to edge
5	Northern Cape Std B	Granular	Quartz	2	Low	Extensive, throughout the sample
6	Northern Cape Ore type 2 C	Granular	Quartz	4	Low	Parallel to foliation
7	Northern Cape Ore Type 5	Specularite	Apatite/ Quartz	2	Medium	Parallel to edge Regular network
8	Northern Cape Std C	Granular	None	1	Low	Perpendicular to edge
9	Northern Cape Std Test1	Granular	None	3	High	Perpendicular to edge
10	Ore Type 4 D2	Granular	Quartz/ Muscovite	2	Low	Parallel to edge
11	Ore Type 4 B	Granular	None	1	Low	Parallel/ Perpendicular to edge
12	Ore Type 3 D	Granular	None	1	Low	Parallel/ Perpendicular to edge
13	Northern Cape Std Test	Granular	None	1	Low	Parallel/ Perpendicular to edge
14	Ore Type 5	Granular	Apatite/ Quartz	2	Low	Parallel Regular network to edge
15	Ore Type 5 C	Granular	Al-silicates/ Apatite	2	Low	None
16	Northern Cape Std A	Granular/ Specularite	None	3	Low	Associated with Specularite
17	Ore Type 4 C	Granular	None	1	Low	Parallel to edge

Group 1: Mono-mineralic hematite samples

These samples can be considered to be mono-mineralic and comprise essentially exclusively of hematite. The samples all show very similar physical characteristics in that they have low porosity, essentially no gangue minerals and they also have similar micro-fracture characteristics.

The samples all exhibit fracturing on the samples edges, the first place in which reduction occurs. The fractures are usually oriented perpendicular to the sample edge ad radiate inwards. The fractures only penetrate as far as the sample has been reduced. Internal fractures occur in a regularly spaced framework.

3.1.1 Sample 3: Ore Type 4 A

This sample is homogeneous and does not have any primary gangue minerals or porosity. Fracturing is generally rare and fractures are predominantly observed at the edge of the sample, where the sample has been reduced. These fractures are radial and only occur perpendicular to the edge of the sample.

A few fractures are observed filled with muscovite indicating that these are pre-existing fractures. A few randomly distributed fractures occur internally within the sample however these fractures are not associated with any gangue minerals

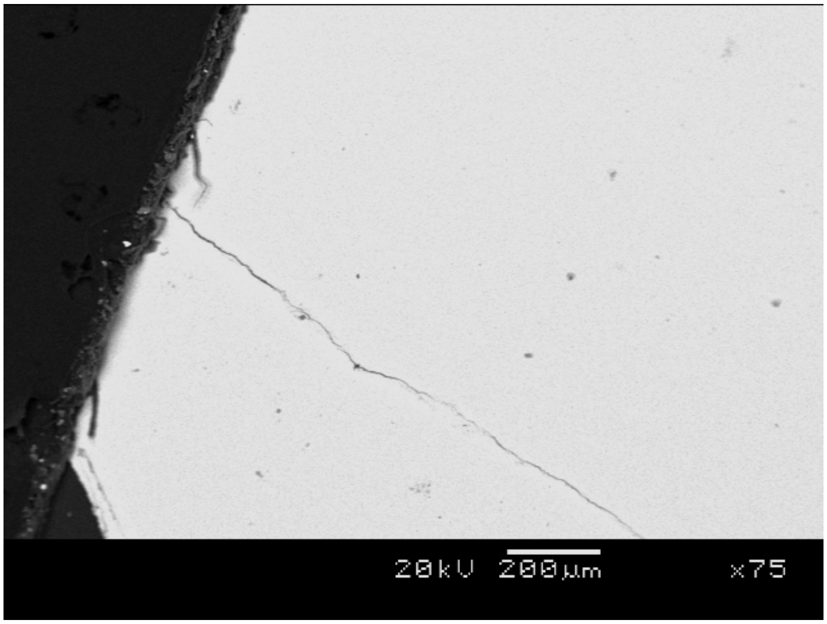

Figure 1. Electron backscatter image of sample 3 showing the homogeneity of the sample. The sample is essentially mono-mineralic and comprises almost exclusively of hematite. Small radial fractures occur at the edge of the sample, where it has been reduced.

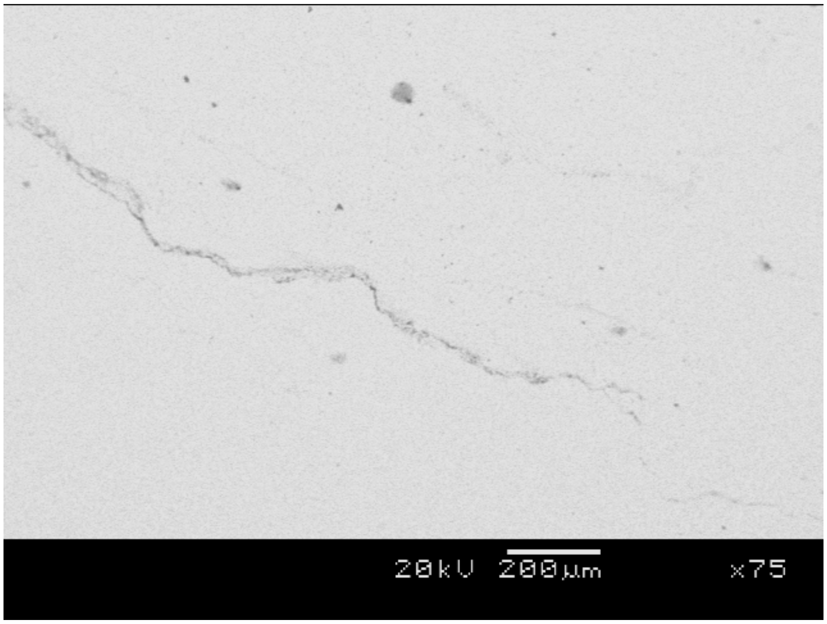

Figure 2. Electron backscatter image of sample 3 showing a rare internal fracture. This fracture is not associated with gangue minerals, porosity or reduction.

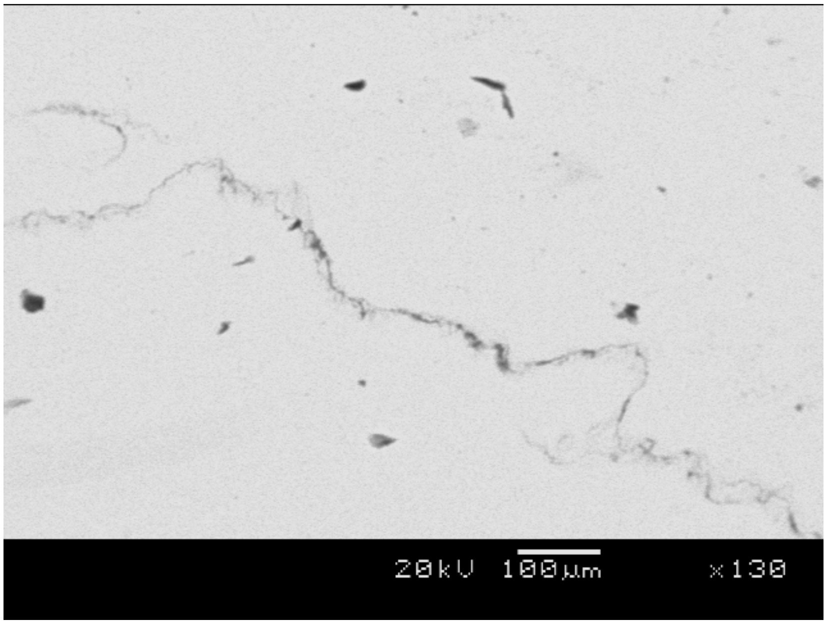

Figure 3. Electron backscatter image of sample 3 showing a pre-existing fracture filled with muscovite.

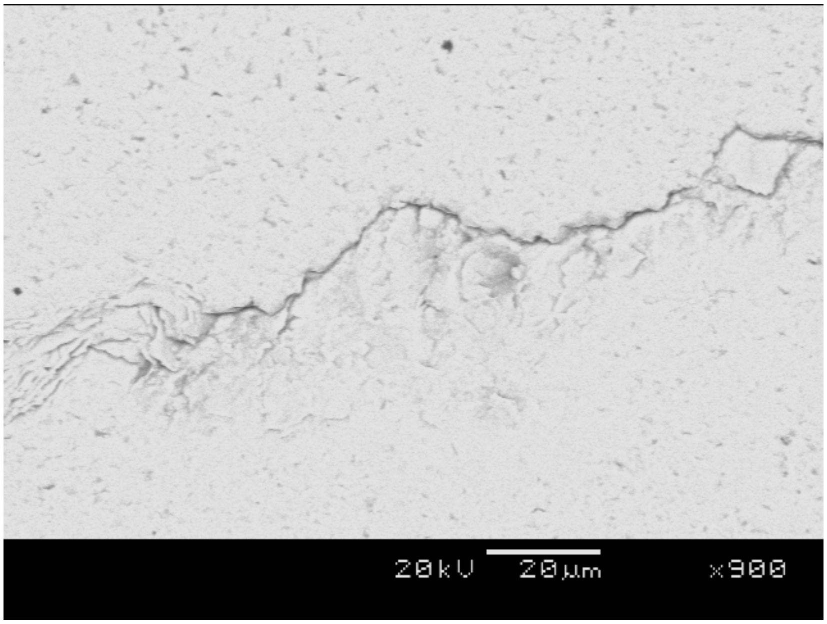

Figure 4. Electron backscatter image of sample 3 showing a rare internal fracture. This fracture is not associated with gangue minerals, porosity or reduction.

3.1.2 Sample 8: Northern Cape Std (C)

This sample is almost completely homogeneous with very little gangue and low porosity. It comprises almost exclusively of granular hematite. The only fracturing observed in the sample occurs at the edge of the sample where it has been reduced. The fractures are perpendicular to the edge of the sample and only penetrate the sample as afar as it has been reduced.

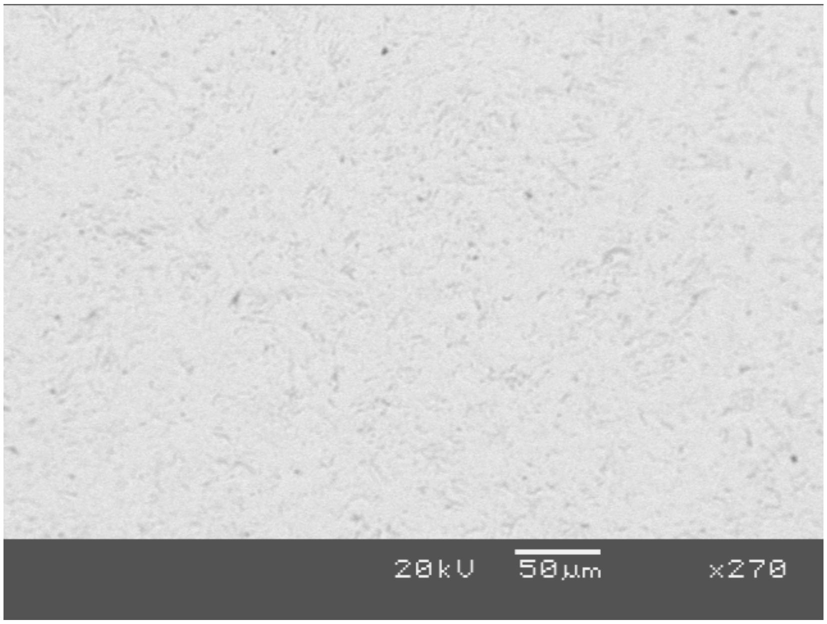

Figure 5. Electron backscatter image of sample 8 showing the homogeneity of the sample. The sample is essentially mono-mineralic and comprises almost exclusively of hematite.

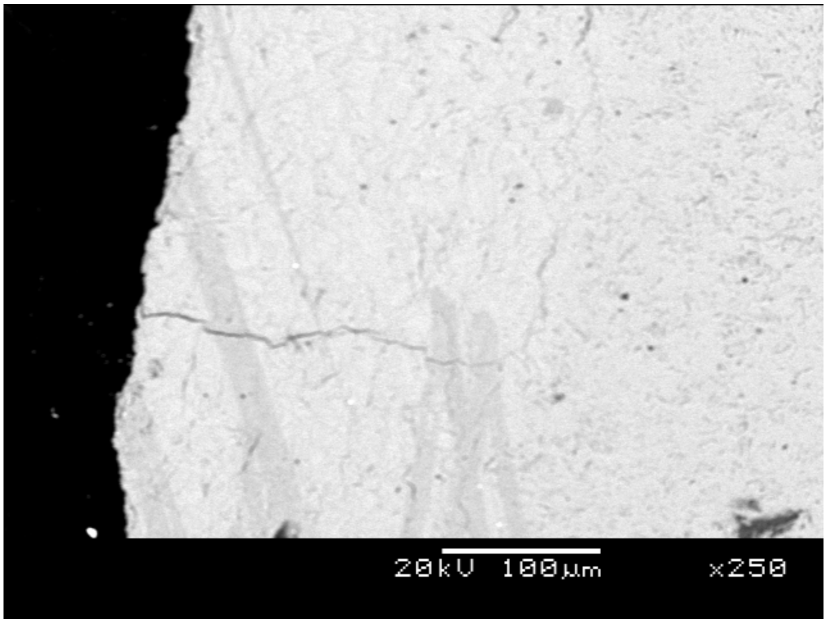

Figure 6. Electron backscatter image of sample 8 showing a fracture perpendicular to the sample edge. The fracture only penetrates as far as the sample has been reduced.

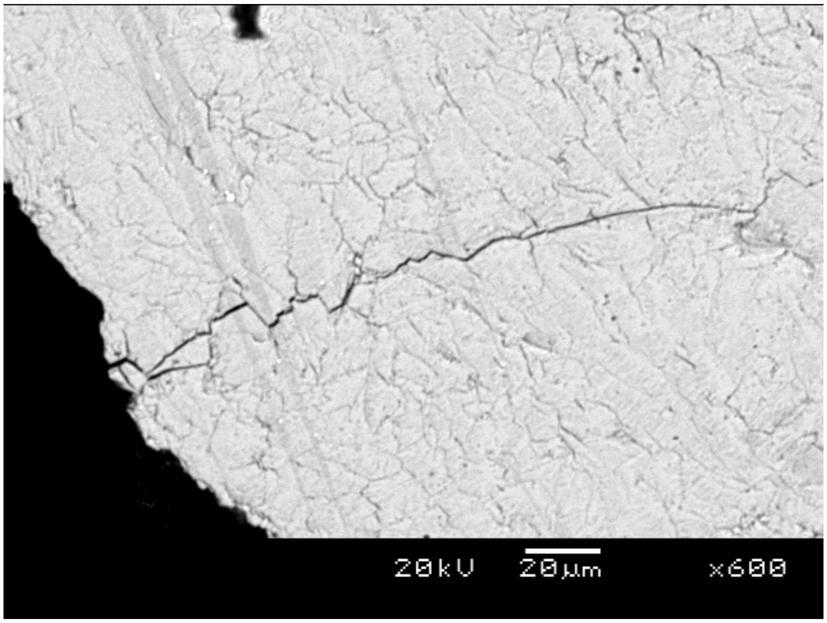

Figure 7. Electron backscatter image of sample 8 showing another radial fracture perpendicular to the edge of the sample.

3.1.3 Sample 4: Northern Cape Std

This sample, as with the other samples observed in this group is a mono-mineralic sample comprised almost exclusively of hematite. Unlike the other samples in this group, this sample has slightly higher porosity. The sample is reduced around the edges and has associated fractures. The interior of the sample, where no reduction has taken place, is homogenous and even small fractures are absent. This may be due to the increased porosity of the sample.

Unlike the other mono-mineralic samples, the fractures formed during reduction occur parallel to the sample edge and not perpendicularly as is more commonly observed.

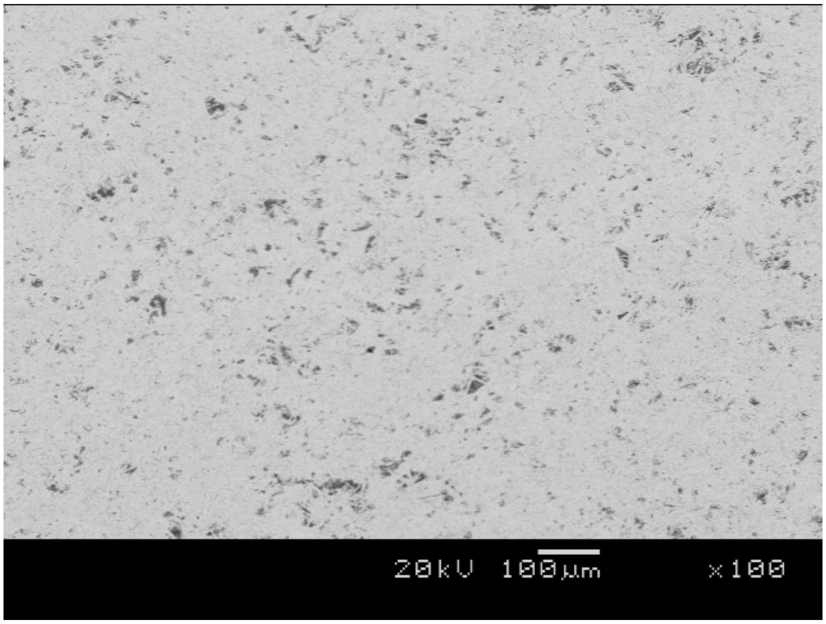

Figure 8. Electron backscatter image of sample 4 showing a homogenous mono-mineralic sample, with slight higher porosity than the other samples in this group.

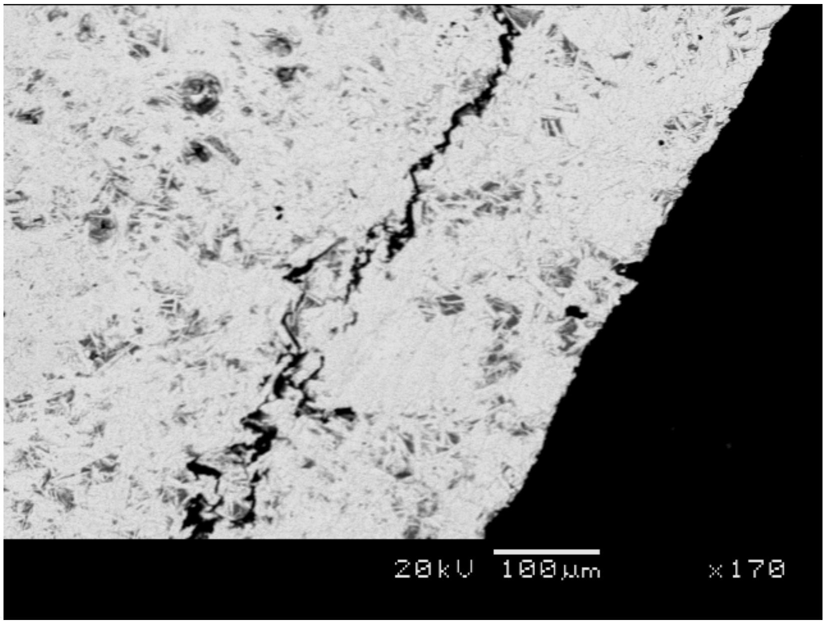

Figure 9. Electron backscatter image of sample 4 showing fractures parallel to the sample edge caused by the volume increase when hematite is reduced to magnetite.

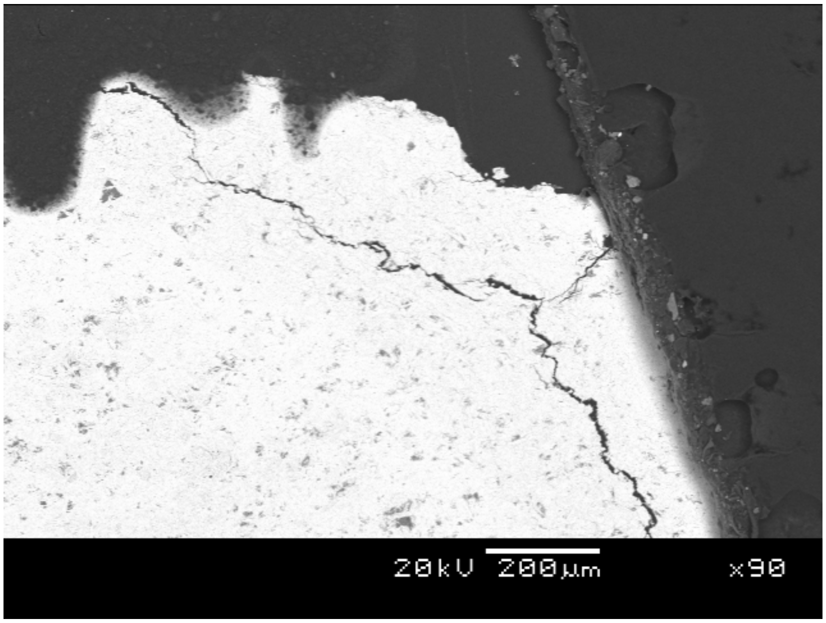

Figure 10. Electron backscatter image of sample 4 showing fractures parallel to the sample edge caused by the volume increase when hematite is reduced to magnetite.

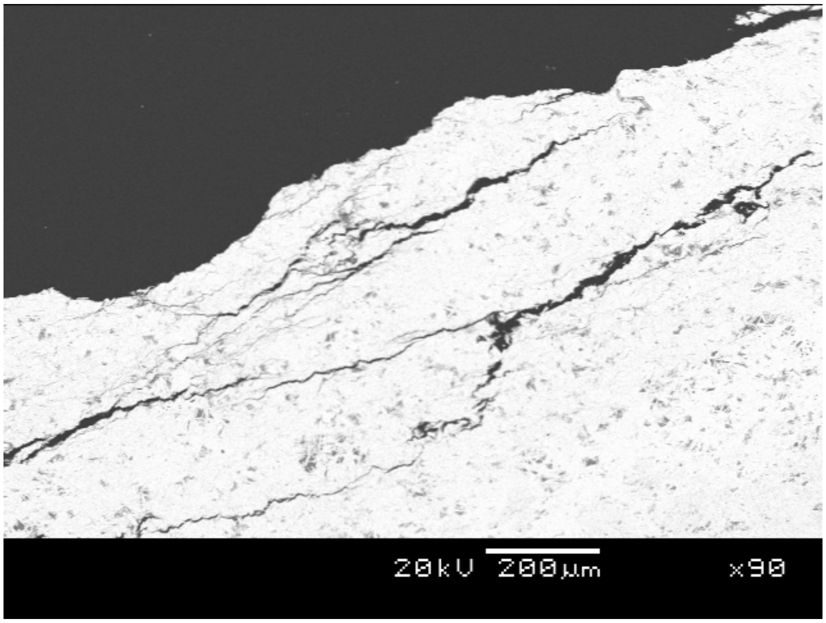

Figure 11. Electron backscatter image of sample 4 showing multiple fractures parallel to the sample edge caused by the volume increase when hematite is reduced to magnetite.

3.1.4 Sample 11: Ore Type 4B

This sample is a mono-mineralic sample comprised almost exclusively of hematite. The sample has very low porosity. Fractures occur throughout the sample wherever the hematite has been reduced. Fractures occur primarily at the edge of the sample both parallel and perpendicular to the sample edge. Where the sample has not been reduced there are no clearly defined fractures.

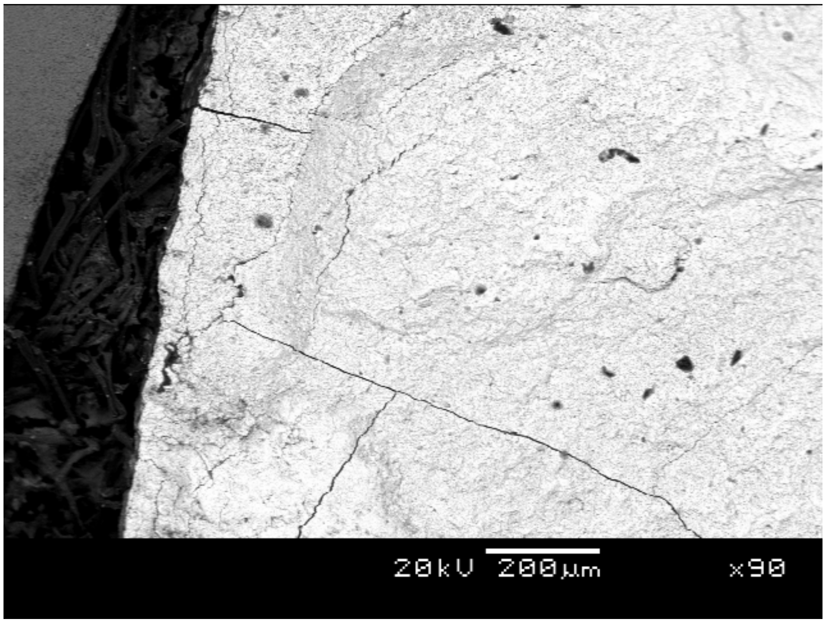

Figure 12. Electron backscatter image of sample 11 showing fractures both perpendicular and parallel to the sample edge where the ore has been reduced.

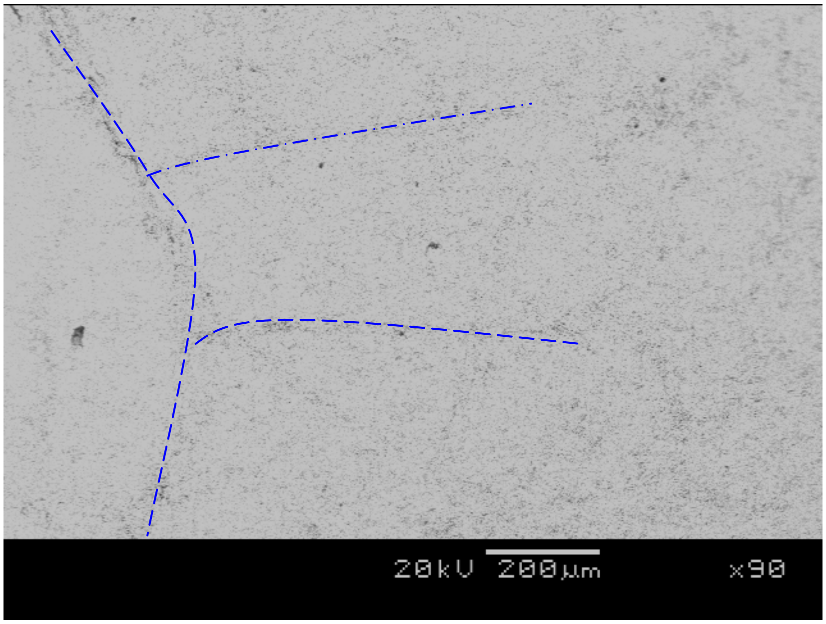

Figure 13. Electron backscatter image of sample showing the homogenous, mono-mineralic interior of the sample. A few proto-fractures appear to have formed (stippled line) however no actual fracturing has taken place.

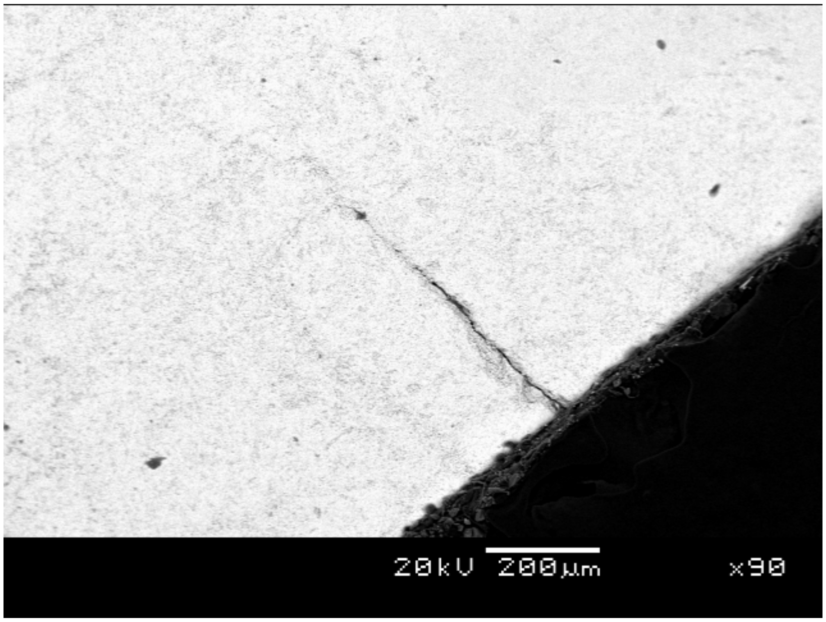

Figure 14. Electron backscatter image of sample 12 showing a small fracture that has developed perpendicular to the sample edge, where the ore has been reduced.

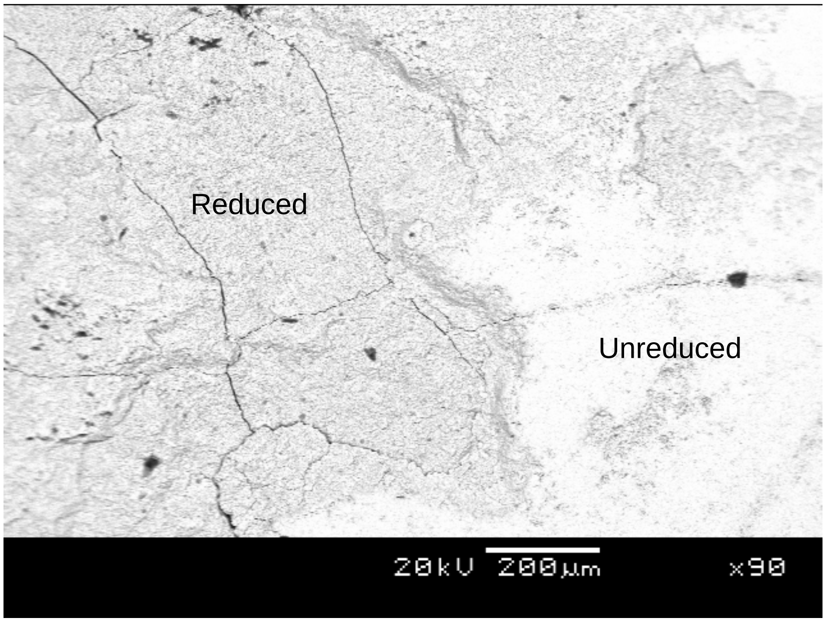

Figure 15. Electron backscatter image of sample 11 showing an area of reduced ore (left) and an area of unreduced ore (right) . Notice the network of fractures that has developed where reduction has taken place.

3.1.5 Sample 12: Ore Type 3 D

This sample is a very low porosity, mono-mineralic hematite sample. There are very few open pores and almost no gangue phases observed. Fracturing occurs primarily at the edge of the sample where it has been reduced. The fractures only penetrate the sample as far as it has been reduced. The interior of the sample is homogenous with no fractures, no gangue, no open pores and no reduction.

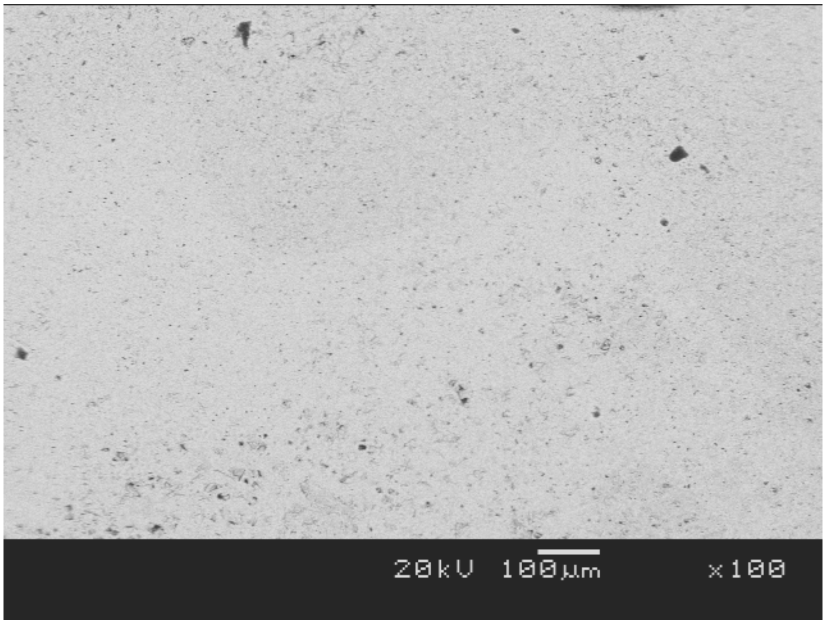

Figure 16. Electron backscatter image of sample 12 showing the homogeneity of the sample. No gangue minerals are observed and the sample has very low porosity.

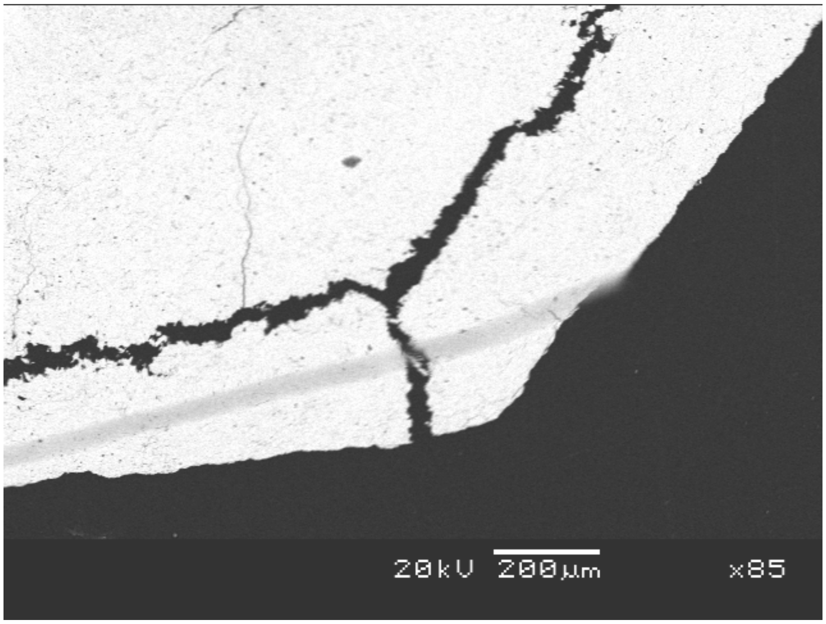

Figure 17. Electron backscatter image of sample 12 showing large fractures perpendicular and parallel to the edge of the sample.

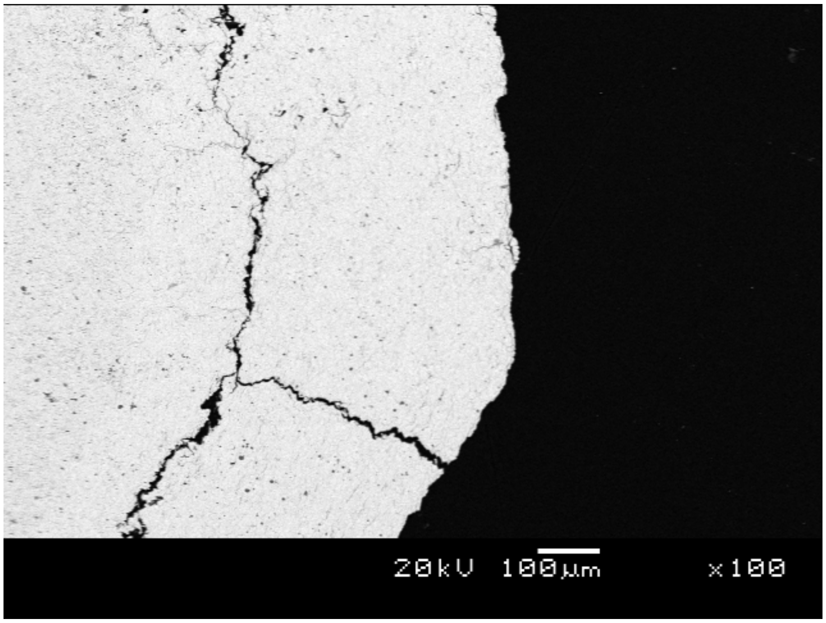

Figure 18. Electron backscatter image of sample 12 large fractures perpendicular and parallel to the edge of the sample.

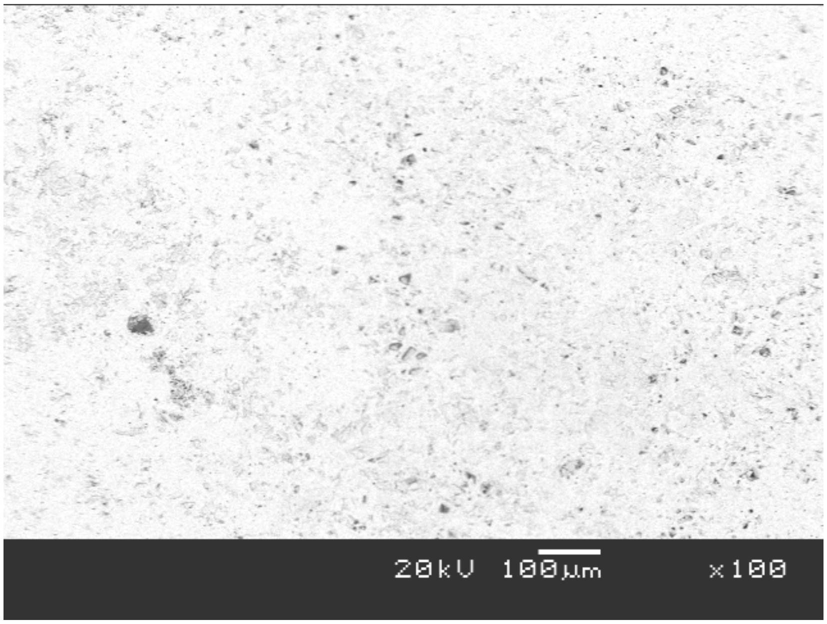

Figure 19. Electron backscatter image of sample 12 showing the homogeneity of the sample.

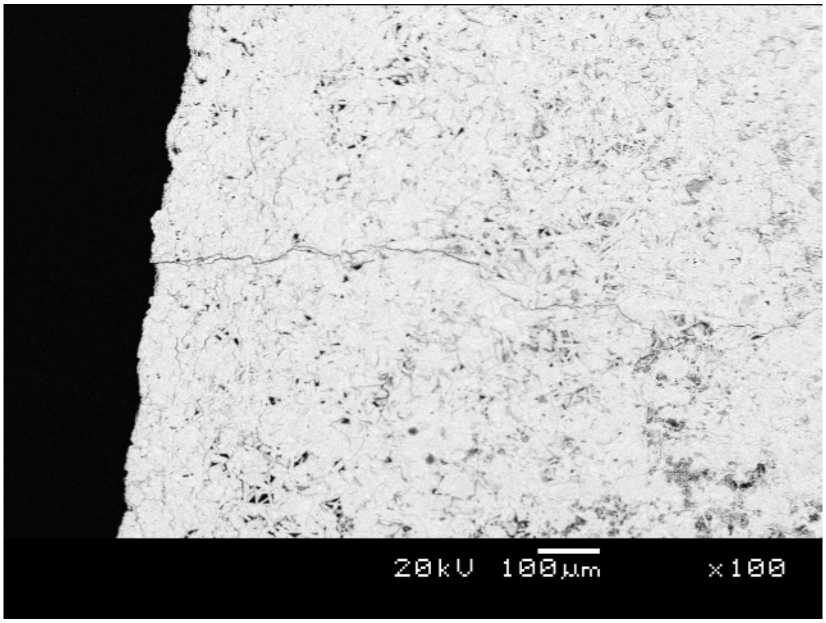

Figure 20. Electron backscatter image of sample 12 large fractures perpendicular and parallel to the edge of the sample.

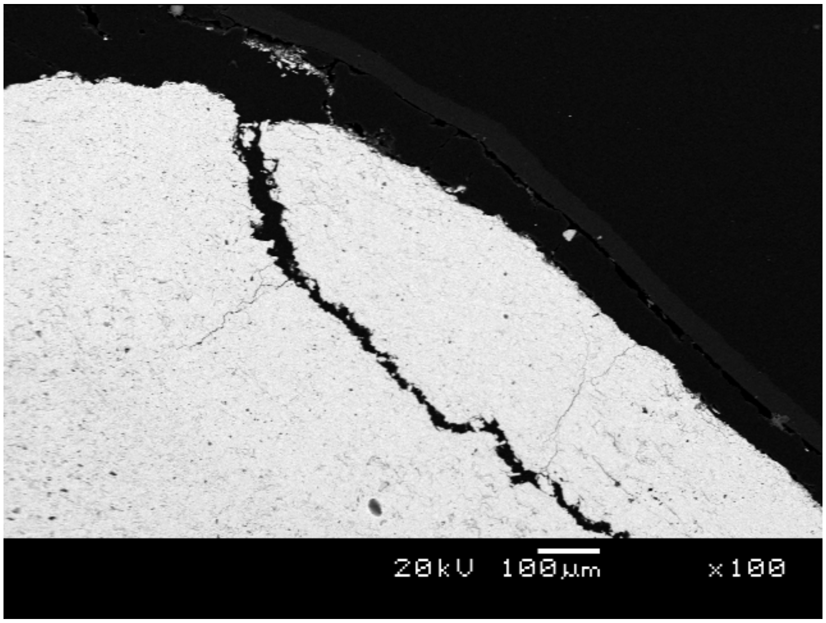

Figure 21. Electron backscatter image of sample 12 large fracture parallel to the edge of the sample. Smaller fractures occur perpendicular to the edge of the sample.

3.1.6 Sample 13: Northern Cape Std Test 7/06/06

This sample is similar to sample 12 in that it comprises predominantly of hematite. The sample has very few open pores and very few gangue minerals. Most fractures that occur within the sample occur at the sample edge where reduction has occurred. The fractures occur both parallel and perpendicular to the sample edge however the fractures that occur parallel to the sample edge are more pervasive.

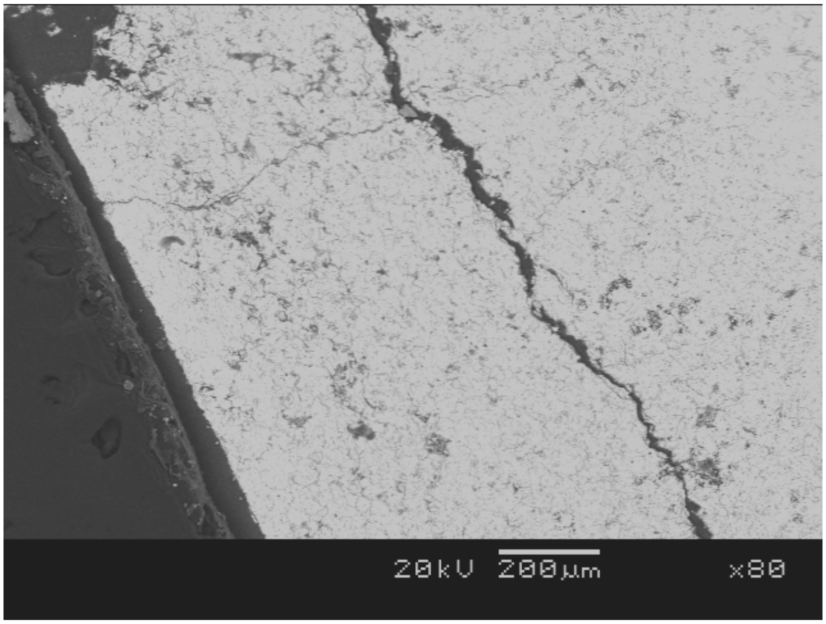

Figure 22. Electron backscatter image of sample 13 showing fractures parallel and perpendicular to the edge of the sample, where the sample has been reduced.

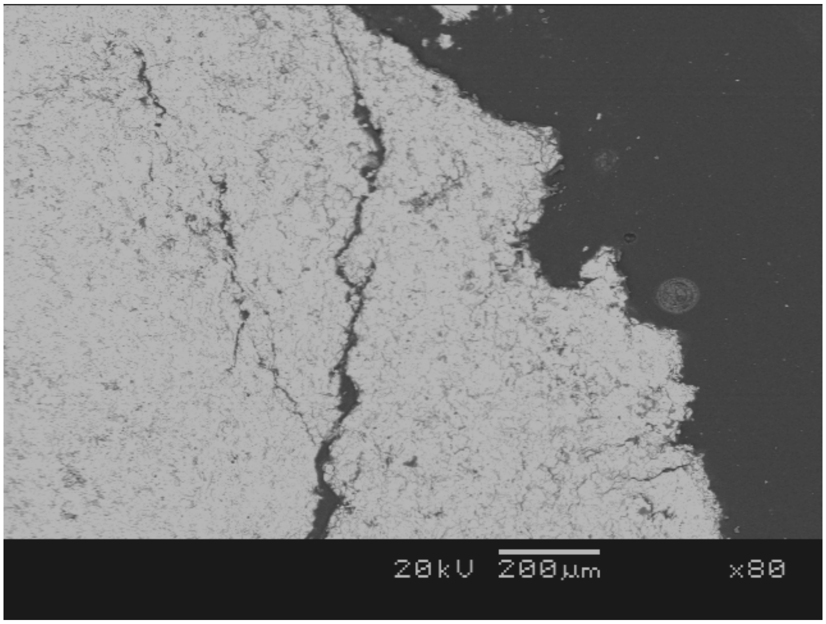

Figure 23. Electron backscatter image of sample 13 showing fractures parallel to the edge of the sample, where the sample has been reduced.

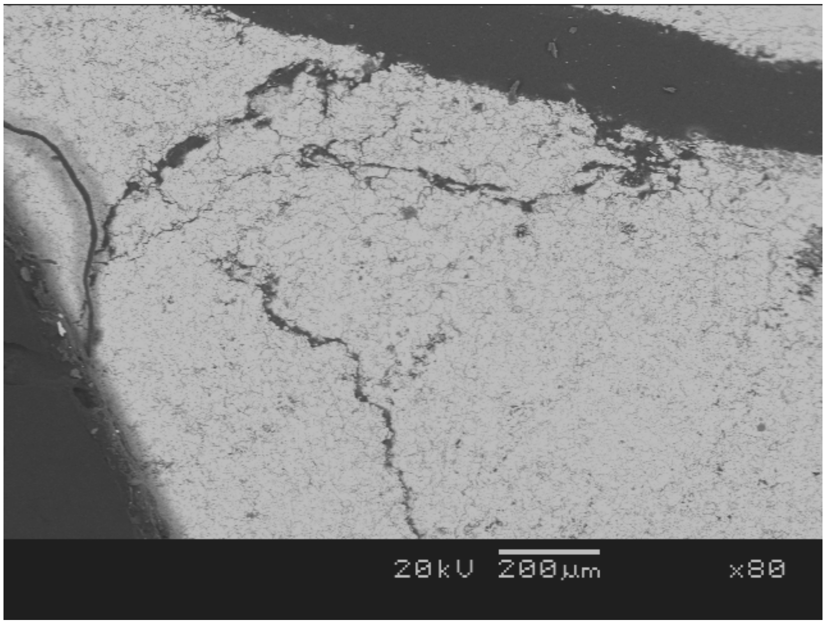

Figure 24. Electron backscatter image of sample 13 showing fractures parallel and perpendicular to the edge of the sample, where the sample has been reduced.

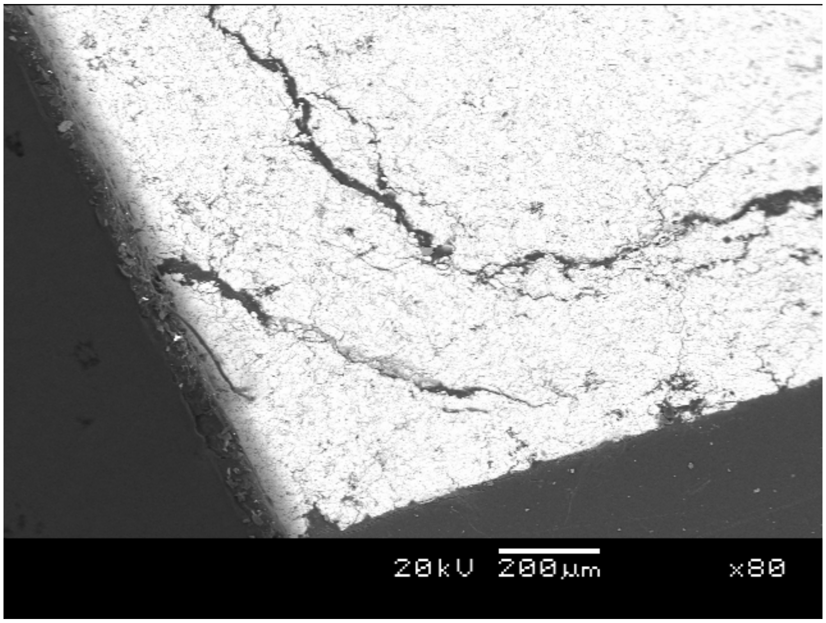

Figure 25. Electron backscatter image of sample 13 showing fractures parallel to the edge of the sample, where the sample has been reduced.

3.1.7 Sample 17: Ore Type 4 C

This sample is a homogeneous mono-mineralic sample comprising almost exclusively of hematite. Most fractures observed in this sample occur at the edge of the sample. The fractures are radial, and occur perpendicular to the edge of the sample. The only other fractures observed in this sample are a regularly spaced set of fractures. The fractures intersect at right angles within the sample.

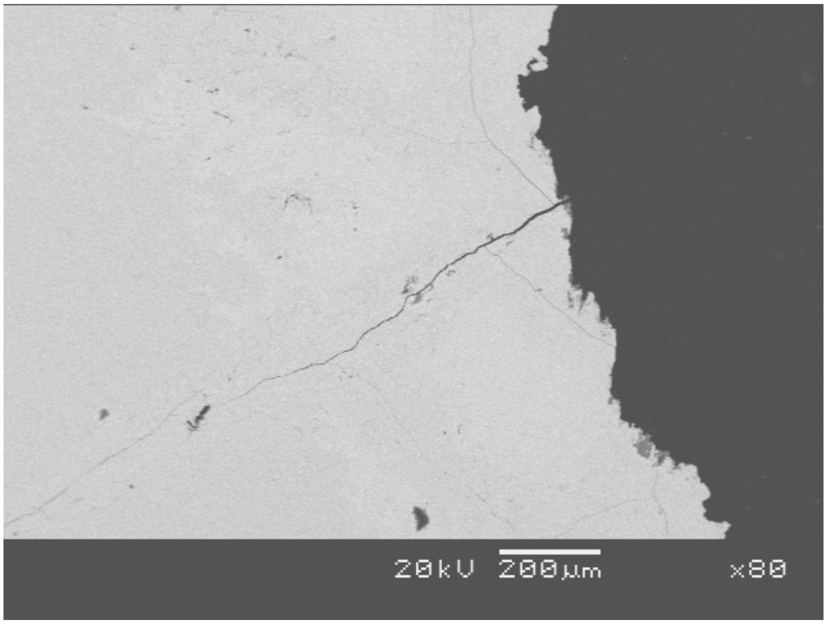

Figure 26. Electron backscatter image of sample 17 showing a fracture perpendicular to the sample edge. The fracture only penetrates as far as the sample has been reduced.

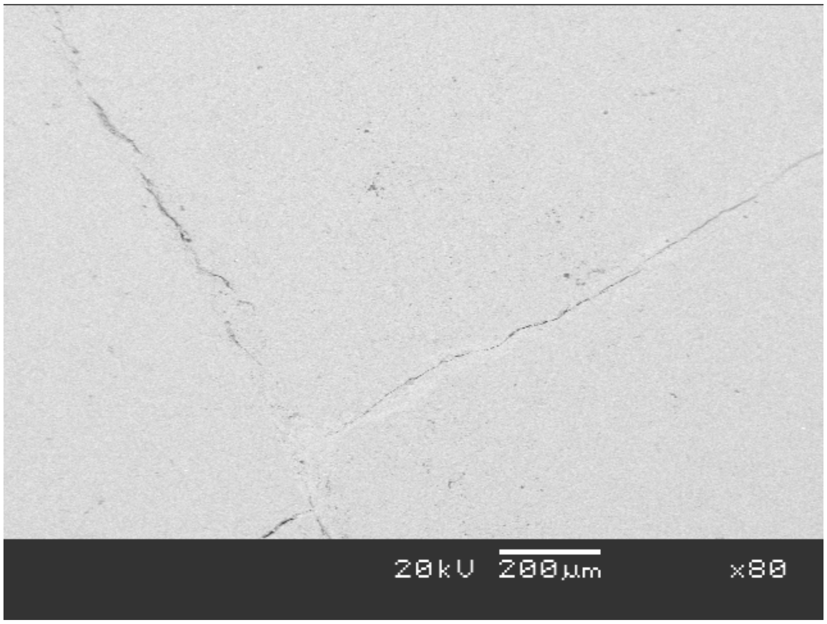

Figure 27. Electron backscatter image of sample 17 showing regularly spaced fracture/joint set in the sample.

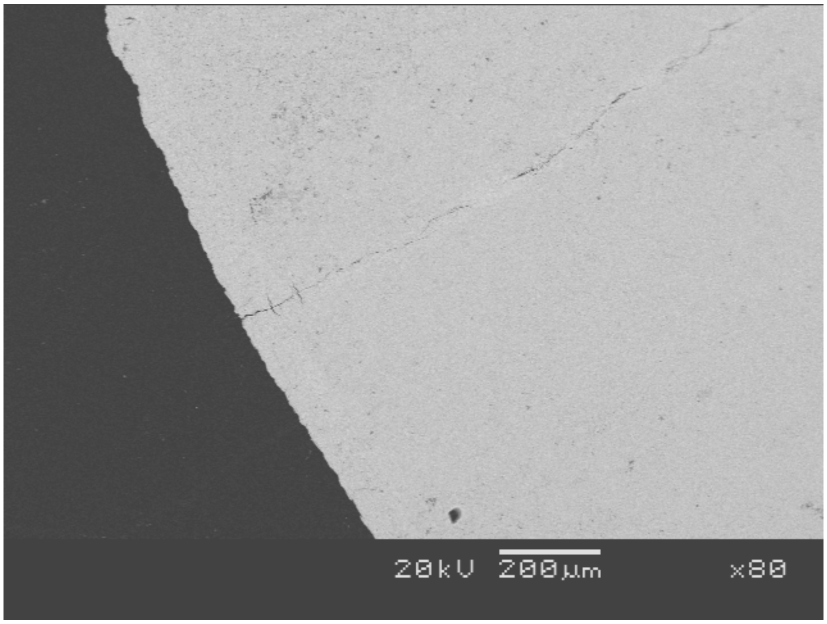

Figure 28. Electron backscatter image of sample 17 showing a fracture perpendicular to the sample edge. The fracture only penetrates as far as the sample has been reduced.

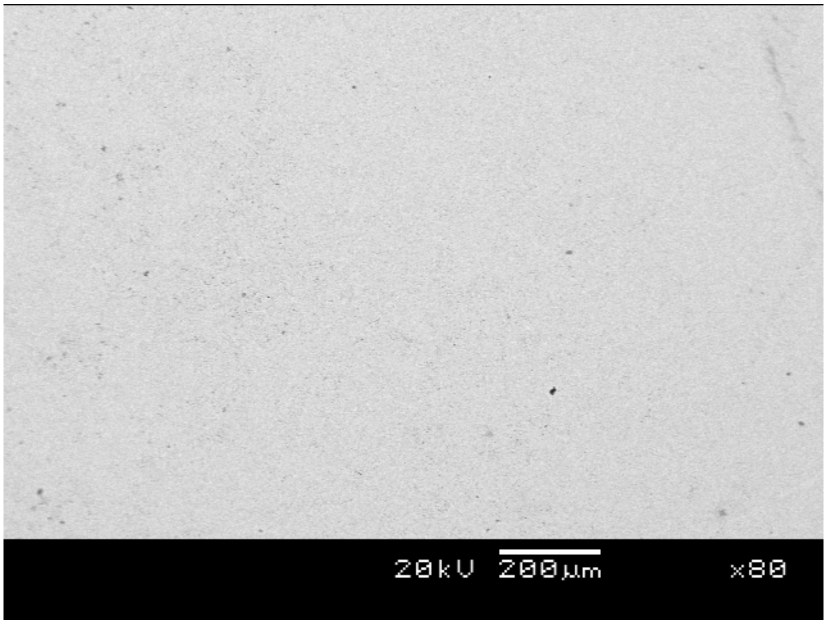

Figure 29. Electron backscatter image of sample 17 showing the homogeneity of the sample. The sample is essentially mono-mineralic and comprises almost exclusively of hematite.

Group 2: Poly-mineralic Samples

This group comprises of samples that have a significant proportion of gangue minerals. The results from the various samples in this group indicates that the presence of gangue minerals alone do not cause fractures to form. However, gangue minerals do influence the direction and intensity of fractures and gangue minerals, especially quartz, tend to fracture more easily than hematite due to their lower competency.

3.2.1 Sample 1: Ore Type 5 (B)

This sample appears to comprise of intergrown hematite and quartz. The sample is extensively fractured with both small and large fractures observed throughout the sample. The presence of gangue minerals appears to facilitate fracturing. Many fractures originate and terminate within gangue minerals without extending into the surrounding hematite.

In this sample it appears as though the presence of gangue minerals only appears to have an impact on the fracture frequency and fracture path up until a certain size of fracture is reached. Thereafter with large fractures, the fracture propagates irrespective of the presence or absence of gangue minerals.

Fractures on the edge of the sample that are directly related to reduction are also observed.

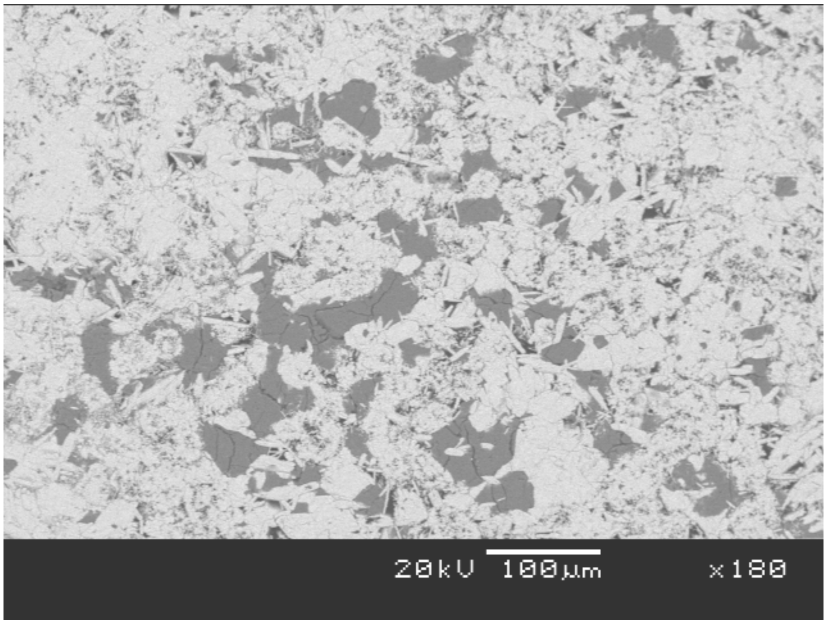

Figure 30. Electron backscatter image of sample 1 showing intergrown hematite (white) and quartz (light grey).

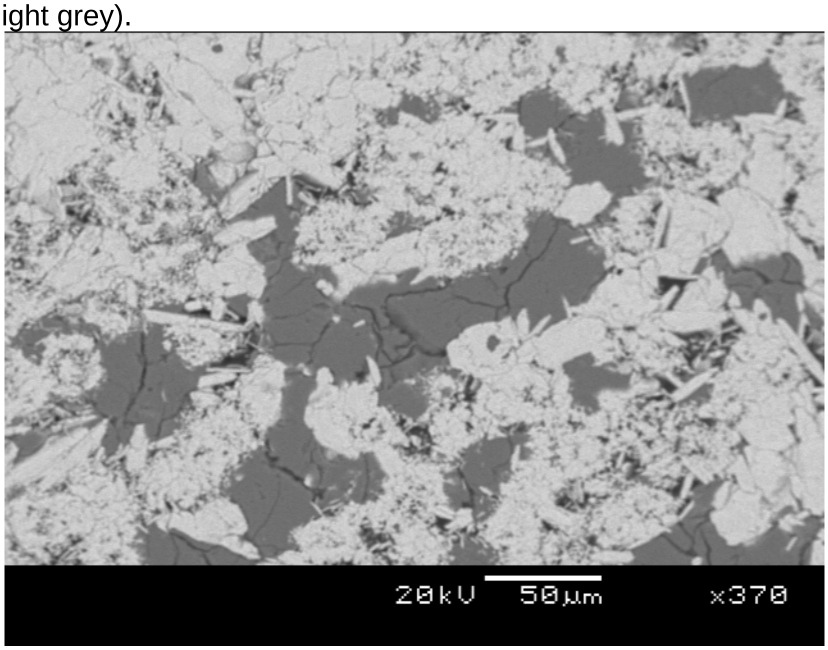

Figure 31. Electron backscatter image of sample 1 showing fractures originating and terminating within quartz (grey) without extending into the surrounding hematite.

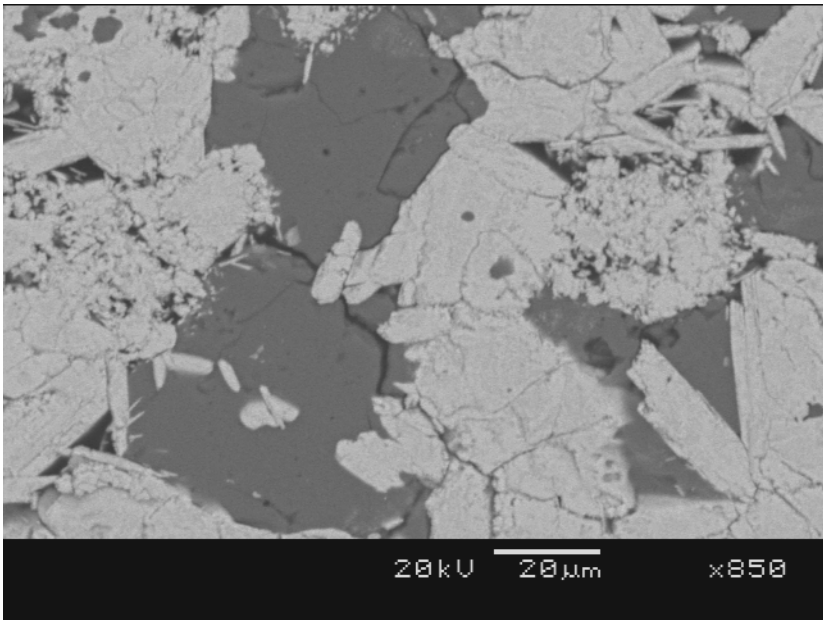

Figure 32. Electron backscatter image of sample 1 showing fractures originating and terminating within quartz (grey) without extending into the surrounding hematite.

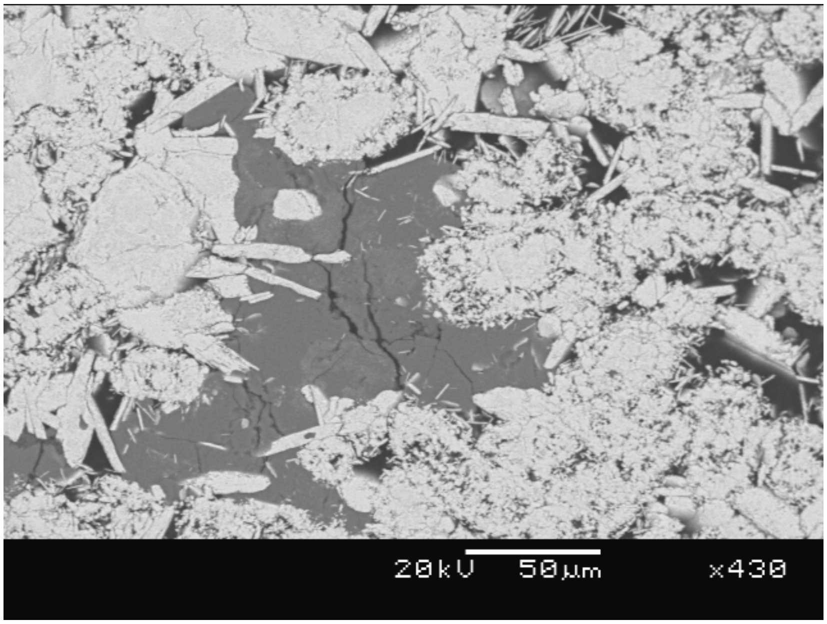

Figure 33 Electron backscatter image of sample 1 showing fractures originating and terminating within quartz without extending into the surrounding hematite.

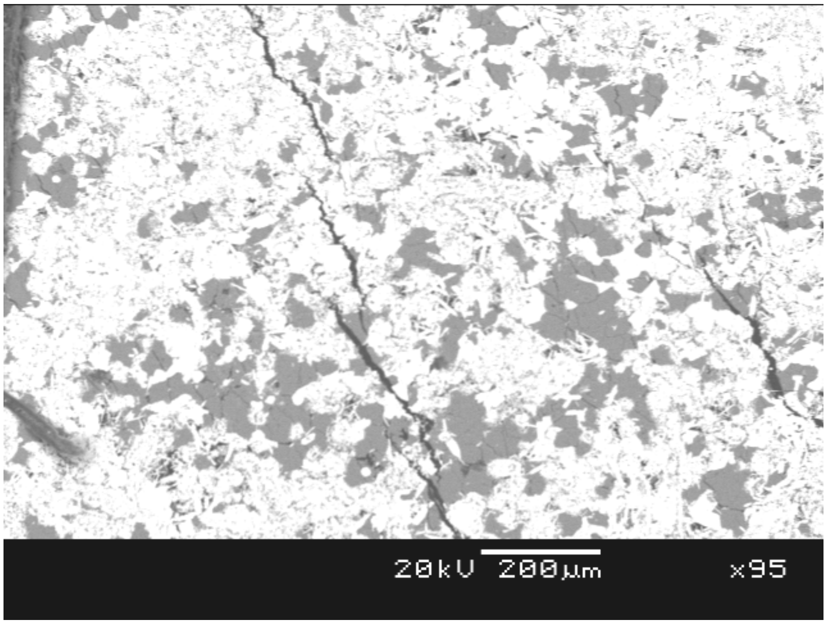

Figure 34. Electron backscatter image of sample 1 showing large fractures that do not appear to be influenced by the sample mineralogy. The fractures propagate through both gangue and ore minerals.

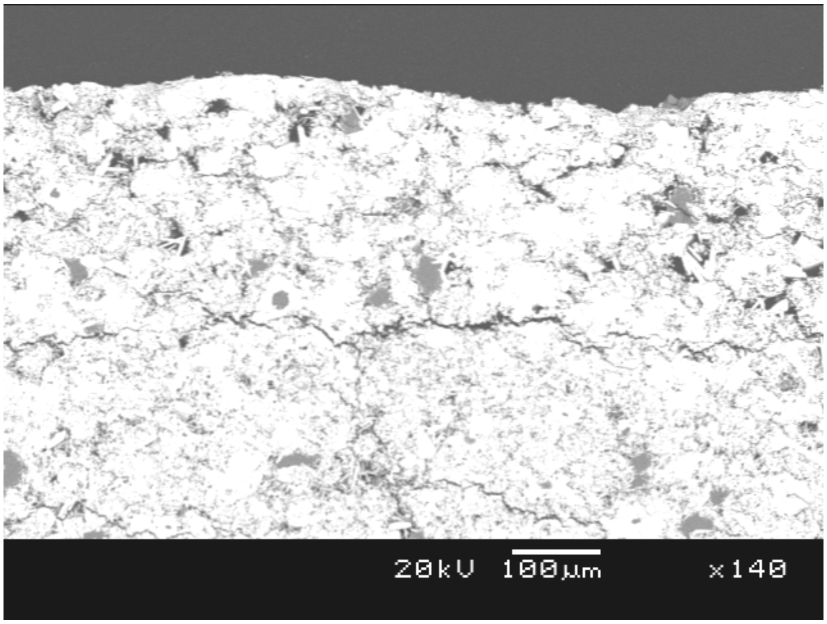

Figure 35. Electron backscatter image of sample 1 showing regularly spaced fractures at the edge of the sample, related to the volume change during the reduction of hematite to magnetite.

3.2.2 Sample 5: Northern Cape Std (B)

This sample contains large amounts of quartz intergrown with hematite throughout the sample. In places the quartz defines very weak banding in the sample as it occurs in a preferred orientation. Fractures are widely developed in the quartz, due to its lower competency, and these fractures do not always extend into the surrounding hematite.

Some fractures propagate parallel to the preferred orientation usually exploiting the less competent quartz phase. Not all the fractures observed exploit the gangue minerals

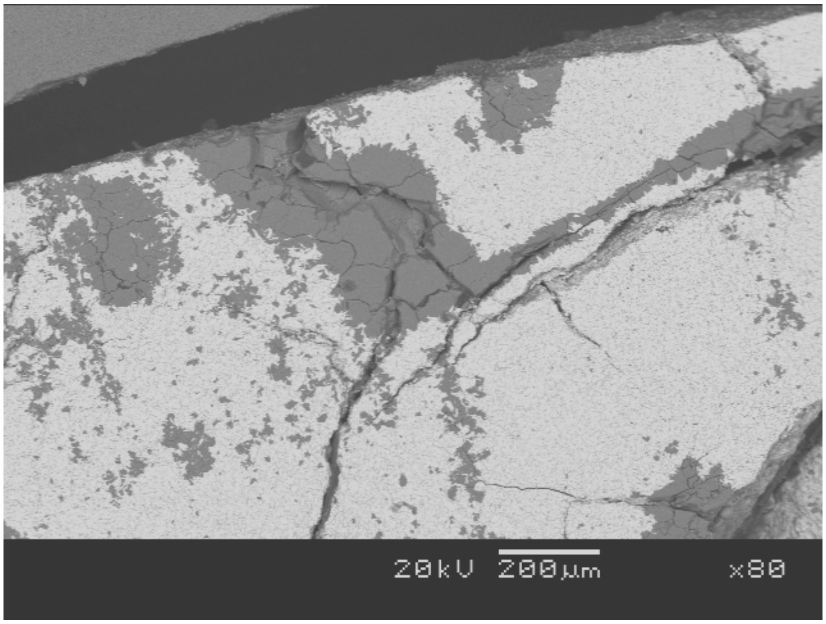

Figure 36. Backscatter electron image of sample 5 showing fractures at the edge of the sample. Notice how the fracture network is better developed when they occur in the gangue phase.

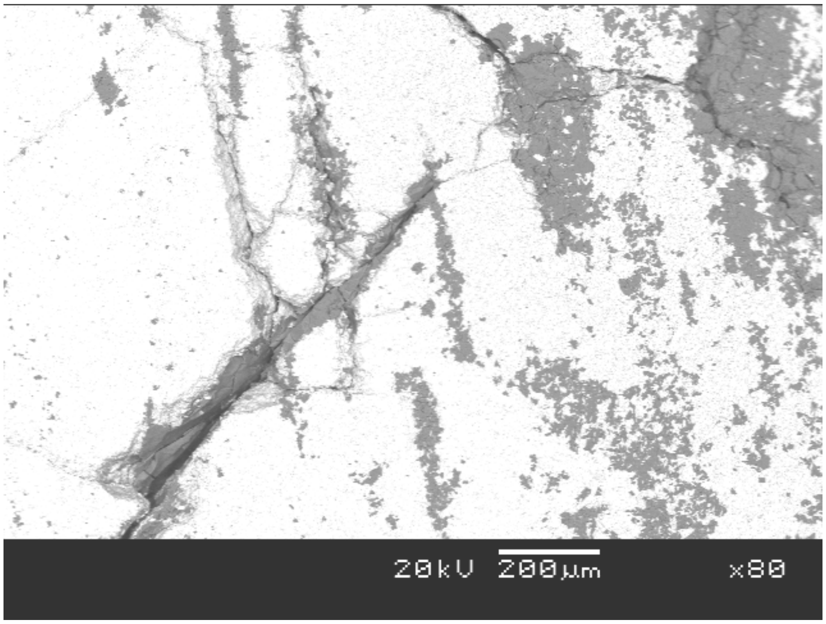

Figure 37. Backscatter electron image of sample 5 showing the quartz defined banding. Some fractures appear to occur parallel to the banding, exploiting the less competent quartz.

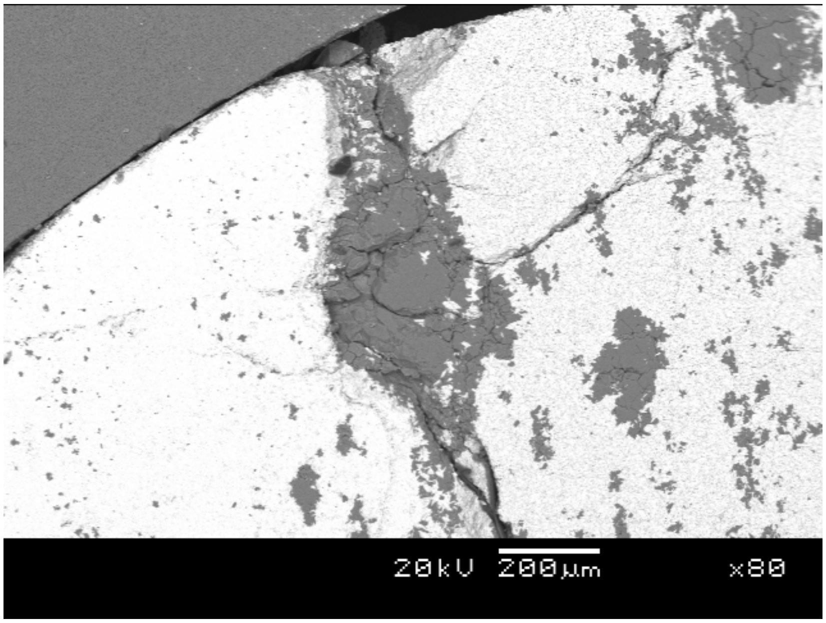

Figure 38. Electron backscatter image of sample 5 showing the development of secondary fractures in quartz.

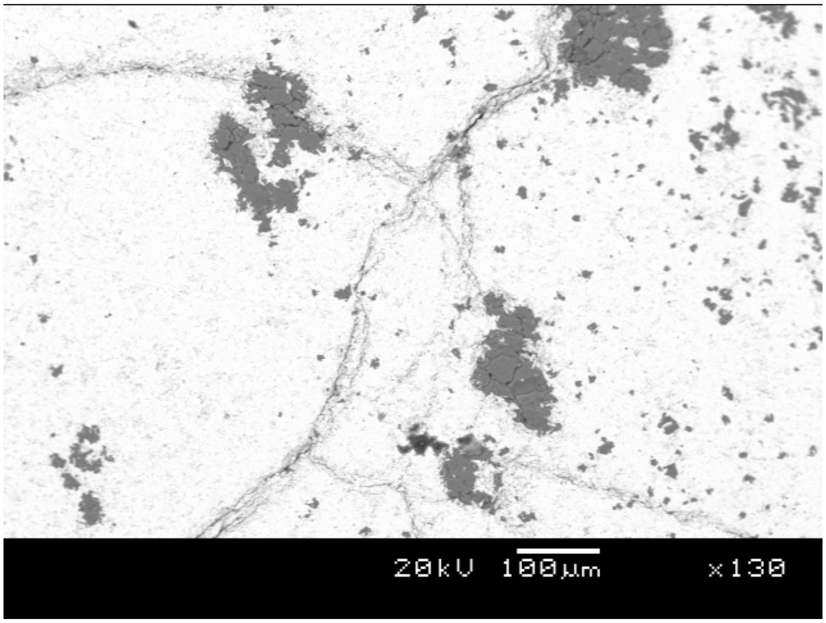

Figure 39. Electron backscatter image of sample 5 showing the relation between fractures and gangue minerals. Although the fractures are not caused by gangue, the distribution of the fractures is influenced. Notice how the fractures always appear to intersect gangue minerals.

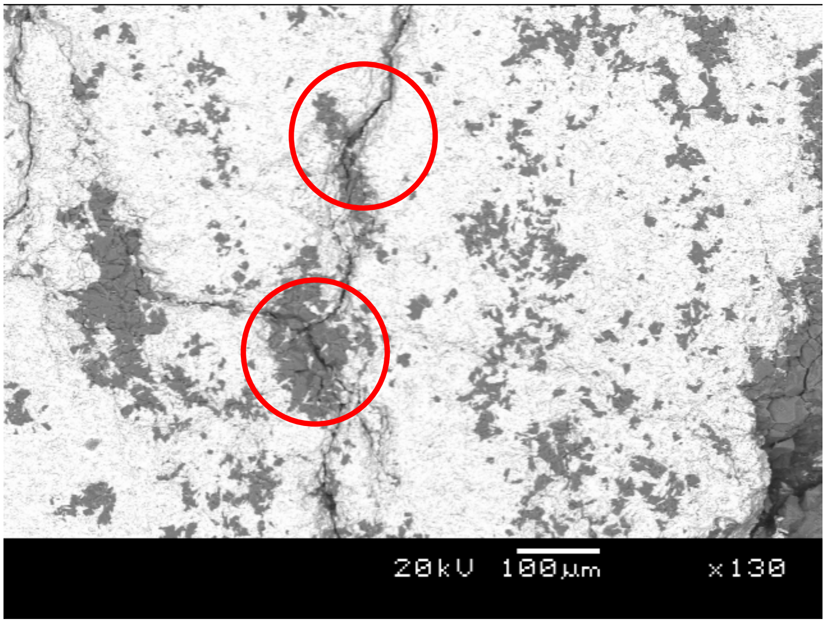

Figure 40. Electron backscatter image of sample 5 showing the dilation of fractures where they occur in gangue.

3.2.3 Sample 7: Ore Type 5 18/06/06

This sample comprises predominantly of specularitic hematite and is relatively porous. Gangue minerals such as apatite occur throughout the sample and appear to have some influence on fracture propagation. In areas where gangue minerals are not present, fractures appear to occur regularly spaced and at regular angles. Fractures are also observed on the edge of samples, these fractures occur parallel to the edge of the sample and are a direct result of sample reduction.

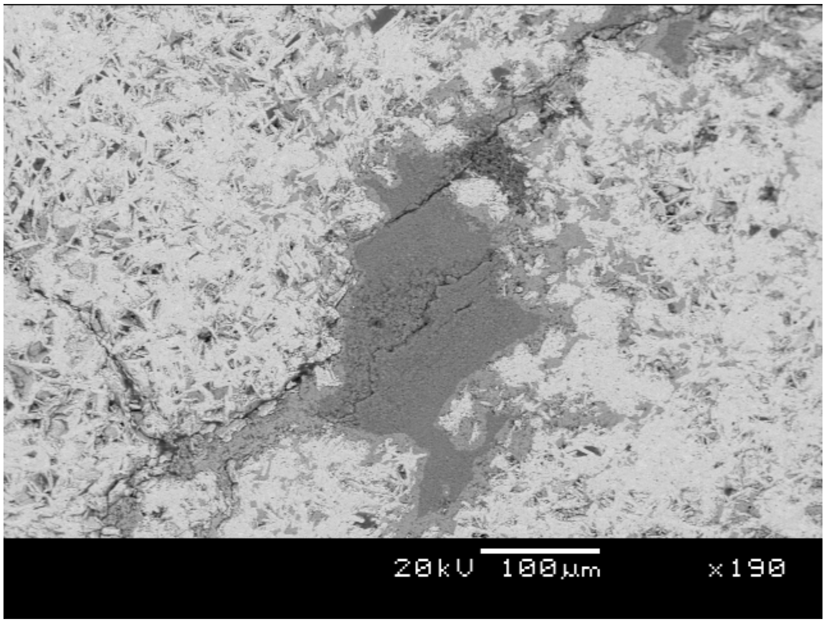

Figure 41. Electron backscatter image of sample 7 showing some secondary fracture development in apatite. The apatite appears to be slightly more competent than quartz.

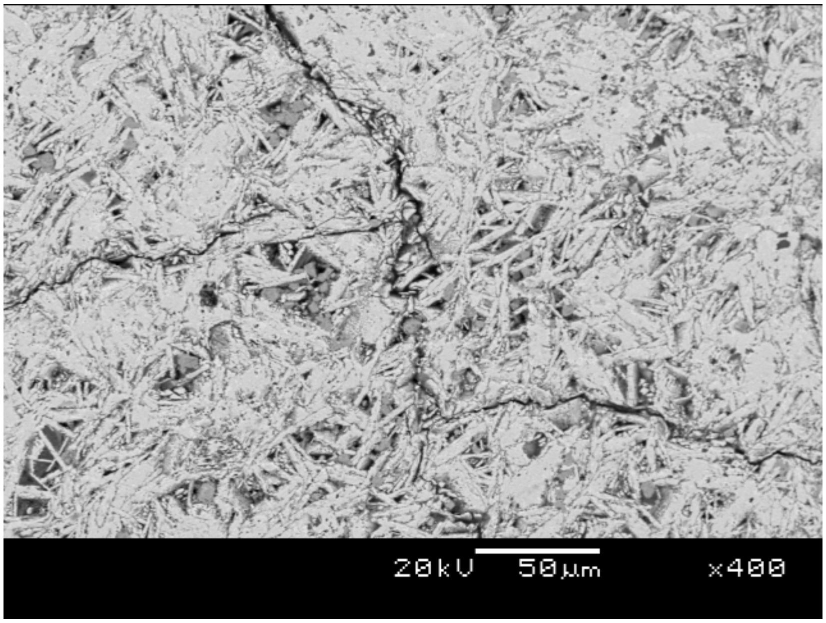

Figure 42. Electron backscatter image of sample 7 showing regularly spaced fractures at the interior of the sample.

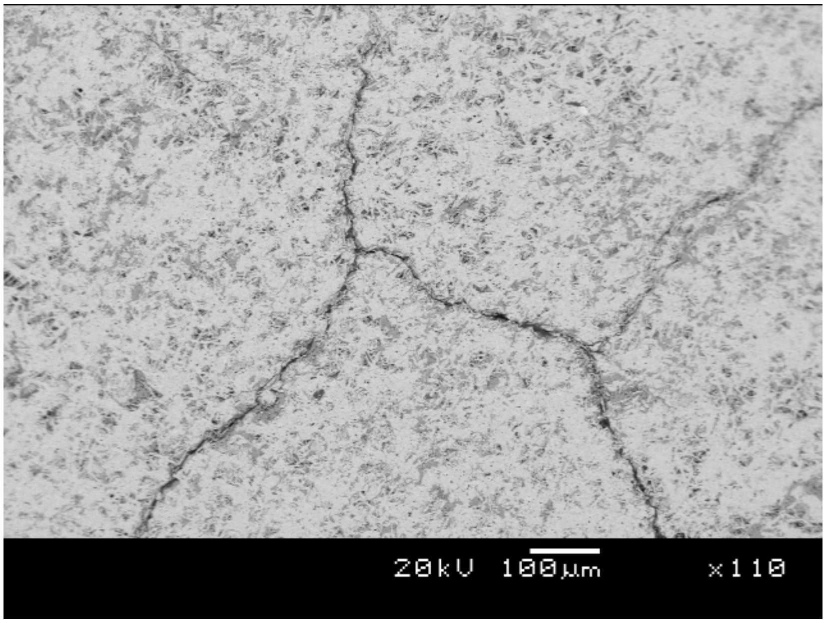

Figure 43. Electron backscatter image of sample 7 showing regularly spaced fractures at the interior of the sample.

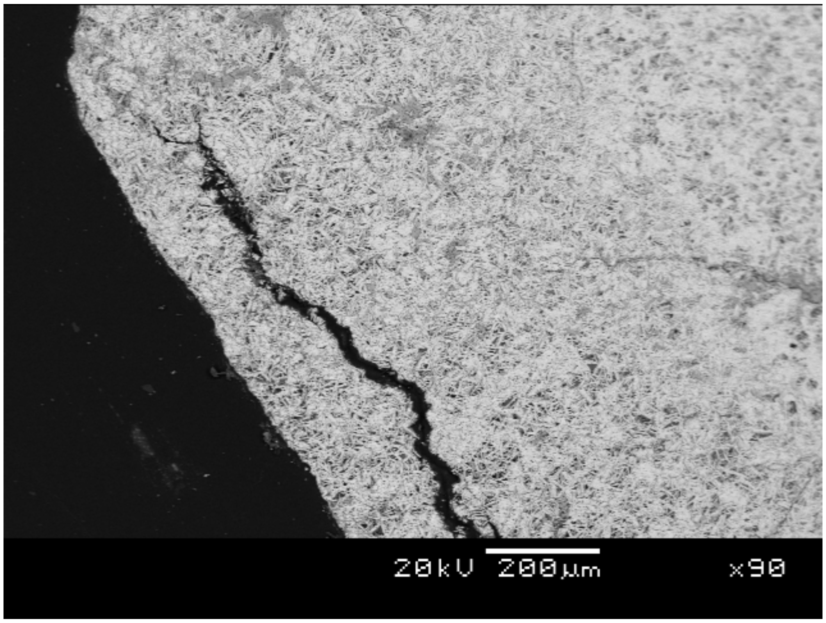

Figure 44. Electron backscatter image of sample 7showing a fracture at the edge of the sample, caused by the volume change during the reduction of hematite to magnetite.

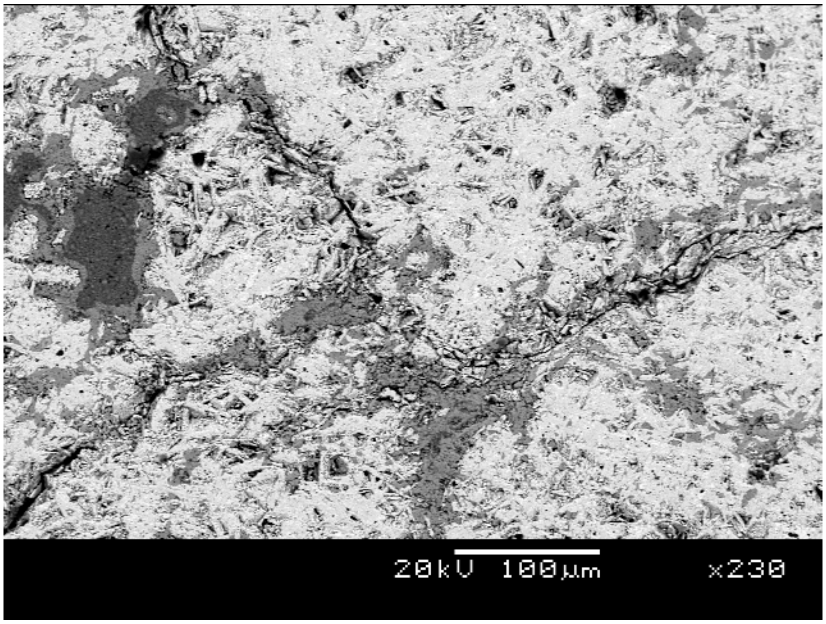

Figure 45. Electron backscatter image of sample 7 showing fractures that appear to occur in association with apatite. Unlike with quartz, there does not appear to be secondary fractures developed within the apatite.

3.2.4 Sample 10: Ore Type 4 D2

The sample is a dense sample with very low porosity. Despite the dense nature of the sample and the abundance of gangue minerals, fracturing is rare and most fractures occur on the edge of the sample, where the sample has been reduced.

Where gangue minerals are present the gangue appears to be fractured more extensively than the surrounding, more competent, hematite. The dearth of fractures may be directly related to the low-porosity of the sample. The sample has only been able to reduce along the edges and therefore there have been no volume changes, and no resultant fracturing internally within the sample.

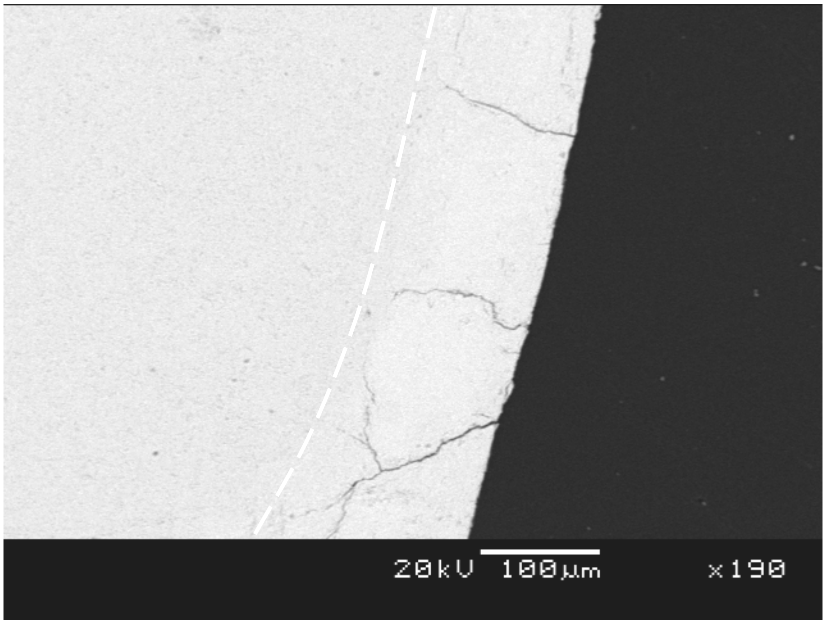

Figure 46. Electron backscatter image of sample 10 showing the development of fractures along the edge of the samples, where it has been reduced. The stippled line indicates where the sample has been reduced.

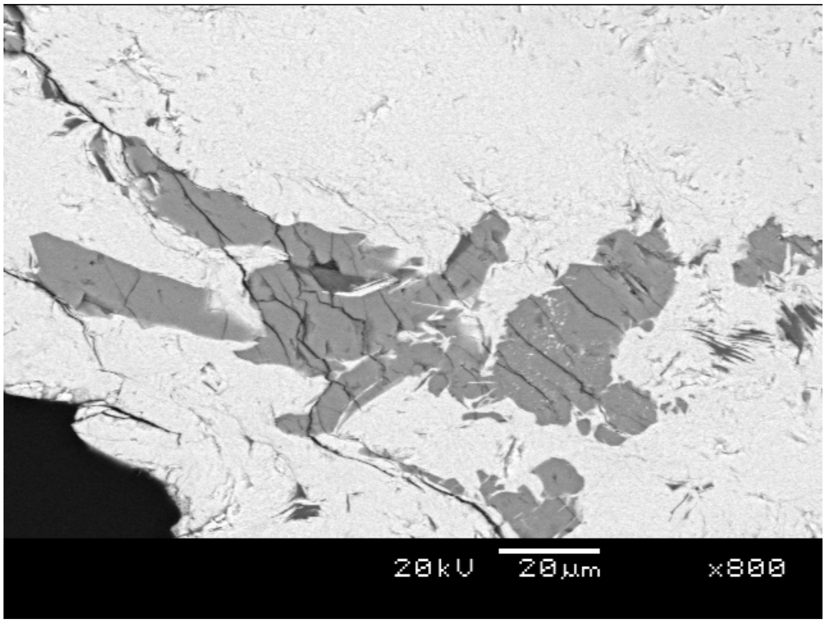

Figure 47. Electron backscatter image of sample 10 showing the development of fractures in quartz. The secondary fractures do not extend into the surrounding hematite.

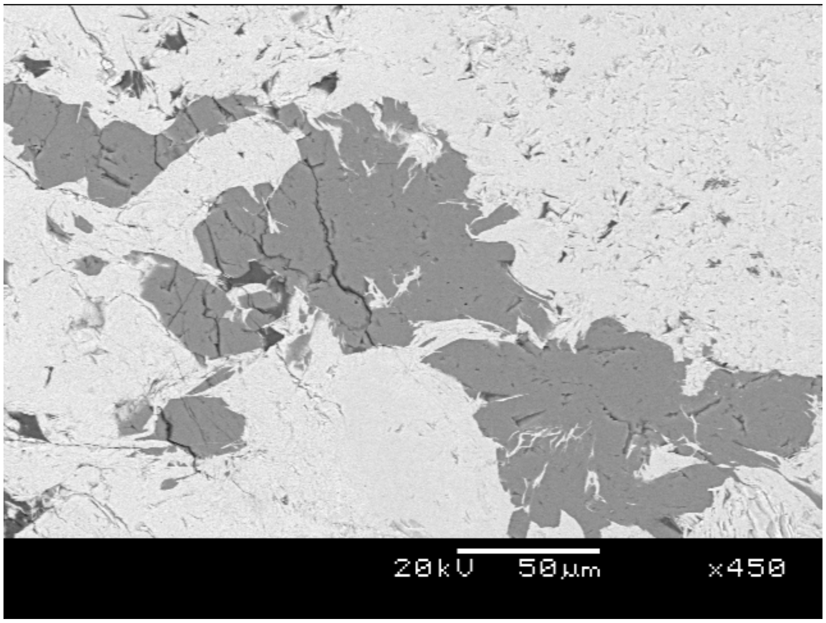

Figure 48. Electron backscatter image of sample 10 showing the development of fractures in quartz. The secondary fractures do not extend into the surrounding hematite.

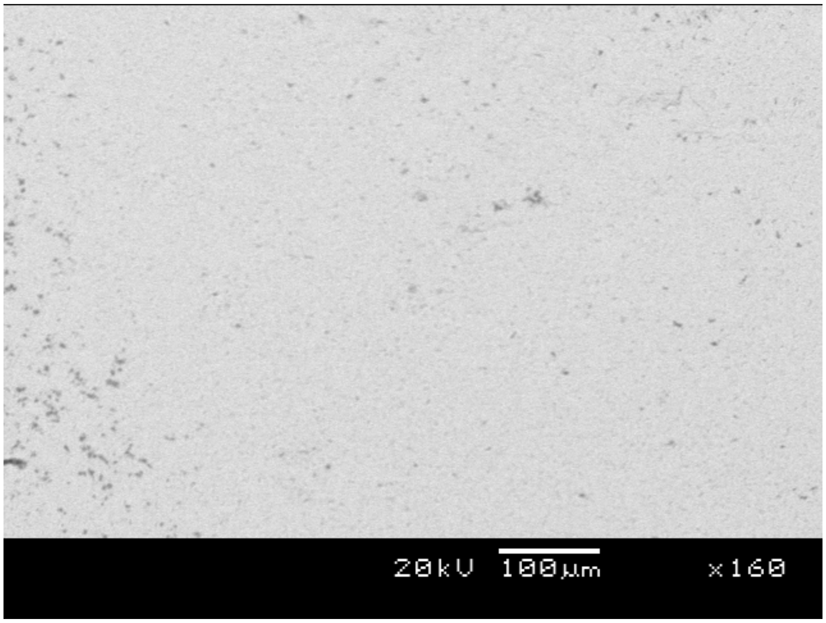

Figure 49. Electron backscatter image of sample 10 showing an area within the sample where no reduction or fracturing has occurred.

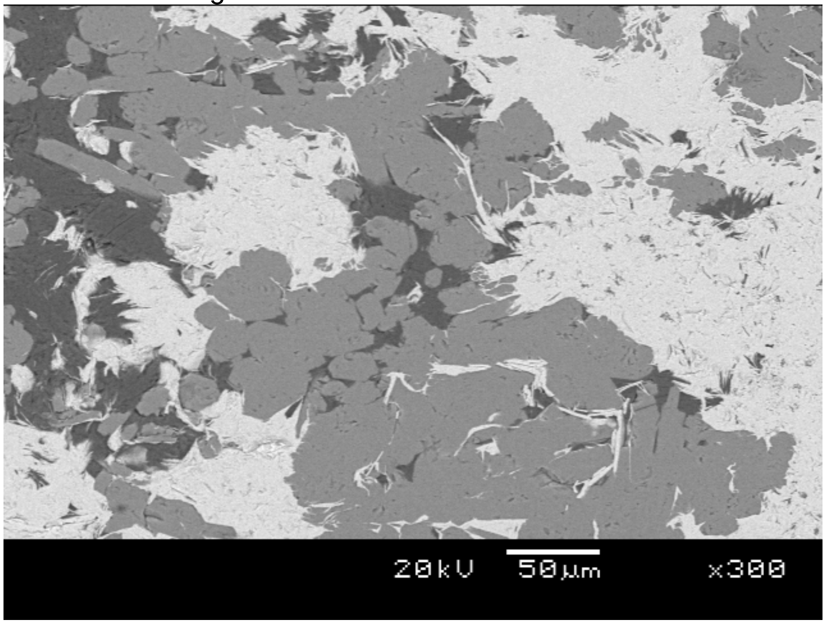

Figure 50. Electron backscatter image of sample 10 showing intergrown hematite and gangue. The presence of gangue phases does not necessarily lead to fracture formation.

3.2.5 Sample 14: Ore Type 5

This sample has relatively large amount of gangue, found intergrown with hematite throughout the sample. Quartz and apatite appear to be the most abundant gangue minerals. The sample has very low porosity and very few fractures. The fractures are usually observed at the edge of the sample, where the sample has been reduced.

Although the presence of gangue may not result in fractures forming, where a fracture intersects gangue minerals the gangue appear to facilitate the development of fractures that do not extend into the surrounding hematite.

In the center of the sample very few fractures are observed. The fractures that do occur are associated with open pores and reduction and are not related to the presence or absence of gangue minerals. The fractures appear to link a series of open pores where reduction has occurred.

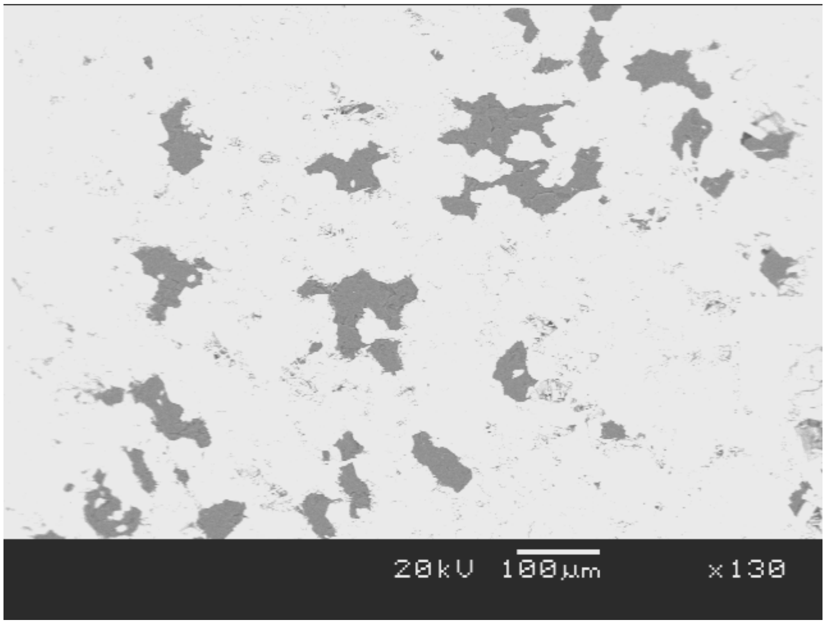

Figure 51. Electron backscatter image of sample 14 showing intergrown hematite and quartz in the center of the sample. There are o fractures observed here as no reduction has been able to occur with the low sample porosity.

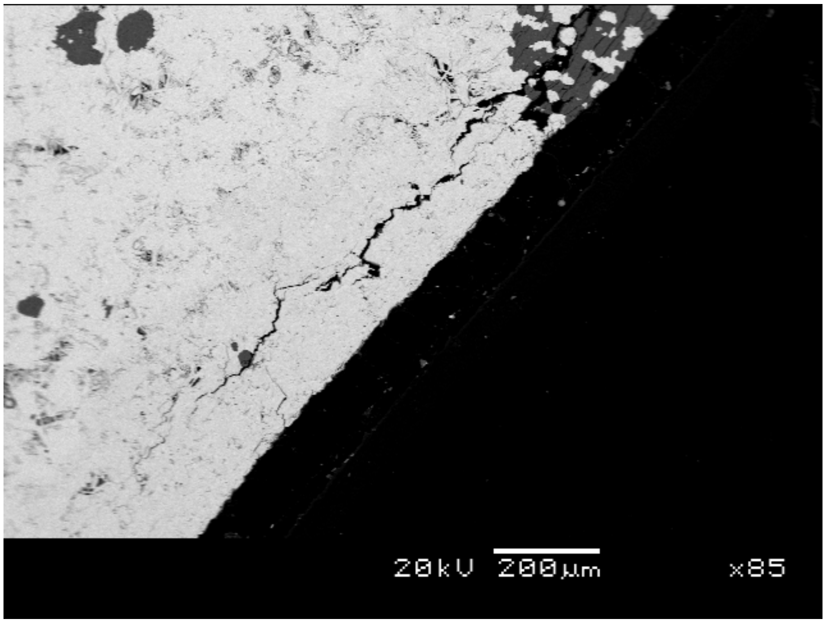

Figure 52. Electron backscatter image of sample 14 showing fractures developed at the edge of the sample where reduction has occurred.

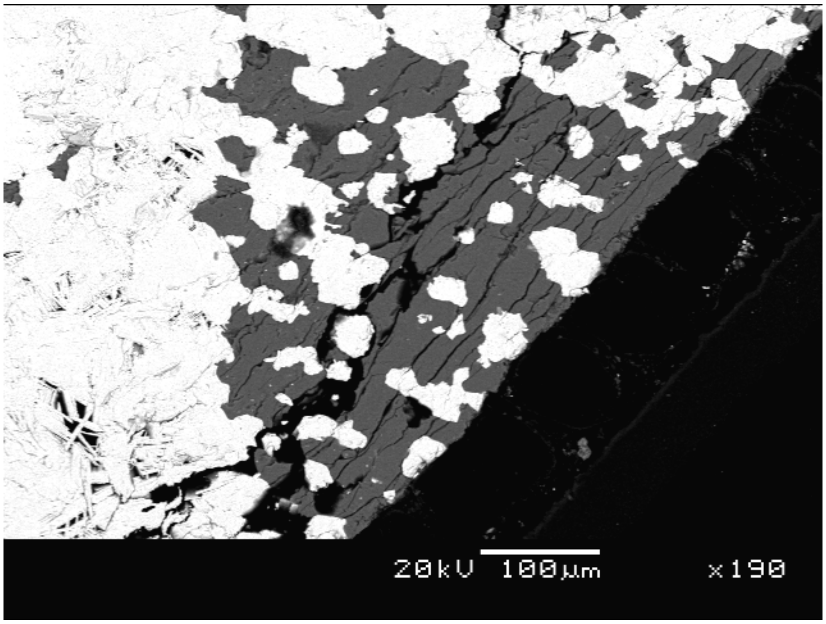

Figure 53. Electron backscatter image of sample 14 showing fractures developed at the edge of the sample where reduction has occurred. Notice how the gangue allows for more extensive development of the fracture network that does not extend into the surrounding hematite.

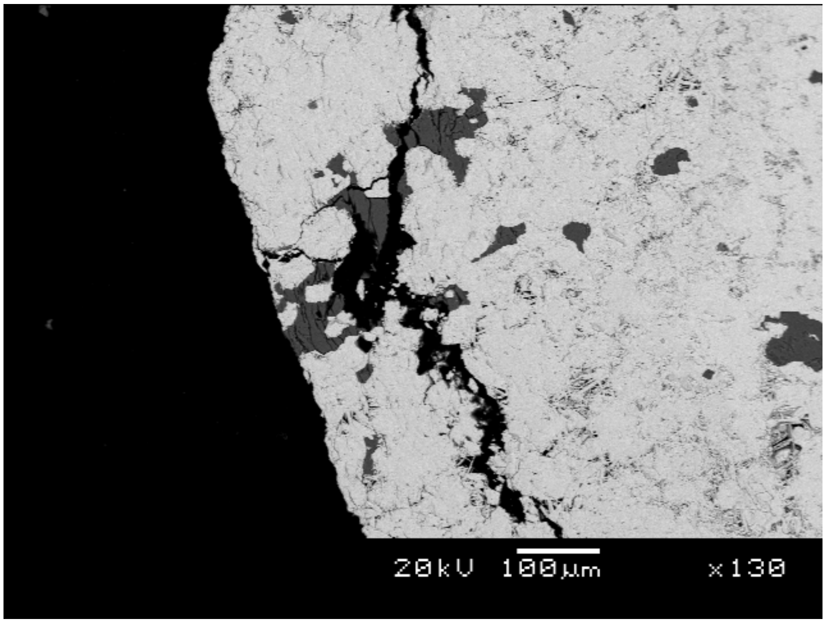

Figure 54. Electron backscatter image of sample 14 showing fractures developed along the edge of the sample where it has been reduced. Where a fracture intersects gangue minerals the gangue appears to facilitate the development of fractures.

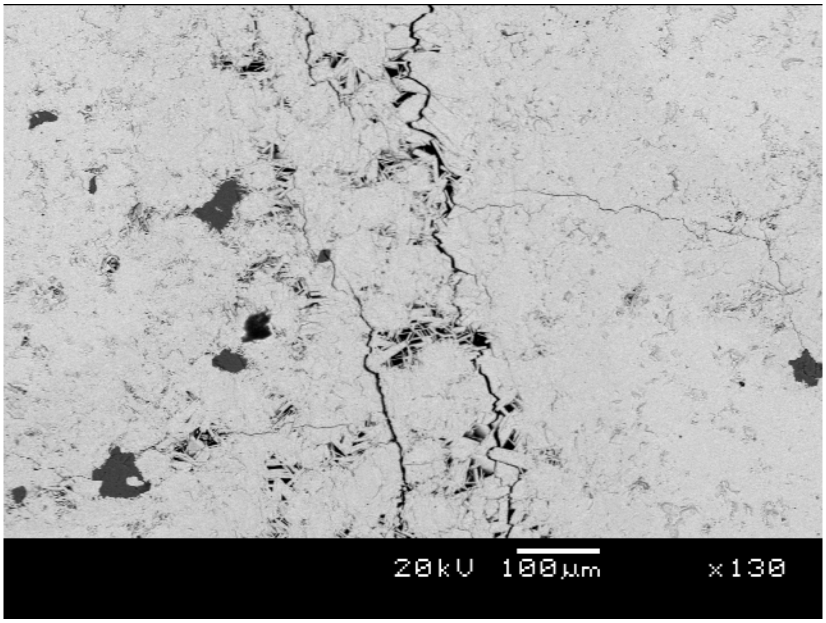

Figure 55. Electron backscatter image of sample 14 showing fractures developed within the sample. The fractures appear to join open pores where reduction has occurred.

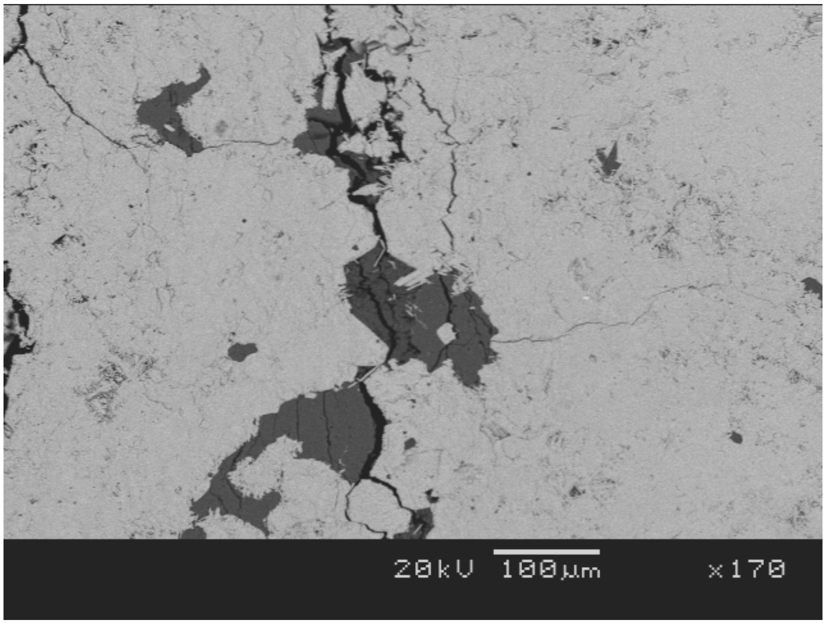

Figure 56. Electron backscatter image of sample 14 showing fractures developed within the sample. Where a fracture intersects gangue minerals the gangue appears to facilitate the development of fractures that do not extend into the surrounding hematite.

3.2.6 Sample 15: Ore Type 5 (C)

This sample comprises intergrown hematite and gangue. The gangue is abundant throughout the sample and comprises predominantly of alumino-silicates. The sample has very low porosity and also has very few fractures.

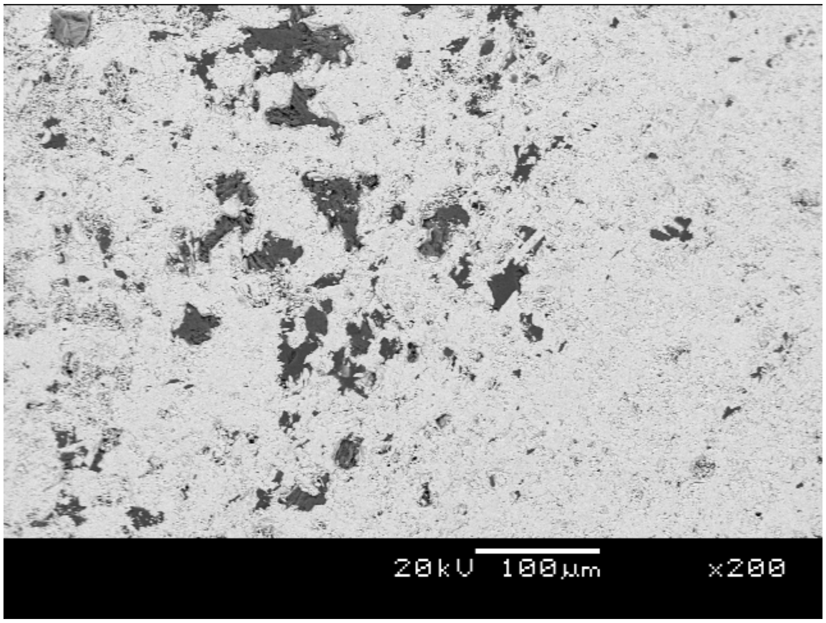

Figure 57. Electron backscatter image of sample 15 showing intergrown hematite and gangue with very low porosity and no visible fractures.

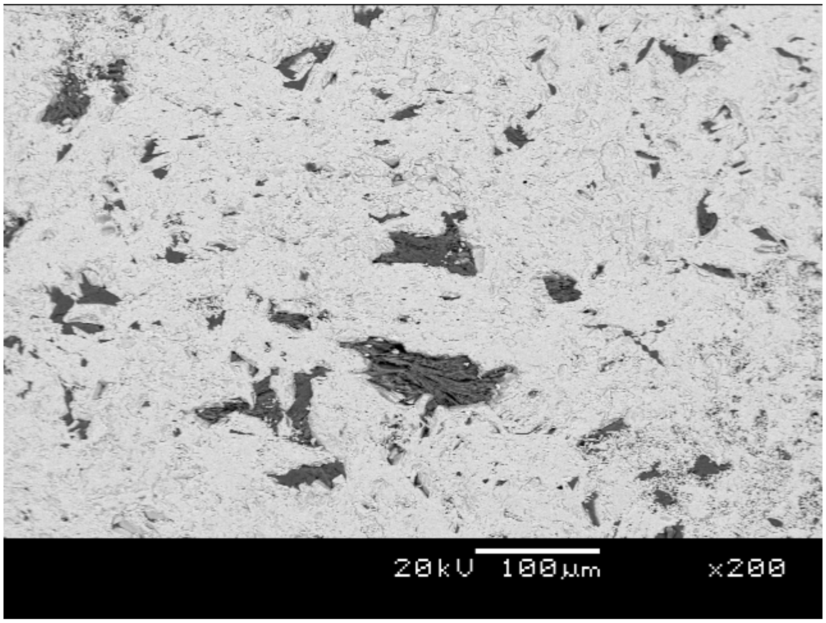

Figure 58. Electron backscatter image of sample 15 showing intergrown hematite and gangue with very low porosity and no visible fractures.

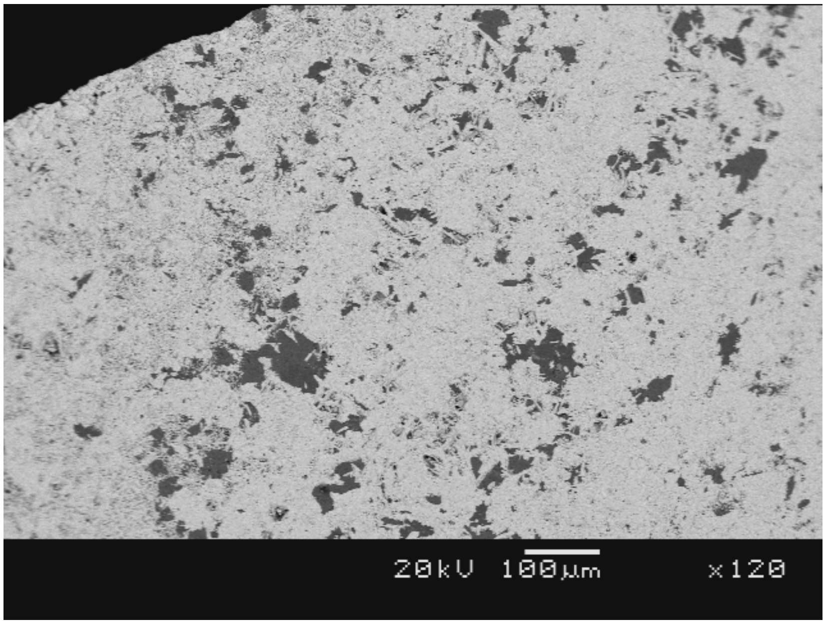

Figure 59. Electron backscatter image of sample 15 showing intergrown hematite and gangue with very low porosity and no visible fractures, even at the edge of the sample where fractures are unusually prolific.

Group 3: Porous Samples

Only two samples are found in this group. Sample 2 comprises of bands of acicular hematite with very high porosity whilst sample 9 has a homogenous high-porosity texture throughout the sample. Both samples do not exhibit extensive fracturing most probably due to the fact that the numerous open voids allow for the volume increase during reduction and therefore prevent extensive fracturing.

3.3.1 Sample 2: Ore Type 3 (B)

This sample comprises predominantly of hematite with very little gangue. The most interesting feature of this sample is the porosity defined banding that appears to have an impact on fracturing. Porous specularite (acicular hematite) would not be affected by the volume increase during reduction and would be more competent in accommodating strain. Therefore fractures would terminate in areas of high porosity.

Where gangue minerals are not present and there are no large changes in porosity, fractures appear to occur evenly spaced at regular intervals and at similar orientations.

The large fractures in this sample are interesting in that they do not occur with a large network of finer fractures or ancillary fractures, as observed in other samples.

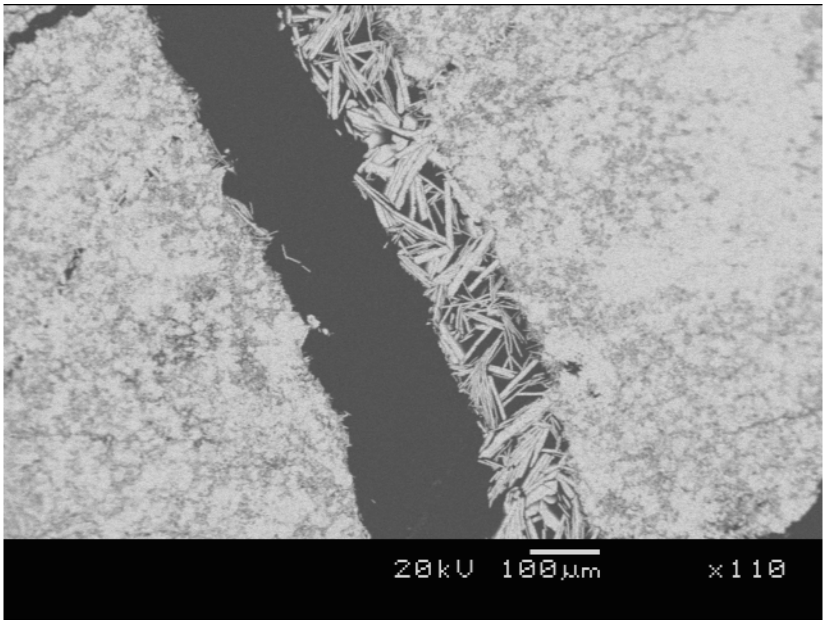

Figure 60. Electron backscatter image of sample 2 showing a very large fracture that has occurred at a boundary between granular hematite (left) and porous specularite (acicular hematite).

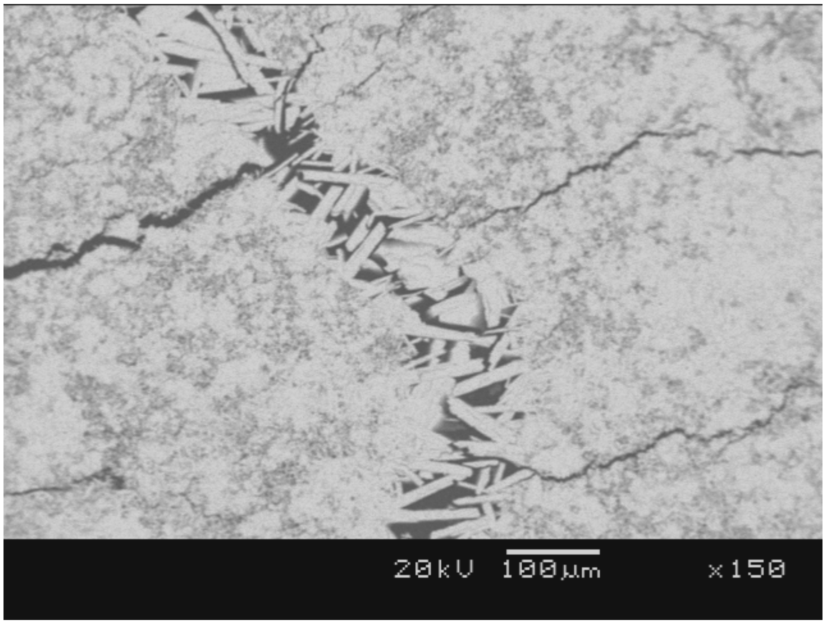

Figure 61. Electron backscatter image of sample 2 showing large fractures originating/terminating in areas of low porosity.

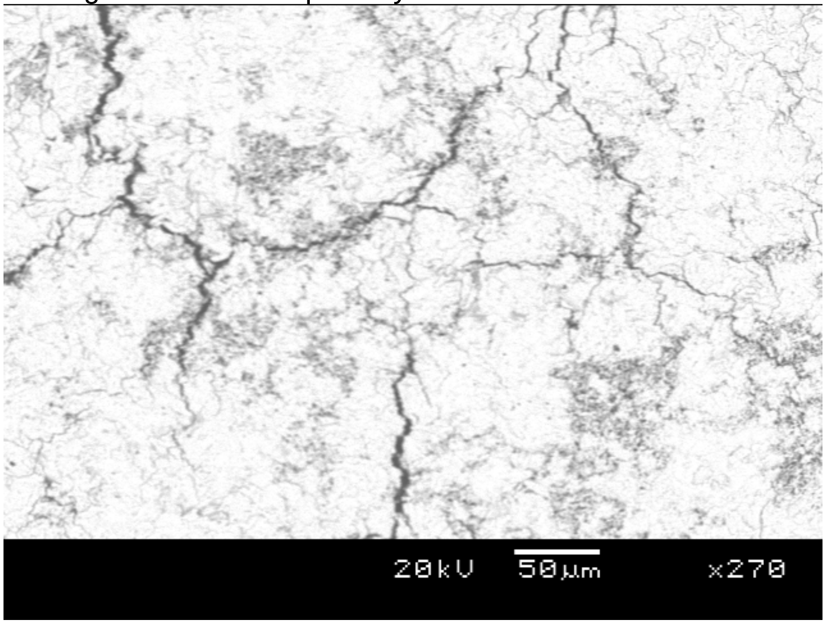

Figure 62. Electron backscatter image of sample 2 showing a network or regularly spaced and oriented fractures formed in an area of dense homogenous ore.

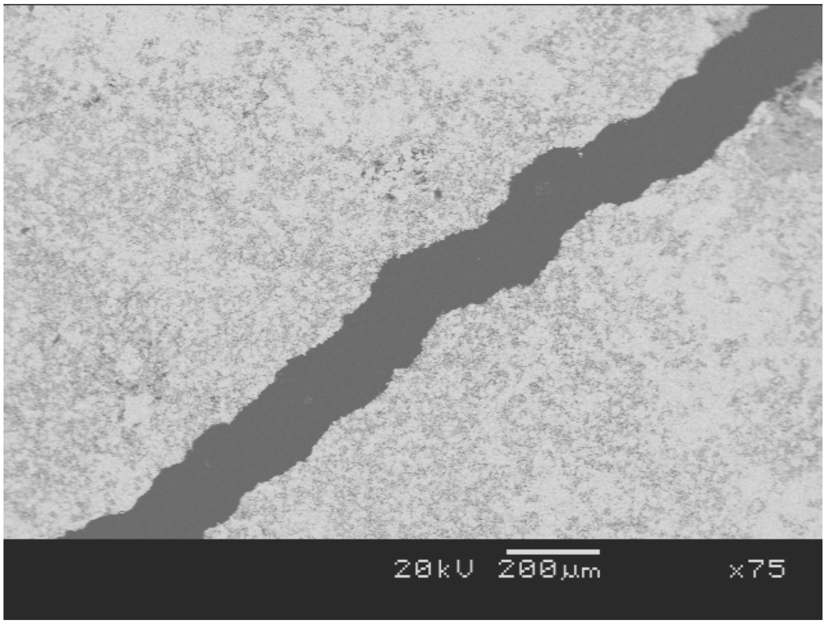

Figure 63. Electron backscatter image of sample 2 showing a large fracture through low porosity granular hematite. The fracture occurs without a large network of feeder fractures or ancillary fractures.

3.3.2 Sample 9: Northern Cape Std Test 1

This sample is a homogenous sample compressing predominantly of granular hematite. The sample is very porous. Most fractures occur at the edge of the sample and are related to the hematite reduction.

Internally within the sample there are not many fractures that have formed. This may be due to the high porosity that allows for the increased in volume during reduction. Where fractures do occur they typically originate and terminate at open pores.

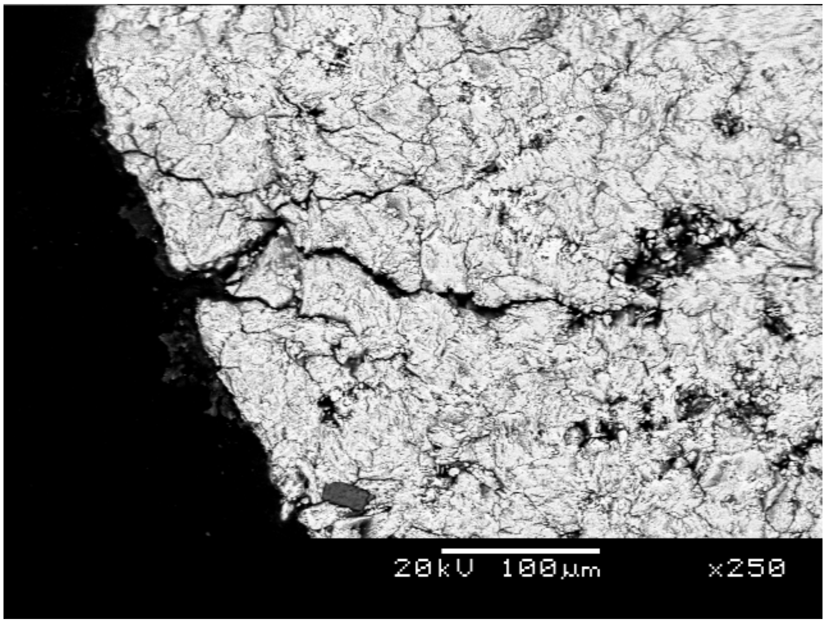

Figure 64. Electron backscatter image of sample 9 showing fractures perpendicular to the sample edge

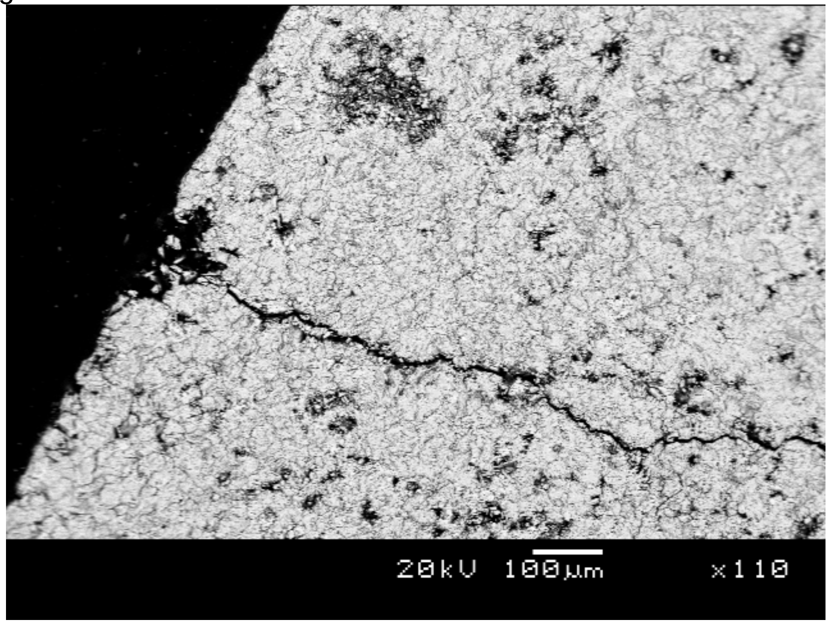

Figure 65. Electron backscatter image of sample 9 showing a fracture perpendicular to the sample edge.

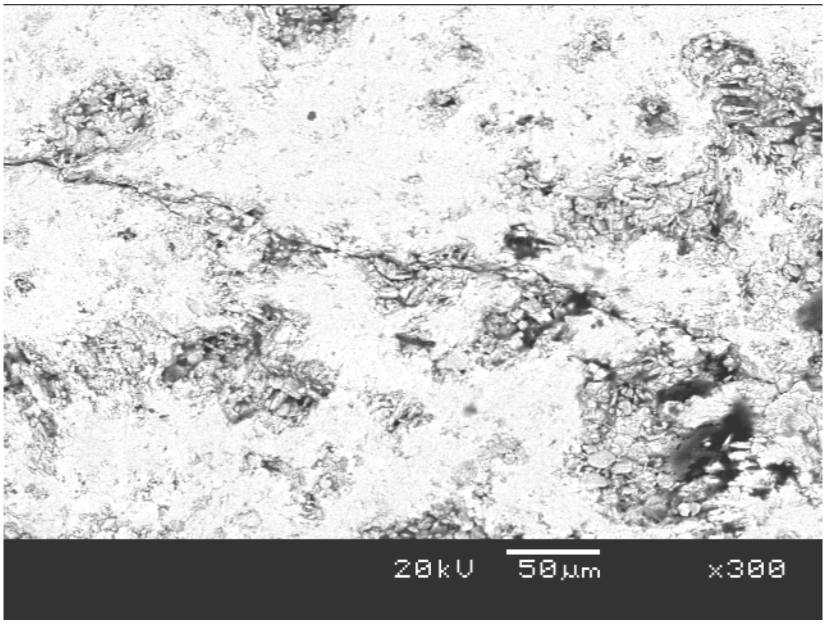

Figure 66. Electron backscatter image of sample 9 showing a fracture within the sample that terminates at an open pore.

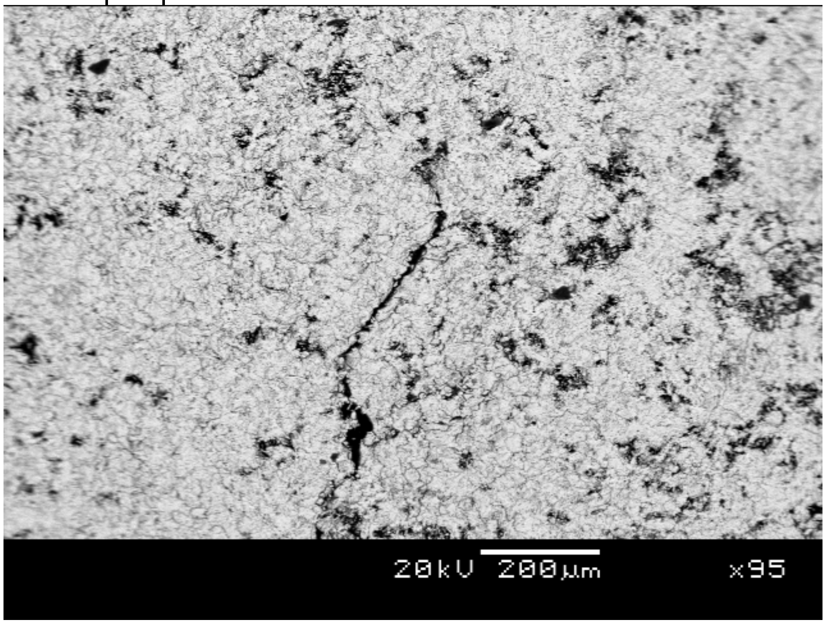

Figure 67. Electron backscatter image of sample 9 showing a fracture that has developed within the sample. Notice the overall sample porosity.

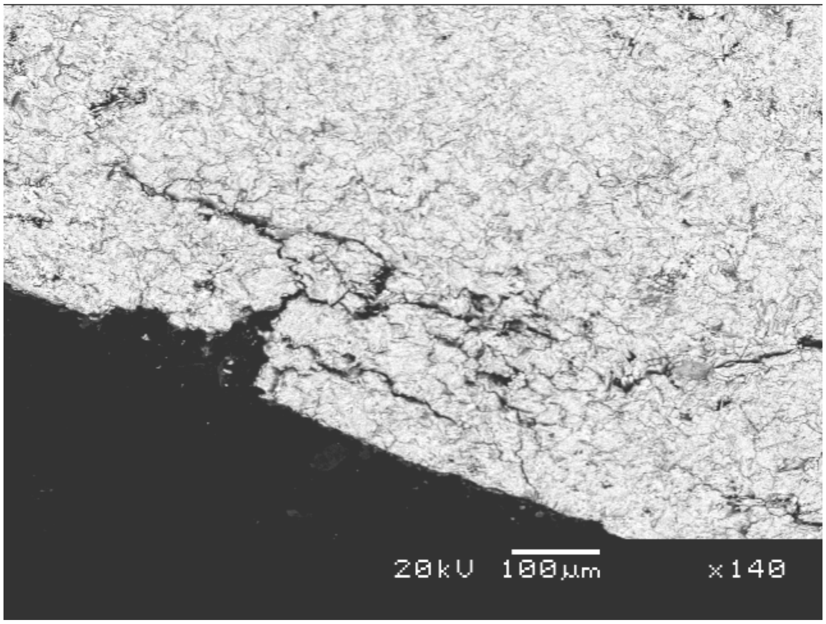

Figure 68. Electron backscatter image of sample 9 showing a fracture network developed parallel and perpendicular to the sample edge.

3.3.3 Sample 16: Northern Cape Std "A"

This sample comprises predominantly of low porosity hematite with very little gangue. Many large and extensive fractures are observed throughout the sample. Fractures are observed in two distinct areas:

1) At or near the sample edge where reduction has occurred.
2) Associated with porous acicular hematite.

The fractures associated with the acicular hematite may be related to the increased porosity in-between the acicular hematite that results in increased reduction, or it may be associated with the brittle nature of the acicular hematite or the increased amount of gangue intergrown with the hematite.

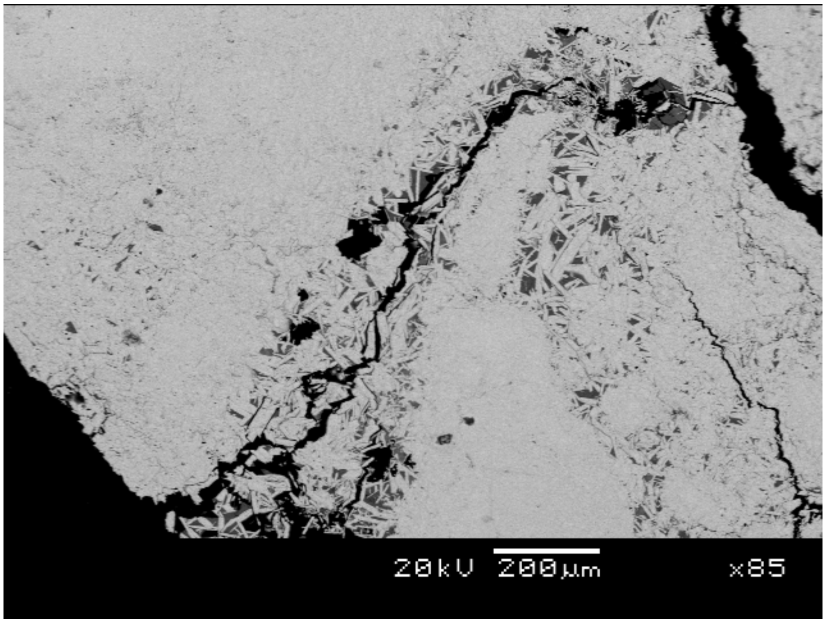

Figure 69. Electron backscatter image of sample 16 showing a large fracture associated with acicular hematite

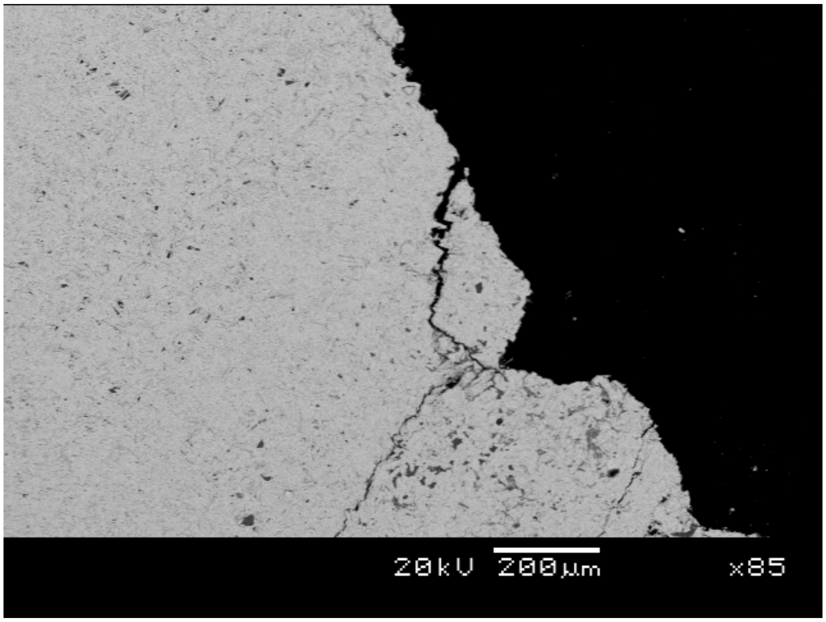

Figure 70. Electron backscatter image of sample 16 showing a small fracture at the edge of the sample associated with reduction of hematite.

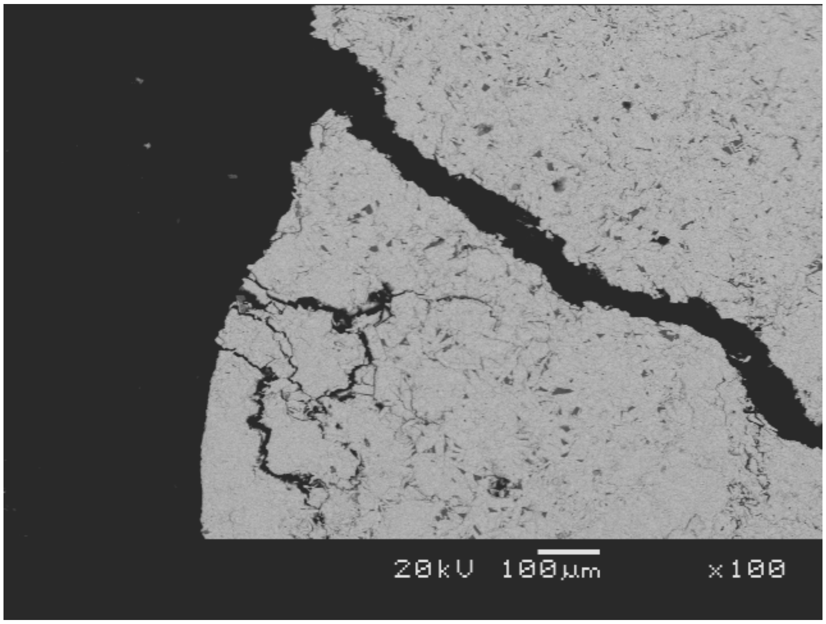

Figure 71. Electron backscatter image of sample 16 showing fractures at the edge of the sample were reduction has taken place.

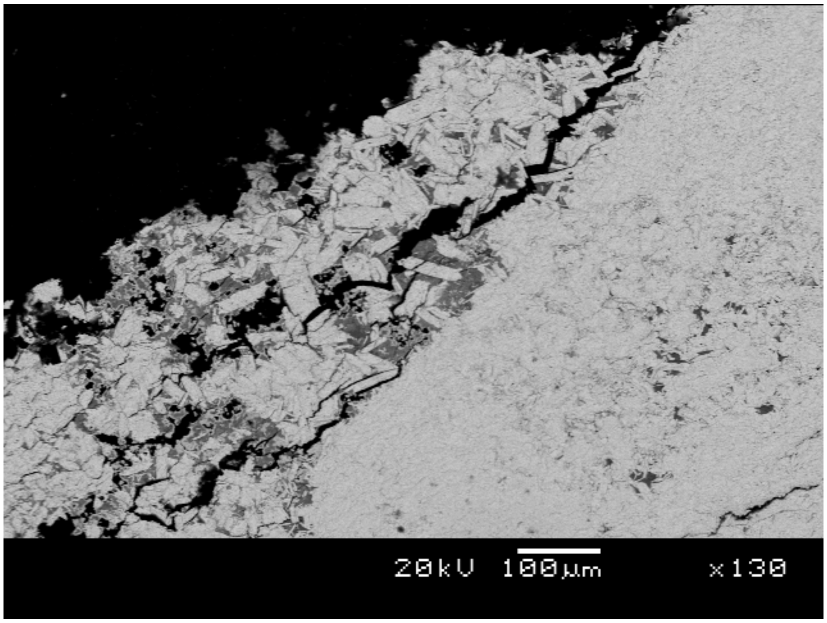

Figure 72. Electron backscatter image of sample 16 showing fractures at the edge of the sample where reduction has taken place. The influence of acicular hematite and gangue minerals is uncertain.

3.4 Group 4: Other

3.4.1 Sample 6: Northern Cape Ore Type 2 C

This sample contains very little gangue and comprise predominantly of hematite. The sample is unique in this study as it is the only sample observed with a clearly observed foliation fabric. The foliation fabric defines the primary plane of weakness in the sample and is an important influence on the fracture that form in the sample. Most fractures occur parallel to the foliation fabric.

Where the foliation fabric is less pronounced or is absent then the fractures appear to occur at regular intervals with similar orientations to form a fracture framework.

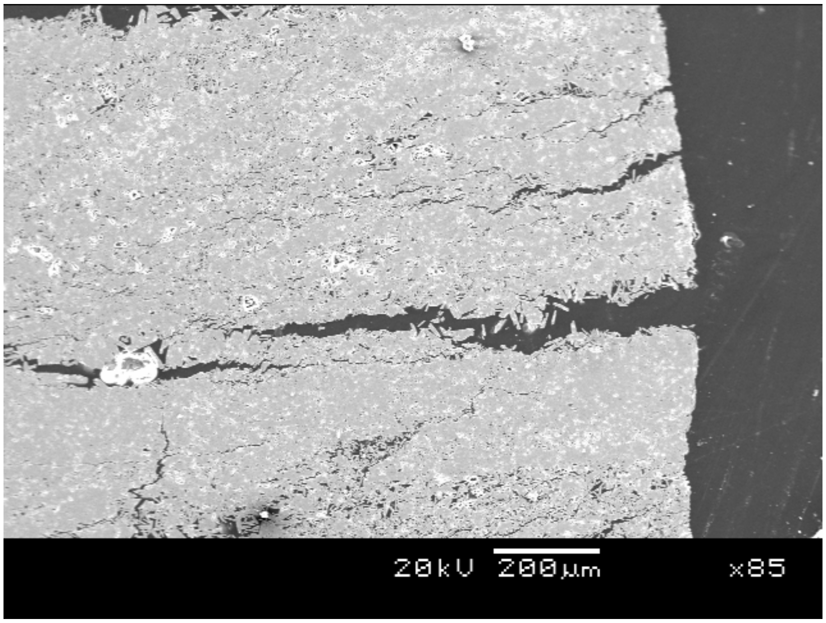

Figure 73. Electron backscatter image of sample 2 showing fractures oriented parallel to the foliation fabric.

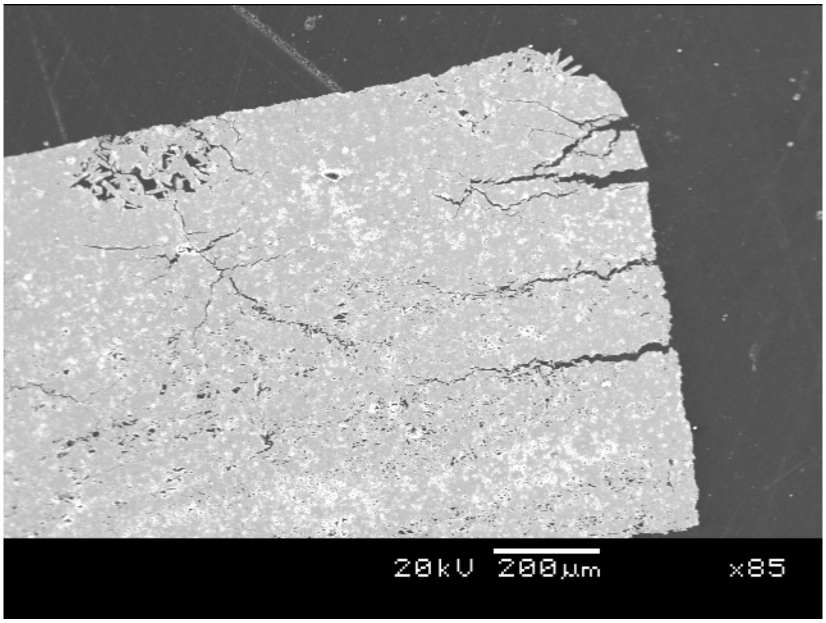

Figure 74. Electron backscatter image of sample 2 showing fractures oriented parallel to the foliation fabric.

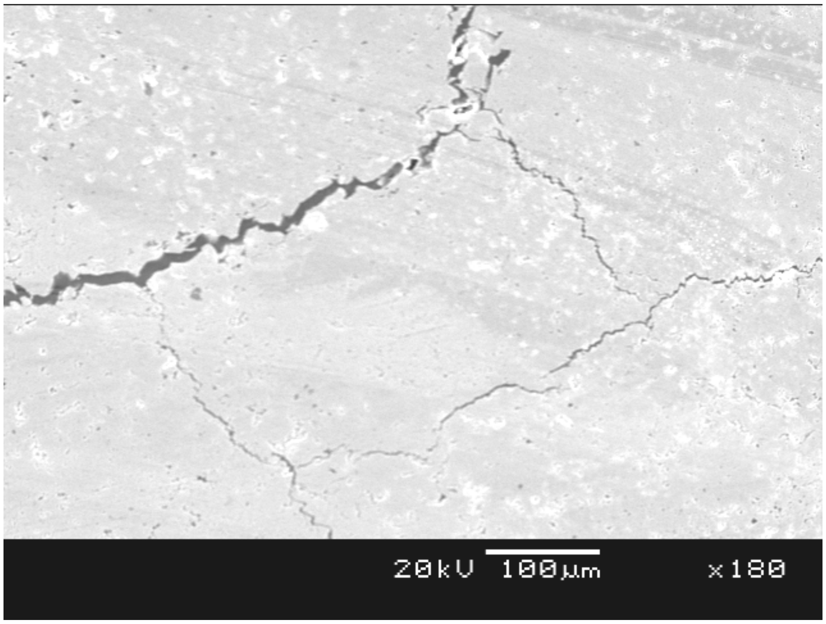

Figure 75. Electron backscatter image of sample 2 showing a regularly spaced network of fractures that occur at right angles to each other. There are no compositional or textural features to influence the fracture orientation.

4.0 CONCLUSION

1. Mono-mineralic particles fracture with radial fractures occurring on the edges of particles penetrating the sample only as far as it has been reduced. These fractures appear to be directly related to the volume change during reduction. Internal fractures do occur in mono-mineralic particles where fractures occur regularly spaced at right angles to one another.

2. It appears as though the presence of gangue minerals only appears to have an impact on the fracture path up until a certain size of fracture is reached. Thereafter with large fractures, the fracture propagates irrespective of the presence or absence of gangue minerals. Fractures often dilate as they pass through gangue minerals and a secondary network of smaller fractures is often developed, especially in quartz. The secondary fractures do not extend into the surrounding hematite.

3. Porous samples appears to be less fractured as the open pores impede fracture formation as the pores is able to accommodate the strain during volume increase during reduction.

4. Features such as internal foliation fabric and/or bedding planes have a significant influence on the orientation of fractures as the foliation/bedding plane is the primary plane of weakness in the sample.

5. Where there are no compositional or textural features in a sample that can have an influence on fracture propagation then fractures will form at regular intervals with similar orientations, often at right angles to one another.

5.0 References

Passchier, C.W. and Trouw, R.A.J. Microtectonics….

PLEASE RECYLCE